Good, Better, Beta

Development and characterization of novel beta cell tracers

Lieke Joosten

ISBN 978-94-028-2167-3

The work presented in this thesis was carried out within the Radboud Institute for Molecular Life Sciences.

The research described in this thesis was financially supported by the People Program (Marie Curie Actions) of the European Union's Seventh Framework Program FP7/2007-2013/ project BetaTrain under REA grant agreement n° 289932, the European Community's Seventh Framework Program FP7/2007-2013/ project BetaImage under grant agreement n° 222980 and project BetaCure, under agreement No. 602812, NIH grant 1R01 AG 030328-01, JDRF grant 3-SRA-2014-32-S-B (to DLE), and JDRF International (37-2011-635).

Cover Crocheted islet of Langerhans made by Riet Joosten. The beta cells will glow in the dark.
Cover design and inside layout Bregje Jaspers | ProefschriftOntwerp.nl
Printed by Ipskamp Printing, Nijmegen, The Netherlands

Good, Better, Beta

Development and characterization of novel beta cell tracers

Proefschrift
ter verkrijging van de graad van doctor
aan de Radboud Universiteit Nijmegen
op gezag van de rector magnificus prof. dr. J.H.J.M. van Krieken,
volgens besluit van het college van decanen
in het openbaar te verdedigen op maandag 2 november 2020
om 10.30 uur precies

door

Lieke Joosten
geboren op 2 november 1983
te Tegelen

Promotoren
Prof. dr. M. Gotthardt
Prof. dr. O.C. Boerman

Copromotoren
Dr. S. Heskamp
Dr. M. Brom

Manusciptcommissie
Prof. dr. N.P. Riksen (voorzitter)
Prof. dr. B.E. de Galan
Prof. dr. P.H. Elsinga (UMC Groningen)

Paranimfen
Rob Joosten
Desirée Bos

Good, Better, Beta

Development and characterization of novel beta cell tracers

Doctoral Thesis
to obtain the degree of doctor
from the Radboud University Nijmegen
on the authority of the Rector Magnificus prof. dr. J.H.J.M. van Krieken,
according to the decision of the Council of Deans
to be defended in public on Monday, November 2, 2020
at 10.30 hours

by

Lieke Joosten
born on November 2, 1983
in Tegelen (The Netherlands)

Supervisors:
Prof. dr. M. Gotthardt
Prof. dr. O.C. Boerman

Co-supervisors:
Dr. M. Brom
Dr. S. Heskamp

Doctoral Thesis Committee:
Prof. dr. N.P. Riksen (Chair)
Prof. dr. B.E. de Galan
Prof. dr. P.H. Elsinga (UMC Groningen)

Paranymphs:
Rob Joosten
Desirée Bos

TABLE OF CONTENTS

CHAPTER 1

Outline

THE IMPORTANCE OF BETA CELL IMAGING

Beta cells are located in the pancreas and form, together with alpha, delta and polypeptide cells, clusters known as the islets of Langerhans. Beta cells produce insulin, which regulates glucose uptake by other cells. When beta cells are functioning correctly and target cells are sensitive to bind insulin, there is a normal blood glucose balance. However, in type 1 diabetes, the beta cell mass is reduced, because the immune system attacks and destroys the beta cells, leading to an imbalance of glucose levels in blood. In type 2 diabetes, cells in the peripheral organs are resistant to insulin, also leading to elevated blood glucose levels. The precise role of beta cells during the development and progression of diabetes is still unknown. To study the role of beta cells in the pathophysiology of diabetes, to monitor new treatment options, or to develop more personalized treatment strategies, a non-invasive method to determine beta cell mass is needed.

Uncontrolled focal growth of beta cells in the pancreas could lead to an insulinoma. Currently, the most widely used molecular imaging strategies to diagnose insulinomas are based on either somatostatin receptor scintigraphy or glucagon-like peptide-1 receptor scintigraphy.

Although the developments for the detection of neuroendocrine tumors have expanded, the search for new tracers for imaging neuroendocrine tumors is ongoing. The first part of this thesis describes the development, improvement and characterization of new radiotracers for beta cell (tumor) imaging. The second part focusses on studies to validate the use of radiolabeled exendin to determine the beta cell mass non-invasively in two animal models of diabetes.

Chapter 2 | General introduction

In this chapter a brief overview of two beta cell related diseases, diabetes and insulinomas, is presented. Possible tracer candidates for visualizing beta cells in both diseases are described, as well as the requirements that an imaging agent should preferably meet, and challenges that we are facing when imaging beta cells in diabetes and insulinomas.

Chapter 3 | Preclinical evaluation of PAC1 targeting with radiolabeled maxadilan

In this chapter the evaluation of a new radiotracer, maxadilan, to image insulinomas is described. Maxadilan targets the PAC1 receptor that is expressed on insulinomas. Radiolabeled maxadilan was able to visualize subcutaneous insulinomas *in vivo* using SPECT.

Chapter 4 | Characterization of ^{111}In-labeled glucose-dependent insulinotropic polypeptide as a radiotracer for neuroendocrine tumors

The feasibility of targeting the glucose-dependent insulinotropic polypeptide receptor (GIPR), that is expressed on neuroendocrine tumors, using a radiolabeled GIP analog is investigated

in this chapter. Subcutaneous GIPR-expressing tumors could be visualized *in vivo* using radiolabeled GIP and SPECT.

Chapter 5 | Enhanced specific activity by multi-chelation of exendin-3 leads to improved *in vivo* beta cell imaging

Of the tracers that we have tested during the last years, radiolabeled exendin seems to best fulfill the criteria for an adequate tracer for both beta cell and insulinoma imaging. To further improve the sensitivity of radiolabeled exendin and broaden its applicability, we have modified exendin by adding six lysine residues and six DTPA moieties. This new exendin-based compound is able to complex more radiometal atoms and as such delivers more activity to a single cell.

Chapter 6 | Efficient reduction of renal uptake of radiolabeled exendin

Using radiolabeled exendin is not only champagne and caviar. One of the challenges when performing SPECT imaging is the high kidney uptake of radiolabeled exendin, which could hamper the visualization of insulinomas. In chapter 6 we have described how to successfully reduce the kidney uptake by modifying exendin by introducing a methionine-isoleucine linker between NOTA and the peptide. This could open a window for exendin as a peptide receptor radionuclide therapeutic.

Chapter 7 | Strain differences determine the suitability of animal models for non-invasive *in vivo* beta cell mass determination with radiolabeled exendin

The second part of the thesis starts with an evaluation which animal model would be most optimal to reliably quantify the beta cell mass non-invasively. In this chapter, a comparison of the behavior of radiolabeled exendin in different animal models and strains is presented. The study showed that rat models are more suitable to study exendin-based beta cell determination than mouse models, because in mice there is significant exendin uptake in the exocrine pancreas as well.

Chapter 8 | Measuring the pancreatic beta cell mass *in vivo* with exendin SPECT during hyperglycemia and severe insulitis

In this chapter the performance of radiolabeled exendin in a type 1 diabetic mouse model under stress conditions has been investigated. Hyperglycemia and severe insulitis do not have a major impact on the determination of the beta cell mass using exendin.

Chapter 9 | Validation of [^{111}In]In-exendin SPECT for the determination of the beta cell mass in BioBreeding Diabetes Prone rats

In chapter 9 radiolabeled exendin was applied to quantitatively assess the beta cell mass non-invasively in a rat model for spontaneous type 1 diabetes. A good correlation between the

pancreatic uptake of radiolabeled exendin and the beta cell mass was found, which was not influenced by insulitis.

Chapter 10 | General discussion and future perspectives

In this final chapter the obtained results are discussed, and a future outlook is given.

CHAPTER 2

Introduction

DIABETES

According to the International Diabetes Federation, worldwide 464 million people are suffering from diabetes in 2019, of which more than 1 million are children with type 1 diabetes. The estimated number of adults living with diabetes is expected to rise to 578 million within ten years[1]. These huge numbers and the immense estimated increase underline the need for proper treatment, early diagnosis or even better, prevention.

Diabetes is a chronic disease in which either the islets of Langerhans in the pancreas are no longer able to produce insulin due to autoimmune destruction of the beta cells (type 1 diabetes (T1D)), or in which cells in peripheral tissue become resistant to insulin. In the latter case, the beta cells are unable to produce enough insulin to overcome the resistance, leading to failure of the beta cells as a consequence of endoplasmic reticulum (ER) stress (type 2 diabetes (T2D)). As the function of beta cells is to guard a normal blood sugar level, failure of these cells results in elevated blood glucose levels, called hyperglycemia. For both types of diabetes, acute or chronic elevation of the blood glucose levels can lead to complications, which can be very severe and even life-threatening. Acute complications are acute elevation of blood glucose levels leading to ketoacidosis, and coma as a result of low blood glucose, which can eventually lead to death. Chronic complications include microvascular diseases, such as retinopathy, nephropathy and neuropathy and macrovascular diseases, like cardiovascular diseases[2]. Currently, the most commonly used treatment for T1D is daily administration of insulin, either by subcutaneous injections or via an insulin pump. This is in contrast to T2D, where the main treatment starts with changing to a healthy lifestyle by increasing exercise or by dietary restrictions. The first-line pharmacological treatment is blood glucose lowering medications (such as metformin), which can be complemented with drugs that stimulate insulin secretion (such as GLP-1 analogs) or drugs that stimulate elimination of glucose (such as SGLT-2 inhibitors)[3].

Currently, most information about beta cell mass in humans is based on autopsy or biopsy studies, which do not show the dynamics in beta cell mass during the progression of diabetes. Functional studies are based on measuring glucose metabolism, (c-peptide levels, oral glucose tolerance tests) and are used as a surrogate to obtain dynamic data. However, these are based on beta cell function rather than on beta cell mass. Measuring only functional beta cells can underestimate the total amount of beta cells. Recently, it was shown that even in longstanding type 1 diabetes, there are still (functional) beta cells present[4, 5]. With this evidence, the dogma that in longstanding type 1 diabetes there is total depletion of beta cells was rebutted. Discrepancies between beta cell function and mass can occur as a result of the presence of dysfunctional beta cells as well as differences in beta cell sensitivity to stimuli. Therefore, a method to accurately measure the beta cell mass *in vivo* would provide a better insight in the pathophysiology of diabetes, and other beta cell related diseases.

INSULINOMAS

Neuroendocrine tumors (NETs) are a heterogeneous group of tumors which can arise throughout the body, but are most commonly found in the intestines, pancreas or lungs[6]. Insulinomas are the most common type of functioning pancreatic neuroendocrine tumors, which originate from the beta cells in the islets of Langerhans. Although the incidence of insulinomas is very low (1-3 per million per year), and >90% of the insulinomas are benign, the clinical symptoms, namely hypoglycemia, are severe and require immediate treatment[7, 8]. Biochemical diagnosis of insulinomas is based on low blood glucose levels or elevated proinsulin, insulin and C-peptide levels in plasma and these tests can be complemented with fasting tests (which result in hypoglycemia if insulinoma is present)[9-11].
Accurate diagnosis and localization of insulinomas to guide therapeutic intervention is essential. Currently, the treatment of choice for insulinomas is surgical removal of the lesion or partial pancreatectomy. Since 10 to 27% of insulinomas are not detected intraoperatively[8], preoperative and/or intraoperative localization of insulinomas is crucial to identify the tumor lesion and to minimize unnecessary surgical interventions.

In this thesis, we describe the development and characterization of new agents to image beta cells in the pancreas as well as to detect insulinomas. Furthermore, we have investigated possibilities to improve glucagon-like peptide 1 receptor (GLP-1R) imaging with GLP-1 analogs, a technique that is currently in clinical use for imaging of insulinomas.

TRACERS FOR BETA CELL IMAGING

The ideal tracer

Nowadays, radionuclide imaging is indispensable for the diagnosis and treatment of tumors and other diseases. Peptide targeted molecular imaging is based on a targeting peptide, which recognizes specific binding sites (such as receptors, antigens) on a certain cell type, being for example tumor cells or immune cells. Labeling of peptides with a radiometal is done via a chelating moiety. After binding of the radiolabeled peptide to the receptor, the whole receptor-peptide-complex can be internalized into the cell, where the chelated radioisotope will be trapped in lysosomes. The peptide will be degraded and the receptor is degraded or can translocate to the cell membrane again, where it is able to bind a new radiolabeled peptide. This process can lead to a high accumulation of the radioisotope in tissues that express the targeted receptor[12]. One of the characteristics of cancer cells is high expression of tumor-associated receptors. This high expression is an advantage for targeted molecular imaging, because it can result in high uptake of the radiolabeled peptide. Ideally, a targeting agent should meet the following criteria: 1) high and specific uptake in tissue of interest, 2) low uptake in non-target

tissue, 3) high affinity for the receptor, 4) fast blood clearance, 5) sufficient metabolic stability, 6) low or no toxicity, and in the case of an agonist 7) a minimal pharmacological effect.
Since insulinomas have high abundance of the GLP-1 receptor, it is reasonable that high amounts of GLP-1 analogs could accumulate into these tumors, and with that it should be relatively easy to detect insulinomas using PET and SPECT. On the contrary, native beta cells in the pancreas are 'healthy' cells and have lower GLP-1 receptor expression. Furthermore, beta cells, together with alpha, delta and polypeptide cells, form the islets of Langerhans which are spread throughout the pancreas and only represent 1-2% of the total pancreatic mass. Hence, imaging of these pancreatic beta cells is much more challenging than imaging tumor cells[13], since tumors consist of more cells than the islets of Langerhans and have increased receptor expression. Thus, the perfect tracer for native beta cell imaging should even meet more requirements. As there are less receptors available for binding, a low peptide dose should be administered to prevent saturation of the receptors. Along with a low peptide dose, a high molar activity is warranted in order to get a sufficient amount of radioactive signal in the organ of interest, to allow detection with SPECT or PET.

Tracers for beta cell imaging

Currently, the most widely used imaging technique for the detection of insulinomas is somatostatin receptor scintigraphy (SRS). Different ligands targeting the somatostatin receptor have been tested, all based on octreotide. For example, a study using [^{111}In]In-DTPA-$_{D}$-Phe^{1}-octreotide reported a detection rate of 53%[14]. A study of Antwi described a detection rate of 33% for [^{68}Ga]DOTATOC[15] and in another study using [^{68}Ga]Ga-DOTA-TATE and [^{68}Ga]Ga-DOTATOC, a sensitivity of 85% has been described for detecting insulinomas[16].
Interestingly, a technique to visualize the pancreatic beta cells in diabetic patients does not exist to date.
Several targets for beta cell imaging have been evaluated, based on their expression pattern in beta cells or in beta-cell derived tumors[17]. Incretins are hormones that are secreted after nutrient intake and stimulate insulin secretion in a glucose-dependent manner[18, 19]. As incretins are key players in controlling the glucose balance, these present interesting targets for beta cell imaging. Two incretin hormones, the glucose-dependent insulinotropic polypeptide (or gastric inhibitory polypeptide (GIP)) and glucagon-like peptide 1 (GLP-1) will be discussed in more detail[18, 19]. Furthermore, as PAC1 also seems to be involved in insulin secretion[20] , this receptor will be discussed as well (Figure 1).

GIP

The GIP receptor (GIPR) belongs to the G-protein coupled receptor family and is expressed in several rodent tissues, like stomach, lung and most important in pancreatic islets[18]. Furthermore, abundant expression of the GIPR has been found in different neuroendocrine tumors, such as gastrointestinal and bronchial tumors, and the highest expression was found

in pancreatic tumors, including insulinomas[21, 22]. The natural GIP ligand has a short biological half-life and is rapidly cleaved by enzymes after release in the circulation[23]. The first pre-clinical study using different radiolabeled GIP analogs was performed by Gourni et al. They described high uptake of a GIP ligand, labeled with either ^{111}In or ^{68}Ga, in GIPR-transfected tumors, and the uptake in the pancreas could be blocked by an excess of unlabeled GIP[24]. As the kidneys are the main excretion route of radiolabeled GIP, high kidney uptake was observed, which could be partially reduced by co-injection of Gelofusine. Autoradiography using iodinated GIP confirmed specific uptake in the islets of Langerhans in the pancreas, as well as specific uptake in pancreatic and bronchial NETs[22]. However, mRNA expression of GIPR has been detected in alpha and beta cells in rats by Moens et al. Nevertheless, it must be noted that they did not study the expression of GIPR on protein level[25].

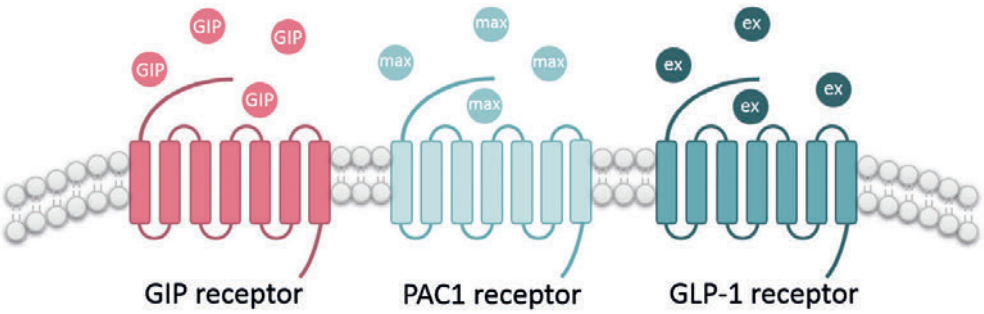

Figure 1. An overview of beta cell specific receptors investigated in the next chapters. Abbreviations: GIP, glucose-dependent insulinotropic polypeptide; PAC1, pituitary adenylate cyclase-activating polypeptide type I; max, maxadilan; GLP-1, glucagon-like peptide 1; ex, exendin.

PAC1

Vasoactive intestinal peptide (VIP)/pituitary adenylate cyclase activating polypeptide (PACAP), and their receptors PAC1, VPAC1 and PAC2, being members of the G-protein coupled receptor family, have emerged as important factors in islet cell function (insulin secretion)[20]. Furthermore, they are involved in growth and differentiation of neuroendocrine tumors, including insulinomas. As these receptors are expressed at high levels in insulinomas and beta cells, they are potential targets for beta cell and insulinoma imaging[26-28].

The natural mammalian ligands of PAC1, PACAP38 and the truncated form PACAP27, also bind VAPC1 and VPAC2. Because these ligands are not selective for the PAC1 receptor and are unstable in plasma[29], they are not suited for *in vivo* targeting of PAC1 receptors. More than two decades ago it was demonstrated that the stable analog maxadilan shared features with ligands of the PACAP family[30, 31]. Maxadilan is a 61-amino acid vasoactive peptide, derived from sand flies[32, 33], and has been demonstrated to bind specifically and with high affinity to the PAC1

receptor, but not to VPAC1 or VPAC2[33]. Thus far, it was unknown whether the PAC1 receptor is an appropriate target for imaging (healthy) beta cells. To the best of our knowledge, no studies were carried out using the PAC1 receptor for imaging insulinomas or for correlating the beta cell mass with uptake of PAC1 receptor targeting ligands. Also, the specificity for beta cells is still unknown. So far, PACAP has been found in glucagon producing alpha cells and insulin producing beta cells, and was expressed in both normal and diabetic islets from rats and humans[34]. However, the specific expression pattern of the PAC1 receptor for beta or other endocrine cells was not explored. Contradictory results have been found by Filipsson *et al.*, who were not able to demonstrate PACAP expression in insulin producing cells[35]. Yet, via in situ hybridization they did show PAC1 receptor expression in pancreatic endocrine cells, but the signal was equal in the exocrine pancreatic tissue. Nevertheless, the PAC1 receptor may be an interesting target for imaging insulinomas, but its potential for both pancreatic beta cell and insulinoma imaging needs to be investigated.

GLP-1R

The glucagon-like peptide 1 receptor (GLP-1R) is also a member of the G-protein coupled receptor family and is involved in beta cell proliferation and insulin secretion upon glucose stimulation. In human, the GLP-1R is mainly expressed in the pancreatic islets, duodenum and neuropituitary[36]. In mice and rats, high expression of the GLP-1R was also found in the lungs[37, 38]. As the GLP-1R is highly expressed on beta cells[39], it is a promising target for imaging beta cells. Exendin is a stable analog of the natural GLP-1R ligand, the hormone GLP-1, and was isolated from the saliva of the *Heloderma suspectum* (Gilamonster)[40]. The feasibility of exendin-4 as an imaging agent was first demonstrated by Gotthardt *et al.* in a preclinical study. Specific uptake of [^{111}In]In-DTPA-exendin-4 was found in GLP-1R expressing organs, such as lungs and pancreas[41]. In addition, in a Rip1Tag2 mouse model insulinomas in the pancreas were visualized using [^{111}In]In-DTPA-exendin-4 and SPECT/CT[42]. Over the years, several groups described exendin-based beta cell imaging using a variety of radioligands[43, 44] or other molecular imaging strategies, like fluorescently labeled exendin[45]. Recently, it was shown that the uptake of exendin in the pancreas was decreased in chemically induced diabetic animals[46, 47]. Radiolabeled exendin has shown great potential to image native beta cells in diabetes. A study of Brom *et al.* showed a significantly lower pancreatic uptake of [^{111}In]In-DTPA-exendin in T1D patients as compared to healthy volunteers, although some individuals with T1D showed pancreatic uptake reaching into the lower range of uptake in healthy volunteers. Furthermore, the signal of the tracer in the pancreas of half of the T1D patients declined to almost the background level, suggesting that small amounts of beta cells can be detected and nonspecific uptake is neglectable[46].

While exendin is a promising tracer for beta cell imaging, its specificity for beta cells varies between species. In mice and pigs there is considerable uptake of exendin in the exocrine pancreas, but the tracer uptake in rats and humans is restricted to the endocrine cells[39, 48]. As

was demonstrated by Brom et al., uptake of exendin correlated with beta cell mass and not with alpha cell mass, indicating the specificity of exendin for beta cells[49].

Challenges of GLP-1R-based beta cell imaging

As mentioned before, to be an ideal tracer, a targeting agent should meet various criteria. Exendin does meet some of these requirements, as it is stable, has high and specific uptake in the beta cells, has high affinity for the GLP-1R, fast blood clearance, and at low doses shows minimal toxicity or pharmacological effects[49, 50]. However, there is GLP-1R expression in non-target organs, like the duodenum, and exendin shows high accumulation in the kidneys. Furthermore, the extent to which the GLP-1R expression changes upon metabolic stress is unknown.

High kidney uptake

The main excretion route of hydrophilic small molecules, such as radiolabeled peptides is via the kidneys (Figure 2). Small molecules enter the kidneys via the bloodstream and are filtered through the glomeruli. Although part of the administered molecules is excreted via the urine, generally a significant part is reabsorbed in the proximal tubules, where different mechanisms of transport can be involved in the reabsorption of these peptides. Exendin is most probably reabsorbed via endocytic receptors that are located near the brush border membrane, as a recent study showed that the uptake of exendin in the kidneys could be reduced in mice that lack megalin, a particular endocytic receptor[51, 52]. After endocytic reabsorption of the radiolabeled peptide, it will be degraded in lysosomes, where the chelated radiometal will residualise, leading to high kidney accumulation.

The high kidney accumulation is a problem mainly for two reasons. First, high renal accumulation of radiolabeled exendin could hamper visualization of insulinomas that are in the vicinity of the kidneys. Second, because of the high kidney uptake, the prolonged radiation burden to the kidneys precludes the applicability of exendin for PRRT. Several successful attempts to reduce the kidney uptake have been described, for example by co-injection with the plasma expander Gelofusine[53, 54]. Also, the use of linkers that are cleaved by lysosomal enzymes, resulting in release of the radiometal-chelator complex into the urine have been described[55]. However, for exendin the use of Gelofusine is not as efficient as for octreotide for example[56]. Therefore, future research on minimizing the renal retention of tracers for beta cell and insulinoma imaging is warranted.

High molar activity

Whereas insulinomas have overexpression of the GLP-1R, the native beta cells in the pancreas have lower GLP-1R expression levels. As there are less binding sites for exendin in these endocrine beta cells, a very low peptide dose is needed to prevent saturation of the receptor. Furthermore, as the amount of beta cells declines in diabetic subjects and the amount of

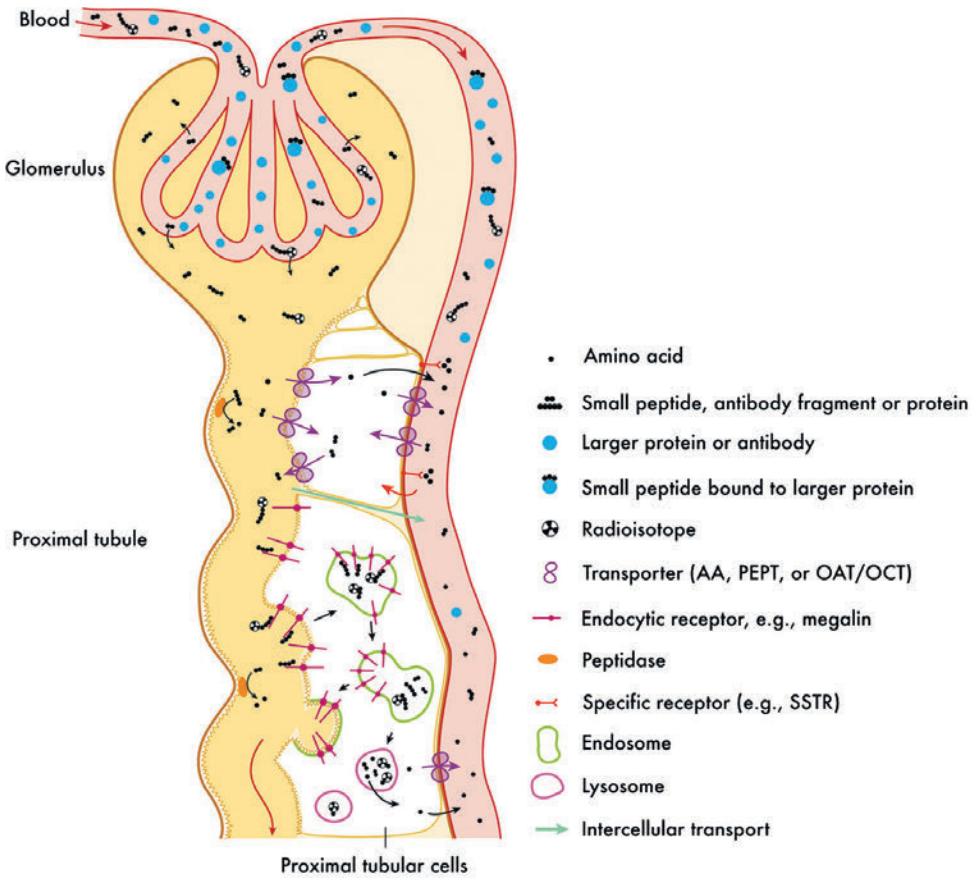

Figure 2. Overview of glomerular and proximal tubular handling of proteins and peptides. AA = amino acid transporter, OCT = organic cation transporter, PEPT = oligopeptide transporter. This figure was originally published in JNM. Vegt et al. Renal Toxicity of Radiolabeled Peptides and Antibody Fragments: Mechanisms, Impact on Radionuclide Therapy, and Strategies for Prevention. J Nucl Med. 2010; 51: 1049-1058. © SNMMI.

beta cells between diabetic and healthy subjects partly overlaps, it is important to deliver high amounts of radiotracer to each single beta cell. Obviously, to be able to detect a sufficient amount of radioactive signal associated with these cells, a tracer with a high molar activity is needed. This can be achieved for example by optimizing the labeling conditions[57] or by introducing peptide modifications that could facilitate a higher molar activity.

Hyperglycemia

One concern when studying the beta cell mass using exendin is a potential influence of hyperglycemia on the GLP-1R expression. Hyperglycemia is one of the main characteristics

of diabetes. It is important that the influence of hyperglycemia on the GLP-1R expression is limited, as the determination of the beta cell mass using radiolabeled exendin depends on the expression of the GLP-1R. Chronic hyperglycemia has been demonstrated to down-regulate GLP-1R expression[58, 59]. This suggests that during development of diabetes the expression of the GLP-1R could change and with that the determination of the beta cell mass would be underestimated. It is therefore important to study the effects of elevated blood glucose levels on beta cell mass measurements using radiolabeled exendin.

Insulitis

Insulitis could also change the expression of the GLP-1R, inherent to the influence of blood glucose levels. Insulitis has been described as infiltration of the islets of Langerhans by lymphocytes, leading to inflammation of the islets and finally destruction of the beta cells[60]. During insulitis, several cytokines (IL-1, IFN-γ, a.o.) are released by immune cells. As not all diabetic patients have autoantibodies against beta cells (ICA, GADA, and IA-2-Ab) and not every patient has insulitis, it is important to unravel whether pro-inflammatory cytokines (e.g. IL-1β and IFN-γ) alter the expression of the GLP-1R. This is important, as the determination of the beta cell mass using radiolabeled exendin depends on the expression of GLP-1R. It has been demonstrated that upon treatment with cytokines the GLP-1R was down-regulated *in vitro*[61]. Similar to hyperglycemia, this might lead to an underestimation of the beta cell mass and thus it needs to be explored to which extend insulitis does have an influence on beta cell mass measurements using exendin.

REFERENCES

1. https://diabetesatlas.org/en/.
2. Forbes JM, Cooper ME. Mechanisms of diabetic complications. *Physiol Rev.* **2013**; 93 (1): 137-188.
3. Aghaei Meybodi HR, Hasanzad M, Larijani B. Path to Personalized Medicine for Type 2 Diabetes Mellitus: Reality and Hope. *Acta Med Iran.* **2017**; 55 (3): 166-174.
4. Keenan HA, Sun JK, Levine J, Doria A, Aiello LP, Eisenbarth G, *et al.* Residual insulin production and pancreatic ss-cell turnover after 50 years of diabetes: Joslin Medalist Study. *Diabetes.* **2010**; 59 (11): 2846-2853.
5. Meier JJ, Bhushan A, Butler AE, Rizza RA, Butler PC. Sustained beta cell apoptosis in patients with long-standing type 1 diabetes: indirect evidence for islet regeneration? *Diabetologia.* **2005**; 48 (11): 2221-2228.
6. Oronsky B, Ma PC, Morgensztern D, Carter CA. Nothing But NET: A Review of Neuroendocrine Tumors and Carcinomas. *Neoplasia.* **2017**; 19 (12): 991-1002.
7. de Herder WW, Niederle B, Scoazec JY, Pauwels S, Kloppel G, Falconi M, *et al.* Well-differentiated pancreatic tumor/carcinoma: insulinoma. *Neuroendocrinology.* **2006**; 84 (3): 183-188.
8. Mehrabi A, Fischer L, Hafezi M, Dirlewanger A, Grenacher L, Diener MK, *et al.* A systematic review of localization, surgical treatment options, and outcome of insulinoma. *Pancreas.* **2014**; 43 (5): 675-686.
9. Granberg D, Oberg K. Neuroendocrine tumours. *Cancer Chemother Biol Response Modif.* **2005**; 22 471-483.
10. Iglesias P, Diez JJ. Management of endocrine disease: a clinical update on tumor-induced hypoglycemia. *Eur J Endocrinol.* **2014**; 170 (4): R147-157.
11. Modlin IM, Tang LH. Approaches to the diagnosis of gut neuroendocrine tumors: the last word (today). *Gastroenterology.* **1997**; 112 (2): 583-590.
12. Gotthardt M, Boermann OC, Behr TM, Behe MP, Oyen WJ. Development and clinical application of peptide-based radiopharmaceuticals. *Curr Pharm Des.* **2004**; 10 (24): 2951-2963.
13. Eriksson O, Laughlin M, Brom M, Nuutila P, Roden M, Hwa A, *et al.* In vivo imaging of beta cells with radiotracers: state of the art, prospects and recommendations for development and use. *Diabetologia.* **2016**; 59 (7): 1340-1349.
14. Krenning EP, Kwekkeboom DJ, Oei HY, de Jong RJ, Dop FJ, Reubi JC, *et al.* Somatostatin-receptor scintigraphy in gastroenteropancreatic tumors. An overview of European results. *Ann N Y Acad Sci.* **1994**; 733 416-424.
15. Antwi K, Fani M, Heye T, Nicolas G, Rottenburger C, Kaul F, *et al.* Comparison of glucagon-like peptide-1 receptor (GLP-1R) PET/CT, SPECT/CT and 3T MRI for the localisation of occult insulinomas: evaluation of diagnostic accuracy in a prospective crossover imaging study. *Eur J Nucl Med Mol Imaging.* **2018**; 45 (13): 2318-2327.
16. Prasad V, Sainz-Esteban A, Arsenic R, Plockinger U, Denecke T, Pape UF, *et al.* Role of (68)Ga somatostatin receptor PET/CT in the detection of endogenous hyperinsulinaemic focus: an explorative study. *Eur J Nucl Med Mol Imaging.* **2016**; 43 (9): 1593-1600.

17. Reubi JC, Waser B. Concomitant expression of several peptide receptors in neuroendocrine tumours: molecular basis for in vivo multireceptor tumour targeting. *Eur J Nucl Med Mol Imaging*. **2003**; 30 (5): 781-793.

18. McIntosh CH, Widenmaier S, Kim SJ. Glucose-dependent insulinotropic polypeptide (Gastric Inhibitory Polypeptide; GIP). *Vitam Horm*. **2009**; 80 409-471.

19. Meier JJ, Nauck MA. Clinical endocrinology and metabolism. Glucose-dependent insulinotropic polypeptide/gastric inhibitory polypeptide. *Best Pract Res Clin Endocrinol Metab*. **2004**; 18 (4): 587-606.

20. Liu M, Yang X, Bai T, Liu Z, Liu T, Wang Y, *et al*. PACAP stimulates insulin secretion by PAC1 receptor and ion channels in beta-cells. *Cell Signal*. **2019**; 61 48-56.

21. Sherman SK, Maxwell JE, Carr JC, Wang D, O'Dorisio MS, O'Dorisio TM, *et al*. GIPR expression in gastric and duodenal neuroendocrine tumors. *J Surg Res*. **2014**; 190 (2): 587-593.

22. Waser B, Rehmann R, Sanchez C, Fourmy D, Reubi JC. Glucose-dependent insulinotropic polypeptide receptors in most gastroenteropancreatic and bronchial neuroendocrine tumors. *J Clin Endocrinol Metab*. **2012**; 97 (2): 482-488.

23. Gault VA, Flatt PR, O'Harte FP. Glucose-dependent insulinotropic polypeptide analogues and their therapeutic potential for the treatment of obesity-diabetes. *Biochem Biophys Res Commun*. **2003**; 308 (2): 207-213.

24. Gourni E, Waser B, Clerc P, Fourmy D, Reubi JC, Maecke HR. The glucose-dependent insulinotropic polypeptide receptor: a novel target for neuroendocrine tumor imaging-first preclinical studies. *J Nucl Med*. **2014**; 55 (6): 976-982.

25. Moens K, Heimberg H, Flamez D, Huypens P, Quartier E, Ling Z, *et al*. Expression and functional activity of glucagon, glucagon-like peptide I, and glucose-dependent insulinotropic peptide receptors in rat pancreatic islet cells. *Diabetes*. **1996**; 45 (2): 257-261.

26. Inagaki N, Kuromi H, Seino S. PACAP/VIP receptors in pancreatic beta-cells: their roles in insulin secretion. *Ann N Y Acad Sci*. **1996**; 805 44-51; discussion 52-43.

27. Moody TW, Nuche-Berenguer B, Jensen RT. Vasoactive intestinal peptide/pituitary adenylate cyclase activating polypeptide, and their receptors and cancer. *Curr Opin Endocrinol Diabetes Obes*. **2016**; 23 (1): 38-47.

28. Tatsuno I, Uchida D, Tanaka T, Saeki N, Hirai A, Saito Y, *et al*. Maxadilan specifically interacts with PAC1 receptor, which is a dominant form of PACAP/VIP family receptors in cultured rat cortical neurons. *Brain Res*. **2001**; 889 (1-2): 138-148.

29. Ahren B. Role of pituitary adenylate cyclase-activating polypeptide in the pancreatic endocrine system. *Ann N Y Acad Sci*. **2008**; 1144 28-35.

30. Arimura A. Pituitary adenylate cyclase activating polypeptide (PACAP): discovery and current status of research. *Regul Pept*. **1992**; 37 (3): 287-303.

31. Arimura A, Shioda S. Pituitary adenylate cyclase activating polypeptide (PACAP) and its receptors: neuroendocrine and endocrine interaction. *Front Neuroendocrinol*. **1995**; 16 (1): 53-88.

32. Lerner EA, Ribeiro JM, Nelson RJ, Lerner MR. Isolation of maxadilan, a potent vasodilatory peptide from the salivary glands of the sand fly Lutzomyia longipalpis. *J Biol Chem.* **1991**; 266 (17): 11234-11236.

33. Moro O, Lerner EA. Maxadilan, the vasodilator from sand flies, is a specific pituitary adenylate cyclase activating peptide type I receptor agonist. *J Biol Chem.* **1997**; 272 (2): 966-970.

34. Portela-Gomes GM, Lukinius A, Ljungberg O, Efendic S, Ahren B, Abdel-Halim SM. PACAP is expressed in secretory granules of insulin and glucagon cells in human and rodent pancreas. Evidence for generation of cAMP compartments uncoupled from hormone release in diabetic islets. *Regul Pept.* **2003**; 113 (1-3): 31-39.

35. Filipsson K, Sundler F, Hannibal J, Ahren B. PACAP and PACAP receptors in insulin producing tissues: localization and effects. *Regul Pept.* **1998**; 74 (2-3): 167-175.

36. Korner M, Stockli M, Waser B, Reubi JC. GLP-1 receptor expression in human tumors and human normal tissues: potential for in vivo targeting. *J Nucl Med.* **2007**; 48 (5): 736-743.

37. Campos RV, Lee YC, Drucker DJ. Divergent tissue-specific and developmental expression of receptors for glucagon and glucagon-like peptide-1 in the mouse. *Endocrinology.* **1994**; 134 (5): 2156-2164.

38. Dunphy JL, Taylor RG, Fuller PJ. Tissue distribution of rat glucagon receptor and GLP-1 receptor gene expression. *Mol Cell Endocrinol.* **1998**; 141 (1-2): 179-186.

39. Tornehave D, Kristensen P, Romer J, Knudsen LB, Heller RS. Expression of the GLP-1 receptor in mouse, rat, and human pancreas. *J Histochem Cytochem.* **2008**; 56 (9): 841-851.

40. Eng J, Kleinman WA, Singh L, Singh G, Raufman JP. Isolation and characterization of exendin-4, an exendin-3 analogue, from Heloderma suspectum venom. Further evidence for an exendin receptor on dispersed acini from guinea pig pancreas. *J Biol Chem.* **1992**; 267 (11): 7402-7405.

41. Gotthardt M, Lalyko G, van Eerd-Vismale J, Keil B, Schurrat T, Hower M, *et al.* A new technique for in vivo imaging of specific GLP-1 binding sites: first results in small rodents. *Regul Pept.* **2006**; 137 (3): 162-167.

42. Wild D, Behe M, Wicki A, Storch D, Waser B, Gotthardt M, *et al.* [Lys40(Ahx-DTPA-111In)NH2]exendin-4, a very promising ligand for glucagon-like peptide-1 (GLP-1) receptor targeting. *J Nucl Med.* **2006**; 47 (12): 2025-2033.

43. Wang Y, Lim K, Normandin M, Zhao X, Cline GW, Ding YS. Synthesis and evaluation of [18F]exendin (9-39) as a potential biomarker to measure pancreatic beta-cell mass. *Nucl Med Biol.* **2012**; 39 (2): 167-176.

44. Wild D, Wicki A, Mansi R, Behe M, Keil B, Bernhardt P, *et al.* Exendin-4-based radiopharmaceuticals for glucagonlike peptide-1 receptor PET/CT and SPECT/CT. *J Nucl Med.* **2010**; 51 (7): 1059-1067.

45. Lehtonen J, Schaffer L, Rasch MG, Hecksher-Sorensen J, Ahnfelt-Ronne J. Beta cell specific probing with fluorescent exendin-4 is progressively reduced in type 2 diabetic mouse models. *Islets.* **2015**; 7 (6): e1137415.

46. Brom M, Woliner-van der Weg W, Joosten L, Frielink C, Bouckenooghe T, Rijken P, *et al.* Non-invasive quantification of the beta cell mass by SPECT with (1)(1)(1)In-labelled exendin. *Diabetologia.* **2014**; 57 (5): 950-959.

47. Selvaraju RK, Velikyan I, Johansson L, Wu Z, Todorov I, Shively J, *et al*. In vivo imaging of the glucagonlike peptide 1 receptor in the pancreas with 68Ga-labeled DO3A-exendin-4. *J Nucl Med*. **2013**; 54 (8): 1458-1463.

48. Eriksson O, Rosenstrom U, Selvaraju RK, Eriksson B, Velikyan I. Species differences in pancreatic binding of DO3A-VS-Cys(40)-Exendin4. *Acta Diabetol*. **2017**; 54 (11): 1039-1045.

49. Brom M, Joosten L, Frielink C, Boerman O, Gotthardt M. (111)In-exendin uptake in the pancreas correlates with the beta-cell mass and not with the alpha-cell mass. *Diabetes*. **2015**; 64 (4): 1324-1328.

50. Brom M, Oyen WJ, Joosten L, Gotthardt M, Boerman OC. 68Ga-labelled exendin-3, a new agent for the detection of insulinomas with PET. *Eur J Nucl Med Mol Imaging*. **2010**; 37 (7): 1345-1355.

51. Vegt E, de Jong M, Wetzels JF, Masereeuw R, Melis M, Oyen WJ, *et al*. Renal toxicity of radiolabeled peptides and antibody fragments: mechanisms, impact on radionuclide therapy, and strategies for prevention. *J Nucl Med*. **2010**; 51 (7): 1049-1058.

52. Vegt E, Melis M, Eek A, de Visser M, Brom M, Oyen WJ, *et al*. Renal uptake of different radiolabelled peptides is mediated by megalin: SPECT and biodistribution studies in megalin-deficient mice. *Eur J Nucl Med Mol Imaging*. **2011**; 38 (4): 623-632.

53. Buitinga M, Jansen T, van der Kroon I, Woliner-van der Weg W, Boss M, Janssen M, *et al*. Succinylated Gelatin Improves the Theranostic Potential of Radiolabeled Exendin-4 in Insulinoma Patients. *J Nucl Med*. **2019**; 60 (6): 812-816.

54. Gotthardt M, van Eerd-Vismale J, Oyen WJ, de Jong M, Zhang H, Rolleman E, *et al*. Indication for different mechanisms of kidney uptake of radiolabeled peptides. *J Nucl Med*. **2007**; 48 (4): 596-601.

55. Uehara T, Rokugawa T, Kinoshita M, Nemoto S, Fransisco Lazaro GG, Hanaoka H, *et al*. (67/68)Ga-labeling agent that liberates (67/68)Ga-NOTA-methionine by lysosomal proteolysis of parental low molecular weight polypeptides to reduce renal radioactivity levels. *Bioconjug Chem*. **2014**; 25 (11): 2038-2045.

56. Vegt E, van Eerd JE, Eek A, Oyen WJ, Wetzels JF, de Jong M, *et al*. Reducing renal uptake of radiolabeled peptides using albumin fragments. *J Nucl Med*. **2008**; 49 (9): 1506-1511.

57. Brom M, Joosten L, Oyen WJ, Gotthardt M, Boerman OC. Improved labelling of DTPA- and DOTA-conjugated peptides and antibodies with 111In in HEPES and MES buffer. *EJNMMI Res*. **2012**; 2 4.

58. Rajan S, Dickson LM, Mathew E, Orr CM, Ellenbroek JH, Philipson LH, *et al*. Chronic hyperglycemia downregulates GLP-1 receptor signaling in pancreatic beta-cells via protein kinase A. *Mol Metab*. **2015**; 4 (4): 265-276.

59. Xu G, Kaneto H, Laybutt DR, Duvivier-Kali VF, Trivedi N, Suzuma K, *et al*. Downregulation of GLP-1 and GIP receptor expression by hyperglycemia: possible contribution to impaired incretin effects in diabetes. *Diabetes*. **2007**; 56 (6): 1551-1558.

60. Campbell-Thompson ML, Atkinson MA, Butler AE, Chapman NM, Frisk G, Gianani R, *et al*. The diagnosis of insulitis in human type 1 diabetes. *Diabetologia*. **2013**; 56 (11): 2541-2543.

61. Ortis F, Naamane N, Flamez D, Ladriere L, Moore F, Cunha DA, *et al*. Cytokines interleukin-1beta and tumor necrosis factor-alpha regulate different transcriptional and alternative splicing networks in primary beta-cells. *Diabetes*. **2010**; 59 (2): 358-374.

Part I

Tracer development

CHAPTER 3

Preclinical evaluation of PAC1 targeting with radiolabeled maxadilan

Lieke Joosten[1], Maarten Brom[1], Martin K. H. Schäfer[2], Otto C. Boerman[1], Eberhard Weihe[2] & Martin Gotthardt[1]

1 Department of Radiology and Nuclear Medicine, Radboud University Medical Center, Nijmegen, The Netherlands

2 Institute of Anatomy and Cell Biology, Department of Molecular Neuroscience, Philipps University of Marburg, Marburg, Germany

Scientific Reports. **2017**; 7 (1): 1751

ABSTRACT

There is an ongoing search for new tracers to optimize imaging of beta cell-derived tumors (insulinomas). The PAC1 receptor, expressed by insulinomas, can be used for targeting of these tumors. Here, we investigated whether radiolabeled maxadilan could be used for insulinoma imaging. Maxadilan was C- or N-terminally conjugated with DTPA (termed maxadilan-DPTA or DTPA-maxadilan respectively). BALB/c nude mice bearing subcutaneous INS-1 tumors were injected with either ^{111}In-labeled maxadilan-DTPA or DTPA-maxadilan. Biodistribution studies were carried out at 1, 2 and 4 hours after injection and SPECT/CT imaging 1 and 4 hours after injection of maxadilan-DTPA-[^{111}In]In. Radiolabeling of maxadilan-DTPA (680 MBq/nmol) was more efficient than of DTPA-maxadilan (55 MBq/nmol). Conjugation with DTPA slightly reduced receptor binding affinity *in vitro*: IC_{50} values were 3.2, 21.0 and 21.0 nM for maxadilan, [^{nat}In]In-DTPA-maxadilan and maxadilan-DTPA-[^{nat}In]In respectively. Upon i.v. injection maxadilan-DTPA-[^{111}In]In accumulated specifically in INS-1 tumors (7.30 ± 1.87%ID/g) and in the pancreas (3.82 ± 0.22%ID/g). INS-1 tumors were clearly visualized by small animal SPECT/CT. In conclusion, this study showed that the high affinity of maxadilan to the PAC1 receptor was maintained after DTPA conjugation. Furthermore, radiolabeled maxadilan-DTPA accumulated specifically in INS-1 tumors and, therefore, may qualify as a useful tracer to image insulinomas.

INTRODUCTION

The most common pancreatic neuroendocrine tumors (NETs) are insulinomas. Insulinomas are tumors derived from the insulin-producing beta cells located in the islets of Langerhans in the pancreas. Clinical symptoms include symptomatic hypoglycemias as well as weight gain (due to increased food intake to compensate for hypoglycemia) and neurological symptoms[1]. Biochemical diagnosis is based on low blood glucose levels or elevated proinsulin, insulin and C-peptide levels in plasma and these tests can be complemented with fasting tests (which results in hypoglycemia if insulinoma is present) [1-3]. The most widely used nuclear medicine imaging strategy for detecting insulinomas is somatostatin receptor scintigraphy (SRS) using ^{111}In-labeled octreotide. SRS is based on targeting somatostatin receptors (SSTR), which are over-expressed in sixty percent of insulinomas[4]. Because the remaining forty percent has either low or no expression of this receptor, many insulinomas are not being detected by scintigraphy based on somatostatin receptor targeting [2-4]. More preferably, PET (Positron Emission Tomography) imaging with octreotide analogs can be used, since PET is more sensitive than SPECT imaging, due to the higher spatial resolution of clinical PET scanners and higher sensitivity in detection of emitted gamma photons. A few promising studies were conducted using SSTR PET/CT, although these studies showed that a small percentage of insulinomas remain undetected [5-8].

More than ten years ago, it was demonstrated that almost all insulinomas express several neuropeptide receptors, including CCK_2 (cholecystokinin), VPAC1 (vasoactive intestinal peptide/PACAP receptor subtype 1) and GLP-1 (glucagon-like peptide 1) receptors [4]. Several preclinical SPECT and PET studies in RipTag2 mouse models using the GLP-1 analogs exendin-3 and exendin-4, showed specific tracer accumulation in insulinomas via the GLP-1 receptor [9-11]. In the first pioneering clinical PET/CT and SPECT/CT studies with exendin-4 in insulinoma patients, small insulinomas, which could not be detected by conventional imaging methods (endoscopic ultrasound, MRI (Magnetic Resonance Imaging), CT (Computed Tomography), SRS) [12-17], were accurately diagnosed. The success of visualizing neuroendocrine tumors is partially dependent on the type of receptors expressed in the tumors, as was shown previously by Baumann et al [5]. For example, malignant insulinomas have a low incidence and expression density of the GLP-1 receptor, but show high expression of the somatostatin receptor, where in benign insulinomas the expression profile is more favorable for the GLP-1R [4, 18, 19]. Therefore, to improve the diagnostic tool box, the search for new tracers for detection of insulinomas is ongoing.

Vasoactive intestinal peptide (VIP)/pituitary adenylate cyclase activating polypeptide (PACAP), and their receptors PAC1, VPAC1 and PAC2 have emerged as important factors in islet cell function (insulin secretion) and growth and differentiation of neuroendocrine tumors including insulinomas. As these receptors are highly expressed in insulinomas and beta cells, they are potential targets for beta cell and insulinoma imaging [20-22].

Using *in vitro* receptor autoradiography with VPAC1 and VPAC2 subtype-selective ligands, insulinomas have been demonstrated to bind high levels of radiolabeled selective VPAC1 receptor ligands, although substantially less than GLP-1 selective ligands [4]. As PAC1, VPAC1 and VPAC2 mRNAs were detected in a rat insulinoma cell line with PAC-1 binding prevailing over that of VPAC1 and VPAC2 [23], the PAC1 receptor seemed to be a promising alternative for targeting insulinomas. The natural mammalian ligands at the PAC1 receptor are PACAP38 and the truncated form PACAP27. They bind to PAC1, VPAC1 and VPAC2, whereas VIP only binds to VPAC1 and VPAC2. Since PACAP38 and PACAP27 are non-selective PAC1/VPAC1/VPAC2 ligands and unstable in plasma [24], they are not suited for *in vivo* targeting of PAC1 receptors. More than two decades ago it was demonstrated that the stable analog maxadilan shared features with ligands of the PACAP family [25, 26]. Maxadilan is a 61-amino acid vasoactive peptide, derived from sand flies [27, 28], and has been demonstrated to bind specifically and with high affinity to the PAC1 receptor but not to either VPAC1 or VPAC2 [28].

In the present study we have examined the ability of ^{111}In-labeled maxadilan to image rat insulinoma xenografts (INS-1) in a nude mouse model. For this purpose maxadilan was either C- or N-terminally conjugated with DTPA to allow labeling with ^{111}In. These compounds were evaluated for their radiolabeling properties and *in vitro* and *in vivo* binding characteristics.

MATERIALS AND METHODS

Peptides

DTPA-conjugated and native maxadilan were purchased from Think Peptides (ProImmune Limited, Oxford, United Kingdom). N-terminal conjugation of DTPA (DTPA-maxadilan) was performed with isothiocyanate-DTPA (Macrocyclics, Dallas, TX, USA) via a beta-alanine spacer and C-terminal conjugation (maxadilan-DTPA) with *p*-NH2-Bn-DTPA via an extra C-terminal glutamic acid. The quality and purity of the peptides was determined using RP-HPLC (reversed-phase high performance liquid chromatography) and mass spectrometry (MS) by the manufacturer. RP-HPLC showed a purity of 95.35%, 93.9% and 100% and a retention time of 15.18 min, 15.81 min and 14.46 for maxadilan, DTPA-maxadilan and maxadilan-DTPA respectively. With MS the expected mass of the peptides was confirmed (6870, 7537 and 7641 Da for maxadilan, DTPA-maxadilan and maxadilan-DTPA respectively). The amino acid sequences of the peptides are shown in Table 1.

Table 1. Amino acid sequence of maxadilan, DTPA-maxadilan and maxadilan-DTPA. Cysteine residues that form disulfide bonds are underlined and indicated by the dotted lines[30].

Peptide	Amino acid sequence
Maxadilan	CDATCQFRKAIDDCQKQAHHSNVLQTSVQTTATFTSMDTSQLPGNSVFKECMKQKKKEFKA
DTPA-Maxadilan	DTPA-beta-A-CDATCQFRKAIDDCQKQAHHSNVLQTSVQTTATFTSMDTSQLPGNSVFKECMKQKKKEFKA
Maxadilan-DTPA	CDATCQFRKAIDDCQKQAHHSNVLQTSVQTTATFTSMDTSQLPGNSVFKECMKQKKKEFKA-E-DTPA

Radiolabeling

DTPA-maxadilan and maxadilan-DTPA were labeled with ^{111}In by adding $^{111}InCl_3$ to 1 µg peptide in 0.1 M MES buffer, pH 5.5. After incubation at room temperature for 20 min, 50 mM EDTA (ethylenediaminetetraacetic acid) (Sigma Aldrich, St. Louis, MO, USA) was added to a final concentration of 5 mM. Quality control was performed by Instant Thin Layer Chromatography (ITLC) on silica gel ITLC strips (Pall Corporation Life Sciences, New York, NY, USA). As a mobile phase 0.1 M EDTA in 0.1 M NH_4Ac, pH 5.5 was used (R_f ^{111}In-maxadilan = 0, R_f ^{111}In-EDTA = 1). The reaction mixture was purified on a disposable PD-10 desalting column (GE Life Sciences, Diegem, Belgium), which was eluted with 10 ml PBS, 0.5% (v/w) bovine serum albumin (BSA) and fractions containing radiolabeled maxadilan were pooled.

Serum stability

Maxadilan-DTPA was labeled with 5 MBq $^{111}InCl_3$ as previously described and incubated with human serum (1:10) at 37°C. Before addition of human serum and 1, 2, 4 and 24 hours after incubation with human serum, samples were taken, mixed with acetonitrile (1:1) and centrifuged for 5 min at 5000g to precipitate serum proteins. The supernatant was analyzed using RP-HPLC on a C_{18} reversed-phase column (Alltima; 4.6 mm x 25 cm; Grace, Breda, The Netherlands) and ITLC. The column was eluted with a linear gradient of 0.1% TFA (trifluoroacetic acid, Lab-Scan, Analytical Sciences, Brussels, Belgium) in acetonitrile (3% to 100% over 10 min) with a flow rate of 1 ml/min. ITLC was performed as described above.

Cell culture

The rat insulinoma cell line INS-1[47] was maintained in RPMI-1640 medium supplemented with 10% fetal bovine serum, 2 mM glutamine, 10 mM HEPES, 50 µM β-mercaptoethanol, 1 mM sodium pyruvate, 100 units/ml penicillin and 100 µg/ml streptomycin, in a humidified 5% CO_2 atmosphere at 37 °C. The cells were harvested by trypsinization with trypsin/EDTA.

Competitive binding assay

The 50% inhibitory concentration (IC_{50}) of maxadilan, DTPA-maxadilan, maxadilan-DTPA, [^{nat}In]In-DTPA-maxadilan and maxadilan-DTPA-[^{nat}In]In was determined using suspensions of INS-1 cells. Labeling of DTPA-maxadilan and maxadilan-DTPA with ^{nat}In was performed as previously

described[9, 48]. Unlabeled and ^{nat}In-labeled peptides were added to the cells (approximately 10 x 10^6 cells in a final volume of 0.5 mL) in Eppendorf tubes to final concentrations ranging from 0.1 to 300 nmol (n=3) together with 1,000 Bq maxadilan-DTPA-[^{111}In]In. After 4 hours incubation on ice, the cells were centrifuged at 3,000 x g, the supernatant was removed and the cells were washed with 1 ml ice-cold PBS and the radioactivity in the cell pellet was determined in a well-type gamma counter (Wallac 1480-Wizard, Perkin-Elmer, Boston, MA, USA). The IC_{50} value was calculated by one-site competition analysis with Graphpad Prism (version 5.03, GraphPad Software, San Diego, CA USA).

Biodistribution studies

All experiments were performed in accordance with Radboud University guidelines. Animal experiments were approved by the Animal Ethical Committee of the Radboud University, Nijmegen, The Netherlands.

In order to assess the feasibility of targeting insulinomas with radiolabeled maxadilan, female BALB/c nude mice (6-8 weeks old) were injected subcutaneously with INS-1 cells (1x10^7 cells in 200 µl). When the tumors had grown to approximately 5 mm in diameter, groups of five mice were injected with either 370 kBq [^{111}In]In-DTPA-maxadilan or maxadilan-DTPA-[^{111}In]In (peptide dose: 13 pmol). For both peptides, an additional group of 5 mice was co-injected with an excess (1,300 pmol) of unlabeled maxadilan to determine the nonspecific binding of the peptides to the cells. Mice were euthanized 2 hours p.i. and blood, muscle, tumor, heart, lung, spleen, pancreas, stomach, intestine, adrenals, kidney and liver were dissected, weighed and the radioactivity concentration was determined.

To examine the pharmacokinetics of maxadilan-DTPA-[^{111}In]In, BALB/c nude mice (n=4/group) were injected with 370 kBq maxadilan-DTPA-[^{111}In]In and mice were euthanized at 1, 2 or 4 hours p.i.. The radioactivity concentration in the organs was measured in a gamma counter.

SPECT of BALB/c nude mice bearing subcutaneous INS-1 tumors

BALB/c nude mice bearing subcutaneous INS-1 tumors were injected intravenously with 9 MBq maxadilan-DTPA-[^{111}In]In (13 pmol). A separate group of tumor-bearing mice was co-injected with an excess of unlabeled maxadilan (1,300 pmol). One and four hours p.i. SPECT/CT images were acquired using a dedicated small animal SPECT scanner (U-SPECT-II, MILabs, Utrecht, The Netherlands). SPECT images were acquired with a 0.6 mm pinhole mouse collimator with an acquisition time of 50 min. The images were reconstructed with OSEM (3 iterations, 16 subsets, voxel size 0.375) using the U-SPECT-Rec software (MILabs, Utrecht, The Netherlands). The settings for the CT were as follows: spatial resolution, 160 µm; 40 kV; 612 µA.

Statistical analysis

Statistical analysis was done using GraphPad Prism version 5.03 for Windows. The unpaired *t* test was used for determination of significance. A *p*-value below 0.05 was considered as significant. For the competitive binding assay the F-test was used to manually calculate significance.

RESULTS

Radiolabeling

[^{111}In]In-DTPA-maxadilan and maxadilan-DTPA-[^{111}In]In could be labeled with a molar activity of 55 and 680 MBq/nmol, respectively. The radiochemical purity after purification exceeded 95%.

Serum stability

The stability of maxadilan-DTPA-[^{111}In]In was analyzed in human serum. The radiochemical purity directly after labeling was >95% (Figure 1A). The radiolabeled peptide remained intact up to 24 hours after incubation in human serum, as is shown in Figure 1B. [^{111}In]In-EDTA and radiolabeled maxadilan have a retention time of 3-4 min and 14.6 min, respectively.

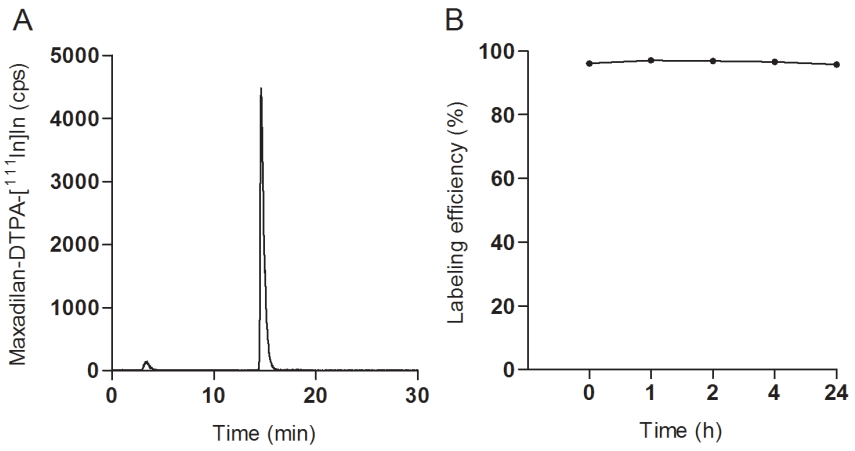

Figure 1. Stability of maxadilan-DTPA-[^{111}In]In in human serum. A) HPLC profile of maxadilan-DTPA-[^{111}In]In directly after labeling. B) Stability analysis of maxadilan-DTPA-[^{111}In]In before and 1, 2, 4 and 24 hours after incubation in human serum at 37°C.

Competitive binding assay

The results of the IC_{50} determination of labeled and unlabeled maxadilan analogs are summarized in Figure 2 and Table 2. Unlabeled maxadilan had the highest affinity (IC_{50} value:

3.2 nM) for the receptor. DTPA conjugation resulted in a somewhat lower affinity as indicated by slightly higher IC_{50} values: 18.3 and 13.2 nM ($p<0.001$ and $p<0.001$) for DTPA-maxadilan and maxadilan-DTPA, respectively. Labeling of DTPA-maxadilan or maxadilan-DTPA with ^{nat}In did not significantly reduce the affinity ($p=0.07$ and $p=0.12$ respectively) compared to the unlabeled compounds.

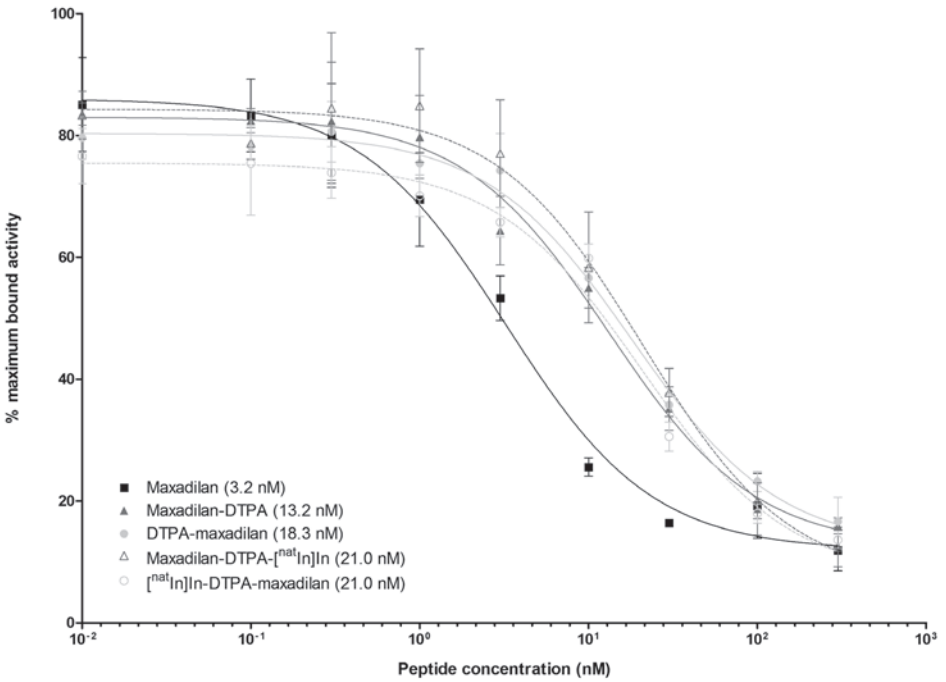

Figure 2. Competitive binding assay (IC_{50}) on INS-1 cells of unlabeled maxadilan, maxadilan-DTPA and DTPA-maxadilan, either unlabeled, or labeled with ^{nat}In. ^{111}In-labeled maxadilan-DTPA was used as radioligand.

Table 2. IC_{50} values and 95% confidence intervals (in nM) of the competitive binding assay on INS-1 cells.

Peptide	IC_{50} (nM)	95% confidence interval (nM)
Maxadilan	3.2	2.1 – 4.9
Maxadilan-DTPA	13.2	8.8 – 19.8
DTPA-maxadilan	18.3	13.2 – 25.3
Maxadilan-DTPA-[^{Nat}In]In	21.0	13.7 – 32.2
[^{Nat}In]In-DTPA-maxadilan	21.0	11.8 – 37.3

Biodistribution studies

The results of the *in vivo* PAC1 receptor targeting study with ^{111}In-labeled maxadilan in BALB/c nude mice bearing subcutaneous INS-1 tumors are summarized in Figure 3. Uptake of maxadilan-DTPA-[^{111}In]In in the tumor was 7.76 ± 1.37 %ID/g, which was significantly higher than that of [^{111}In]In-DTPA-maxadilan (4.82 ± 0.87 %ID/g) (p=0.0037). Also, pancreatic uptake was significantly higher for maxadilan-DTPA-[^{111}In]In compared to [^{111}In]In-DTPA-maxadilan, (3.87 ± 0.56 %ID/g and 2.73 ± 0.35 %ID/g respectively, p=0.0048). Accumulation in both tumor and pancreas could be blocked by an excess of unlabeled maxadilan, demonstrating specific uptake of the peptides via the PAC1 receptor (1.54 ± 0.49 %ID/g and 1.24 ± 0.48 %ID/g for maxadilan-DTPA-[^{111}In]In and [^{111}In]In-DTPA-maxadilan respectively in tumor tissue and 0.59 ± 0.07 %ID/g and 0.43 ± 0.04 %ID/g respectively for pancreatic uptake). Renal uptake was very high and similar for both peptides (148 ± 3 and 145 ± 19 %ID/g for [^{111}In]In-DTPA-maxadilan and maxadilan-DTPA-[^{111}In]In, respectively), which could not be blocked with an excess of unlabeled maxadilan. Furthermore, in all other dissected organs, except for blood and spleen, receptor-mediated uptake of maxadilan was observed. Since these results showed that maxadilan-DTPA-[^{111}In]In has higher accumulation in tumor and pancreatic tissue than [^{111}In]In-DTPA-maxadilan, this peptide was used to study the pharmacokinetics. Figure 4 shows the fast clearance of the peptide from the blood. Furthermore, tumor accumulation peaked at one hour after injection (7.30 ± 1.87 %ID/g) and decreased slightly over time (5.85 ± 1.17 %ID/g and 5.49 ± 0.66 %ID/g after 2 and 4 hours (not significant)). A similar trend was observed for the uptake in the pancreas: 3.82 ± 0.22 %ID/g at 1 hour p.i., 2.71 ± 0.36 %ID/g at 2 hours p.i. and 2.55 ± 0.07 %ID/g at 4 hours p.i.. Renal uptake increased over time, while the specific accumulation in the liver decreased. Table 3 gives an overview of the tumor-to-normal-organ ratios for ^{111}In-labeled maxadilan-DTPA.

Table 3. Tumor-to-normal-organ ratios for ^{111}In-labeled maxadilan-DTPA. Mean ± SD are shown.

Time p.i. (h)	Tumor-to-Blood	Tumor-to-Muscle	Tumor-to-Pancreas	Tumor-to-Kidney
1	44.62 ± 10.63	11.45 ± 3.75	2.01 ± 0.35	0.06 ± 0.02
2	139.65 ± 24.28	10.59 ± 2.25	2.34 ± 0.35	0.04 ± 0.01
4	314.74 ± 40.82	11.83 ± 1.91	2.04 ± 0.23	0.04 ± 0.01

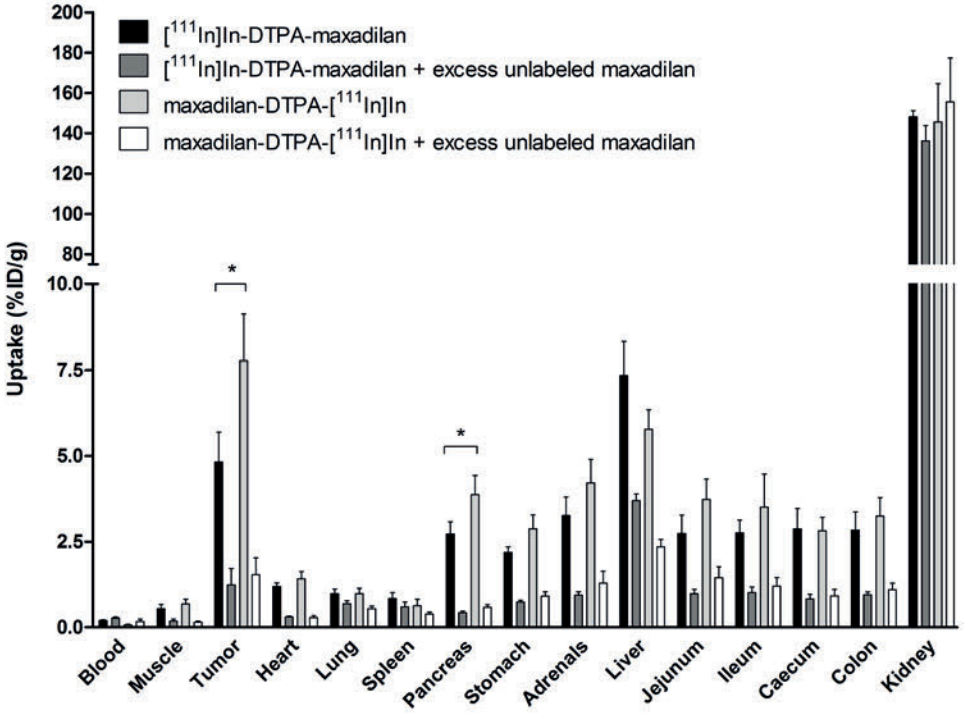

Figure 3. Biodistribution of ^{111}In-labeled DTPA-maxadilan and maxadilan-DTPA in BALB/c nude mice bearing subcutaneous INS-1 tumors. Values are expressed as a percentage of the injected dose per gram of tissue (n=5 mice per group, error bars SD). Blocking was performed by coinjection of a 100-fold excess of unlabeled maxadilan. Mice were dissected 2 hours after injection.

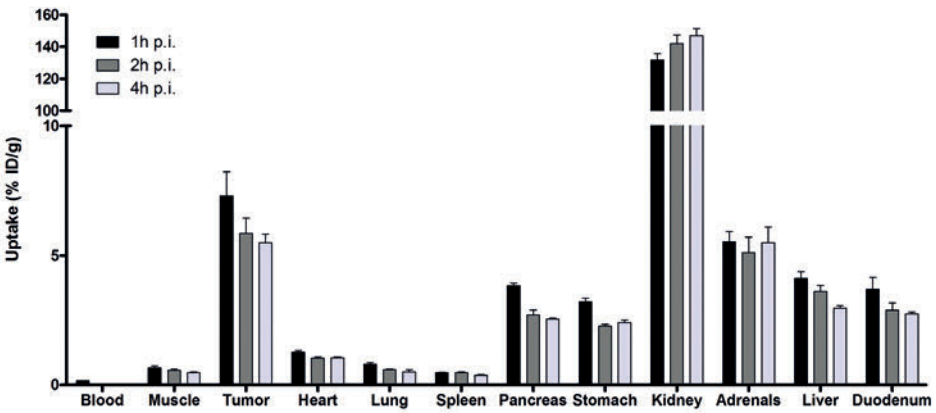

Figure 4. Biodistribution of ^{111}In-labeled maxadilan-DTPA in BALB/c nude mice bearing subcutaneous INS-1 tumors. Values are expressed as a percentage of the injected dose per gram of tissue (n=4 mice per group, error bars SD). Mice were dissected 1, 2 and 4 hours after injection to study the pharmacokinetics.

SPECT of BALB/c nude mice bearing subcutaneous INS-1 tumors

SPECT/CT images of BALB/c nude mice bearing subcutaneous INS-1 tumors are shown in Figure 5.

Images were acquired one and four hours after injection of ^{111}In-labeled maxadilan-DTPA and INS-1 tumors in the right shoulder were clearly visualized. In addition to tumor and kidney, accumulation of the tracer in the liver was observed. Figure 5C shows the image of a mouse which was co-injected with an excess of unlabeled maxadilan. The tumor on the right shoulder was not visualized with SPECT/CT, demonstrating specific uptake via the PAC1 receptor.

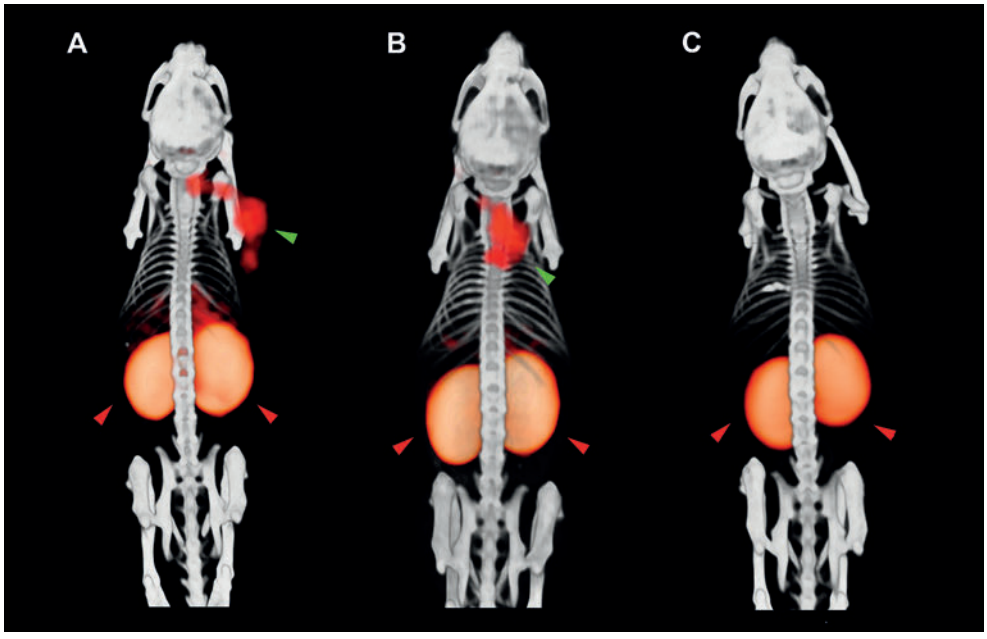

Figure 5. Fused SPECT/CT images of BALB/c nude mice bearing subcutaneous INS-1 tumors on the right shoulder (green arrow), obtained one and four hours p.i.. Image of a mouse injected with 9 MBq of maxadilan-DTPA-[^{111}In]In, 1 hour (A), 4 hours (B), and a mouse with 9 MBq of maxadilan-DTPA-[^{111}In]In and a 100 fold excess of unlabeled maxadilan (C). Kidneys are indicated with red arrows. Uptake in the abdomen is also seen, mainly in liver (A and B).

DISCUSSION

We demonstrate here for the first time that indeed radiolabeled maxadilan is a promising new tool to image subcutaneously transplanted insulinomas in mice.

We were able to radiolabel maxadilan with ^{111}In with high specific activity while preserving the affinity for the PAC1 receptor. High and specific uptake of this tracer in both subcutaneous INS-

1 tumors and pancreas was found. SPECT imaging clearly visualized the s.c. INS-1 xenografts. Both pancreatic as well as tumor uptake were receptor mediated, as was demonstrated by blocking experiments with unlabeled maxadilan.

Since the conjugation of a DTPA moiety can affect the affinity of the peptide for the receptor, the peptide was conjugated with DPTA at either the C- or the N-terminus and the molecules were compared. The maximum molar activity of maxadilan-DTPA-[^{111}In]In was at least twelve times higher than that of [^{111}In]In-DTPA-maxadilan. This could possibly be explained by hindrance of the radiometal incorporation into the DTPA molecule, due to either the secondary or tertiary structure of maxadilan or a conformational change in the peptide as a result of the conjugation. Conjugation of DTPA to either the C-or N-terminus of maxadilan influenced the receptor binding affinity significantly. Maxadilan contains four cysteine residues, which form two disulfide bridges, one of which is located close to the N-terminus. Furthermore, it is known that the N-terminal residues of maxadilan are important for receptor binding [23, 29]. Therefore, it was thought likely that conjugation of DTPA to the N-terminus could influence the binding affinity. However, it has also been shown in previous studies that when the disulfide bridge at the N-terminal part of maxadilan is removed or changed, the receptor binding capacity of maxadilan is preserved[29, 30]. Nevertheless, as was determined in our *in vivo* biodistribution studies, the C-terminally modified maxadilan-DTPA-[^{111}In]In analog showed higher uptake in the tumor, therefore this compound was used for further characterization.

The biodistribution shows specific accumulation of maxadilan in most organs. This is in line with the widespread PAC1 receptor expression and function in the pituitary, adrenal medulla, pancreas, stomach, colon, lung, and heart [31, 32]. As demonstrated in the SPECT images, maxadilan-DTPA-[^{111}In]In clearly visualized the subcutaneous INS-1 tumors and they were easily distinguished from the specific accumulation of radiolabeled maxadilan in various other tissues.

Other preclinical studies using INS-1 tumor-bearing mice have shown that GLP-1 receptor targeting ligands, labeled either with ^{111}In, ^{68}Ga or ^{18}F, show a more favorable biodistribution compared to this maxadilan tracer. Although those previously-studied tracers show high tumor and kidney uptake similar to maxadilan, the tumor-to-normal-organ ratios are more optimal, which can be correlated with expression levels of the different receptors that are targeted[9, 33, 34]. Future studies need to be conducted to compare radiolabeled maxadilan with existing relevant PET agents in animals, before moving to clinical trials.

Recently, clinical imaging techniques such as ^{68}Ga-labeled somatostatin receptor imaging and radiolabeled GLP-1 receptor imaging were introduced for diagnosis of insulinomas. These tracers would be useful for differentiating benign from malignant tumors or in diagnosis of metastatic NETS. However, the sensitivity is not optimal and false positive or false negative cases continue to be described using somatostatin receptor targeting [8, 19, 35]. False negative-SSTR PET/CT could be explained by small lesions (missed because the resolution of the scanner is not sufficient to detect them) or low somatostatin receptor expression (leading to

a low signal which cannot be detected as the sensitivity of the scanner is not sufficient). A solution to the latter problem would be the use of a combination of different radiotracers, thus targeting alternative receptors. This was also suggested by Reubi et al., who conducted an elegant *in vitro* study proving that a cocktail of three different ligands was able to detect all tested NETs [36]. Tumors with no or low receptor density, which would be missed *in vivo* when using only one radiotracer, have a higher probability of being detected when multiple receptors are targeted. In addition, if one of the tracers had a very high uptake in the tumor, this high uptake could help to overcome the limited spatial resolution and also visualization of small lesions.

In addition to diagnostic imaging, some somatostatin analogs, when radiolabeled with a beta emitter, are used as therapeutic agents[37]. Due to the high accumulation of radiolabeled maxadilan in the kidneys, and to a lesser extent in other organs, the feasibility of peptide receptor radionuclide therapy with maxadilan would be questionable. Insulinomas may not be the only NETs in which radiolabeled maxadilan could play a diagnostic role. In a study carried out by Pisegna et al. high expression levels of the PAC1 receptor in rat gastric ECL (enterochromaffin-like) cells were observed [38, 39]. Currently, [^{111}In]In-DTPA-octreotide or [^{68}Ga]Ga-DOTATOC/[^{68}Ga]Ga-DOTA-octreotide are used for the detection of gastric neuroendocrine tumors, which originate from ECL cells [40]. Furthermore, PAC1 receptor expression has been demonstrated in Lewis lung tumor transplants [41]. Radiolabeled maxadilan could therefore be a possible candidate for detecting both ECL derived tumors and a subtype of small cell lung cancer, in addition to somatostatin receptor tomography. Moreover, there is evidence that there is high expression of PAC1 in human tumors such as paragangliomas, neuroblastomas, pituitary adenomas and endometrial cancers [42-45] with expression found also in human lung cancers[46]. Importantly, most of these studies were conducted *in vitro*, so *in vivo* studies are needed to explore the ratio between peptide uptake in PAC1 receptor positive tumors and that in normal tissues where PAC1 is widely expressed.

In conclusion, radiolabeled maxadilan accumulates efficiently and specifically in INS-1 tumors and could potentially be used for *in vivo* PAC1 targeting in patients with insulinoma. Radiolabeled maxadilan, therefore, represents a new tracer to image insulinomas using SPECT in addition to or in combination with octreotide and exendin for the identification of benign or malignant insulinoma. Furthermore, the expression of PAC1 in other human tumors indicates a broader application for the usage of radiolabeled maxadilan. Thus, the newly generated PAC1 selective high affinity radiopeptide maxadilan can be employed for multireceptor tumor targeting *in vivo*.

ACKNOWLEDGEMENTS

We would like to thank J. K. Sosabowski (Centre for Molecular Oncology, Barts Cancer Institute, Queen Mary University of London) for her help with editing the manuscript.

AUTHOR CONTRIBUTIONS

L.J., M.B., O.B. and M.G. contributed in the design of the study, M.S. and E.W. contributed to the new compound, L.J. and M.B. performed the experiments and analyzed the data, L.J. wrote the manuscript, M.S., E.W., and M.B. contributed to the introduction and discussion. All authors reviewed and edited the manuscript.

ADDITIONAL INFORMATION

Competing financial interests

No potential conflict of interest relevant for this article was reported.

REFERENCES

1. Iglesias P, Diez JJ. Management of endocrine disease: a clinical update on tumor-induced hypoglycemia. *European journal of endocrinology / European Federation of Endocrine Societies.* **2014**; 170 (4): R147-157.
2. Granberg D, Oberg K. Neuroendocrine tumours. *Cancer chemotherapy and biological response modifiers.* **2005**; 22 471-483.
3. Modlin IM, Tang LH. Approaches to the diagnosis of gut neuroendocrine tumors: the last word (today). *Gastroenterology.* **1997**; 112 (2): 583-590.
4. Reubi JC, Waser B. Concomitant expression of several peptide receptors in neuroendocrine tumours: molecular basis for in vivo multireceptor tumour targeting. *European journal of nuclear medicine and molecular imaging.* **2003**; 30 (5): 781-793.
5. Baumann T, Rottenburger C, Nicolas G, Wild D. Gastroenteropancreatic neuroendocrine tumours (GEP-NET) - Imaging and staging. *Best practice & research. Clinical endocrinology & metabolism.* **2016**; 30 (1): 45-57.
6. Bodei L, Sundin A, Kidd M, Prasad V, Modlin IM. The status of neuroendocrine tumor imaging: from darkness to light? *Neuroendocrinology.* **2015**; 101 (1): 1-17.
7. Prasad V, Sainz-Esteban A, Arsenic R, Plockinger U, Denecke T, Pape UF, *et al.* Role of (68)Ga somatostatin receptor PET/CT in the detection of endogenous hyperinsulinaemic focus: an explorative study. *European journal of nuclear medicine and molecular imaging.* **2016**; 43 (9): 1593-1600.
8. Sharma P, Arora S, Karunanithi S, Khadgawat R, Durgapal P, Sharma R, *et al.* Somatostatin receptor based PET/CT imaging with 68Ga-DOTA-Nal3-octreotide for localization of clinically and biochemically suspected insulinoma. *The quarterly journal of nuclear medicine and molecular imaging : official publication of the Italian Association of Nuclear Medicine.* **2016**; 60 (1): 69-76.
9. Brom M, Oyen WJ, Joosten L, Gotthardt M, Boerman OC. 68Ga-labelled exendin-3, a new agent for the detection of insulinomas with PET. *European journal of nuclear medicine and molecular imaging.* **2010**; 37 (7): 1345-1355.
10. Wild D, Behe M, Wicki A, Storch D, Waser B, Gotthardt M, *et al.* [Lys40(Ahx-DTPA-111In)NH2] exendin-4, a very promising ligand for glucagon-like peptide-1 (GLP-1) receptor targeting. *Journal of nuclear medicine : official publication, Society of Nuclear Medicine.* **2006**; 47 (12): 2025-2033.
11. Wild D, Wicki A, Mansi R, Behe M, Keil B, Bernhardt P, *et al.* Exendin-4-based radiopharmaceuticals for glucagonlike peptide-1 receptor PET/CT and SPECT/CT. *Journal of nuclear medicine : official publication, Society of Nuclear Medicine.* **2010**; 51 (7): 1059-1067.
12. Christ E, Wild D, Ederer S, Behe M, Nicolas G, Caplin ME, *et al.* Glucagon-like peptide-1 receptor imaging for the localisation of insulinomas: a prospective multicentre imaging study. *The lancet. Diabetes & endocrinology.* **2013**; 1 (2): 115-122.
13. Christ E, Wild D, Forrer F, Brandle M, Sahli R, Clerici T, *et al.* Glucagon-like peptide-1 receptor imaging for localization of insulinomas. *The Journal of clinical endocrinology and metabolism.* **2009**; 94 (11): 4398-4405.

14. Sowa-Staszczak A, Pach D, Mikolajczak R, Macke H, Jabrocka-Hybel A, Stefanska A, *et al*. Glucagon-like peptide-1 receptor imaging with [Lys40(Ahx-HYNIC- 99mTc/EDDA)NH2]-exendin-4 for the detection of insulinoma. *European journal of nuclear medicine and molecular imaging*. **2013**; 40 (4): 524-531.

15. Wild D, Macke H, Christ E, Gloor B, Reubi JC. Glucagon-like peptide 1-receptor scans to localize occult insulinomas. *The New England journal of medicine*. **2008**; 359 (7): 766-768.

16. Antwi K, Fani M, Nicolas G, Rottenburger C, Heye T, Reubi JC, *et al*. Localization of Hidden Insulinomas with (6)(8)Ga-DOTA-Exendin-4 PET/CT: A Pilot Study. *Journal of nuclear medicine : official publication, Society of Nuclear Medicine*. **2015**; 56 (7): 1075-1078.

17. Eriksson O, Velikyan I, Selvaraju RK, Kandeel F, Johansson L, Antoni G, *et al*. Detection of metastatic insulinoma by positron emission tomography with [(68)ga]exendin-4-a case report. *The Journal of clinical endocrinology and metabolism*. **2014**; 99 (5): 1519-1524.

18. Christ E, Wild D, Reubi JC. Glucagonlike peptide-1 receptor: an example of translational research in insulinomas: a review. *Endocrinology and metabolism clinics of North America*. **2010**; 39 (4): 791-800.

19. Wild D, Christ E, Caplin ME, Kurzawinski TR, Forrer F, Brandle M, *et al*. Glucagon-like peptide-1 versus somatostatin receptor targeting reveals 2 distinct forms of malignant insulinomas. *Journal of nuclear medicine : official publication, Society of Nuclear Medicine*. **2011**; 52 (7): 1073-1078.

20. Inagaki N, Kuromi H, Seino S. PACAP/VIP receptors in pancreatic beta-cells: their roles in insulin secretion. *Annals of the New York Academy of Sciences*. **1996**; 805 44-51; discussion 52-43.

21. Moody TW, Nuche-Berenguer B, Jensen RT. Vasoactive intestinal peptide/pituitary adenylate cyclase activating polypeptide, and their receptors and cancer. *Current opinion in endocrinology, diabetes, and obesity*. **2016**; 23 (1): 38-47.

22. Tatsuno I, Uchida D, Tanaka T, Saeki N, Hirai A, Saito Y, *et al*. Maxadilan specifically interacts with PAC1 receptor, which is a dominant form of PACAP/VIP family receptors in cultured rat cortical neurons. *Brain research*. **2001**; 889 (1-2): 138-148.

23. Borboni P, Porzio O, Pierucci D, Cicconi S, Magnaterra R, Federici M, *et al*. Molecular and functional characterization of pituitary adenylate cyclase-activating polypeptide (PACAP-38)/vasoactive intestinal polypeptide receptors in pancreatic beta-cells and effects of PACAP-38 on components of the insulin secretory system. *Endocrinology*. **1999**; 140 (12): 5530-5537.

24. Ahren B. Role of pituitary adenylate cyclase-activating polypeptide in the pancreatic endocrine system. *Annals of the New York Academy of Sciences*. **2008**; 1144 28-35.

25. Arimura A. Pituitary adenylate cyclase activating polypeptide (PACAP): discovery and current status of research. *Regulatory peptides*. **1992**; 37 (3): 287-303.

26. Arimura A, Shioda S. Pituitary adenylate cyclase activating polypeptide (PACAP) and its receptors: neuroendocrine and endocrine interaction. *Frontiers in neuroendocrinology. 1***995**; 16 (1): 53-88.

27. Lerner EA, Ribeiro JM, Nelson RJ, Lerner MR. Isolation of maxadilan, a potent vasodilatory peptide from the salivary glands of the sand fly Lutzomyia longipalpis. *The Journal of biological chemistry*. **1991**; 266 (17): 11234-11236.

28. Moro O, Lerner EA. Maxadilan, the vasodilator from sand flies, is a specific pituitary adenylate cyclase activating peptide type I receptor agonist. *The Journal of biological chemistry.* **1997**; 272 (2): 966-970.

29. Lerner EA, Iuga AO, Reddy VB. Maxadilan, a PAC1 receptor agonist from sand flies. *Peptides.* **2007**; 28 (9): 1651-1654.

30. Moro O, Wakita K, Ohnuma M, Denda S, Lerner EA, Tajima M. Functional characterization of structural alterations in the sequence of the vasodilatory peptide maxadilan yields a pituitary adenylate cyclase-activating peptide type 1 receptor-specific antagonist. *The Journal of biological chemistry.* **1999**; 274 (33): 23103-23110.

31. Vamos Z, Ivic I, Cseplo P, Toth G, Tamas A, Reglodi D, *et al.* Pituitary Adenylate Cyclase-Activating Polypeptide (PACAP) Induces Relaxations of Peripheral and Cerebral Arteries, which are Differentially Impaired by Aging. *Journal of molecular neuroscience : MN.* **2014**; 54 (3): 535-542.

32. Yada T, Sakurada M, Ihida K, Nakata M, Murata F, Arimura A, *et al.* Pituitary adenylate cyclase activating polypeptide is an extraordinarily potent intra-pancreatic regulator of insulin secretion from islet beta-cells. *The Journal of biological chemistry.* **1994**; 269 (2): 1290-1293.

33. Kiesewetter DO, Gao H, Ma Y, Niu G, Quan Q, Guo N, *et al.* 18F-radiolabeled analogs of exendin-4 for PET imaging of GLP-1 in insulinoma. *European journal of nuclear medicine and molecular imaging.* **2012**; 39 (3): 463-473.

34. Rylova SN, Waser B, Del Pozzo L, Tonnesmann R, Mansi R, Meyer PT, *et al.* Approaches to Improve the Pharmacokinetics of Radiolabeled Glucagon-Like Peptide-1 Receptor Ligands Using Antagonistic Tracers. *Journal of nuclear medicine : official publication, Society of Nuclear Medicine.* **2016**; 57 (8): 1282-1288.

35. Prasad V, Sainz-Esteban A, Arsenic R, Plockinger U, Denecke T, Pape UF, *et al.* Role of Ga somatostatin receptor PET/CT in the detection of endogenous hyperinsulinaemic focus: an explorative study. *European journal of nuclear medicine and molecular imaging.* **2016**;

36. Reubi JC, Waser B. Triple-peptide receptor targeting in vitro allows detection of all tested gut and bronchial NETs. *Journal of nuclear medicine : official publication, Society of Nuclear Medicine.* **2015**; 56 (4): 613-615.

37. van der Zwan WA, Bodei L, Mueller-Brand J, de Herder WW, Kvols LK, Kwekkeboom DJ. GEPNETs update: Radionuclide therapy in neuroendocrine tumors. *European journal of endocrinology / European Federation of Endocrine Societies.* **2015**; 172 (1): R1-8.

38. Zeng N, Athmann C, Kang T, Lyu RM, Walsh JH, Ohning GV, *et al.* PACAP type I receptor activation regulates ECL cells and gastric acid secretion. *The Journal of clinical investigation.* **1999**; 104 (10): 1383-1391.

39. Zeng N, Kang T, Lyu RM, Wong H, Wen Y, Walsh JH, *et al.* The pituitary adenylate cyclase activating polypeptide type 1 receptor (PAC1-R) is expressed on gastric ECL cells: evidence by immunocytochemistry and RT-PCR. *Annals of the New York Academy of Sciences.* **1998**; 865 147-156.

40. Cavallaro A, Zanghi A, Cavallaro M, Lo Menzo E, Di Carlo I, Di Vita M, *et al.* The role of 68-Ga-DOTATOC CT-PET in surgical tactic for gastric neuroendocrine tumors treatment: our experience: a case report. *International journal of surgery.* **2014**; 12 Suppl 1 S225-231.

41. Kalmbach N, Krasel C, Schafer MKH, Bunemann M, Weihe E. Molecular and functional characterization of PACAP/VIP receptors in Lewis lung carcinoma cells. *Pneumologie.* **2012**; 66 A604.

42. Reubi JC, Laderach U, Waser B, Gebbers JO, Robberecht P, Laissue JA. Vasoactive intestinal peptide/pituitary adenylate cyclase-activating peptide receptor subtypes in human tumors and their tissues of origin. *Cancer research.* **2000**; 60 (11): 3105-3112.

43. Robberecht P, Vertongen P, Velkeniers B, de Neef P, Vergani P, Raftopoulos C, *et al.* Receptors for pituitary adenylate cyclase activating peptides in human pituitary adenomas. *The Journal of clinical endocrinology and metabolism.* **1993**; 77 (5): 1235-1239.

44. Robberecht P, Woussen-Colle MC, Vertongen P, De Neef P, Hou X, Salmon *I, et al.* Expression of pituitary adenylate cyclase activating polypeptide (PACAP) receptors in human glial cell tumors. *Peptides.* **1994**; 15 (4): 661-665.

45. Vertongen P, Devalck C, Sariban E, De Laet MH, Martelli H, Paraf F, *et al.* Pituitary adenylate cyclase activating peptide and its receptors are expressed in human neuroblastomas. *Journal of cellular physiology.* **1996**; 167 (1): 36-46.

46. Busto R, Prieto JC, Bodega G, Zapatero J, Fogue L, Carrero I. VIP and PACAP receptors coupled to adenylyl cyclase in human lung cancer: a study in biopsy specimens. *Peptides.* **2003**; 24 (3): 429-436.

47. Asfari M, Janjic D, Meda P, Li G, Halban PA, Wollheim CB. Establishment of 2-mercaptoethanol-dependent differentiated insulin-secreting cell lines. *Endocrinology.* **1992**; 130 (1): 167-178.

48. Brom M, Joosten L, Oyen WJ, Gotthardt M, Boerman OC. Radiolabelled GLP-1 analogues for in vivo targeting of insulinomas. *Contrast media & molecular imaging.* **2012**; 7 (2): 160-166.


3

CHAPTER 4

Characterization of ^{111}In-labeled glucose-dependent insulinotropic polypeptide as a radiotracer for neuroendocrine tumors

Lieke Joosten[1*], Stefanie M. A. Willekens[1,2*], Otto C. Boerman[1], Maarten Brom[1] & Martin Gotthardt[1]

1 Department of Radiology and Nuclear Medicine, Radboud University Medical Center, Nijmegen, The Netherlands
2 Division of Nuclear Medicine and Molecular Imaging, Department of Imaging and Pathology, University Hospitals and KU Leuven, Leuven, Belgium

* Lieke Joosten and Stefanie M. A. Willekens contributed equally to this work

Scientific Reports. **2018**; 8 (1): 2948

ABSTRACT

Somatostatin receptor targeting is considered the standard nuclear medicine imaging technique for visualization of neuroendocrine tumors (NETs). Since not all NETs over-express somatostatin receptors, the search for novel targets to visualize these NETs is ongoing. Many NETs, expressing low somatostatin receptor levels, have been shown to express glucose-dependent insulinotropic polypeptide (GIP) receptors (GIPR). Here, we evaluated the performance of [Lys^{37}(DTPA)]N-acetyl-GIP_{1-42}, a newly synthesized GIP analog to investigate whether NET imaging via GIPR targeting is feasible. Therefore, [Lys^{37}(DTPA)]N-acetyl-GIP_{1-42} was radiolabeled with ^{111}In with a molar activity up to 1.2 TBq/μmol and both its *in vitro* and *in vivo* receptor targeting properties were examined. *In vitro*, ^{111}In-labeled [Lys^{37}(DTPA)]N-acetyl-GIP_{1-42} showed receptor mediated binding to BHK-GIPR positive cells, NES2Y cells and isolated islets. *In vivo*, both NES2Y and GIPR-transfected BHK tumors were visualized on SPECT/CT. Furthermore, co-administration of an excess unlabeled GIP_{1-42} lowered tracer uptake from 0.7 ± 0.2 %ID/g to 0.6 ± 0.01 %ID/g (p=0.78) in NES2Y tumors and significantly lowered tracer uptake from 3.3 ± 0.8 to 0.8 ± 0.2 %ID/g (p=0.0001) in GIPR-transfected BHK tumors. In conclusion, ^{111}In-labeled [Lys^{37}(DTPA)]N-acetyl-GIP_{1-42} shows receptor mediated binding in various models. Furthermore, both GIPR-transfected BHK tumors and NES2Y tumors were visible on SPECT/CT using this tracer. Therefore, ^{111}In-labeled [Lys^{37}(DTPA)]N-acetyl-GIP_{1-42} SPECT seems promising for visualization of somatostatin receptor negative NETs.

INTRODUCTION

Targeting of peptide hormone receptors, expressed on tumors, is a valuable tool for *in vivo* molecular imaging and radionuclide therapy of a variety of neuroendocrine tumors (NETs). Successful tumor targeting relies on over-expression of target receptors on cancer cells when compared to their expression levels in healthy tissues [1, 2]. Nowadays, somatostatin receptor targeting is a standard procedure for NET detection [3-6] and radionuclide therapy with ^{90}Y- and ^{177}Lu-labeled somatostatin analogs was proven beneficial to patients with NET [7]. However, not all NETs show elevated somatostatin receptor expression levels. Therefore, false negative results may occur in all NET types and somatostatin receptor imaging displays limited sensitivity for some types of NET, such as insulinomas (80-90% on [^{68}Ga]Ga-DOTA-TATE PET) [3, 5, 8-10] and medullary thyroid carcinoma (MTC) for which the detection rate is below 40-60% [11].

A variety of alternative peptide receptors, such as cholecystokinin (CCK) receptors [12], vasoactive intestinal peptide (VIP) receptors [13] and glucagon-like peptide 1 (GLP-1) receptors (GLP-1R) [14] are expressed on NETs. Recent findings showed glucose-dependent insulinotropic polypeptide (GIP) receptor (GIPR) expression in gastric, duodenal and bronchial NETs [15, 16]. Furthermore, approximately 90% of somatostatin receptor negative NETs are GIPR positive [16]. In 2013, Sherman et al. pointed out that GIPR is a promising target for NET imaging and therapy due to its favorable expression pattern [17] and the feasibility of GIPR targeting was shown in a GIPR over-expressing tumor model using a truncated GIP_{1-30} analog [18].

GIP is secreted from the intestinal K cells after nutrient ingestion [19] and together with GLP-1, it enhances glucose-induced insulin secretion upon receptor binding on pancreatic beta cells, the so-called incretin effect [20, 21]. Since insulinomas are NETs derived from pancreatic beta cells, incretin receptors are expected to be ideal candidate receptors for insulinoma imaging. Indeed, GLP-1R targeting tracers, such as ^{68}Ga- or ^{111}In-labeled exendin, can be applied for non-invasive *in vivo* insulinoma detection [22-24]. However, since malignant insulinomas display differential GLP-1R and somatostatin receptor expression patterns [25], detection rates of these tumors remain limited to 50% by scintigraphy. Interestingly, GLP-1R negative malignant insulinomas and a majority of somatostatin negative NETs express enhanced GIPR levels [16], rendering this receptor an interesting target for NET and insulinoma imaging.

Since it was described that GIP_{1-30} exhibits reduced receptor binding affinity when compared to the full length peptide GIP_{1-42} [26, 27], we have investigated the potential of a newly synthesized GIP_{1-42} analog, ^{111}In-labeled [Lys^{37}(DTPA)]N-acetyl-GIP_{1-42} (Figure 1) as a radiotracer for NET imaging, starting from the initial hypothesis that a full-length peptide-based tracer might show improved characteristics for *in vivo* NET imaging when compared to GIP_{1-30}. Therefore, we optimized the radiolabeling procedure and investigated its binding and internalization kinetics using GIPR-positive tumor cells (BHK-GIPR). Furthermore, we have also explored the tracer binding characteristics to NES2Y cells (a human beta cell-derived cell line, representing a more realistic model in terms of receptor expression) [28] and isolated islets of Langerhans.

Finally, subcutaneous BHK-GIPR and NES2Y tumors were visualized by SPECT after injection of ^{111}In-labeled [Lys^{37}(DTPA)]N-acetyl-GIP$_{1-42}$.

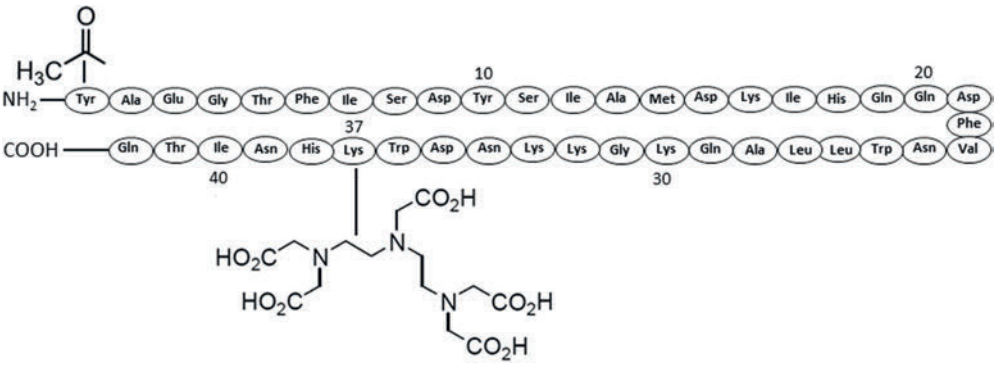

Figure 1. Amino acid sequence and molecular modifications of [Lys^{37}(DTPA)]N-acetyl-GIP$_{1-42}$.

METHODS

Radiolabeling

[Lys^{37}(DTPA)]N-acetyl-GIP$_{1-42}$ (MW = 5422 g/mol) (referred to as DTPA-GIP$_{1-42}$ and GIP$_{1-42}$ (MW = 5046.7 g/mol) were purchased from Peptide Specialty Laboratories (PSL GmbH, Heidelberg, Germany). DTPA was conjugated to the ε-amino group of the Lysine (K37) and the N-terminal tyrosine was acetylated to reduce its susceptibility to endopeptidases (Figure 1). DTPA-GIP$_{1-42}$ was dissolved in 0.5 *M* MES (2-(N-morpholino)ethanesulfonic acid) buffer, pH 5.5 and stored at 4°C until use. 150 MBq $^{111}InCl_3$ (Mallinckrodt Pharmaceuticals, 's Hertogenbosch, The Netherlands) was added to 1 µg DTPA-GIP$_{1-42}$ together with 5 volumes of 0.5 M MES buffer (1:5 relation ^{111}In:buffer), pH 5.5 and incubated for 20 min at room temperature. After incubation, EDTA (Sigma Aldrich, St. Louis, MO, USA) and Tween-80 (Sigma Aldrich) were added to a final concentration of 5 mM and 0.1%, respectively. The labeling mixture was purified by solid-phase extraction using a hydrophilic-lipophilic balance (HLB) cartridge (30 mg, Waters Oasis, Milford, MA, USA), to eliminate unincorporated ^{111}In. The cartridge was activated with 1 ml ethanol, washed with 2 ml water and conditioned with 1 ml of 0.5 M MES, pH 5.5. Subsequently, the cartridge was loaded with the labeling mixture, washed with 1 ml 0.5 M MES and 2 ml water and [^{111}In]In-DTPA-GIP$_{1-42}$ was eluted from the cartridge with 200 µL 100% ethanol. For *in vivo* use, purified labeled peptide was diluted in phosphate buffered saline (PBS), 0.5% bovine serum albumin (BSA) (w/v) to obtain a final ethanol concentration of less than 10%. Radiochemical purity of [^{111}In]In-DTPA-GIP$_{1-42}$ was determined by instant thin-layer chromatography (ITLC) (ITLC-SG, Agilent Technologies, Lake Forest, CA, USA), using 0.1 M EDTA in 0.1 M NH_4Ac

(Sigma Aldrich), pH 5.5 as a mobile agent and by reversed-phase high performance liquid chromatography (RP-HPLC) using an Eclipse XDB C18 column (Agilent Technologies). The column was eluted with 0.1% trifluoroacetic acid (TFA) in H_2O (0-5 minutes) followed by a linear gradient from 3% to 100% acetonitrile with 0.1% TFA over 10 minutes (flow rate: 1 ml/minute).

Serum Stability Analysis

For the serum stability analysis, DTPA-GIP_{1-42} was labeled with $^{111}InCl_3$ at a molar activity of 27 GBq/µmol. Radiochemical purity of [^{111}In]In-DTPA-GIP_{1-42} directly after labeling was determined by ITLC-SG (Agilent Technologies) and RP-HPLC as described above. A sample of the labeling mixture was incubated in human serum (1:10) at 37°C. After 1, 2, 4 and 24 hours, a sample was taken and serum proteins were precipitated by adding acetonitrile. This mixture was centrifuged and after dilution, the radiochemical purity of the compound in the supernatant was analyzed using ITLC and RP-HPLC as described above.

Cell Culture

Baby hamster kidney cells, transfected with the human GIPR (BHK-GIPR cells) were maintained in DMEM Glutamax (cat. Nr. 6195, GIBCO, BRL Life Sciences Technologies, Bleiswijk, The Netherlands) supplemented with 10% fetal bovine serum (FCS), (HyClone, Celbio, Logan, UT, USA) and 1 mg/ml G418, in a humidified atmosphere containing 5% CO_2 at 37°C. The human beta cell line NES2Y was cultured as described previously (28). Briefly, cells were maintained in RPMI 1640 (R0883, GIBCO) supplemented with 10% FCS, (HyClone, Celbio), 2 m*M* L-glutamine (Sigma Aldrich), 100 U/ml penicillin (Sigma Aldrich) and 100 µg/ml streptomycin (Sigma Aldrich) (complete RPMI), in a humidified atmosphere containing 5% CO_2 at 37°C.

Competitive binding assay

The 50% inhibitory concentration (IC_{50}) of [^{111}In]In-DTPA-GIP_{1-42} was determined using NES2Y cells. NES2Y cells were seeded at a density of 200,000 cells/well in 24-well plates and incubated overnight at 37°C. The cells were washed with binding buffer (RPMI + 0.5% BSA (w/v)) and DTPA-GIP_{1-42} was added at a final concentration ranging from 1.0 – 100 µM along with a trace amount of [^{111}In]In-DTPA-GIP_{1-42} (4.6 kBq = 2.7 fmol). After o/n (15 hours) incubation at 37°C, cells were washed with binding buffer and cell-associated activity was measured in a well type gamma counter (Wallac 2480 wizard, Perkin Elmer). Under these conditions, internalization may occur. We therefore designate the results of this competitive binding assay as "apparent IC_{50}" values rather than IC_{50}.

Internalization kinetics

The internalization kinetics of [^{111}In]In-DTPA-GIP_{1-42} was determined as previously described [38] using BHK-GIPR transfected cells and NES2Y cells. BHK-GIPR transfected cells and NES2Y cells were seeded in 24-well plates with a density of 50,000 and 200,000 cells/well, respectively

and incubated overnight at 37°C. Cells were washed with binding buffer and incubated with approximately 1.6 kBq [^{111}In]In-DTPA-GIP$_{1-42}$ (2.7 fmol) for 1, 2, 4 and 24 hours at 37°C. After incubation, cells were washed twice with binding buffer. To determine the surface-bound fraction, ice-cold acid buffer (0.1 M acetic acid, 154 mM NaCl, pH 2.5) was added and cells were incubated for 10 minutes at 4°C. After washing the cells twice with binding buffer to make sure that all surface-bound tracer was removed from the cells, the cell-associated activity was measured in a well type gamma counter. After removal of the surface-bound activity, the internalized fraction was represented by the remaining cell-associated activity. The internalized fraction (remaining cell-associated activity after acid wash) and the receptor bound fraction (activity removed by acid wash) were determined in a well-type gamma counter.

Animals

All animal experiments were approved by the Animal Welfare Body of the Radboud University, Nijmegen, The Netherlands and carried out in accordance with their guidelines. Six to eight weeks old, female BALB/c nude mice and C3H mice were purchased from Janvier labs (Le Genest Saint Isle, France). For all *in vivo* experiments, 6-8 weeks old female BALB/c nude mice were injected subcutaneously in the right shoulder with 0.2 ml of a 2.5 x 10^7 cells/ml suspension of BHK-GIPR transfected cells or with 0.2 ml of a 2.5 x 10^7 cells/ml suspension of NES2Y cells mixed with matrigel (2:1) in the right shoulder. When the tumor reached a diameter of 2-5 mm, mice were randomly divided in groups.

Islet Isolation

Islets of Langerhans were isolated from donor C3H mice by collagenase digestion as follows. Mice were euthanized by CO_2/O_2 suffocation and 2 ml of ice cold RPMI 1640 containing 1 mg/ml collagenase type V (Sigma Aldrich) were infused via the pancreatic duct *in situ*. After dissection, the perfused pancreata were collected in serum free medium containing collagenase and kept on ice until digestion. Pancreata were digested for 12 min at 37°C. Digestion was stopped by adding RPMI medium containing 10% FCS, 2 mM L-glutamine, 100 U/ml penicillin and 100 U/ml streptomycin (complete RPMI). After washing, digested pancreata were passed through a mesh. Afterwards, islets were purified on a discontinuous Ficoll gradient (densities: 1.108; 1.096; 1.037; Cellgro by Mediatech Inc, Manassas, VA, USA) by centrifugation at 625 x g for 16 min without brake. Islets were collected from the intersection of the second and third layer and remaining Ficoll was removed by washing with complete RPMI. Isolated islets were cultured overnight in complete RPMI medium in a humidified atmosphere containing 5% CO_2 at 37°C.

In Vitro Binding to Isolated Islets

After overnight recovery from the isolation procedure, islets from the donor C3H mice were collected, counted and resuspended in complete RPMI. After transwell saturation using binding buffer, islets were transferred to 24 well transwell plates (200 islets per transwell) (Corning

Inc. Tewksbury, MA, USA) and washed with binding buffer. Subsequently, approximately 8 kBq [^{111}In]In-DTPA-GIP$_{1-42}$ (13.5 fmol) was added followed by incubation for 24 hours at 37°C. To investigate the GIPR-mediated binding, 25 µg of unlabeled GIP$_{1-42}$ was added together with [^{111}In]In-DTPA-GIP$_{1-42}$ in a separate set of wells. After incubation, islets were washed extensively with binding buffer and islet-associated radioactivity was measured in a well type gamma counter.

Peptide Dose Escalation Study

To determine the optimal peptide dose of DTPA-GIP$_{1-42}$, BHK-GIPR transfected tumor bearing BALB/c nude mice (n=5/group) were injected intravenously with approximately 3 MBq [^{111}In]In-DTPA-GIP$_{1-42}$ (0.05 µg) in the tail vein and were co-injected with escalating amounts of unlabeled DTPA-GIP$_{1-42}$ (0.05 µg – 1.95 µg), resulting in final peptide doses ranging from 0.1 to 2 µg/mouse (0.02 – 0.4 nmol/mouse) (5 groups, n=5/group). Four hours after injection, mice were euthanized by CO_2/O_2 suffocation and tumors and other relevant tissues (heart, muscle, lung, spleen, pancreas, kidney, liver, stomach and duodenum) were dissected, weighed and measured in a well type gamma counter. The percentage injected dose per gram of tissue (%ID/g) was determined for each tissue.

Biodistribution Studies

BALB/c nude mice bearing BHK-GIPR transfected tumors were injected intravenously with approximately 3 MBq (peptide dose 0.2 µg = 0.04 nmol) of [^{111}In]In-DTPA-GIP$_{1-42}$ via the tail vein. At various time points after injection (1, 4 and 24 hours), mice were euthanized by CO_2/O_2 suffocation and blood, tumor and other relevant tissues were dissected, weighed and measured in a well type gamma counter. The percentage injected dose per gram (%ID/g) was calculated for each tissue. To determine whether the GIP$_{1-42}$ uptake was GIPR mediated, 25 µg of unlabeled GIP$_{1-42}$ was co-injected in a separate group (n=5) and mice were euthanized four hours post-injection. BALB/c nude mice bearing NES2Y tumors (n=5) were injected intravenously with approximately 3 MBq (peptide dose 0.2 µg = 0.04 nmol) of [^{111}In]In-DTPA-GIP$_{1-42}$ via the tail vein. One hour after injection, mice were euthanized by CO_2/O_2 suffocation and blood, tumor and other relevant tissues were dissected, weighed and measured in a well type gamma counter. The percentage injected dose per gram (%ID/g) was determined for each tissue. To determine whether the GIP$_{1-42}$ uptake was GIPR mediated, 25 µg of unlabeled GIP$_{1-42}$ was co-injected in a separate group (n=2) and mice were euthanized one hours post-injection.

SPECT/CT

One (BHK-GIPR tumors and NES2Y tumors) or four (BHK-GIPR tumors) hours (n=2/group) prior to SPECT imaging, BALB/c nude mice were injected intravenously in the tail vein with 20.6 ± 0.7 MBq [^{111}In]In-DTPA-GIP$_{1-42}$ (peptide dose 0.2 µg (=0.04 nmol) in 200 µl injection fluid). SPECT/CT scans were acquired on a dedicated small animal SPECT/CT scanner (U-SPECT-II, Milabs, Utrecht, The Netherlands) with a 1.0 mm mouse collimator, using 36 bed positions and

an acquisition time of 30 minutes (BHK-GIPR tumors) or 45 minutes (NES2Y tumors). After SPECT acquisition, CT (65 kV, 615 µA, 1 bed position) was acquired as an anatomical reference. SPECT scans were reconstructed using U-SPECT-II reconstruction software (U-SPECT-Rec, Milabs, Utrecht, The Netherlands) with the following settings: selection of the lower ^{111}In photopeak (152-183 keV), corrected for two backgrounds (135-151 keV and 184-211 keV), pixel based OSEM, voxel size 0.4 mm^3 and 1 iteration over 16 subsets.

Statistics

All values are expressed as mean ± standard deviation (SD). Statistical analysis was performed using unpaired two-tailed t-test using GraphPad Prism v5.03 (GraphPad Software Inc., San Diego, CA, USA). The level of significance was set at $p<0.05$.

RESULTS

Radiolabeling and Serum Stability

DTPA-GIP$_{1-42}$ could be labeled with ^{111}In with a molar activity of up to 1.2 TBq/µmol. Radiochemical purity exceeded 95% as determined by RP-HPLC and ITLC, resulting in a final molar activity exceeding 712.5 MBq/nmol when starting with 150 MBq $^{111}InCl_3$. Figure 2A shows the HPLC analysis of the labeling mixture. [^{111}In]In-EDTA eluted with a retention time of 3 minutes, whereas ^{111}In-labeled DTPA-GIP$_{1-42}$ had a retention time of 14 minutes. After 12 minutes, a very small impurity (< 2%) eluted from the column. Since GIP is known to be prone to inactivation by dipeptidyl peptidase IV (DPP IV), the stability of [^{111}In]In-DTPA-GIP$_{1-42}$ was analyzed in human serum. The results of this stability analysis are shown in Figure 2B and 2C. Up to 4 hours of incubation in human serum, [^{111}In]In-DTPA-GIP$_{1-42}$ remained intact. After 24 hours of incubation in human serum, 73% of the activity was still found as intact radiolabeled peptide, as determined by HPLC.

In vitro binding and internalization kinetics

The results of the apparent IC_{50} determination are shown in Figure 3A. The apparent IC_{50} of DTPA-GIP$_{1-42}$ is 4.8 µ*M* (95% confidence interval: 0.7 – 32.8 µ*M*). However, the low internalization rate described below, render the observed value more likely to be a true IC_{50} rather than an apparent IC_{50}. Figure 3B summarizes the binding and internalization kinetics of [^{111}In]In-DTPA-GIP$_{1-42}$ by BHK-GIPR transfected cells and NES2Y cells as determined *in vitro*. Both cell lines displayed similar binding and internalization characteristics. After 1 hour, 0.6 ± 0.1% and 0.6 ± 0.02% of the added [^{111}In]In-DTPA-GIP$_{1-42}$ was bound to BHK-GIPR transfected cells and NES2Y cells, respectively. At this time point, the internalized fractions were 1.1 ± 0.1% and 1.5 ± 0.3%, respectively. After 24 hours, the binding values had increased to 13.8 ± 1.7% and 8.6 ± 1.5%, respectively and the internalization values to 4.2 ± 0.6% and 4.7 ± 3.6% for BHK-GIPR and NES2Y

cells, respectively. All values were corrected for non-specific binding, as determined by the addition of 25 µg unlabeled GIP_{1-42} which significantly reduced the binding and internalization at all time points indicating GIPR-mediated binding in both cell lines ($p<0.05$). Figure 4 shows the *in vitro* binding characteristics of [^{111}In]In-DTPA-GIP_{1-42} to 200 isolated islets of C3H mice. After 24 hours, 0.22 ± 0.01 fmol [^{111}In]In-DTPA-GIP_{1-42} bound to the islets. Addition of 25 µg unlabeled GIP_{1-42} reduced the binding to 0.03 ± 0.01 fmol, indicating specific binding of the tracer to the GIPR on the islets of Langerhans.

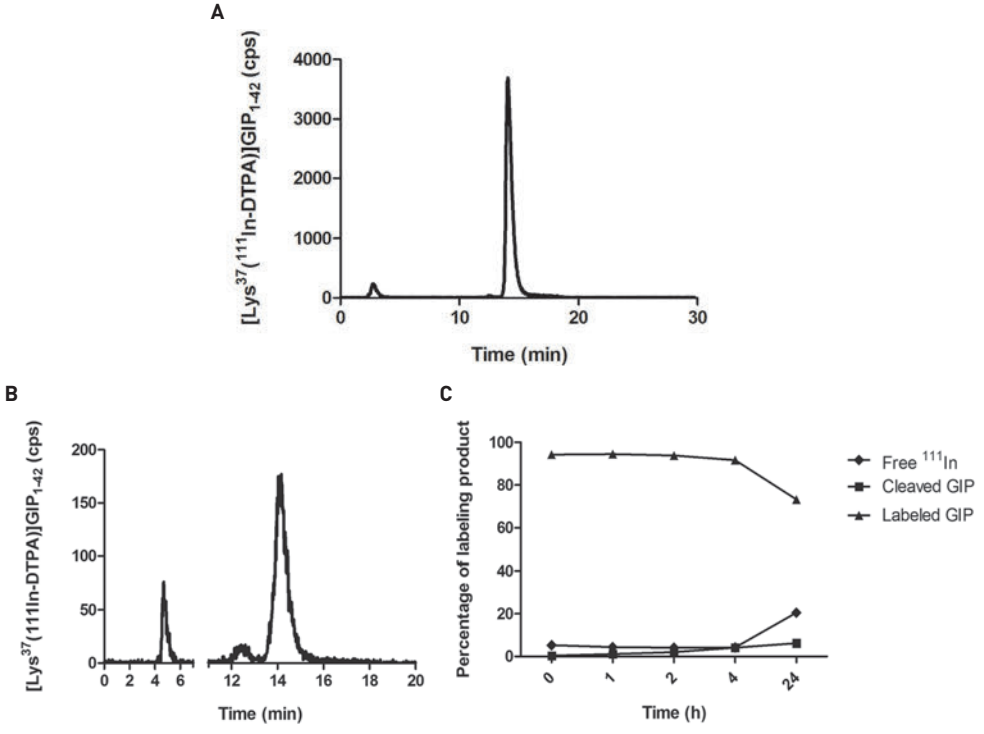

Figure 2. a) Radiochemical purity analysis of [^{111}In]In-DTPA-GIP_{1-42} as determined by HPLC, immediately after labeling. b) HPLC profile of [^{111}In]In-DTPA-GIP_{1-42} after 24 hours of incubation in human serum. c) Overview of stability behavior after various incubation times in human serum.

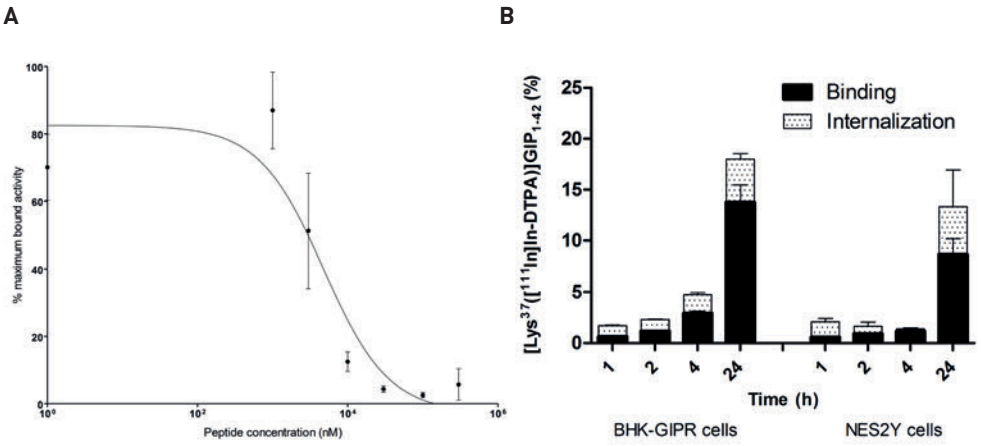

Figure 3. In vitro characterization a) Competition binding assay (apparent IC_{50}) of DTPA-GIP_{1-42} on NES2Y cells. [^{111}In]In-DTPA-GIP_{1-42} was used as a radiotracer b) binding and internalization kinetics of [^{111}In]In-DTPA-GIP_{1-42} in BHK-GIPR positive cells and NES2Y cells. Cell bound and internalized fractions are corrected for non-specific binding and accumulation, as determined by co-incubation with an excess unlabeled GIP_{1-42}.

Peptide Dose Escalation Study

The effect of the peptide dose on tumor targeting was studied in BALB/c nude mice with subcutaneous BHK-GIPR tumors and the results are summarized in Figure 5A. The DTPA-GIP_{1-42} dose had a pronounced effect on tumor uptake, which decreased significantly at peptide doses exceeding 0.2 µg (Figure 5A and 5B). Highest tumor uptake of [^{111}In]In-DTPA-GIP_{1-42} was observed at peptide doses $\leq$0.2 µg (0.04 nmol) per mouse: 5.2 ± 1.4 %ID/g at 4 hours post-injection. Administration of 0.5 µg (0.1 nmol) as a peptide dose resulted in a significantly lower tumor uptake: 2.4 ± 0.7 %ID/g (p=0.008) (figure 5B). Four hours post-injection, [^{111}In]In-DTPA-GIP_{1-42} also showed uptake in various organs such as the lung, spleen, pancreas, liver, stomach and duodenum. The high uptake in the kidneys has been described as being the result of tubular reabsorption through the scavenger receptors cubilin and megalin, which is the case for many peptides [30]. As the kidney uptake of radiolabeled DTPA-GIP_{1-42} cannot be inhibited by an excess of unlabeled peptide, tubular reabsorption indeed appears to be the cause of the high kidney uptake. Raw data of this biodistribution study are shown in Table 1.

Table 1. Raw data of the peptide dose escalation study in BALB/c nude mice with subcutaneous BHK-GIPR tumors shown in Figure 5A. Values are expressed as percentage injected dose per gram tissue (%ID/g) and presented as mean ± SD.

	0.1 µg (n=5)	0.2 µg (n=5)	0.5 µg (n=5)	1.0 µg (n=5)	2.0 µg (n=5)
Blood	0.03 ± 0.01	0.05 ± 0.01	0.05 ± 0.01	0.06 ± 0.02	0.07 ± 0.05
Tumor	0.15 ± 0.03	0.13 ± 0.02	0.14 ± 0.05	0.14 ± 0.03	0.16 ± 0.03
Muscle	4.69 ± 0.85	5.19 ± 1.36	2.36 ± 0.67	2.88 ± 0.34	1.92 ± 0.09
Heart	0.13 ± 0.03	0.16 ± 0.03	0.16 ± 0.02	0.18 ± 0.02	0.17 ± 0.02
Lung	0.36 ± 0.07	0.52 ± 0.12	0.58 ± 0.19	0.61 ± 0.08	0.56 ± 0.13
Spleen	0.65 ± 0.10	0.69 ± 0.18	0.59 ± 0.15	0.78 ± 0.08	0.71 ± 0.07
Pancreas	0.17 ± 0.03	0.23 ± 0.05	0.20 ± 0.05	0.26 ± 0.04	0.21 ± 0.04
Kidney	237.3 ± 17.75	265 ± 38.01	213.8 ± 41.68	287.25 ± 33.58	256.96 ± 28.78
Liver	1.60 ± 0.31	1.53 ± 0.32	1.55 ± 0.37	1.74 ± 0.24	1.83 ± 0.35
Stomach	0.41 ± 0.09	0.42 ± 0.09	0.41 ± 0.03	0.53 ± 0.10	0.44 ± 0.07
Duodenum	0.49 ± 0.10	0.57 ± 0.15	0.53 ± 0.07	0.75 ± 0.27	0.93 ± 0.66
Tumor/Blood	143.4 ± 15.75	109.8 ± 13.06	52.55 ± 18.37	50.28 ± 7.42	37.95 ± 16.30
Tumor/Muscle	33.69 ± 10.64	41.12 ± 5.16	19.08 ± 8.46	20.94 ± 5.02	12.23 ± 2.94
Tumor/Kidney	0.02 ± 0.01	0.02 ± 0.00	0.01 ± 0.00	0.01 ± 0.00	0.01 ± 0.00
Tumor/Heart	35.64 ± 2.05	33.10 ± 5.33	14.58 ± 4.15	16.45 ± 3.02	11.22 ± 1.42
Tumor/Lung	12.96 ± 1.16	10.04 ± 1.82	4.19 ± 0.72	4.81 ± 0.82	3.58 ± 0.83

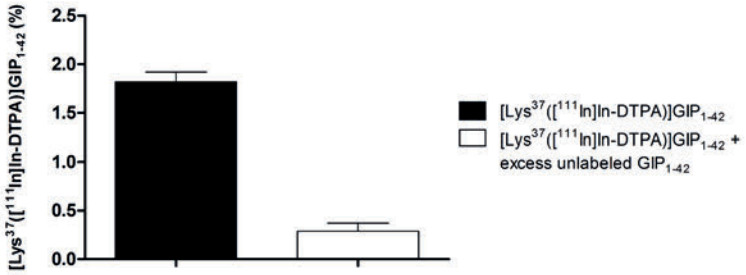

Figure 4. Binding of [^{111}In]In-DTPA-GIP$_{1-42}$ to isolated islets. The solid bar represents binding of [^{111}In]In-DTPA-GIP$_{1-42}$. The white bar represents binding of [^{111}In]In-DTPA-GIP$_{1-42}$ in the presence of an excess unlabeled GIP$_{1-42}$.

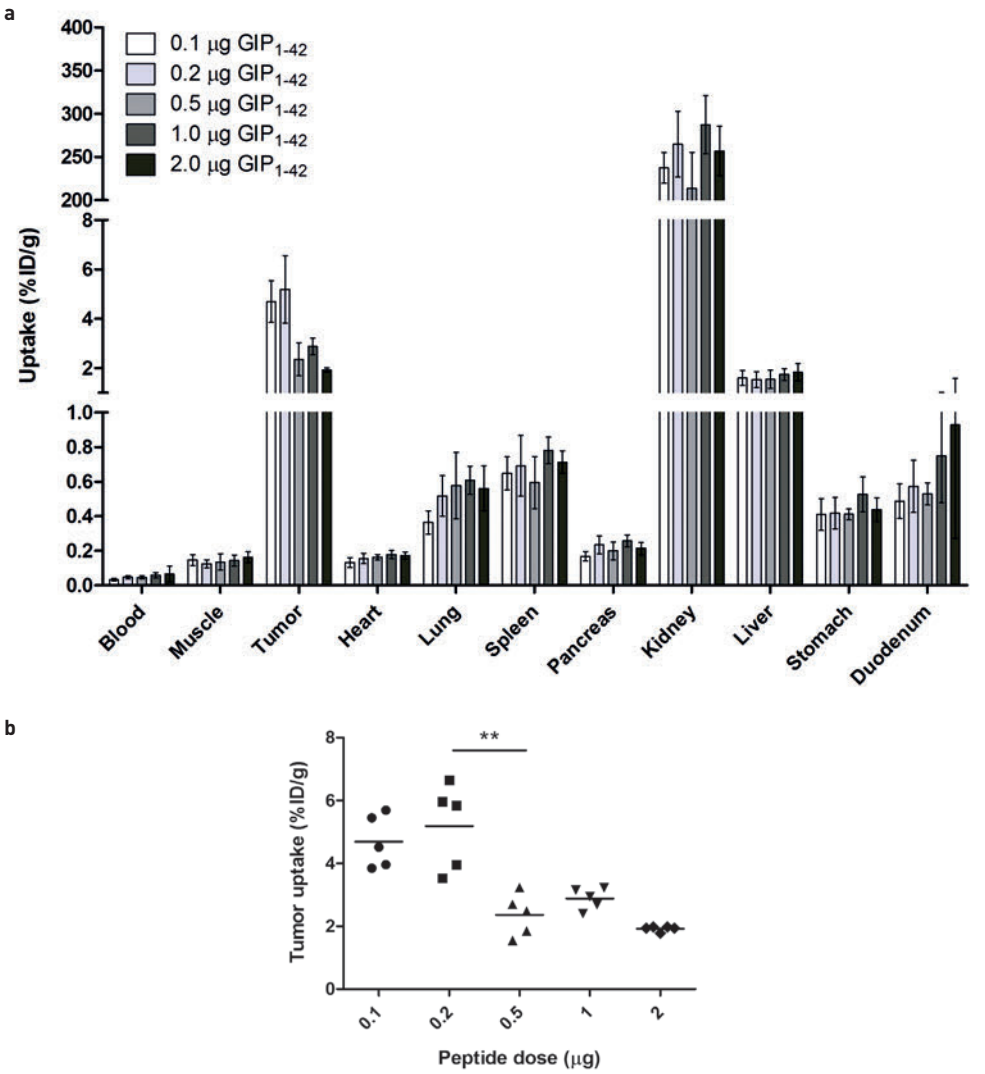

Figure 5. a) Peptide dose escalation study in BALB/c nude mice with subcutaneous BHK-GIPR tumors. Values are expressed as percentage injected dose per gram tissue (%ID/g) (n=5). b) Tumor uptake of [^{111}In]In-DTPA-GIP$_{1-42}$ using different peptide doses. Tumor uptake was significantly higher (**p=0.008) at peptide doses smaller than 0.5 µg (0.1 nmol).

Biodistribution Studies

Figure 6A summarizes the biodistribution of [^{111}In]In-DTPA-GIP$_{1-42}$ in BALB/c nude mice bearing a subcutaneous BHK-GIPR transfected tumor. One hour after injection, highest tumor uptake was observed: 4.7 ± 0.8 %ID/g. After 4 and 24 hours, tumor uptake decreased to 3.3 ± 0.8 %ID/g and 2.0 ± 0.2 %ID/g, respectively (Figure 6A). Co-administration of an excess unlabeled

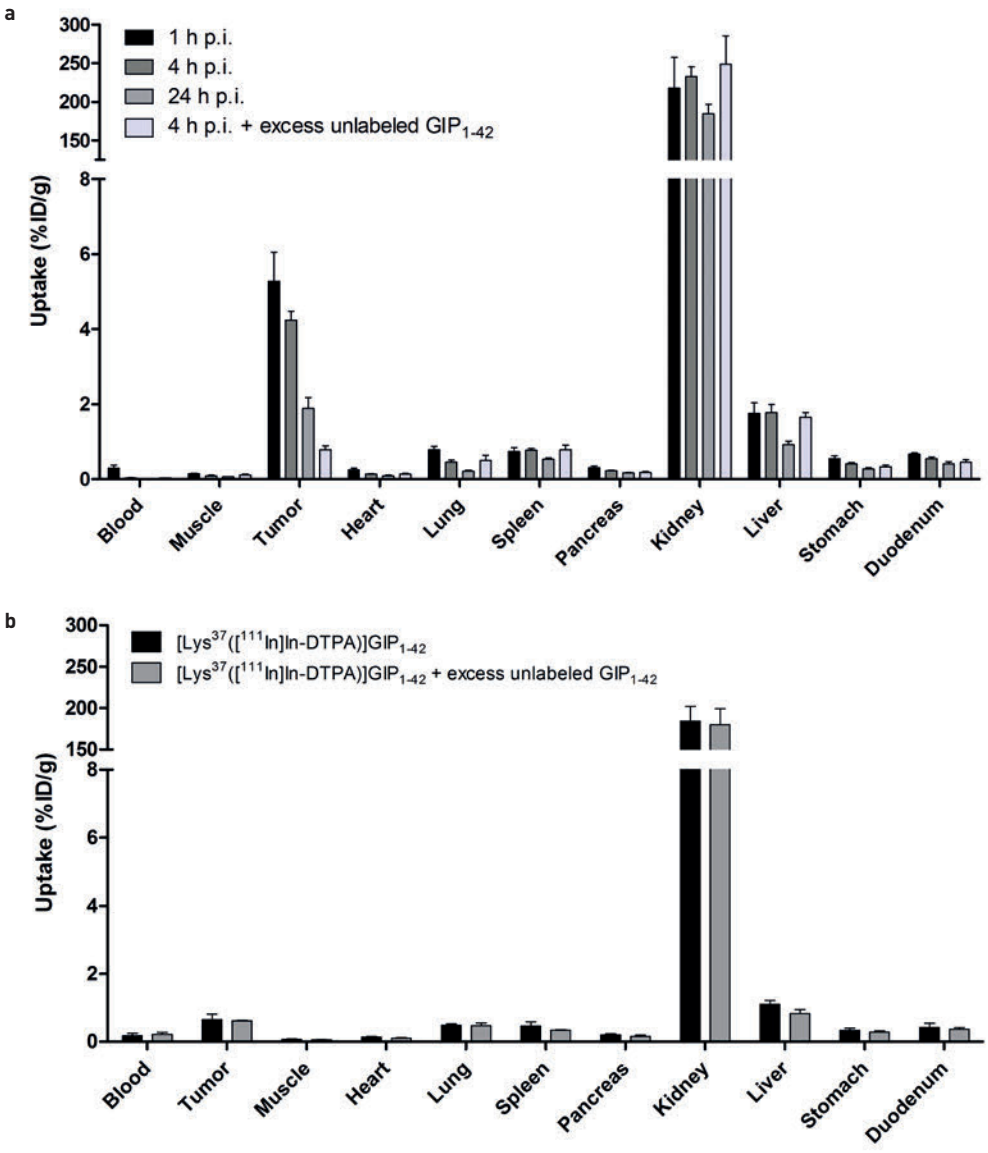

Figure 6. a) Biodistribution study of [^{111}In]In-DTPA-GIP$_{1-42}$ in BALB/c nude mice bearing subcutaneous BHK-GIPR tumors at 1, 4 and 24 hours after tracer injection. Values are expressed as percentage injected dose per gram tissue (%ID/g) (n=5). Blocking was performed by co-injection of 25 µg unlabeled GIP$_{1-42}$ (n=5). b) Biodistribution study of [^{111}In]In-DTPA-GIP$_{1-42}$ in BALB/c nude mice bearing subcutaneous NES2Y tumors, 1 hour after tracer injection. Values are expressed as percentage injected dose per gram tissue (%ID/g) (n=5). Blocking was performed by co-injection of 25 µg unlabeled GIP$_{1-42}$ (n=2).

GIP_{1-42} significantly lowered tumor uptake to 0.8 ± 0.2 %ID/g (p=0.0001) 4 hours after injection, indicating GIPR-mediated tumor uptake. One hour after injection, tumor uptake in NES2Y tumors was 0.7 ± 0.2 %ID/g (Figure 6B). Co-administration of an excess unlabeled GIP_{1-42} lowered tumor uptake to 0.6 ± 0.01 %ID/g (p=0.78) Raw data of these biodistribution studies are shown in Tables 2 and 3.

SPECT/CT

One and four hours after injection of [^{111}In]In-DTPA-GIP_{1-42}, BHK-GIPR transfected tumors were clearly visible on SPECT/CT (Figures 7A and 7B). Co-injection of an excess unlabeled GIP_{1-42} completely blocked tracer uptake in the BHK-GIPR transfected tumor (Figure 7C). Also in mice bearing NES2Y tumors, clear tumor uptake was observed 1 hour after tracer injection (Figure 8A and 8B). Furthermore, co-injection of an excess unlabeled GIP_{1-42} prevented tracer uptake in NES2Y tumors, suggesting GIPR-mediated tracer uptake in these tumors.

Table 2. Raw data of the biodistribution study of [^{111}In]In-DTPA-GIP_{1-42} in BALB/c nude mice bearing subcutaneous BHK-GIPR tumors at 1, 4 and 24 hours after tracer injection shown in Figure 6A. Values are expressed as percentage injected dose per gram tissue (%ID/g) and presented as mean ± SD.

	1 hour p.i. (n=5)	4 hours p.i. (n=5)	4 hours p.i. + excess unlabeled (n=5)	24 hours p.i. (n=5)	p-value
Blood	0.25 ± 0.12	0.05 ± 0.02	0.03 ± 0.01	0.02 ± 0.01	
Tumor	4.69 ± 0.75	3.27 ± 0.77	0.86 ± 0.20	1.95 ± 0.21	0.0001
Muscle	0.14 ± 0.02	0.08 ± 0.01	0.07 ± 0.01	0.06 ± 0.20	
Heart	0.20 ± 0.03	0.12 ± 0.02	0.10 ± 0.02	0.08 ± 0.03	
Lung	0.55 ± 0.08	0.33 ± 0.08	0.33 ± 0.11	0.18 ± 0.60	
Spleen	0.60 ± 0.09	0.53 ± 0.17	0.52 ± 0.12	0.49 ± 0.08	
Pancreas	0.30 ± 0.04	0.19 ± 0.02	0.15 ± 0.02	0.14 ± 0.03	0.01
Kidney	210.9 ± 22.93	227.9 ± 15.46	227.1 ± 25.81	172.75 ± 21.28	
Liver	1.10 ± 0.15	1.16 ± 0.26	1.09 ± 0.27	0.70 ± 0.16	
Stomach	0.50 ± 0.12	0.36 ± 0.07	0.27 ± 0.02	0.26 ± 0.07	
Duodenum	0.56 ± 0.09	0.45 ± 0.05	0.39 ± 0.07	0.38 ± 0.04	
Tumor/Blood	21.76 ± 7.93	77.60 ± 21.65	29.76 ± 10.10	129.79 ± 68.35	
Tumor/Muscle	34.97 ± 4.70	40.43 ± 11.33	12.45 ± 1.14	36.35 ± 11.38	
Tumor/Kidney	0.02 ± 0.01	0.01 ± 0.00	0.00 ± 0.00	0.01 ± 0.00	
Tumor/Heart	23.58 ± 3.41	29.00 ± 9.68	8.89 ± 0.83	25.51 ± 5.31	
Tumor/Lung	8.64 ± 1.05	10.09 ± 2.91	2.68 ± 0.51	11.27 ± 2.95	

Table 3. Raw data of the biodistribution study of [^{111}In]In-DTPA-GIP$_{1-42}$ in BALB/c nude mice bearing subcutaneous NES2Y tumors shown in Figure 6B. Values are expressed as percentage injected dose per gram tissue (%ID/g) and presented as mean ± SD.

	1 hour p.i. (n=5)	1 hour p.i. + excess unlabeled (n=5)	p-value
Blood	0.18 ± 0.07	0.21 ± 0.06	
Tumor	0.65 ± 0.16	0.62 ± 0.01	0.70
Muscle	0.07 ± 0.01	0.06 ± 0.01	
Heart	0.14 ± 0.02	0.10 ± 0.02	
Lung	0.49 ± 0.04	0.47 ± 0.08	
Spleen	0.46 ± 0.12	0.34 ± 0.01	
Pancreas	0.20 ± 0.04	0.16 ± 0.04	0.20
Kidney	184.38 ± 17.56	180.17 ± 19.22	
Liver	1.11 ± 0.11	0.83 ± 0.12	
Stomach	0.34 ± 0.06	0.28 ± 0.04	
Duodenum	0.42 ± 0.12	0.37 ± 0.04	
Tumor/Blood	3.96 ± 0.76	3.01 ± 0.88	
Tumor/Muscle	9.43 ± 1.12	11.09 ± 2.05	
Tumor/Kidney	0.00 ± 0.00	0.00 ± 0.00	
Tumor/Heart	4.83 ± 0.96	6.09 ± 1.14	
Tumor/Lung	1.38 ± 0.45	1.33 ± 0.24	

DISCUSSION

In this study, we investigated the potential of [^{111}In]In-DTPA-GIP$_{1-42}$ for NET detection. The tracer showed GIPR-mediated binding to BHK-GIPR positive cells and NES2Y cells, and to isolated islets *in vitro*. Optimal GIPR-mediated tumor targeting of BHK-GIPR positive tumors *in vivo*, was observed 1 hour post injection using a peptide dose of 0.2 µg (0.04 nmol). Furthermore, both BHK-GIPR transfected tumors and NES2Y tumors were visualized by SPECT.

It has been described that C-terminally truncated GIP analogs, such as GIP$_{1-30}$, exhibit reduced receptor binding affinity when compared to intact GIP$_{1-42}$, while retaining their full insulinotropic effect [26, 27]. Since the goal of this study was to apply the analog for *in vivo* imaging, high receptor affinity should be preserved rather than biological activity. Therefore, we selected GIP$_{1-42}$ as a basis for our radiotracer. Another point of consideration while designing a GIPR targeting radiotracer, is the susceptibility of the native peptide to DPP IV degradation [31]. Since it was shown that several N-terminal modifications showed increased half-life *in vitro* [32, 33], we acetylated the N-terminal tyrosine residue to obtain a better DPP IV degradation-resistant tracer. Indeed, we observed that the tracer remained stable in serum for at least 4 hours after incubation and even after 24 hours of incubation 73% of the tracer remained intact.

In order to obtain high quality images, high target-to-background ratios are required. Tracer metabolites labeled with a radiometal via a chelator, can be trapped in the lysosomes upon tracer internalization and degradation, resulting in enhanced tracer accumulation in the target cells [23, 34]. Therefore, we investigated tracer internalization rates *in vitro*. Internalization kinetics of the tracer were comparable and relatively slow: after 24 hours, both BHK-GIPR positive and NES2Y cells showed similar internalization rates of 4.2 ± 0.6 %ID/g and 4.7 ± 3.6 %ID/g, respectively. Interestingly, the majority of the tracer was bound to the cell surface in both cell lines. These observations could be explained by very recent findings of Ismail *et al.* indicating that N-terminal acetylation of the peptide hampers receptor internalization [35].

In BHK-GIPR positive tumors, GIP_{1-42} doses lower than 0.5 µg (0.1 nmol) resulted in maximal tumor accumulation. This indicates that administration of higher peptide doses results in partial saturation of the GIPR *in vivo*. However, since the tracer could be labeled with a molar activity up to 1.2 TBq/µmol, administration of an activity dose for imaging is still feasible. For *in vivo* SPECT imaging, high tumor-to-blood ratios are required. However, since tracer uptake in the blood was still very low at a peptide dose of 0.2 µg, we selected this dose as the optimal dose for *in vivo* imaging since it resulted in the highest absolute tumor uptake.

Although [^{111}In]In-DTPA-GIP_{1-42} showed high and specific tumor uptake in GIPR-transfected GIPR tumors, tumor uptake in NES2Y tumors was lower and co-injection of an excess unlabeled GIP_{1-42} did not result in significantly lower tracer uptake. This clear difference in tracer uptake might be explained by the completely different origin and purpose of both cell lines. While the BHK-GIPR cell line was created to express artificially high receptor levels, the NES2Y cells are derived from patients with congenital hyperinsulinism of infancy (28). Since these cells do not overexpress the target receptor and it is known that the natural expression levels of the GIPR are much lower compared to its brother incretin peptide GLP-1 [36], the lower uptake is to be expected. As for the blocking study, the small size of the blocking group (n=2) impairs generation of representative results. Therefore, the obtained significance level (p=0.78) might be distorted. On the SPECT images however, tracer accumulation was observed in NES2Y tumors but was no longer observed after co-injection of an excess unlabeled GIP_{1-42} (Figure 8C), suggesting specific tumor targeting. Nevertheless, several tracer characteristics might be optimized to further improve tumor targeting. Firstly, other N-terminal modifications than acetylation, such as glucitol or pyroglutamil insertion, have been shown to improve the half-life of the peptide in the presence of DPP IV [32, 33] and might also result in higher internalization rates. Secondly, receptor binding and internalization might increase with longer circulation times. As shown in our biodistribution studies, [^{111}In]In-DTPA-GIP_{1-42} is cleared from the blood very rapidly, hampering longer tracer circulation and thus higher tumor uptake. Several methods such as PEGylation, multimerization or introduction of free fatty acid tails might increase circulation time [37] and thereby tracer accumulation in the tumor. However, a good balance between tracer retention in blood and tracer targeting dynamics has to be found in order to obtain favorable target-to-background ratios for *in vivo* imaging.

[^{111}In]In-DTPA-GIP$_{1-42}$ was produced at a high molar activity and showed receptor mediated binding to various GIPR expressing cells *in vitro*. Subcutaneous BHK-GIPR positive tumors showed GIPR-mediated tracer accumulation with optimal *in vivo* targeting 1 hour post-injection, at a peptide dose of 0.2 µg (0.04 nmol). Furthermore, although very low, uptake of a GIP-based tracer was demonstrated for the first time in a human beta-cell derived tumor. Unfortunately, specificity of tracer binding could not be shown due to the small size of the blocking group. In conclusion, [^{111}In]In-DTPA-GIP$_{1-42}$ shows promising results as a radiotracer for NET imaging. However, the initial working hypothesis that a full-length peptide-based tracer might show improved characteristics for *in vivo* NET imaging when compared to GIP$_{1-30}$ could not be confirmed.

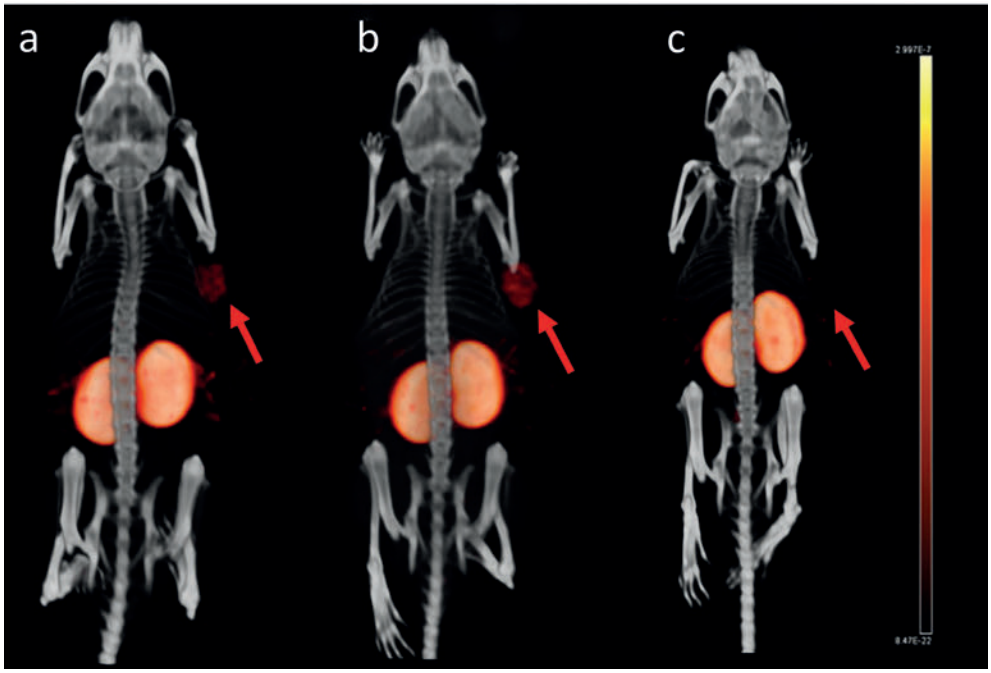

Figure 7. Maximum intensity projection (MIP) SPECT/CT images of a BALB/c nude mouse bearing a subcutaneous BHK-GIPR tumor 1 hour after injection (a), 4 hours after injection (b) and 4 hours after injection and co-injection with 25 µg unlabeled GIP$_{1-42}$ (c).

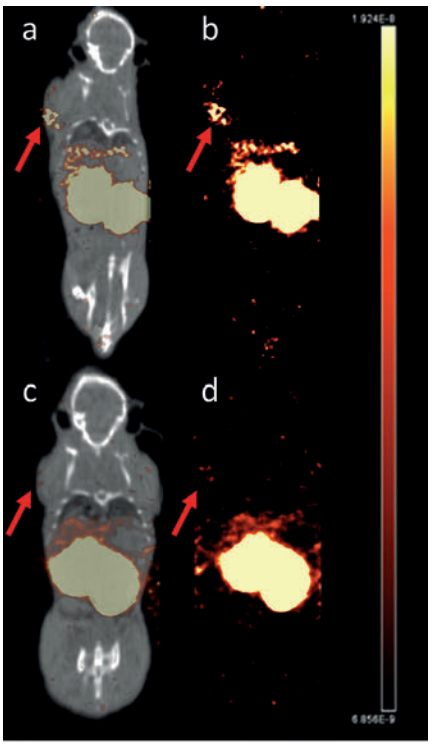

Figure 8. SPECT/CT (a) and SPECT (b) of a BALB/c nude mouse bearing a subcutaneous NES2Y tumor, 1 hour after injection and SPECT/CT (c) and SPECT (d) after co-injection with 25 µg unlabeled GIP_{1-42}.

ETHICAL APPROVAL

All animal experiments were approved by the Animal Welfare Body of the Radboud University, Nijmegen, The Netherlands and carried out in accordance with their guidelines.

ACKNOWLEDGEMENTS

The research leading to these results has received funding from the People Programme (Marie Curie Actions) of the European Union's Seventh Framework Programme FP7/2007-2013/ under REA grant agreement n° 289932. The authors declare that there is no conflict of interest. SW is a postdoctoral fellow of the research foundation Flanders (FWO). We thank the biotechnicians of PRIME for their assistance in the animal experiments, Jacob Hecksher-Sørensen of Novo Nordisk for kindly providing us with BHK-GIPR cells and Roger James of the University of Leicester for kindly providing us with NES2Y cells.

AUTHOR CONTRIBUTION STATEMENT

SMAW and LJ designed and performed the experiments; acquired, analyzed and interpreted data; and drafted and critically revised the manuscript. OCB, MB and MG provided a substantial contribution to conception and design, and data interpretation. OCB, MB and MG critically revised the manuscript for intellectual content. All authors approved the final version of the manuscript. MG is responsible for the integrity of the manuscript as a whole.

ADDITIONAL INFORMATION

Competing interests: MG is patent holder in the field.
Data availability statement: all data are available at the department of Nuclear medicine of the Radboud University medical center, Nijmegen.

REFERENCES

1. Reubi JC. Peptide receptors as molecular targets for cancer diagnosis and therapy. *Endocrine reviews*. **2003**; 24 (4): 389-427.
2. Schottelius M, Wester HJ. Molecular imaging targeting peptide receptors. *Methods*. **2009**; 48 (2): 161-177.
3. Krenning EP, Kwekkeboom DJ, Bakker WH, Breeman WA, Kooij PP, Oei HY, *et al*. Somatostatin receptor scintigraphy with [111In-DTPA-D-Phe1]- and [123I-Tyr3]-octreotide: the Rotterdam experience with more than 1000 patients. *European journal of nuclear medicine*. **1993**; 20 (8): 716-731.
4. Lamberts SW, Bakker WH, Reubi JC, Krenning EP. Somatostatin-receptor imaging in the localization of endocrine tumors. *The New England journal of medicine*. **1990**; 323 (18): 1246-1249.
5. Modlin IM, Tang LH. Approaches to the diagnosis of gut neuroendocrine tumors: the last word (today). *Gastroenterology*. **1997**; 112 (2): 583-590.
6. Yang J, Kan Y, Ge BH, Yuan L, Li C, Zhao W. Diagnostic role of Gallium-68 DOTATOC and Gallium-68 DOTATATE PET in patients with neuroendocrine tumors: a meta-analysis. *Acta Radiol*. **2014**; 55 (4): 389-398.
7. Bodei L, Mueller-Brand J, Baum RP, Pavel ME, Horsch D, O'Dorisio MS, *et al*. The joint IAEA, EANM, and SNMMI practical guidance on peptide receptor radionuclide therapy (PRRNT) in neuroendocrine tumours. *European journal of nuclear medicine and molecular imaging*. **2013**; 40 (5): 800-816.
8. Joseph K, Stapp J, Reinecke J, Skamel HJ, Hoffken H, Benning R, *et al*. [Receptor scintigraphy using 111In-pentetreotide in endocrine gastroenteropancreatic tumors]. *Nuklearmedizin. Nuclear medicine*. **1993**; 32 (6): 299-305.
9. Prasad V, Sainz-Esteban A, Arsenic R, Plockinger U, Denecke T, Pape UF, *et al*. Role of (68)Ga somatostatin receptor PET/CT in the detection of endogenous hyperinsulinaemic focus: an explorative study. *European journal of nuclear medicine and molecular imaging*. **2016**; 43 (9): 1593-1600.
10. Nockel P, Babic B, Millo C, Herscovitch P, Patel D, Nilubol N, *et al*. Localization of Insulinoma Using 68Ga-DOTATATE PET/CT Scan. *J Clin Endocrinol Metab*. **2017**; 102 (1): 195-199.
11. Gotthardt M, Behe MP, Beuter D, Battmann A, Bauhofer A, Schurrat T, *et al*. Improved tumour detection by gastrin receptor scintigraphy in patients with metastasised medullary thyroid carcinoma. *European journal of nuclear medicine and molecular imaging*. **2006**; 33 (11): 1273-1279.
12. Reubi JC, Schaer JC, Waser B. Cholecystokinin(CCK)-A and CCK-B/gastrin receptors in human tumors. *Cancer research*. **1997**; 57 (7): 1377-1386.
13. Reubi JC, Laderach U, Waser B, Gebbers JO, Robberecht P, Laissue JA. Vasoactive intestinal peptide/pituitary adenylate cyclase-activating peptide receptor subtypes in human tumors and their tissues of origin. *Cancer research*. **2000**; 60 (11): 3105-3112.
14. Reubi JC, Waser B. Concomitant expression of several peptide receptors in neuroendocrine tumours: molecular basis for in vivo multireceptor tumour targeting. *European journal of nuclear medicine and molecular imaging*. **2003**; 30 (5): 781-793.

15. Sherman SK, Maxwell JE, Carr JC, Wang D, O'Dorisio MS, O'Dorisio TM, *et al.* GIPR expression in gastric and duodenal neuroendocrine tumors. *The Journal of surgical research.* **2014**; 190 (2): 587-593.

16. Waser B, Rehmann R, Sanchez C, Fourmy D, Reubi JC. Glucose-dependent insulinotropic polypeptide receptors in most gastroenteropancreatic and bronchial neuroendocrine tumors. *The Journal of clinical endocrinology and metabolism.* **2012**; 97 (2): 482-488.

17. Sherman SK, Carr JC, Wang D, O'Dorisio MS, O'Dorisio TM, Howe JR. Gastric inhibitory polypeptide receptor (GIPR) is a promising target for imaging and therapy in neuroendocrine tumors. *Surgery.* **2013**; 154 (6): 1206-1213; discussion 1214.

18. Gourni E, Waser B, Clerc P, Fourmy D, Reubi JC, Maecke HR. The glucose-dependent insulinotropic polypeptide receptor: a novel target for neuroendocrine tumor imaging-first preclinical studies. *Journal of nuclear medicine : official publication, Society of Nuclear Medicine.* **2014**; 55 (6): 976-982.

19. Mortensen K, Christensen LL, Holst JJ, Orskov C. GLP-1 and GIP are colocalized in a subset of endocrine cells in the small intestine. *Regulatory peptides.* **2003**; 114 (2-3): 189-196.

20. Elrick H, Stimmler L, Hlad CJ, Jr., Arai Y. Plasma Insulin Response to Oral and Intravenous Glucose Administration. *The Journal of clinical endocrinology and metabolism.* **1964**; 24 1076-1082.

21. McIntyre N, Holdsworth CD, Turner DS. New Interpretation of Oral Glucose Tolerance. *Lancet.* **1964**; 2 (7349): 20-21.

22. Brom M, Oyen WJ, Joosten L, Gotthardt M, Boerman OC. 68Ga-labelled exendin-3, a new agent for the detection of insulinomas with PET. *European journal of nuclear medicine and molecular imaging.* **2010**; 37 (7): 1345-1355.

23. Gotthardt M, Fischer M, Naeher I, Holz JB, Jungclas H, Fritsch HW, *et al.* Use of the incretin hormone glucagon-like peptide-1 (GLP-1) for the detection of insulinomas: initial experimental results. *European journal of nuclear medicine and molecular imaging.* **2002**; 29 (5): 597-606.

24. Wild D, Macke H, Christ E, Gloor B, Reubi JC. Glucagon-like peptide 1-receptor scans to localize occult insulinomas. *The New England journal of medicine.* **2008**; 359 (7): 766-768.

25. Wild D, Christ E, Caplin ME, Kurzawinski TR, Forrer F, Brandle M, *et al.* Glucagon-like peptide-1 versus somatostatin receptor targeting reveals 2 distinct forms of malignant insulinomas. *Journal of nuclear medicine : official publication, Society of Nuclear Medicine.* **2011**; 52 (7): 1073-1078.

26. Maletti M, Altman JJ, Hoa DH, Carlquist M, Rosselin G. Evidence of functional gastric inhibitory polypeptide (GIP) receptors in human insulinoma. Binding of synthetic human GIP 1-31 and activation of adenylate cyclase. *Diabetes.* **1987**; 36 (11): 1336-1340.

27. Wheeler MB, Gelling RW, McIntosh CH, Georgiou J, Brown JC, Pederson RA. Functional expression of the rat pancreatic islet glucose-dependent insulinotropic polypeptide receptor: ligand binding and intracellular signaling properties. *Endocrinology.* **1995**; 136 (10): 4629-4639.

28. Adams GG, Uddin A, Vives-Pi M, Pujol-Borrell R, James RF. Characterisation of the NES2Y cell line and its use in the production of human glucose-responsive insulin producing (hGRIP) cell lines by cell-cell fusion. *Islets.* **2009**; 1 (2): 117-123.

29. Coenen HH, Gee AD, Adam M, Antoni G, Cutler CS, Fujibayashi Y, *et al*. Consensus nomenclature rules for radiopharmaceutical chemistry - Setting the record straight. *Nucl Med Biol*. **2017**; 55 v-xi.

30. Gotthardt M, van Eerd-Vismale J, Oyen WJ, de Jong M, Zhang H, Rolleman E, *et al*. Indication for different mechanisms of kidney uptake of radiolabeled peptides. *J Nucl Med*. **2007**; 48 (4): 596-601.

31. Kieffer TJ, McIntosh CH, Pederson RA. Degradation of glucose-dependent insulinotropic polypeptide and truncated glucagon-like peptide 1 in vitro and in vivo by dipeptidyl peptidase IV. *Endocrinology*. **1995**; 136 (8): 3585-3596.

32. O'Harte FP, Mooney MH, Flatt PR. NH2-terminally modified gastric inhibitory polypeptide exhibits amino-peptidase resistance and enhanced antihyperglycemic activity. *Diabetes*. **1999**; 48 (4): 758-765.

33. Gault VA, Flatt PR, O'Harte FP. Glucose-dependent insulinotropic polypeptide analogues and their therapeutic potential for the treatment of obesity-diabetes. *Biochemical and biophysical research communications*. **2003**; 308 (2): 207-213.

34. Gotthardt M, Boermann OC, Behr TM, Behe MP, Oyen WJ. Development and clinical application of peptide-based radiopharmaceuticals. *Current pharmaceutical design*. **2004**; 10 (24): 2951-2963.

35. Ismail S, Dubois-Vedrenne I, Laval M, Tikhonova IG, D'Angelo R, Sanchez C, *et al*. Internalization and desensitization of the human glucose-dependent-insulinotropic receptor is affected by N-terminal acetylation of the agonist. *Molecular and cellular endocrinology*. **2015**;

36. De Marinis YZ, Salehi A, Ward CE, Zhang Q, Abdulkader F, Bengtsson M, *et al*. GLP-1 inhibits and adrenaline stimulates glucagon release by differential modulation of N- and L-type Ca2+ channel-dependent exocytosis. *Cell Metab*. **2010**; 11 (6): 543-553.

37. Pathak V, Vasu S, Gault VA, Flatt PR, Irwin N. Sequential induction of beta cell rest and stimulation using stable GIP inhibitor and GLP-1 mimetic peptides improves metabolic control in C57BL/KsJ db/db mice. *Diabetologia*. **2015**; 58 (9): 2144-2153.

38. Laverman P, Roosenburg S, Gotthardt M, Park J, Oyen WJ, de Jong M, *et al*. Targeting of a CCK(2) receptor splice variant with (111)In-labelled cholecystokinin-8 (CCK8) and (111)In-labelled minigastrin. *European journal of nuclear medicine and molecular imaging*. **2008**; 35 (2): 386-392.


4

CHAPTER 5

Enhanced molar activity by multi-chelation of exendin-3 leads to improved *in vivo* beta cell imaging

Lieke Joosten[1], Maarten Brom[1], Hanneke Peeters[1], Sandra Heskamp[1], Martin Béhé[2], Otto C. Boerman[1] & Martin Gotthardt[1]

1 Department of Radiology and Nuclear Medicine, Radboud University Medical Center, Nijmegen, The Netherlands
2 Center for Radiopharmaceutical Sciences ETH-PSI-USZ, Paul Scherrer Institut, Villigen, Switzerland

Molecular Pharmaceutics. **2018**; 15 (2): 486-494

ABSTRACT

Glucagon like peptide-1 receptor (GLP-1R) targeting using radiolabeled exendin is a promising approach to non-invasively visualize and determine beta cell mass (BCM), which could help to unravel the pathophysiology of diabetes. However, saturation of the GLP-1R on beta cells occurs at low peptide doses, since the number of receptors expressed under physiological conditions is low. Therefore, tracers with high molar activities are required to sensitively image small variations in BCM. Here, we describe a novel exendin-3-based radiotracer with multiple chelators and determined its potential for *in vivo* beta cell imaging.

Exendin-3 was modified by adding six lysine residues C-terminally conjugated with one, two or six DTPA moieties. All compounds were labeled with ^{111}In and their GLP-1R affinity was determined *in vitro* using GLP-1R expressing cells. The *in vivo* behavior of the ^{111}In-labeled tracers was examined in BALB/c nude mice with a subcutaneous GLP-1R expressing tumor (INS-1). Brown Norway rats were used for SPECT visualization of the pancreatic BCM.

Addition of six lysine and six DTPA residues (hexendin(40-45)) resulted in a seven-fold increase in molar activity (from 0.73 GBq/nmol to 5.54 GBq/nmol). IC_{50} values varied between 5.2 and 69.5 nM. All compounds with two or six lysine and DTPA residues had a significantly lower receptor affinity than [Lys^{40}(DTPA)]exendin-3 (4.4 nM, $p < 0.05$). The biodistribution in mice revealed no significant decrease in pancreatic uptake after addition of six lysine and DTPA molecules. Hexendin(40-45) showed a six-fold increase in absolute ^{111}In uptake in the pancreas of Brown Norway rats compared to [Lys^{40}(DTPA)]exendin-3 (182.7 ± 42.3 kBq vs. 28.8 ± 6.0 kBq, $p<0.001$). Visualization of the pancreas on SPECT was improved using hexendin(40-45), due to the higher count rate, achieved at the same peptide dose.

In conclusion, hexendin(40-45) showed an improved visualization of the pancreas with SPECT. This tracer holds promise to sensitively and specifically detect small variations in BCM.

INTRODUCTION

Currently, 422 million people worldwide are suffering from diabetes, and it is expected that this number will have doubled by 2030 [1]. These dramatic numbers underline the importance for research aiming to improve diagnosis and treatment of the disease. Gaining better insight into the pathophysiology of the different types of diabetes is therefore one of the major goals of current diabetes research.

The diagnosis of diabetes is currently based on laboratory tests, such as blood glucose measurements and oral glucose tolerance testing. However, they do not provide information about the underlying pathophysiological processes and can only detect the downstream consequences (i.e. impaired glucose tolerance) of processes that have started years before diagnosis. Currently, the loss of beta cell mass (BCM) and beta cell function (not being directly related to mass) proceeding to overt hyperglycemia is gaining attention and determination of BCM has emerged as a field of diabetes research [2]. To date, biopsy and autopsy studies of diabetic patients are the only source of information regarding BCM. However, this only provides information at one time point [3] and pancreatic biopsies in T1D patients have been shown to be associated with a high rate of serious complications [4]. Therefore, there is a clear need for a non-invasive method to measure the loss of BCM in individual patients. A promising approach addressing this urgent issue would be a sensitive, specific and non-invasive imaging method to detect viable beta cells in the pancreas, which would also enable determination of the exact relation between the BCM and beta cell function during the course of the disease [5, 6]. The high technological demands for *in vivo* beta cell imaging and the need for a highly sensitive and specific imaging method displaying a high target-to-background ratio have been discussed extensively in the literature [5, 7-10]. Namely, the low amount of beta cells (only a few gram) and the diffuse distribution throughout the pancreas represent a major challenge for *in vivo* imaging [6]. Recently, it has been shown that radiolabeled exendin is a promising tracer to visualize pancreatic beta cells *in vivo* in rodents and humans [6, 11]. Exendin-3 is an analog of GLP-1 (glucagon-like peptide-1) and binds with high affinity to the GLP-1 receptor (GLP-1R) which is specifically expressed on the pancreatic beta cells as well as on beta cell derived tumors [12, 13]. In order to improve image quality, enabling better delineation of the pancreas (which can be hampered by the proximity of the kidneys accumulating radioactivity), higher uptake of radiolabeled exendin-3 in the pancreas is warranted to obtain optimal count rates and high signal-to-background ratios. Since the GLP-1R is expressed at relatively low levels on beta cells in healthy rodents (as compared to for example neuroendocrine tumors massively overexpressing somatostatin receptors) and the total BCM is decreased in diabetic animals, the receptor is saturated at comparably low peptide doses. It has been demonstrated that the maximum peptide dose for exendin imaging of pancreatic beta cells in mice and rats is 20 pmol per injection [14, 15]. In order to achieve optimal SPECT image quality, labeling of exendin with very high molar activities is required.

Previously, an exendin analog with six extra lysine residues at the C-terminus has been described (Table 1)[16]. The addition of lysine residues would theoretically allow the conjugation of multiple DTPA moieties to produce a tracer with a higher molar activity. In the present study, we have tested five novel variants of exendin-3 by adding multiple DTPA moieties to the C-terminal lysine residues and we evaluated whether 1) the molar activity would be enhanced, 2) the modifications would influence the affinity for the GLP-1R, 3) targeting to beta cells would be increased (in terms of absolute radioactivity concentration) and 4) image quality would be improved.

Table 1. Amino acid sequence of ZP10A, exendin-4, exendin-3 and GLP1. Amino acids homologous to GLP-1 are in bold.

Peptide	Amino acid sequence
Poly-Lysine-exendin-4 (ZP10A)[16]	**H**G**EGTFTSD**L**S**KQM**E**EE**A**VRL**FI**E**WL**KN**G**GPSSGAPPPSKKKKKK-NH_2
Exendin-4	**H**G**EGTFTSD**L**S**KQM**E**EE**A**VRL**FI**E**WL**KN**G**GPSSGAPPPS-NH_2
Exendin-3	**H**SD**GTFTSD**L**S**KQM**E**EE**A**VRL**FI**E**WL**KN**G**GPSSGAPPPS-NH_2
GLP-1	HAEGTFTSDVSSYLEGQAAKEFIAWLVKGRG-NH_2

MATERIALS AND METHODS

Peptides and radionuclides

$^{111}InCl_3$ was obtained from Mallinckrodt Medical (Petten, The Netherlands) and the DTPA-exendin-3 peptides were purchased from Peptide Specialty Laboratories (PSL, Heidelberg, Germany). The exendin-3 compounds with 6 additional lysine residues are referred to as hexendin (hexa-lysine-exendin-3) hereafter. One or multiple DTPA molecules were conjugated to the ε-amino group of C-terminal lysines at different positions. The structure, names and molecular weights of the peptides are shown in Table 2. Exendin-3, with DTPA conjugated to lysine at position 40 ([Lys^{40}(DTPA)]exendin-3), was used as the reference in this study.

Table 2. Structure, name and molecular mass of exendin-3 derivatives. The lysine position to which DTPA is conjugated is indicated between parentheses (), the lysine residues and DTPA moieties attached are marked in bold.

Peptide	Amino Acid Sequence	Molecular weight (Da)
[Lys^{40}(DTPA)]exendin-3	HSDGTFTSDLSKQMEEEAVRLFIEWLKNGGPSS-GAPPPS**K(DTPA)**	4816.3
Hexendin(40)	HSDGTFTSDLSKQMEEEAVRLFIEWLKNGGPSS-GAPPPS**K(DTPA)KKKKK**	5345.7
Hexendin(45)	HSDGTFTSDLSKQMEEEAVRLFIEWLKNGGPSS-GAPPPS**KKKKKK(DTPA)**	5345.7
Hexendin(40+45)	HSDGTFTSDLSKQMEEEAVRLFIEWLKNGGPSS-GAPPPS**K(DTPA)KKKKK(DTPA)**	5720.8
Hexendin(40+41)	HSDGTFTSDLSKQMEEEAVRLFIEWLKNGGPSS-GAPPPS**K(DTPA)K(DTPA)KKKK**	5724.5
Hexendin(40-45)	HSDGTFTSDLSKQMEEEAVRLFIEWLKNGGPSS-GAPPPS**K(DTPA)K(DTPA)K(DTPA)K(DTPA)K(DTPA)K(DTPA)**	7235.6

Radiolabeling of DTPA-exendin-3 analogs with ^{111}In

The peptides were dissolved in metal-free 0.1 M MES (2-(*N*-morpholino) ethanesulfonic acid, Sigma Aldrich, St. Louis, MO, USA), pH 5.5 [17]. $^{111}InCl_3$ was added to 0.1 M MES buffer, pH 5.5, containing the respective peptide: One volume of $^{111}InCl_3$ was mixed with two volumes of MES buffer. After incubation for 20 min at room temperature, 50 mM EDTA (ethylenediaminetetraacetic acid) (Sigma Aldrich) was added to a final concentration of 5 mM. Subsequently, 10% Tween-80 (Sigma Aldrich) in PBS was added to a final concentration of 0.1% to prevent sticking of the peptide to the reaction vial. The maximum specific activity of each analog was determined by performing a series of radiolabeling reactions ranging from 75 to 300 MBq for [Lys^{40}(DTPA)] exendin-3, hexendin(40), hexendin(45), and hexendin(40+45) (200 pmol of peptide was added to the reaction mixture) and 75 to 900 MBq for hexendin(40+41) and hexendin(40-45) (100 pmol of peptide was added to the reaction mixture). Radiochemical purity was determined by instant thin layer chromatography on silica-gel strips (ITLC-SG Biodex, Shirley, NY, USA) using 0.1 M EDTA in 0.1 M NH_4Ac as a mobile phase (R_f ^{111}In-labeled peptides = 0, R_f ^{111}In-EDTA = 1).

The radiolabeled peptides were purified by solid-phase extraction using an HLB (hydrophilic-lipophilic balance reversed-phase sorbent) cartridge (Waters Oasis©, Milford, MA, USA) as described previously [18]. For conditioning and washing of the cartridge, 1 ml 0.1 M MES was used.

Cell culture

For *in vivo* experiments the rat insulinoma cell line INS-1 was used [19]. INS-1 cells were cultured in RPMI-1640 medium supplemented with 10% fetal calf serum, 2 mM glutamine, 100 units/ml penicillin, 100 µg/ml streptomycin, 10 mM HEPES, 50 µM β-mercaptoethanol and 1 mM sodiumpyruvate. CHL-cells transfected with the human GLP-1 receptor (a kind gift of

Brigitte Lankat-Buttgereit, Marburg) were used for the *in vitro* experiments. CHL-GLP-1R cells were maintained in Dulbecco's Modified Eagle's Medium (DMEM) GlutaMAX (Gibco, Invitrogen, Breda, The Netherlands), supplemented with 10% fetal calf serum, 100 units/ml penicillin, 100 µg/ml streptomycin, Geneticin (G418) sulphate solution (0.5 mg/ml final concentration), 1 mM sodiumpyruvate and 0.1 mM non-essential amino acids. Cells were maintained in a humidified 5% CO_2 atmosphere at 37 °C.

Competitive binding assay

The relative affinity of the exendin analogs for the GLP-1R was determined in a competitive binding assay using CHL-GLP-1R cells. CHL-GLP-1R cells were seeded in six-well plates at 1 x 10^6 cells/well 2 days prior to the experiment. All peptides were labeled with ^{nat}In. A five-fold molar excess of ^{nat}In prepared in 0.02 M HCl was added to the peptides and two volumes of 0.1 M MES buffer. After incubation at room temperature for 20 min, 10% Tween-80 was added to a final concentration of 0.1%. Serial dilutions of these 'cold-labeled' compounds were prepared in DMEM GlutaMAX with 0.5% *w/v* BSA (bovine serum albumin). Cells were washed once with GlutaMAX with 0.5% *w/v* BSA and the 'cold-labeled' peptides were added at a final concentration ranging from 0.1-1000 nM along with 1 kBq (1.4 fmol) ^{111}In-labeled [Lys^{40}(DTPA)] exendin-3. After incubation on ice for 4 hours, cells were washed with ice-cold GlutaMAX with 0.5% *w/v* BSA and the cells were harvested with 0.1 M NaOH. Cell-associated radioactivity was determined in a γ-counter (Wallac 1480-Wizard, Perkin Elmer, Boston, MA, USA) and the IC_{50} (half-maximal inhibitory concentration) was calculated using GraphPad Prism (version 5.03, GraphPad Software, San Diego California USA).

Biodistribution at equimolar doses

All animal experiments were performed according to national laws and regulations and approved by the animal welfare body of the Radboud University. To examine the *in vivo* GLP-1R targeting properties of the ^{111}In-labeled exendin analogs, six to eight weeks old female BALB/cRJ nu mice (Janvier, Saint-Berthevin, France) were inoculated subcutaneously with 1 x 10^7 INS-1 cells in 200 µl RPMI medium. Mice were randomly divided into 12 groups (n=5 per group). Each group was injected intravenously with 0.1-0.7 MBq of one of the following ^{111}In-labeled peptides: [Lys^{40}(DTPA)]exendin-3, hexendin(40), hexendin(45), hexendin(40+45), hexendin(40+41) or hexendin(40-45)). Equimolar doses of the labeled analogs were administered (20 pmol) to the mice. For each analog, an additional group of 5 mice was co-injected with an excess (2 nmol) of unlabeled Lys^{40}exendin-3 to determine the biodistribution of the tracer while blocking the GLP-1 receptors *in vivo*. After two hours, mice were euthanized by CO_2/O_2 asphyxiation. Relevant organs were dissected, weighed and counted in a γ-counter. For each tissue sample the uptake was calculated and presented as the percentage of the injected dose per gram tissue (%ID/g).

Biodistribution at different molar doses

Because hexendin(40+41) and hexendin(40-45) can be labeled at higher molar activities, it allows injection of a lower peptide dose. To investigate whether administering a lower peptide dose could lead to higher uptake of the tracer in the target tissue (in terms of %ID/g), BALB/c nude mice with a s.c. INS-1 tumor were injected with 4 pmol of hexendin(40+41) or hexendin(40-45) and compared to injection of 20 pmol of [Lys^{40}(DTPA)]exendin-3. For all compounds 0.2 MBq of the ^{111}In-labeled peptide was injected. To determine the non-GLP-1R mediated biodistribution of the tracers, for each peptide an additional group of 5 mice was co-injected with an excess (2 nmol) of unlabeled Lys^{40}exendin-3. The *ex vivo* biodistribution was performed as described above.

SPECT

To compare the ability of the tracers to visualize GLP-1R expressing cells in the pancreas, SPECT studies were carried out in male Brown Norway (BN) rats. Two groups of rats (n=5) received 19.4 ± 1.3 MBq (20 pmol) of either ^{111}In-labeled [Lys^{40}(DTPA)]exendin-3 or hexendin(40-45). An additional group received [^{111}In]In-hexendin(40-45) at a 7.5-fold higher activity dose (20 pmol, 149.1 ± 3.8 MBq (n=4)) to investigate the effect of the activity dose on the image quality. SPECT scans were acquired under isoflurane/O_2 anesthesia two hours after injection of the radiolabeled peptide using a dedicated small animal SPECT/CT scanner (U-SPECT-II, MILabs, Utrecht, The Netherlands). Images were acquired for 50 min, using a 1.0 mm multi-pinhole general purpose mouse and rat collimator. Rats were euthanized by CO_2/O_2 asphyxiation and the *ex vivo* biodistribution was determined as described above. Absolute uptake in the pancreas and kidneys was calculated by multiplying the injected dose (MBq) by the uptake in the organs (percent injected dose in the total dissected organ).

Images were reconstructed using the U-SPECT-Rec Software (MILabs, Utrecht, The Netherlands,). Inveon Research Workplace (Preclinical Solutions, Siemens Medical Solutions USA, Inc., Knoxville, TN, USA) was used to quantify the pancreatic uptake of the ^{111}In-labeled peptides by drawing a volume of interest over the pancreas and in the abdomen (below the kidneys) as a background region. The image quality was determined quantitatively by calculating the ratio of the mean activity in the pancreas region and the activity in the background region (signal-to-background ratio) [20].

Statistical analysis

Data were analyzed using GraphPad Prism software version 5.03 for Windows. One-way ANOVA followed by a Tukey test was used to determine significance. A *p*-value below 0.05 was considered significant. For the competitive binding assay the F-test was used to manually calculate significance.

RESULTS

Molar activity

The maximum molar activity of the ^{111}In-labeled exendin analogs and the theoretical maximum molar activity (assuming all DTPA-molecules chelating ^{111}In) are summarized in Table 3. For all tracers the radiochemical purity exceeded 99% after purification. The molar activity of [Lys^{40}(DTPA)]exendin-3 (0.73 GBq/nmol) was similar to that of the exendin-3 analogs with 6 lysine residues and only one DTPA attached (hexendin(40) and hexendin(45): 0.69 and 0.67 GBq/nmol). The molar activity of hexendin(40+41) and hexendin(40+45) was approximately two-fold higher (1.66 and 1.32 GBq/nmol, respectively) compared to the reference peptide. Finally, hexendin(40-45) could be labeled with a molar activity of 5.54 GBq/nmol, which is 7.5-times higher than that of the reference peptide. Furthermore, the radiolabeling of [Lys^{40}(DTPA)] exendin-3 resulted in 42% of the theoretical maximum molar activity, whereas 54% of the theoretical maximum molar activity was reached for hexendin(40-45).

Table 3. Maximum and theoretical specific activity of exendin-3 derivatives. The maximum theoretical specific activity calculated for exendin-3, conjugated with one, two or six DTPA molecules, with the assumption that 1 nmol of ^{111}In will be complexed in 1 nmol of DTPA.

Compound	Maximum specific activity achieved (GBq/nmol)	Maximum theoretical specific activity (GBq/nmol)
[Lys^{40}(DTPA)]exendin-3	0.73	1.72
Hexendin(40)	0.69	1.72
Hexendin(45)	0.67	1.72
Hexendin(40+41)	1.66*	3.44
Hexendin(40+45)	1.32	3.44
Hexendin(40-45)	5.54	10.33

* The labeling is not reproducible, and varies from 0.85 GBq/nmol to 4.24 GBq/nmol.

Competitive binding assay

In Figure 1 the results of the competitive binding assay on CHL-GLP-1R cells are shown. The IC_{50} values of all peptides were in the low nanomolar range. The IC_{50} of hexendin(40) and hexendin(45) were 5.2 and 6.3 nM respectively. The IC_{50} of hexendin(40+45), hexendin(40+41) and hexendin(40-45) were 10.1 , 19.2 and 69.5 nM, respectively. All peptides, except hexendin(40), had a significantly lower affinity for the receptor than the reference peptide (4.4 nM, $p < 0.05$).

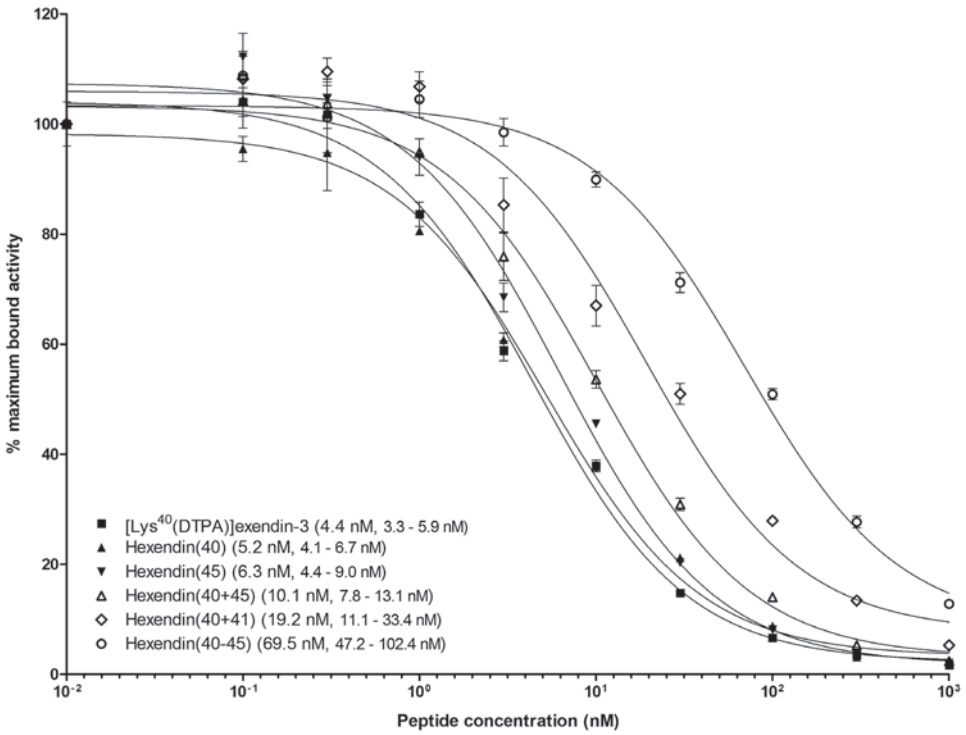

Figure 1. Curves of the competitive binding assay (IC_{50}) on CHL-GLP-1R cells. ^{111}In-labeled [Lys^{40}(DTPA)]-exendin-3 was used as radiotracer. The IC_{50} values and 95% confidence intervals in nM are given between parentheses ().

Biodistribution at equimolar doses

Figure 2 shows the biodistribution of all ^{111}In-labeled exendin analogs (at a peptide dose of 20 pmoles) in BALB/c nude mice with a subcutaneous INS-1 tumor two hours post injection. ^{111}In-labeled [Lys^{40}(DTPA)]exendin-3 showed the highest uptake (33.8 ± 7.6 %ID/g) in the INS-1 tumor. C-terminal addition of six lysine residues (hexendin(40)) reduced the tumor uptake to 19.8 ± 5.8 %ID/g ($p<0.05$). Conjugation of multiple DTPA molecules did not affect the tumor uptake significantly compared to hexendin(40) (hexendin(40+45): 15.9 ± 1.3 %ID/g, hexendin(40+41): 22.9 ± 7.3 %ID/g, hexendin(40-45): 19.9 ± 9.2 %ID/g). The pancreatic uptake of hexendin(40) (7.60 ± 1.50 %ID/g) was lower than that of [Lys^{40}(DTPA)]exendin-3 (11.97 ± 4.04 %ID/g). Hexendin with two or more DTPA molecules showed similar pancreatic uptake as [Lys^{40}(DTPA)]exendin-3: hexendin(40+41) (10.77 ± 2.87 %ID/g) and hexendin(40-45) (9.77 ± 2.72 %ID/g). Accumulation in the tumor and the pancreas could be blocked by an excess of unlabeled exendin-3, proving GLP-1R mediated uptake for all compounds. Furthermore, the lungs, stomach and duodenum also showed receptor-mediated uptake of exendin-3. Renal uptake of all peptides was high and could not be blocked by an excess of unlabeled exendin-3.

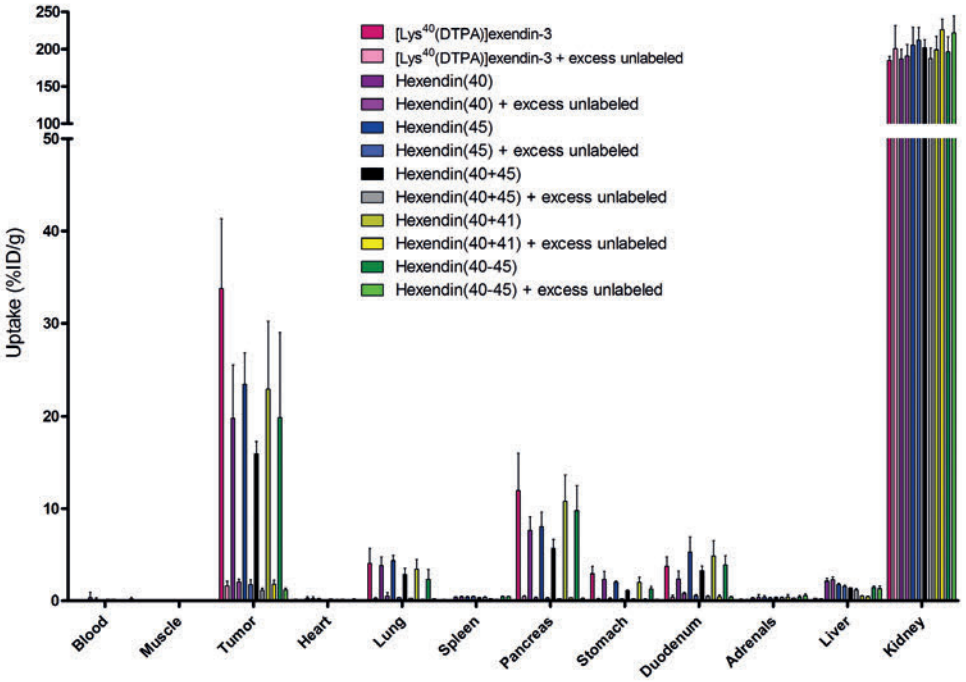

Figure 2. Biodistribution of ^{111}In-labeled exendin-3 derivatives in BALB/c nude mice bearing a subcutaneous INS-1 tumor. Values are expressed as a percentage of the injected dose per gram of tissue (n=5 mice per group, error bars SD).

Biodistribution at different molar doses

In order to assess whether the uptake of the tracer in the pancreas could be further enhanced by reducing the administered peptide dose, the biodistribution of 20 pmol of the reference peptide was compared to that of 4 pmol of hexendin(40+41) and hexendin(40-45) (Figure 3). When the standard [Lys^{40}(DTPA)]exendin-3 dose of 20 pmol was given, the uptake in tumor was 28.3 ± 12.2 %ID/g. A peptide dose of 4 pmol resulted in a tumor uptake of 23.7 ± 5.8 and 16.7 ± 3.3 %ID/g, respectively for hexendin(40+41) and hexendin(40-45), which was not significantly different. Pancreatic uptake was 13.3 ± 1.9 %ID/g for [Lys^{40}(DTPA)]exendin-3 at the standard peptide dose, while this was 9.5 ± 1.7 and 9.8 ± 2.2 %ID/g for hexendin(40+41) ($p<0.05$) and hexendin(40-45) ($p<0.05$) respectively, at a peptide dose of 4 pmol. Renal uptake did not change significantly.

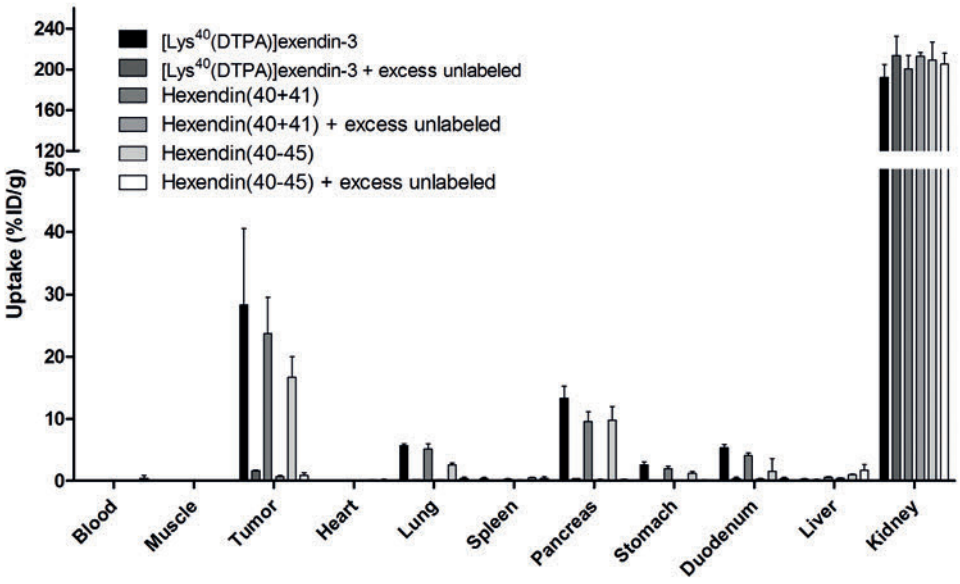

Figure 3. Biodistribution of ^{111}In-labeled [Lys^{40}(DTPA)]exendin-3 (20 pmol), hexendin(40+41) (4 pmol) and hexendin(40-45) (4 pmol) in BALB/c nude mice with a subcutaneous INS-1 tumor. Values are expressed as %ID/g (n=5 mice per group, error bars SD).

SPECT

Addition of multiple DTPA molecules allowed for labeling at a higher molar activity. Therefore, in the final experiment, we radiolabeled hexendin(40-45) at a high molar activity and we investigated whether visualization of the pancreas with SPECT could be improved by administering a higher activity dose (at equimolar peptide doses), compared to labeling of hexendin(40-45) or [Lys^{40}(DTPA)]exendin-3 at a low molar activity. Figure 4 shows the biodistribution profiles of ^{111}In-labeled [Lys^{40}(DTPA)]exendin-3 and hexendin(40-45) in BN rats. Pancreatic uptake was higher for [Lys^{40}(DTPA)]exendin-3 (0.17 ± 0.05 %ID/g) than for hexendin(40-45), either labeled at a low (LA) or high (HA) molar activity (0.09 ± 0.01 ($p<0.01$) and 0.10 ± 0.02 %ID/g ($p<0.05$) respectively). The absolute uptake in pancreas and kidneys was assessed for all three tracers and is shown in Figure 5. The absolute pancreatic uptake of [Lys^{40}(DTPA)]exendin-3 (28.8 ± 6.0 kBq) and hexendin(40-45) (19.9 ± 1.5 kBq) did not differ significantly, when labeled at the same molar activity. However, injection with a high activity dose of hexendin(40-45) resulted in an absolute uptake in the pancreas which was 9 times higher than injection of a low activity dose (182.7 ± 42.3 kBq compared to 19.9 ± 1.5 kBq, $p<0.001$). The absolute renal uptake was six-fold higher: 42.52 ± 2.68 MBq vs. 7.17 ± 3.16 MBq ($p<0.001$). Typical images of rats injected with [Lys^{40}(DTPA)]exendin-3 or hexendin(40-45), labeled at a low molar activity are shown in Figure 6A and 6B. The image quality improved when hexendin(40-45) with a high molar activity was

administered (Figure 6C). The pancreas-to-background ratio (Figure 7) increased to 18.8 ± 4.3 for hexendin(40-45) (HA), compared to 6.6 ± 1.9 for [Lys^{40}(DTPA)]exendin-3 (LA) and 10.9 ± 2.2 for hexendin(40-45) (LA). ($p<0.001$).

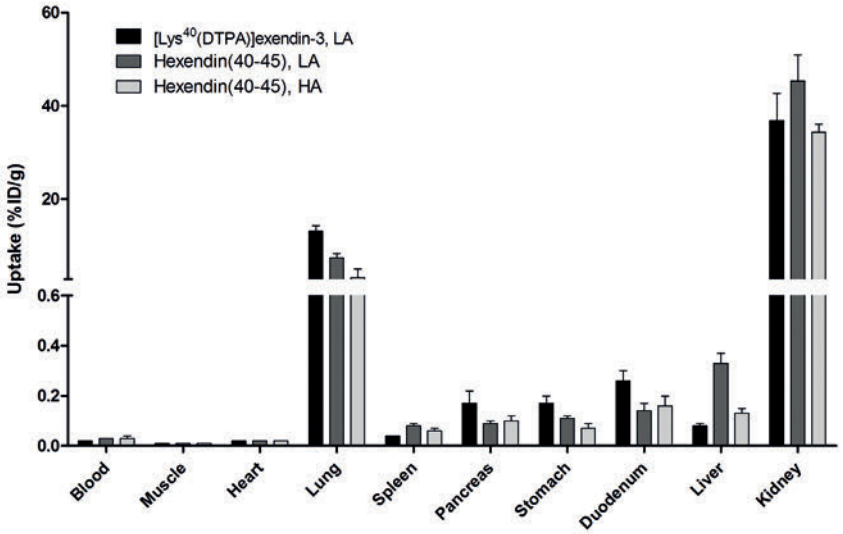

Figure 4. Biodistribution of ^{111}In-labeled [Lys^{40}(DTPA)]exendin-3 and hexendin(40-45) in Brown Norway rats. Values are expressed as %ID/g (n=5 rats per group for the LA (low activity) and n=4 rats per group for the HA (high activity), error bars SD).

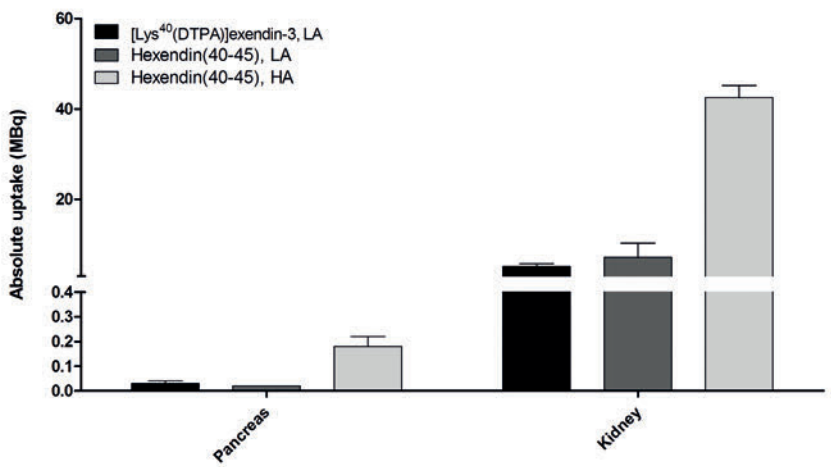

Figure 5. Absolute uptake of ^{111}In-labeled [Lys^{40}(DTPA)]exendin-3 and hexendin(40-45) in pancreas and kidney.

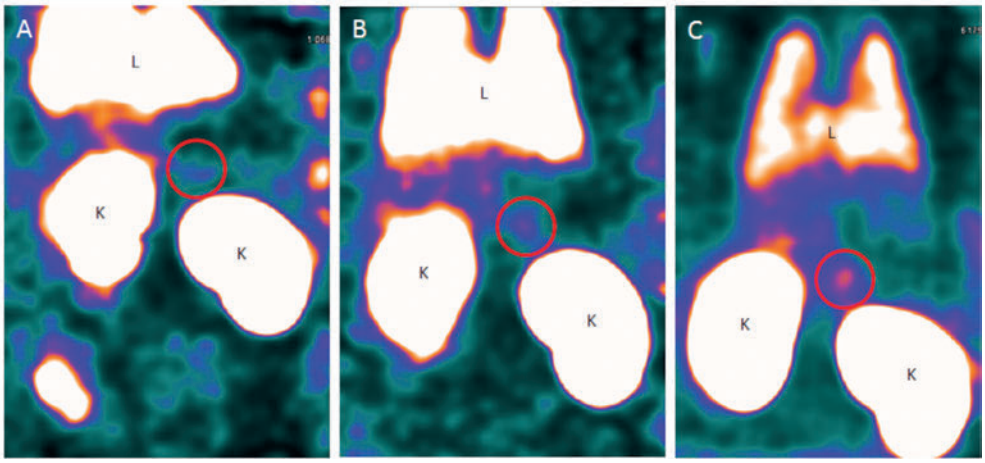

Figure 6. Coronal slices of SPECT images of Brown Norway rats, obtained two hours after injection of the peptide. (A) 20 pmol ^{111}In-labeled [Lys^{40}(DTPA)]exendin-3 (19.1 ± 2.4 MBq) (B) 20 pmol ^{111}In-labeled hexendin(40-45) (18.4 ± 0.2 MBq) (C) 20 pmol ^{111}In-labeled hexendin(40-45) (149.1 ± 3.8 MBq). Lungs are indicated with L, kidneys with K and the pancreas is delineated with a red circle.

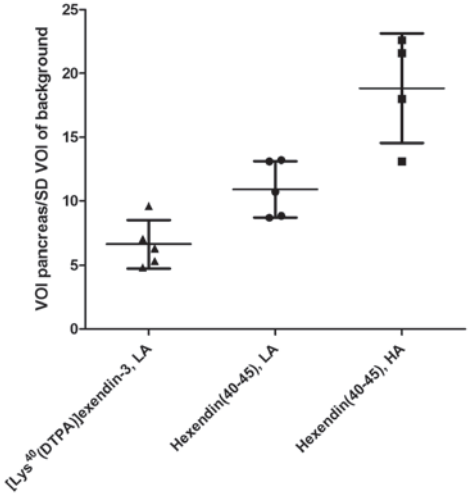

Figure 7. Signal-to-background ratio.

DISCUSSION

In this study, a novel exendin analog was presented that can be labeled at a seven-fold higher molar activity as compared to [Lys^{40}(DTPA)]exendin-3. The relative pancreatic uptake of this new tracer with six lysine and DTPA moieties (expressed as %ID/g) in mice was comparable to that of the reference peptide, however, the absolute activity uptake of hexendin(40-45) in the pancreas was nine-fold higher. This increased pancreas activity resulted in an almost three-fold improvement of the signal-to-background ratio of the images and clearly improved pancreas visualization.

Breeman *et al*. optimized labeling conditions to reach higher molar activities to avoid receptor saturation or pharmacological (side)effects [21]. When using optimal labeling conditions, like metal-free materials, appropriate temperatures or buffers still leaves room for improvement, a modification of the compound is an additional approach to enhance the molar activity.

Conjugation of five extra lysine residues to the C-terminus of [Lys^{40}(DTPA)]exendin-3 allowed to attach multiple DTPA moieties. The $^{111}InCl_3$ incorporation in hexendin(40-45) was twenty percent more efficient, relatively, than in the reference peptide, leading to a very clear absolute increase in molar activity from 0.73 GBq/nmol to 5.54 GBq/nmol.

The increased molar activity obtained in this study allowed us to administer either lower amounts of peptide or higher amounts of radioactivity at equal peptide doses of the tracer. Although lowering the peptide dose did not lead to an increased relative accumulation in target tissues, injecting a higher amount of radioactivity led to enhanced absolute accumulation of radiolabeled exendin. Background activity increased to a lesser extent, resulting in improved target-to-background ratios and improved visualization of the pancreas on SPECT. This represents a clear improvement for *in vivo* imaging as low peptide doses of exendin should be administered to avoid receptor saturation [14]; as stated previously, this is of even more importance for beta cell quantification in the pancreas of diabetic individuals with lower BCM and thus a lower number of GLP-1R available for binding.

Although administration of higher ligand doses may be possible in clinical studies, also for peptides or antibodies which are biologically active, like exendin, it is of great interest to administer low pharmacological doses to limit the potential (biological) side-effects of the tracer. Using hexendin(40-45) for instance, the peptide dose administered to patients could be reduced almost seven times, thereby preventing side-effects, while maintaining a sufficient amount of radioactivity (150 MBq).

A disadvantage of multi-chelated compounds is the higher radioactivity accumulation in the kidneys. In preclinical imaging studies this is not a limiting factor, while in clinical studies this would result in unfavorably high radiation doses to the kidneys.

In our view, the multi-chelation approach presented here has high translational potential, because it is widely applicable, not only for different SPECT tracers, but also for PET tracers and other peptides or antibodies. When the labeling procedure of an antibody, for example, is

restricted to a low temperature, the multi-chelation approach could help to improve the molar activity. In addition, several antibody-based imaging agents are also limited by the protein dose that can be administered without saturating the tumor-associated receptor (e.g. PD-L1, IGF-1R) [22, 23]. Also, for evaluation of tracer molecules, this technology facilitates determination of optimal (low) tracer doses *in vivo*.

The concept of conjugating more than one chelator molecule to one mole of antibody was demonstrated almost three decades ago. In the respective study from Boniface *et al.*, an increase in molar activity was found by increasing the cDTPA:MAb (monoclonal antibody) conjugation ratio [24]. A major difference between their study and the study presented here, is the conjugation method. When conjugating antibodies, the chelator moieties are randomly bound to the antibody, possibly in the binding domain and thereby influencing the affinity or immunoreactivity of the antibody. In the present study, the DTPA moieties were conjugated site-specifically to additional Lysine residues. By F-moc protection of the lysines that should not be conjugated, random conjugation interference in the binding domain was prevented.

Multi-chelated compounds should, at least theoretically, also be more sensitive in detecting tumors with a very low receptor density, or very small tumors or metastases, since more radioactivity can be delivered per receptor molecule while uptake in non-receptor expressing background remains low. In addition, this approach may help to make radiotracers suitable for autoradiography studies as the detection limit of autoradiography is dependent on target saturation and thus limits the tracer amount used. Finally, the potential of non-internalizing peptides with antagonistic features for tumor detection might be increased by improving radioactivity accumulation (which is lower due to lack of internalization) in the target tissue.

In conclusion, despite slightly decreased relative uptake of the tracer in the pancreas in rats, our multi-chelator approach led to an increase in signal-to-background ratio as a result of the improved molar activity. The higher target organ radioactivity accumulation led to improved visibility of pancreatic tissue in SPECT images in rodents. This technology may represent a major asset for reliable quantitative measurements of BCM *in vivo* for diabetes research. Moreover, this approach has great potential for translation to other peptides and chelators/radionuclides, where it is essential to perform examination with high molar activity.

ACKNOWLEDGEMENTS

We thank Bianca Lemmers, Kitty Lemmens, Iris Lamers-Elemans and Henk Arnts (Central Animal Facility, Radboud university medical center, Nijmegen, The Netherlands) for their expertise in the *in vivo* studies.

Our work was supported by NIH grant 1R01 AG 030328-01, the European Union's Seventh Framework Programme project BetaImage, under grant agreement No. 222980 and project BetaCure, under agreement No. 602812.

REFERENCES

1. http://www.who.int/mediacentre/factsheets/fs312/en/.
2. Gotthardt M, Eizirik DL, Cnop M, Brom M. Beta cell imaging - a key tool in optimized diabetes prevention and treatment. *Trends Endocrinol Metab.* **2014**; 25 (8): 375-377.
3. Brom M, Andralojc K, Oyen WJ, Boerman OC, Gotthardt M. Development of radiotracers for the determination of the beta-cell mass in vivo. *Current pharmaceutical design.* **2010**; 16 (14): 1561-1567.
4. Krogvold L, Edwin B, Buanes T, Ludvigsson J, Korsgren O, Hyoty H, *et al.* Pancreatic biopsy by minimal tail resection in live adult patients at the onset of type 1 diabetes: experiences from the DiViD study. *Diabetologia.* **2014**; 57 (4): 841-843.
5. Gotthardt M. Beta cell imaging--why we need it and what has been achieved. *Current pharmaceutical design.* **2010**; 16 (14): 1545-1546.
6. Eriksson O, Laughlin M, Brom M, Nuutila P, Roden M, Hwa A, *et al.* In vivo imaging of beta cells with radiotracers: state of the art, prospects and recommendations for development and use. *Diabetologia.* **2016**; 59 (7): 1340-1349.
7. Andralojc K, Srinivas M, Brom M, Joosten L, de Vries IJ, Eizirik DL, *et al.* Obstacles on the way to the clinical visualisation of beta cells: looking for the Aeneas of molecular imaging to navigate between Scylla and Charybdis. *Diabetologia.* **2012**; 55 (5): 1247-1257.
8. Goke B. What are the potential benefits of clinical beta-cell imaging in diabetes mellitus? *Current pharmaceutical design.* **2010**; 16 (14): 1547-1549.
9. A, Schibli R, Behe M. Targets and probes for non-invasive imaging of beta-cells. *European journal of nuclear medicine and molecular imaging.* **2016**;
10. Moore A. Advances in beta-cell imaging. *European journal of radiology.* **2009**; 70 (2): 254-257.
11. Brom M, Woliner-van der Weg W, Joosten L, Frielink C, Bouckenooghe T, Rijken P, *et al.* Non-invasive quantification of the beta cell mass by SPECT with In-labelled exendin. *Diabetologia.* **2014**;
12. Lankat-Buttgereit B, Goke R, Stockmann F, Jiang J, Fehmann HC, Goke B. Detection of the human glucagon-like peptide 1(7-36) amide receptor on insulinoma-derived cell membranes. *Digestion.* **1994**; 55 (1): 29-33.
13. Reubi JC, Waser B. Concomitant expression of several peptide receptors in neuroendocrine tumours: molecular basis for in vivo multireceptor tumour targeting. *European journal of nuclear medicine and molecular imaging.* **2003**; 30 (5): 781-793.
14. Brom M, Oyen WJ, Joosten L, Gotthardt M, Boerman OC. 68Ga-labelled exendin-3, a new agent for the detection of insulinomas with PET. *European journal of nuclear medicine and molecular imaging.* **2010**; 37 (7): 1345-1355.
15. Wild D, Behe M, Wicki A, Storch D, Waser B, Gotthardt M, *et al.* [Lys40(Ahx-DTPA-111In)NH2] exendin-4, a very promising ligand for glucagon-like peptide-1 (GLP-1) receptor targeting. *Journal of nuclear medicine : official publication, Society of Nuclear Medicine.* **2006**; 47 (12): 2025-2033.

16. Thorkildsen C, Neve S, Larsen BD, Meier E, Petersen JS. Glucagon-like peptide 1 receptor agonist ZP10A increases insulin mRNA expression and prevents diabetic progression in db/db mice. *The Journal of pharmacology and experimental therapeutics*. **2003**; 307 (2): 490-496.

17. Brom M, Joosten L, Oyen WJ, Gotthardt M, Boerman OC. Improved labelling of DTPA- and DOTA-conjugated peptides and antibodies with 111In in HEPES and MES buffer. *EJNMMI research*. **2012**; 2 4.

18. Brom M, Franssen GM, Joosten L, Gotthardt M, Boerman OC. The effect of purification of Ga-68-labeled exendin on in vivo distribution. *EJNMMI research*. **2016**; 6 (1): 65.

19. Asfari M, Janjic D, Meda P, Li G, Halban PA, Wollheim CB. Establishment of 2-mercaptoethanol-dependent differentiated insulin-secreting cell lines. *Endocrinology*. **1992**; 130 (1): 167-178.

20. van Hoorn RA, Vriens D, Postema JW, Arens AI, Pfestroff A, Oyen WJ, *et al*. The influence of SPECT reconstruction algorithms on image quality and diagnostic accuracy in phantom measurements and 99mTc-sestamibi parathyroid scintigraphy. *Nuclear medicine communications*. **2014**; 35 (1): 64-72.

21. Breeman WA, De Jong M, Visser TJ, Erion JL, Krenning EP. Optimising conditions for radiolabelling of DOTA-peptides with 90Y, 111In and 177Lu at high specific activities. *European journal of nuclear medicine and molecular imaging*. **2003**; 30 (6): 917-920.

22. Heskamp S, Hobo W, Molkenboer-Kuenen JD, Olive D, Oyen WJ, Dolstra H, *et al*. Noninvasive Imaging of Tumor PD-L1 Expression Using Radiolabeled Anti-PD-L1 Antibodies. *Cancer research*. **2015**; 75 (14): 2928-2936.

23. Heskamp S, van Laarhoven HW, Molkenboer-Kuenen JD, Franssen GM, Versleijen-Jonkers YM, Oyen WJ, *et al*. ImmunoSPECT and immunoPET of IGF-1R expression with the radiolabeled antibody R1507 in a triple-negative breast cancer model. *Journal of nuclear medicine : official publication, Society of Nuclear Medicine*. **2010**; 51 (10): 1565-1572.

24. Boniface GR, Izard ME, Walker KZ, McKay DR, Sorby PJ, Turner JH, *et al*. Labeling of monoclonal antibodies with samarium-153 for combined radioimmunoscintigraphy and radioimmunotherapy. *Journal of nuclear medicine : official publication, Society of Nuclear Medicine*. **1989**; 30 (5): 683-691.

CHAPTER 6

Efficient reduction of renal uptake of radiolabeled exendin

Lieke Joosten[1], Cathelijne Frielink[1], Tom Jansen[1], Daphne Lobeek[1], Fritz Andreae[2], Sandra Heskamp[1], Martin Gotthardt[1] & Maarten Brom[1]

1 Department of Radiology and Nuclear Medicine, Radboud University Medical Center, Nijmegen, The Netherlands
2 Forschungs- und Entwicklungs GmbH, piCHEM, Grambach, Austria

Manuscript in preparation

ABSTRACT

PET/CT imaging of the glucagon-like peptide-1 receptor (GLP-1R) using radiolabeled exendin is a highly promising imaging method to detect insulinomas. However, high renal accumulation of radiolabeled exendin could hamper the detection of small insulinomas in close proximity to the kidneys. We report a new exendin analog with a cleavable methionine-isoleucine (Met-Ile-Mal) linker to reduce renal uptake. We performed *ex vivo* biodistribution and PET/CT studies to assess uptake of this radiolabeled tracer in insulinomas, kidneys, and pancreas.

The C-terminus of exendin-4 was extended with a Met-Ile-linker, to which NOTA was conjugated (NOTA-MI-exendin-4). Exendin-4 with conjugated NOTA was used as control (NOTA-exendin-4). The affinity of both peptides for the GLP-1R was determined in a competitive binding assay using GLP-1R transfected CHL cells. The renal retention of ^{68}Ga-labeled compounds was compared in non-tumor bearing C3H mice. Subsequently, the tumor uptake in INS-1 tumor-bearing BALB/c nude mice was determined with *ex vivo* biodistribution and visualized by PET/CT.

The affinity for the GLP-1R was 9.6 and 4.0 nM for NOTA-exendin-4 and NOTA-MI-exendin-4, respectively. In C3H mice, a significantly lower uptake of ^{68}Ga-labeled NOTA-MI-exendin-4 in the kidneys 4 hours post injection (72.7 ± 3.9 %ID/g) was observed, compared to NOTA-exendin-4 (207.7 ± 17.4 %ID/g) ($p<0.0001$). [^{68}Ga]Ga-NOTA-MI-exendin-4 uptake in INS-1 tumors was stable over time (29.3 ± 6.9 %ID/g at 1 hour and 25.0 ± 8.0 %ID/g at 4 hours p.i.) and was similar to tumor uptake of [^{68}Ga]Ga-NOTA-exendin-4 (27.8 ± 4.9 %ID/g at 1 hour and 24.9 ± 9.3 %ID/g at 4 hours p.i.). For both tracers, INS-1 tumors were clearly visualized using PET/CT, while kidney uptake was significantly lower for [^{68}Ga]Ga-NOTA-MI-exendin-4 in comparison to [^{68}Ga]Ga-NOTA-exendin-4.

[^{68}Ga]Ga-NOTA-MI-exendin-4 showed reduced renal retention, while preserving INS-1 tumor uptake. Therefore, this promising new tracer might improve the sensitivity of PET/CT to detect insulinomas.

INTRODUCTION

Insulinomas are functioning neuroendocrine tumors, which originate from the beta cells in the pancreatic islets of Langerhans. Although the incidence of insulinomas is very low (0.4%), and only a small percentage of insulinomas are malignant (>90% of the insulinomas is benign), the clinical symptoms, namely hypoglycemia, are severe and require adequate treatment[1, 2]. Accurate localization of insulinomas to guide therapeutic intervention is essential. Currently, the treatment of choice for insulinomas is surgical removal of the lesion or partial pancreatectomy. Since 10% to 27% of insulinomas are not detected intraoperatively[2], preoperative and/or intraoperative localization of insulinomas is of pivotal importance to identify the tumor lesion and to minimize unnecessary surgical intervention. A highly promising recently developed clinical imaging strategy to visualize insulinomas and native beta cells in the pancreas is based on glucagon-like peptide-1 receptor (GLP-1R) targeting using radiolabeled exendin and either SPECT/CT or PET/CT[3-5]. The GLP-1R is highly and specifically expressed on beta cells and is therefore the most promising target for the detection of (benign) insulinomas. Furthermore, recent studies suggest that this imaging method is preferred over somatostatin receptor scintigraphy (SRS)[4]. Exendin-4 is a stable analog of the natural, unstable GLP-1 ligand and binds with high affinity to the GLP-1R. In addition to high accumulation in insulinomas, radiolabeled exendin-4 also shows high renal uptake, as a result of tubular reabsorption in the kidneys.

In certain cases, high renal uptake may be of concern as insulinomas are often very small in size (≤ 2 cm)[1, 2] and located in close proximity to the kidneys, especially lesions located in the pancreatic tail, as demonstrated by several clinical trials [3, 4, 6, 7]. This may hamper visualization of these lesions. Another concern is that [^{68}Ga]Ga-exendin PET scans of patients can display a white halo around the kidneys, a serious reconstruction artefact as a result of the high kidney uptake[8]. Obviously, these artefacts can hamper the detection of tumor lesions, but cannot be solved currently by using different reconstruction algorithms.

Over the past years, several successful strategies to reduce renal uptake of radiolabeled peptides have been described. For example, van Eerd *et al.*, were the first to show reduced renal uptake of ^{111}In-labeled octreotide by pre-injection of Gelofusine[9]. Likewise, Vegt *et al.* obtained the same results in human volunteers[10]. Furthermore, Hammond *et al.*, used the amino acids lysine and arginine to block the tubular re-uptake of [^{111}In]In-DTPA-octreotide[11], which was also shown to be effective in patients with neuroendocrine tumors[12]. In a rat study, Gelofusine was shown to reduce renal uptake of ^{111}In-labeled exendin by almost 19%[13]. A similar effect was found in human volunteers[14]. Blocking the tubular reabsorption of radiolabeled exendin using amino acids is, however, not effective[13]. Thus, in order to further reduce the kidney uptake of radiolabeled exendin, a new approach is demanded.

Wu *et al.* have shown that a methionine conjugate, labeled with gallium-67, was rapidly excreted from the kidneys[15]. Based on the conclusions of the latter study, Uehara *et al.*

reported a methionine-isoleucine linker between NOTA and a Fab fragment of a mAb against HER2. They observed a reduction in kidney uptake of almost 88%, which could be attributed to the additional linker that was introduced[16]. These two studies evoked the question whether the translation of the methionine-isoleucine linker to exendin-4 could help to reduce the renal uptake of exendin.

The purpose of this study is to develop and characterize a novel exendin analog, which is based on NOTA-exendin-4, with an additional methionine-isoleucine linker between the chelator and the peptide (NOTA-MI-exendin-4). The peptide has been labeled with gallium-68 and its uptake in kidneys, pancreas and GLP-1R-expressing tumors in mice was compared to ^{68}Ga-labeled NOTA-exendin-4 by *ex vivo* biodistribution and PET/CT studies. Furthermore, this concept was validated using a different chelator (NODAGA) and a different radiometal (indium-111).

MATERIALS AND METHODS

Peptides and radionuclides

NOTA-exendin-4, Lys^{40}[Mep((S-)NOTA-**M**et-**I**le-Mal-)] exendin-4 (referred to as NOTA-MI-exendin-4), NODAGA-exendin-4, Lys^{40}[Mep((S-)NODAGA-**M**et-**I**le-Mal-)]exendin-4 (referred to as MI-NODAGA-exendin-4) and [Lys^{40}(DTPA)]exendin-3 were purchased from piCHEM (Graz, Austria).

Control peptides [Lys^{40}(DTPA)]exendin-3, [Lys^{40}(NOTA)]exendin-4 and [Lys^{40}(NODAGA)]exendin-4 (piCHEM) were conjugated with p-NCS-benzyl-functionalized DTPA, NOTA or NODAGA to the ε-amino group of the lysine at position 40.

To obtain NOTA-MI-exendin-4 and NODAGA-MI-exendin-4, exendin-4 was modified with a Mep (mercapto-proionic acid) at the lysine side chain at position 40. The spacer molecule, methionyl-isoleucine was modified at the C-terminus with N-(2-aminoethyl)maleimide as the thiol reactive cross-linker, whereas the corresponding chelator (NOTA-Bn-SCN or NODAGA-Bn-SCN) was attached at the N-terminus of methionine. Finally, the chelator-spacer group was conjugated via the maleimide to the mercapto-propionyl moiety at the lysine of exendin-4 at position 40. An overview of the structure of these peptides is given in Figure 1 and Table 1.

$^{111}InCl_3$ was obtained from Mallinckrodt Medical (Petten, The Netherlands) and ^{68}Ga was eluted from a ^{68}Ge/^{68}Ga generator (GalliaPharm Generator, Eckert & Ziegler Eurotope, Berlin, Germany) with 0.1 M HCl (Rotem GmbH, Israel) at a flow rate of 1mL/min.

Table 1. Name, abbreviation, molecular mass and amino acid sequence of exendin-4 derivatives.

Peptide	Abbreviation	Molecular weight (Da)	Amino Acid sequence
[Lys^{40}(DTPA)]-exendin-3	DTPA-exendin-3	4816.3	HSDGTGTSDLSKQMEEEAVRLFIEWLKNGGPSSGAPPPS-K(DTPA)-NH_2
Exendin-4	Exendin-4	4186.6	HGEGTFTSDLSKQMEEEAVRLFIEWLKNGGPSSGAPPPS-NH_2
[Lys^{40}(NODAGA)]-exendin-4	NODAGA-exendin-4	4673.6	HGEGTFTSDLSKQMEEEAVRLFIEWLKNGGPSSGAPPPS-**K(NODAGA-Bn-SCN)-**NH_2
Lys^{40}[Mep[(S-)NODAGA-Met-Ile-Mal-)]-exendin-4	NODAGA-MI-exendin-4	5308.95	HGEGTFTSDLSKQMEEEAVRLFIEWLKNGGPSSGAPPPS-**K(Mep[NODAGA-Bn-SCN-Met-Ile-Mal])-**NH_2
[Lys^{40}(NOTA)]-exendin-4	NOTA-exendin-4	5237.1	HGEGTFTSDLSKQMEEEAVRLFIEWLKNGGPSSGAPPPS-**K(NOTA-Bn-SCN)-**NH_2
Lys^{40}[Mep[(S-)NOTA-Met-Ile-Mal-)]-exendin-4	NOTA-MI-exendin-4	4765.3	HGEGTFTSDLSKQMEEEAVRLFIEWLKNGGPSSGAPPPS-**K(Mep[NOTA-Bn-SCN-Met-Ile-Mal])-**NH_2

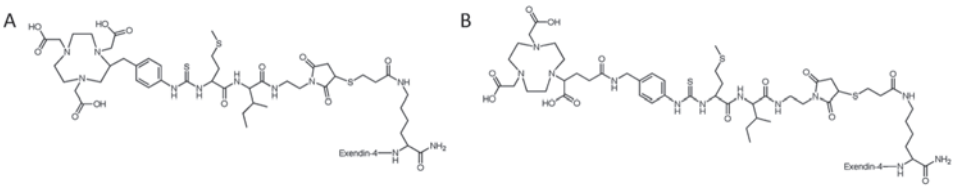

Figure 1. Structures of NOTA-MI-exendin (A) and NODAGA-MI-exendin-4 (B).

Radiolabeling of exendin-4 analogs with ^{68}Ga

The peptides were labeled with ^{68}Ga by adding 2.5 M HEPES (4-(2-hydroxyethyl)-1-piperazineethanesulfonic acid, Sigma Aldrich) to 35-100 MBq ^{68}Ga in Ultrapure 0.1 M HCl and 1 µg of peptide. After incubation at 95°C for 5 min, EDTA and Tween-80 were added to a final concentration of 5 mM and 0.1%, respectively. Quality control was performed by RP-HPLC (reversed-phase high performance liquid chromatography) and ITLC (instant thin layer chromatography). RP-HPLC was done using a C_{18} reversed-phase column (Alltima; 4.6 mm x 25 cm; Grace, Breda, The Netherlands). For elution a linear gradient of 0.1% TFA (trifluoroacetic acid, Lab-Scan, Analytical Sciences, Brussels, Belgium) in acetonitrile (3% to 100% over 10 min) with a flow rate of 1 ml/min was used. ^{68}Ga-colloid content was determined with ITLC: 1.25 M NH_4Ac, pH 5.5: dimethylformamide (DMF) (1:1) (R_f ^{68}Ga-hydroxide = 0, R_f ^{68}Ga-labeled peptide and ^{68}Ga-EDTA = 1)[17]. Purification was performed by solid-phase extraction using an HLB (hydrophilic-lipophilic balance reversed-phase sorbent) cartridge (Waters Oasis©, Milford, MA, USA). Activation and washing of the cartridge was done with 100% ethanol and water, respectively.

Radiolabeling of DTPA-exendin-3, NOTA-exendin-4 and NOTA-MI-exendin-4 with ^{111}In

DTPA-exendin-3, NOTA-exendin-4 and NOTA-MI-exendin-4 were labeled with ^{111}In by mixing 150, 30 and 30 MBq of $^{111}InCl_3$, respectively, with 0.5 M MES (2-(*N*-morpholino) ethanesulfonic acid, Sigma Aldrich, St. Louis, MO, USA), pH 5.5 and 1 µg of the respective peptide, followed by incubation at room temperature for 20 min. After labeling, Tween-80 and 50 mM EDTA (ethylenediaminetetraacetic acid) (Sigma Aldrich) were added to a final concentration of 0.1% and 5 mM, respectively. Purification was performed by solid-phase extraction using an HLB column and washing and conditioning of the cartridge was done with 1 ml 0.5 M MES. The labeling efficiency was analyzed using instant thin layer chromatography on silica-gel strips (ITLC-SG Biodex, Shirley, NY, USA) using 0.1 M EDTA in 0.1 M NH_4Ac as a mobile phase (R_f ^{111}In-labeled peptide = 0, R_f ^{111}In-EDTA = 1).

Serum stability of ^{68}Ga-labeled exendin-4 analogs

NOTA-MI-exendin-4, NOTA-exendin-4, NODAGA-MI-exendin-4 and NODAGA-exendin-4 were labeled with ^{68}Ga at a specific activity of 60, 35, 100 and 35 MBq/µg respectively and quality

control and purification was performed as described above. The radiolabeled compounds were incubated in human serum (1:10) at 37°C and samples were taken after 1 and 2 hour incubation. Supernatant was analyzed using RP-HPLC after acetonitrile precipitation of the proteins. RP-HPLC was performed as described previously.

Cell culture

CHL-cells transfected with the human GLP-1R (a kind gift of Brigitte Lankat-Buttgereit, Marburg, Germany) were maintained in Dulbecco's Modified Eagle's Medium (DMEM) GlutaMAX (Gibco, Invitrogen, Breda, The Netherlands), supplemented with 10% fetal calf serum, 100 units/ml penicillin, Geneticin (G418) sulphate solution (0.5 mg/ml final concentration), 100 µg/ml streptomycin, 1 mM sodiumpyruvate and 0.1 mM non-essential amino acids. The INS-1 cell line (rat insulinoma) was maintained in RPMI-1640 medium supplemented with 10% fetal bovine serum, 2 mM glutamine, 10 mM HEPES, 50 µM β-mercaptoethanol, 1 mM sodium pyruvate, 100 units/ml penicillin and 100 µg/ml streptomycin[18]. Cells were maintained in a humidified 5% CO_2 atmosphere at 37 °C.

Competitive binding assay (IC_{50})

A competitive binding assay using CHL-GLP-1R cells was performed to compare the affinity of both MI-peptides with their respective control peptides. Cells were grown to confluency overnight at 37°C, after plating $1x10^6$ cells per well in a 6-wells plate. Cells were washed with binding buffer (DMEM GlutaMAX + 0.5% bovine serum albumin) and a trace amount of ^{111}In-labeled DTPA-exendin-3 (150 MBq/µg, as previously described) (0.8 kBq, 0.9 fmol) was added to the cells, together with increasing amounts of unlabeled NOTA-exendin-4, NOTA-MI-exendin-4, NODAGA-exendin-4 or NODAGA-MI-exendin-4, ranging from 0.1 to 1000 nM. After incubation for 4 h at 0°C, cells were washed twice with binding buffer, harvested with 0.1 M NaOH and cell associated activity was measured in a gamma counter (WIZARD, 2480 Automatic Gamma Counter, Perkin Elmer, Boston, MA, USA). The IC_{50} value (half-maximal inhibitory concentration) was calculated using GraphPad Prism using one-site competition (version 5.03, GraphPad Software, San Diego California USA).

Animal studies

The project (2015-0071) was approved by the Nijmegen Medical Center animal ethics committee (RUDEC) and the Dutch animal ethics comittee (CCD) of the Radboud University and performed according to the Institute of Laboratory Animal Research Guidelines.

C3H mice were purchased from Charles River Laboratories (L'Arbresle, France) and BALB/cRJ nu mice from Janvier (Saint-Berthevin, France).

Mice were housed in a pathogen-free environment in ventilated filter-topped cages (5 mice per cage), had *ad libitum* access to water and chow and were allowed to adapt to laboratory conditions for 1 week before the start of the experiments.

Biodistribution of [^{68}Ga]Ga-NOTA-exendin-4 and [^{68}Ga]Ga-NOTA-MI-exendin-4 in healthy mice

The distribution of ^{68}Ga-labeled NOTA-exendin-4 and NOTA-MI-exendin-4 were compared in female healthy C3H mice of 8-13 weeks old. Mice were randomized into 8 groups (n = 4-5 per group,) and received an intravenous injection with 20 pmol of either [^{68}Ga]Ga-NOTA-MI-exendin-4 (1.7 MBq) or [^{68}Ga]Ga-NOTA-exendin-4 (1,4 MBq). At 1, 2 and 4 hours after injection mice were euthanized by CO_2/O_2 asphyxiation and relevant organs were dissected, weighed, and measured in a gamma-counter. For each tissue sample, the uptake was calculated and presented as the percentage of the injected dose per gram tissue (%ID/g).
Two additional groups of mice (n = 2/group) received an excess of unlabeled (2 nmol) peptide (the same peptide as the tracer) to determine non-specific uptake at 4 hours after injection.

Biodistribution and PET/CT of [^{68}Ga]Ga-NOTA-exendin-4 and [^{68}Ga]Ga-NOTA-MI-exendin-4 in mice with a subcutaneous INS-1 tumor

To assess the influence of the Met-Ile-linker on the uptake of the radiolabeled exendin-4 in tumor tissue, an experiment was conducted in male BALB/cRJ nu mice (13 weeks old) with subcutaneous INS-1 tumors. Mice were inoculated subcutaneously with 3 x 10^6 INS-1 cells in 200 µl RPMI medium and after growth of the tumor to appropriate size (approx. 0.1 cm^3) assigned randomly into groups of five animals. One, 2 and 4 hours after injection of [^{68}Ga]Ga-NOTA-MI-exendin-4 or [^{68}Ga]Ga-NOTA-exendin-4 (1.6 MBq), mice were anesthetized by isoflurane/O_2 and underwent PET/CT. Two additional groups of mice received a co-injection of the tracer with an excess of unlabeled peptide (n=2/group). PET/CT images were acquired for 30-40 min with a small-animal PET/CT scanner (Inveon™; Preclinical Solutions, Siemens Medical Solutions USA, Inc., Knoxville, TN, USA). After PET/CT acquisition, the biodistribution of the radiolabeled peptides was determined as described above. Reconstruction of the images was performed as follows: OSEM3D/SPMAP reconstruction, 256 x 256 matrix, 2 OSEM3D iterations, 18 MAP iterations and a resolution of 0.075 mm uniform variance. The settings for the CT were as following: spatial resolution 113 µm, 80 kV, 500 µA, exposure time 300 msec.

Biodistribution of [^{68}Ga]Ga-NODAGA-exendin-4 and [^{68}Ga]Ga-NODAGA-MI-exendin-4 in healthy mice

We have evaluated the combination of the methionine-isoleucine linker with NODAGA-exendin-4 in female C3H mice of 8-13 weeks old as well. The molar activity obtained with both NODAGA-conjugated peptides is higher than that of the NOTA-conjugated peptides. If there is a comparable biodistribution of NOTA-MI-exendin-4 and NODAGA-MI-exendin-4, the higher molar activity for the NODAGA-MI-peptide could be beneficial in PET/CT studies. A higher molar activity allows the injection of a higher radioactive dose at the standard peptide dose, which could lead to and enhanced absolute uptake. Mice (n = 4-5 per group) received an intravenous injection with 20 pmol of either [^{68}Ga]Ga-NOTA-MI-exendin-4 (1,7 MBq),

[^{68}Ga]Ga-NOTA-exendin-4 (1,4 MBq), [^{68}Ga]Ga-NODAGA-MI-exendin-4 (4,1 MBq) or [^{68}Ga]Ga-NODAGA-exendin-4 (3.7 MBq). At one, two and four hours after injection the biodistribution was performed as described previously. Four additional groups of mice (n = 2) received an excess of unlabeled (2 nmol) peptide (the same peptide as the tracer) to determine receptor-mediated binding and their biodistribution was determined four hours after injection.

Biodistribution of [^{111}In]In-NOTA-exendin-4 and [^{111}In]In-NOTA-MI-exendin-4 in healthy mice

The biodistribution of ^{111}In-labeled NOTA-MI-exendin-4 and NOTA-exendin-4 was determined in female C3H mice (Charles River Laboratories, Calco, Italy) of 9-10 weeks old. Mice were injected intravenously with 20 pmol of either [^{111}In]In-NOTA-MI-exendin-4 or [^{111}In]In-NOTA-exendin-4 (3,7 MBq) (n=3 per group). To determine receptor-mediated binding additional groups of mice received an excess of unlabeled NOTA-MI-exendin-4 or NOTA-exendin-4 (2 nmol) together with the labeled peptide (n=2 per group).
Four hours after injection the biodistribution was performed as described previously.

Dosimetry

Biodistribution data of [^{68}Ga]Ga-NOTA-exendin-4 and [^{68}Ga]Ga-NOTA-MI-exendin-4 in mice with a subcutaneous INS-1 tumor were used for dosimetric calculations. The kidney self-dose was calculated based on the radioactivity distribution in the kidneys. The time-integrated activity coefficients (MBq-h/MBq) were calculated using mono-exponential curve-fitting between the imaging time points. As last data point, an extrapolation of the remaining uptake value within the kidneys of 10 times the radioactive half-life of ^{68}Ga was used for NOTA-exendin-4, and 10 times the biological half-life of the peptide for NOTA-MI-exendin-4. OLINDA/EXM application (version 2.1) was used to calculate the absorbed kidney dose in mice using the 25 g RADAR model. The mice data was then used to calculate the expected absorbed kidney doses per injected activity in humans using the equation[19, 20]:

$$\left(\frac{\%IA}{organ}\right)human = \left[\left(\frac{\%IA}{g}\ mouse \times Mmouse\ (kg)\right]\right] \times \left(\frac{m\ (g)}{M\ (kg)}\right) human$$

with $\frac{\%IA}{g}$ and $\frac{\%IA}{organ}$ the percentage of the injected activity concentration and per organ, respectively, and m the organ mass and M the total human or mouse body weight. Subsequently, the extrapolated human residence times were used as input in an 80 kg male reference model in OLINDA/EXM application (Version 2.1).

Statistical analysis

All data were analyzed using GraphPad Prism software version 5.03 for Windows. The Student's t-test or the One-way ANOVA followed by a Tukey's test were used to determine significance.

For the IC_{50} binding assay the F-test was used to manually calculate significance. A *p*-value below 0.05 was considered significant. All data are presented as mean ± standard deviation.

RESULTS

Radiolabeling

Labeling of NOTA-exendin-4 and NOTA-MI-exendin-4, with ^{68}Ga resulted in a maximum specific activity up to 275 GBq/µmol and 242 GBq/µmol, respectively. After purification, radiochemical purity exceeded 98%. Labeling of NODAGA-exendin-4 and NODAGA-MI-exendin-4 with ^{68}Ga resulted in a maximum specific activity up to 457 GBq/µmol and 667 GBq/µmol, respectively. After purification, the radiochemical purity exceeded 95% for [^{68}Ga]Ga-NODAGA-exendin-4 and 85% for [^{68}Ga]Ga-NODAGA-MI-exendin-4.

Serum stability

Two hours after incubation in serum, >94% of the gallium-68 was still coupled to NOTA-MI-exendin-4 and had the most favourable stability compared to [^{68}Ga]Ga-NODAGA-exendin-4 (93%), [^{68}Ga]Ga-NOTA-exendin-4 (92%) and [^{68}Ga]Ga-NODAGA-MI-exendin-4 (47%) (Figure 2).

Competitive binding assay (IC_{50})

The IC_{50} values of NOTA-exendin-4 and NOTA-MI-exendin-4 were 4.0 nM (2.5 – 6.3 nM) and 9.6 nM (7.0 – 12.8), respectively. The IC_{50} values of NODAGA-Exendin-4 and NODAGA-MI-exendin-4 were 4.7 nM (3.4 – 6.4 nM) and 5.2 nM (3.8 – 7.2 nM) respectively. A significant difference in affinity was found between NOTA-exendin-4 and NOTA-MI-exendin-4 and between NODAGA-MI-exendin-4 and NOTA-MI-exendin-4 ($p < 0.01$). The competitive binding curves and their respective 95% confidential intervals are presented in Figure 3.

Biodistribution of [^{68}Ga]Ga-NOTA-exendin-4 and [^{68}Ga]Ga-NOTA-MI-exendin-4 in healthy mice

The biodistribution of ^{68}Ga-labeled NOTA-MI-exendin-4 was compared to that of the reference peptide NOTA-exendin-4 in healthy mice (Figure 4). The overall distribution pattern of the radiolabeled compounds was similar, with very rapid clearance of the peptides from the circulation. A significant difference in renal uptake of ^{68}Ga-labeled NOTA-MI-exendin-4 one hour post injection (151.7 ± 17.0 %ID/g), compared to NOTA-exendin-4 (203.2 ± 15.3 %ID/g) ($p<0.0001$) was found, which was even more pronounced (up to 65% difference) four hours p.i. (72.7 ± 3.9 %ID/g vs 207.7 ± 17.4 %ID/g respectively, $p<0.0001$) (Figure 4B).

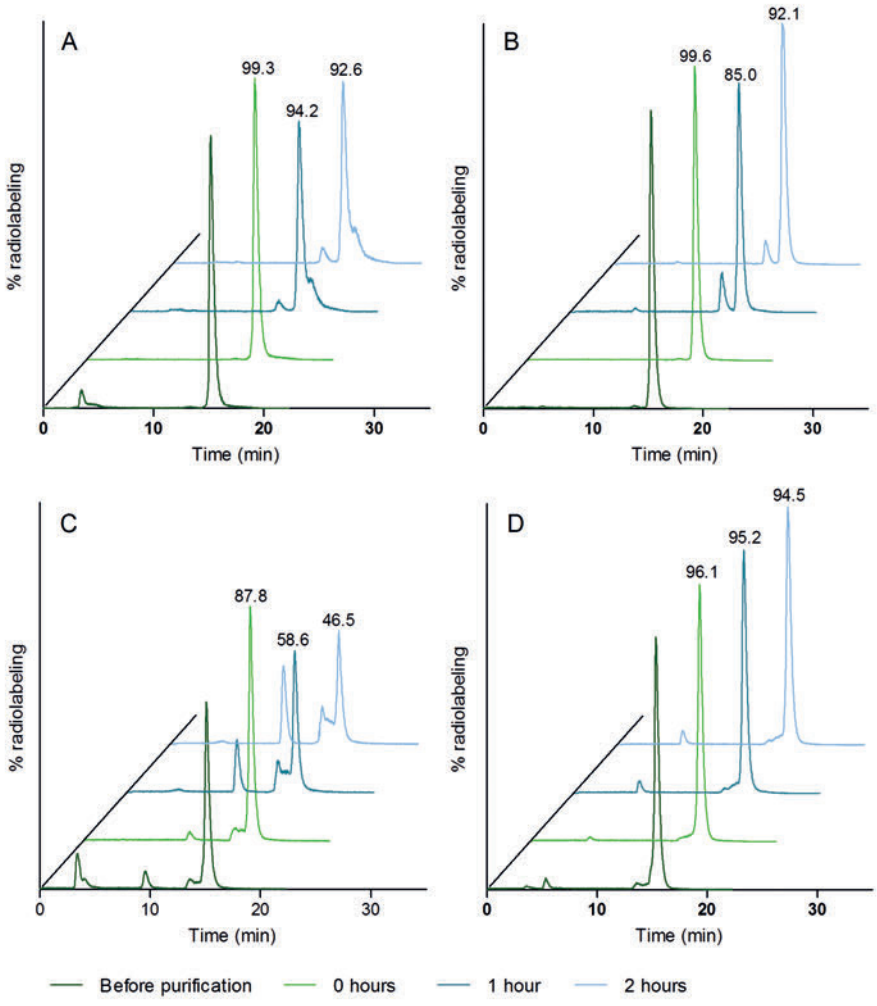

Figure 2. Stability of ^{68}Ga-labeled NODAGA-exendin-4 (A), NOTA-exendin-4 (B), NODAGA-MI-exendin-4 (C) and NOTA-MI-exendin-4 (D) before purification, and before and 1 and 2 h after incubation in human serum at 37°C. Graphs show HPLC profiles.

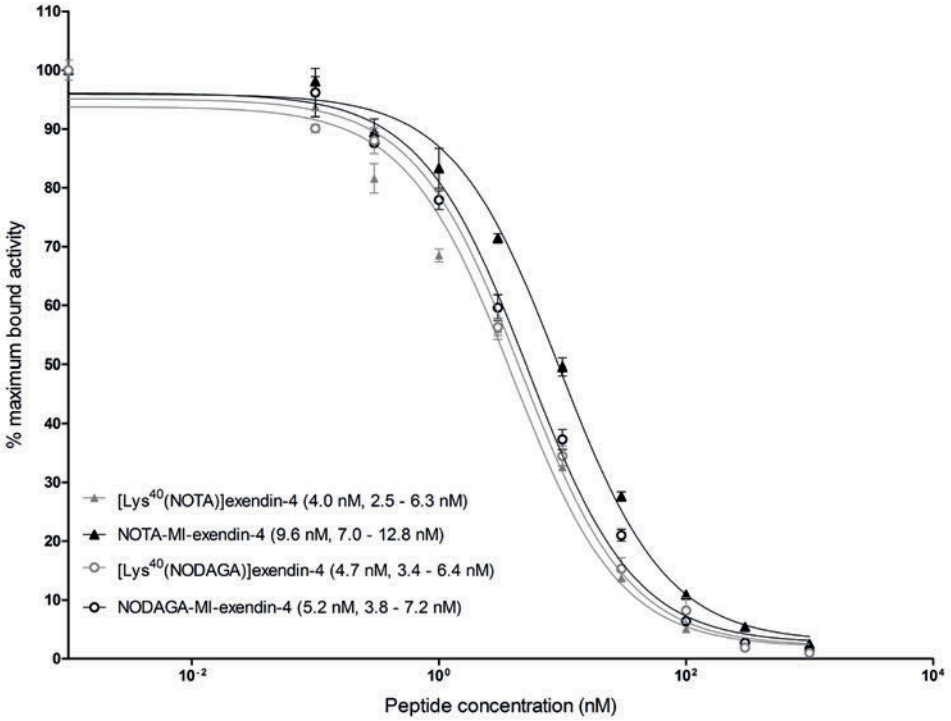

Figure 3. Competitive binding assay (IC_{50}) of NOTA-exendin-4, NOTA-MI-exendin-4, NODAGA-exendin-4 and NODAGA-MI-exendin-4 on CHL cells transfected with the GLP-1R. ^{111}In-labeled DTPA-exendin-4 was used as tracer.

Similarly, pancreatic uptake of [^{68}Ga]Ga-NOTA-MI-exendin-4 also decreased over time (22.2 ± 2.3% and 11.6 ± 1.4% at 1 hour and 4 hours p.i., respectively, while that of [^{68}Ga]Ga-NOTA-exendin-4 remained stable (21.5 ± 1.2% and 18.3 ± 3.4% at 1 hour and 4 hours. p.i., respectively (Figure 4A)). However, the difference in kidney uptake (65%) between both peptides was higher than the difference in pancreatic uptake (37%) at four hours p.i. (Figure 4D). These findings led to a more favourable pancreas-to-kidney ratio for [^{68}Ga]Ga-NOTA-MI-exendin-4 (0.16 ± 0.01) than for [^{68}Ga]Ga-NOTA-exendin-4 (0.09 ± 0.01) at four hours after injection ($p<0.0001$) (Figure 4C).
Co-injection of unlabeled exendin-4 showed that the uptake of the radiolabeled peptides in the pancreas, lungs and duodenum (transition from stomach to duodenum) could be blocked by an excess unlabeled peptide and therefore was GLP-1 receptor mediated. Raw data of this biodistribution study is shown in Table 2.

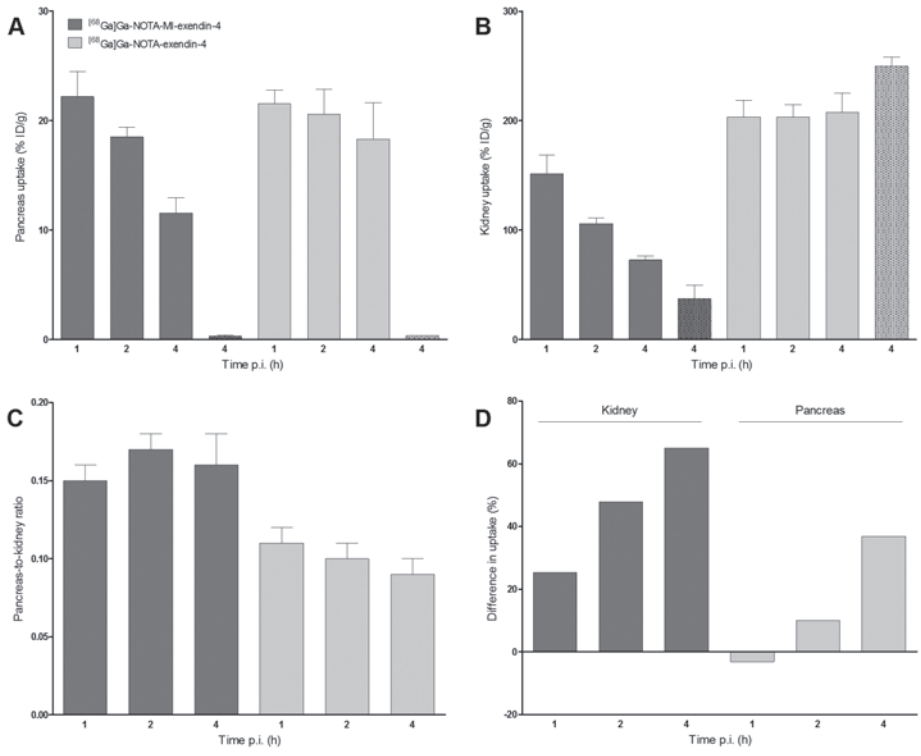

Figure 4. Biodistribution of ^{68}Ga-labeled NOTA-exendin-4 and NOTA-MI-exendin-4 in healthy C3H mice, 1, 2 and 4 hours after injection. Pancreatic uptake (A), kidney uptake (B), pancreas-to-kidney-ratio (C), difference in kidney and pancreatic uptake between both peptides (D). Receptor saturation was performed by coinjection of a 100-fold excess of unlabeled peptide 4 hours after injection (dotted bars). Values are expressed as percentage injected dose per gram of tissue (%ID/g) (n=4-5 mice per group, error bars SD).

Table 2. Biodistribution of ^{68}Ga-labeled NOTA-exendin-4 and NOTA-MI-exendin-4 in C3H mice. Kidney and pancreas data are shown in Figure 4. Values are expressed as percentage injected dose per gram tissue (%ID/g).

	[^{68}Ga]Ga-NOTA-exendin-4				**[^{68}Ga]Ga-NOTA-MI-exendin-4**			
	1 h (n=5)	**2 h (n=5)**	**4 h (n=4)**	**4 h + excess unlabeled (n=2)**	**1 h (n=5)**	**2 h (n=5)**	**4 h (n=5)**	**4 h + excess unlabeled (n=2)**
Blood	0.36 ± 0.02	0.16 ± 0.01	0.11 ± 0.01	0.10 ± 0.00	0.48 ± 0.05	0.28 ± 0.02	0.17 ± 0.02	0.12 ± 0.00
Muscle	0.07 ± 0.00	0.04 ± 0.01	0.05 ± 0.02	0.03 ± 0.01	0.08 ± 0.01	0.05 ± 0.01	0.04 ± 0.02	0.02 ± 0.00
Heart	0.29 ± 0.02	0.19 ± 0.02	0.16 ± 0.04	0.09 ± 0.00	0.37 ± 0.04	0.24 ± 0.04	0.15 ± 0.03	0.07 ± 0.01
Lung	18.68 ± 1.64	14.59 ± 1.49	12.85 ± 3.13	0.44 ± 0.10	21.05 ± 3.26	19.58 ± 1.30	13.13 ± 1.00	0.45 ± 0.10
Spleen	0.27 ± 0.05	0.22 ± 0.02	0.27 ± 0.13	0.21 ± 0.01	0.26 ± 0.03	0.25 ± 0.08	0.15 ± 0.03	0.10 ± 0.01
Pancreas	21.52 ± 1.24	20.57 ± 2.27	18.30 ± 3.35	0.36 ± 0.03	22.19 ± 2.27	18.52 ± 0.86	11.55 ± 1.40	0.35 ± 0.05
Kidney	203.20 ± 15.27	203.18 ± 11.35	207.66 ± 17.43	249.77 ± 8.34	151.67 ± 17.03	106.04 ± 4.89	72.74 ± 3.90	37.68 ± 12.04
Liver	0.43 ± 0.05	0.39 ± 0.02	0.42 ± 0.06	0.50 ± 0.00	0.53 ± 0.06	0.47 ± 0.04	0.37 ± 0.04	0.37 ± 0.14
Stomach	5.38 ± 0.43	4.44 ± 0.71	4.58 ± 0.18	0.21 ± 0.01	5.83 ± 0.99	4.53 ± 0.78	3.14 ± 0.10	0.19 ± 0.04
Duodenum	5.43 ± 1.25	4.87 ± 1.50	4.52 ± 0.38	0.26 ± 0.02	5.97 ± 0.39	4.79 ± 0.95	3.11 ± 0.58	1.09 ± 0.21

Biodistribution and PET/CT of [^{68}Ga]Ga-NOTA-exendin-4 and [^{68}Ga]Ga-NOTA-MI-exendin-4 in mice with a subcutaneous INS-1 tumor

Figure 5A shows that the high accumulation of both [^{68}Ga]Ga-NOTA-exendin-4 and [^{68}Ga]Ga-NOTA-MI-exendin-4 in INS-1 tumors was stable over time ([^{68}Ga]Ga-NOTA-MI-exendin-4: 29.3 ± 6.9 %ID/g at 1 h and 25.0 ± 8.0 %ID/g at 4 h p.i.; [^{68}Ga]Ga-NOTA-exendin-4: 27.8 ± 4.9 %ID/g at 1 h and 24.9 ± 9.3 %ID/g at 4 h p.i.). Furthermore, a remarkably reduced kidney uptake up to 66% for [^{68}Ga]Ga-NOTA-MI-exendin-4 was seen over 4 h (Figure 5B), which was not observed for [^{68}Ga]Ga-NOTA-exendin-4. The tumor-to-kidney ratio was 0.20 ± 0.10 for [^{68}Ga]Ga-NOTA-exendin-4, compared to 0.80 ± 0.30 for [^{68}Ga]Ga-NOTA-MI-exendin-4 ($p<0.001$) and was most optimal four hours after injection (Figure 5C). Raw data of this biodistribution study are shown in Table 3.

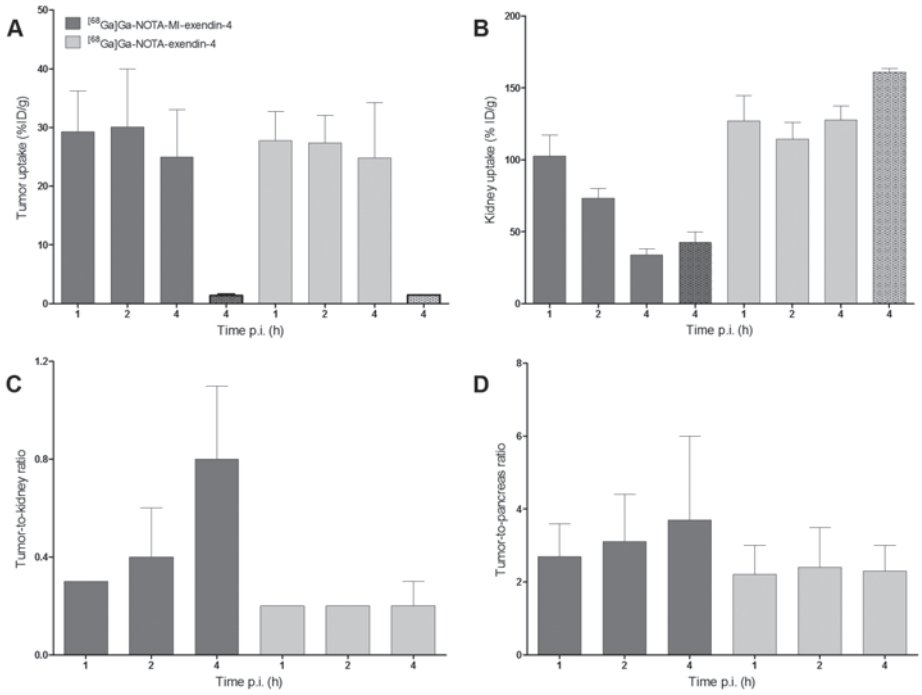

Figure 5. Biodistribution of ^{68}Ga-labeled NOTA-exendin-4 and NOTA-MI-exendin-4 in BALB/c nude mice bearing subcutaneous CHL-GLP1R tumors 1, 2 and 4 hours after injection. Tumor uptake (A), kidney uptake (B), tumor-to-kidney-ratio (C), Tumor-to-pancreas ratio (D). Receptor saturation was performed by coinjection of a 100-fold excess of unlabeled peptide 4 hours after injection (dotted bars). Values are expressed as percentage injected dose per gram of tissue (%ID/g) (n=4-5 mice per group, error bars SD).

Table 3. Biodistribution of ^{68}Ga-labeled NOTA-exendin-4 and NOTA-MI-exendin-4 in BALB/c nude mice bearing a subcutaneous INS-1 tumor. Kidney and tumor data are shown in Figure 5. Values are expressed as percentage injected dose per gram tissue (%ID/g).

	[^{68}Ga]Ga-NOTA-exendin-4				**[^{68}Ga]Ga-NOTA-MI-exendin-4**			
	1 h (n=5)	**2 h (n=5)**	**4 h (n=5)**	**4 h + excess unlabeled (n=2)**	**1 h (n=5)**	**2 h (n=5)**	**4 h (n=5)**	**4 h + excess unlabeled (n=2)**
Blood	0.25 ± 0.04	0.14 ± 0.01	0.11 ± 0.01	0.06 ± 0.01	0.33 ± 0.01	0.22 ± 0.02	0.14 ± 0.01	0.12 ± 0.03
Muscle	0.05 ± 0.01	0.04 ± 0.01	0.08 ± 0.05	0.03 ± 0.02	0.04 ± 0.01	0.04 ± 0.02	0.02 ± 0.01	0.03 ± 0.00
Tumor	27.75 ± 4.94	27.39 ± 4.67	24.85 ± 9.33	1.45 ± 0.02	29.32 ± 6.91	30.12 ± 9.89	24.96 ± 8.04	1.35 ± 0.25
Heart	0.20 ± 0.02	0.15 ± 0.01	0.14 ± 0.02	0.05 ± 0.00	0.24 ± 0.03	0.18 ± 0.02	0.13 ± 0.01	0.08 ± 0.02
Lung	4.34 ± 0.85	4.49 ± 0.85	3.14 ± 0.46	0.22 ± 0.04	6.33 ± 1.54	5.77 ± 1.18	3.69 ± 0.64	0.31 ± 0.01
Spleen	0.28 ± 0.03	0.30 ± 0.04	0.31 ± 0.07	0.17 ± 0.00	0.28 ± 0.08	0.23 ± 0.04	0.21 ± 0.05	0.08 ± 0.01
Pancreas	13.06 ± 2.22	12.25 ± 2.90	10.66 ± 0.89	0.29 ± 0.01	11.41 ± 2.74	10.39 ± 1.94	7.61 ± 2.14	0.30 ± 0.02
Kidney	127.18 ± 17.26	114.33 ± 11.75	127.74 ± 9.47	160.95 ± 2.54	102.60 ± 14.80	73.37 ± 6.66	34.15 ± 4.16	42.51 ± 7.25
Liver	0.56 ± 0.03	0.45 ± 0.04	0.53 ± 0.06	0.47 ± 0.06	0.51 ± 0.04	0.43 ± 0.06	0.33 ± 0.04	0.22 ± 0.03
Stomach	2.46 ± 0.45	2.03 ± 0.30	2.07 ± 0.27	0.12 ± 0.01	2.86 ± 0.32	2.35 ± 0.14	1.59 ± 0.66	0.20 ± 0.08
Duodenum	3.39 ± 1.37	4.00 ± 0.45	4.18 ± 0.59	0.35 ± 0.14	3.89 ± 1.59	4.49 ± 1.15	2.42 ± 1.56	0.35 ± 0.03

The images in Figure 6F reveal reduced renal uptake and improved discrimination between the left and right kidney when using ^{68}Ga-labeled exendin-4 with the Met-Ile-linker, while maintaining a significant signal in the INS-1 tumor. This in contrast to the images of [^{68}Ga]Ga-NOTA-exendin-4, where the kidneys could not be discriminated from each other due to the high renal retention (Figure 6C).

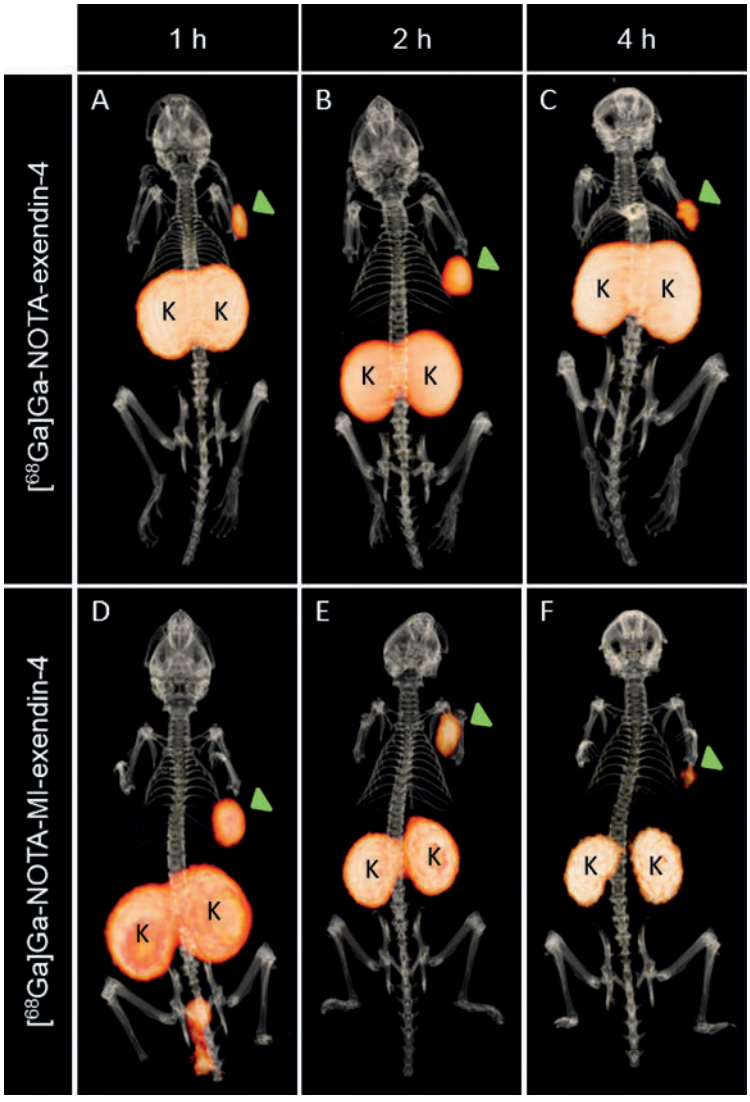

Figure 6. Fused PET/CT images of BALB/c nude mice bearing subcutaneous CHL-GLP-1R tumors (green arrow). Mice were injected with 1.6 MBq of either [^{68}Ga]Ga-NOTA-exendin-4 (A, B and C) or [^{68}Ga]Ga-NOTA-MI-exendin-4 (D, E and F). Images were obtained 1 hour (A and D), 2 hours (B and E) and 4 hours (C and F) after injection. Kidneys are indicated with K.

Dosimetry

The estimated absorbed doses per injected activity for mice were 266 and 232 mSv/MBq for [^{68}Ga]Ga-NOTA-exendin-4 and [^{68}Ga]Ga-NOTA-MI-exendin-4, respectively. For human, the estimated absorbed doses were 0.20 and 0.17 mSv/MBq respectively. The use of [^{68}Ga]Ga-NOTA-MI-exendin-4 reduced the estimated absorbed kidney dose in both mice and human by 12%.

Biodistribution of [^{68}Ga]Ga-NODAGA-exendin-4 and [^{68}Ga]Ga-NODAGA-MI-exendin-4 in healthy mice

The complete biodistribution of [^{68}Ga]Ga-NODAGA-exendin-4 and [^{68}Ga]Ga-NODAGA-MI-exendin-4 in healthy C3H mice is presented in Table 4. The overall distribution pattern of these compounds is similar with very rapid elimination from the blood.

The addition of the cleavable linker lowers renal uptake by almost 40% at 4 hours after injection of [^{68}Ga]Ga-NODAGA-MI-exendin-4. When comparing the renal retention of [^{68}Ga]Ga-NODAGA-MI-exendin-4 with [^{68}Ga]Ga-NODAGA-exendin-4, a difference of almost 58% was found (109.3 ± 7.0 %ID/g vs 257.9 ± 21.2 %ID/g respectively, $p<0.0001$) four hours after injection. Similarly, uptake in the pancreas also decreased over time. Four hours after injection, pancreatic uptake of [^{68}Ga]Ga-NODAGA-MI-exendin-4 was 53% less than the pancreatic uptake of [^{68}Ga]Ga-NODAGA-exendin-4 ($p<0.0001$). A significant difference in pancreas-to-kidney ratio was found only 2 h after injection (0.11 ± 0.01 for [^{68}Ga]Ga-NODAGA-MI-exendin-4 and 0.09 ± 0.01 for [^{68}Ga]Ga-NODAGA-exendin-4, $p=0.01$). Furthermore, co-injection of an excess of unlabeled exendin-4 showed that the uptake of all radiolabeled peptides in the pancreas, lungs and duodenum could be blocked by coinjection of an excess unlabeled peptide and was therefore GLP-1 receptor mediated. Overall, a higher pancreas-to-kidney ratio was found for [^{68}Ga]Ga-NOTA-MI-exendin-4 (0.17 ± 0.01) compared to [^{68}Ga]Ga-NODAGA-MI-exendin-4 (0.11 ± 0.01) ($p<0.0001$).

Biodistribution of [^{111}In]In-NOTA-exendin-4 and [^{111}In]In-NOTA-MI-exendin-4 in healthy mice

Table 5 presents the total biodistribution of ^{111}In-labeled NOTA-exendin-4 and NOTA-MI-exendin-4 four hours after injection. The overall distribution of both compounds is similar. However, a significantly higher lung uptake was found for [^{111}In]In-NOTA-MI-exendin-4 compared to [^{111}In]In-NOTA-exendin-4 ($p<0.01$), in contrast to the other GLP-1R expressing organs (pancreas, stomach/duodenum), were the uptake did not significantly differ. Interestingly, the renal clearance as observed for the ^{68}Ga-labeled peptides was not found for [^{111}In]In-NOTA-MI-exendin-4. At four hours post injection, kidney uptake was 175.2 ± 23.0 %ID/g and 202.6 ± 3.9 %ID/g for [^{111}In]In-NOTA-MI-exendin-4 and [^{111}In]In-NOTA-exendin-4, respectively ($p=0.11$).

Table 4. Biodistribution of ^{68}Ga-labeled NODAGA-exendin-4 and NODAGA-MI-exendin-4 in C3H mice. Values are expressed as percentage injected dose per gram tissue (%ID/g).

	[^{68}Ga]Ga-NODAGA-exendin-4				[^{68}Ga]Ga-NODAGA-MI-exendin-4			
	1h (n=5)	**2h (n=5)**	**4h (n=5)**	**4h + excess unlabeled (n=2)**	**1h (n=5)**	**2h (n=5)**	**4h (n=5)**	**4h + excess unlabeled (n=2)**
Blood	0.37 ± 0.03	0.17 ± 0.01	0.10 ± 0.01	0.05 ± 0.00	0.56 ± 0.06	0.29 ± 0.02	0.21 ± 0.01	0.18 ± 0.01
Muscle	0.09 ± 0.03	0.05 ± 0.01	0.05 ± 0.00	0.04 ± 0.01	0.09 ± 0.01	0.05 ± 0.01	0.04 ± 0.01	0.02 ± 0.00
Heart	0.29 ± 0.04	0.22 ± 0.06	0.17 ± 0.02	0.06 ± 0.01	0.34 ± 0.04	0.21 ± 0.01	0.15 ± 0.01	0.08 ± 0.01
Lung	25.81 ± 3.02	18.55 ± 3.24	12.69 ± 1.54	0.51 ± 0.09	17.94 ± 3.17	11.41 ± 1.97	11.08 ± 2.07	0.65 ± 0.12
Spleen	0.27 ± 0.06	0.21 ± 0.01	0.21 ± 0.03	0.12 ± 0.00	0.27 ± 0.02	0.20 ± 0.03	0.18 ± 0.03	0.13 ± 0.01
Pancreas	24.27 ± 3.33	22.57 ± 1.93	21.68 ± 2.28	0.43 ± 0.05	16.87 ± 0.66	14.43 ± 1.33	10.18 ± 0.79	0.44 ± 0.02
Kidney	256.21 ± 9.82	242.37 ± 14.65	257.85 ± 21.22	276.33 ± 14.53	179.32 ± 8.38	131.16 ± 19.13	109.26 ± 7.03	98.21 ± 8.35
Liver	0.41 ± 0.03	0.37 ± 0.02	0.39 ± 0.05	0.28 ± 0.00	0.74 ± 0.05	0.57 ± 0.03	0.50 ± 0.02	0.39 ± 0.04
Stomach	6.05 ± 0.80	5.23 ± 1.01	5.71 ± 1.34	0.22 ± 0.04	4.11 ± 0.63	3.36 ± 0.77	2.67 ± 0.25	0.24 ± 0.01
Duodenum	5.98 ± 1.78	5.67 ± 0.84	5.07 ± 1.05	0.22 ± 0.01	4.77 ± 0.96	3.49 ± 1.35	2.38 ± 0.18	0.68 ± 0.26

Table 5. Biodistribution of ^{111}In-labeled NOTA-exendin-4 and NOTA-MI-exendin-4 in C3H mice. Values are expressed as percentage injected dose per gram tissue (%ID/g).

	[^{111}In]In-NOTA-exendin-4		[^{111}In]In-NOTA-MI-exendin-4	
	4h (n=3)	**4h + excess unlabeled (n=2)**	**4h (n=3)**	**4h + excess unlabeled (n=2)**
Blood	0.20 ± 0.01	0.20 ± 0.00	0.24 ± 0.02	0.24 ± 0.00
Muscle	0.06 ± 0.00	0.08 ± 0.01	0.06 ± 0.01	0.07 ± 0.01
Heart	0.19 ± 0.02	0.18 ± 0.00	0.25 ± 0.01	0.17 ± 0.01
Lung	8.88 ± 1.15	0.75 ± 0.15	15.42 ± 0.85	1.05 ± 0.09
Spleen	0.39 ± 0.02	0.38 ± 0.00	0.41 ± 0.03	0.49 ± 0.04
Pancreas	14.81 ± 0.62	0.47 ± 0.00	14.30 ± 0.52	0.64 ± 0.06
Kidney	202.62 ± 3.92	207.22 ± 6.19	175.20 ± 22.97	214.05 ± 7.39
Liver	0.93 ± 0.02	1.03 ± 0.02	1.32 ± 0.06	1.54 ± 0.00
Stomach	3.37 ± 0.32	0.30 ± 0.01	4.18 ± 0.53	0.43 ± 0.03
Duodenum	2.60 ± 2.18	0.44 ± 0.01	6.08 ± 2.09	0.83 ± 0.11

DISCUSSION

Complete surgical resection of insulinomas remains challenging. Pre-operative imaging with radiolabeled exendin can be used to identify and localize tumor lesions, however some lesions (namely in the pancreatic tail close to the left kidney) may be missed because they are masked by the high kidney uptake. The present study demonstrated a significantly lower renal uptake of radiolabeled exendin, after introducing a methionine-isoleucine linker. The high accumulation in subcutaneous GLP-1R-expressing INS-1 tumors was preserved. Therefore, this new compound may enable an improved visualization of small insulinomas located in the vicinity of the kidneys.

The mechanism behind high renal uptake is not fully understood. Tubular reabsorption of radiolabeled exendin-4 has been described as one of the major causes[13], but expression of the GLP-1R on porcine proximal tubular cells has been reported as well[21]. However, exendin uptake in the kidneys cannot be blocked by an excess of unlabeled exendin, thus the contribution of GLP-1R mediated uptake in the tubules seems to play only a minor role. In general, peptides enter the kidneys via the bloodstream and are filtered through the glomeruli. Instead of being excreted, the peptides are reabsorbed in the proximal tubules[22], most probably via endocytic receptors that are located near the brush border membrane[23]. After endocytosis, the peptides will finally end up in lysosomes, where they are cleaved into amino acids by enzymes[22]. As radiolabeled exendin-4 is a residualizing compound, it will get trapped in the lysosomes instead of excreted, leading to high accumulation of the tracer.

In this study, high kidney uptake of [^{68}Ga]Ga-NOTA-exendin-4 was observed at early time points after injection, which did not decrease over time. On the contrary, [^{68}Ga]Ga-NOTA-MI-exendin-4 showed rapid clearance from the kidneys (a difference of 66% between 1 and 4 hours in the BALB/c nude mice) and therefore had a much shorter renal retention time. This is in line with the findings as reported by Uehara et al. They have shown a reduced kidney uptake when introducing a methionine-isoleucine linker between the chelator and the compound[16]. Furthermore, they published an antibody fragment with a newly designed cleavable linker, Methionine-Valine-Lysine (MVK). This new compound displayed an even lower renal uptake than the antibody with the methionine-isoleucine linker. More recently, an exendin-4 analog containing the MVK-linker was developed. Similar to our study, they reported a stable tumor uptake (around 25 %ID/g at 1 and 2 hours p.i.) of the ^{68}Ga-labeled compound, but found a striking decrease in renal accumulation. Two hours p.i., the uptake of [^{68}Ga]Ga-NOTA-MVK-Cys^{40}-Leu^{14}-Exendin-4 was 33% of the control. Similarly, the kidney uptake of our ligand was 36% of the control, which was even more pronounced 4 hours after injection (73% of the control)[24].

Both studies using the MVK-linker showed that the main radiometabolite in the urine was radiolabeled NOTA-Met and the ligand was cleaved between Methionine and Valine by the renal brush border membrane enzyme, neutral endopeptidase (NEP)[24, 25]. Uehara *et al.* performed a direct comparison between both linkers and postulated that the methionine-isoleucine linker

is cleaved during lysosomal proteolysis rather than cleavage at the brush border membrane, due to higher retention in the kidneys[25]. The exact mechanism and location behind the cleavage of the methionine-isoleucine linker remains to be unravelled.

Importantly, [^{68}Ga]Ga-NOTA-MI-exendin-4 already showed less kidney uptake one hour after injection, in contrast to [^{68}Ga]Ga-NOTA-exendin-4, whereas uptake in the other GLP-1R expressing organs was similar at this time point. Furthermore, uptake in the INS-1 tumor did not change over time, showing that binding to and retention in tumor tissue was not impaired. These findings suggest that degradation of the peptide was restricted to the kidneys, but we did find lower uptake over time in other GLP-1R mediated organs, like the pancreas, lungs and duodenum as well. This cannot be explained by a difference in binding capacity, since the baseline uptake (1 hour p.i.) was similar for both tracers. Also, the *in vitro* binding affinity for the GLP-1R was very high for both tracers. A different internalization rate of the peptide in different organs, the abundance of the GLP-1R in tumor tissue, or absence of the cleavable enzyme might explain the different retention times. Of course, a lower uptake in the pancreas can even improve the detection of insulinomas, as almost all insulinomas are located in the pancreas. Accordingly, the tumor-to-pancreas ratio could also be improved.

In addition, the pancreas-to-kidney and tumor-to-kidney ratio of [^{68}Ga]Ga-NOTA-MI-exendin-4 were almost three and four times higher (respectively) than for [^{68}Ga]Ga-NOTA-exendin-4, 4 hours after injection. Even 4 hours after injection of ^{68}Ga-labeled exendin-4 PET scans can be acquired of patients with an insulinoma with a very good image quality.

Other attempts in decreasing renal exendin uptake based on cleavable linkers have been reported, but were not successful so far. Jodal *et al.*[26] introduced a meprin ß (a protease on the brush border membrane of the kidneys) cleavable linker to exendin-4. After labeling with ^{111}In they did not find a reduced kidney uptake in CD1 nu/nu mice. Whether this could be explained by exendin-4 not being recognized by the targeted protease for cleavage or by the use of the radiometal that was used is not known. Interestingly, when comparing [^{111}In]In-NOTA-exendin-4 and [^{111}In]In-NOTA-MI-exendin-4 in C3H mice (Table 5), we also did not find a decreased renal uptake. The same was reported for [^{111}In]In-DTPA-Met-octreotide[27]. Moreover, Yim *et al.* reported that the addition of an N$^{\varepsilon}$-maleoyl-L-lysyl-glycine (MAL) linker between [^{64}Cu]Cu-NODAGA and exendin-4 did not prove effective in reducing the kidney uptake in rats[28]. Again, whether this is a matter of animal model, radionuclide or cleavable linker used, remains unknown. Although the approach of the above mentioned studies were unsuccessful, many other studies showed that cleavable linkers can be effective in reducing kidney retention[29].

To date, the best approach for reducing kidney uptake is co-injection of Gelofusine or amino acids. Gotthardt *et al.* used Gelofusine to inhibit the renal uptake of [^{111}In]In-DTPA-exendin-4. They found a reduction of 19% in the kidneys of Wistar rats[13]. In healthy volunteers, Gelofusine reduced kidney uptake of [^{111}In]In-DTPA-exendin-4 by 18.1 ± 4.2%[14]. Both approaches, coinjection of Gelofusine or the introduction of a cleavable linker are a step forward towards the use of radiolabeled exendin for peptide receptor radionuclide therapy (PRRT), which could

be an alternative treatment for patients that are not eligible for surgery (i.e. metastasized insulinomas or insulinomas near vessels or ducts).

Another approach to prevent renal retention of exendin-4 is by a different radiolabeling approach which is not based on radiometals. For example [^{18}F]-exendin-4 demonstrated rapid clearance from the kidneys in Sprague-Dawley rats; 17 ± 3 %ID/g at 1 hour p.i. to 2.8 ± 0.4 %ID/g at 4 hours p.i., which is beneficial regarding visualization of lesions in close proximity to the kidneys. However, they also observed decreased uptake in the pancreas (0.18 ± 0.02 %ID/g at 1 h p.i. to 0.13 ± 0.004 %ID/g at 4 h p.i.[130]. The absorbed kidney dose was 0.3 mSv/MBq (based on extrapolation of rat data). This makes [^{18}F]-exendin-4 promising for safely visualizing beta cells and insulinomas, which is however, restricted for diagnostic purposes as this radiolabeling technique does not allow coupling of therapeutic radionuclides.

In our study, a kidney-to-kidney absorbed dose in human of 0.17 mSv/MBq was estimated for [^{68}Ga]Ga-NOTA-MI-exendin-4, which was twelve percent lower than for [^{68}Ga]Ga-NOTA-exendin-4 (0.20 mSv/MBq). Although [^{68}Ga]Ga-NOTA-MI-exendin-4 showed a much more favorable biodistribution than [^{68}Ga]Ga-NOTA-exendin-4, this was not reflected in the estimated kidney absorbed dose values. This might be explained by the short physical half-life of ^{68}Ga as the main contributor for the absorbed doses for both peptides. Importantly, the reduced uptake of our new compound in pancreas and kidney, and the preserved high uptake in tumor tissue, improves the ratio between target and non-target organs and could therefore be important in the next step towards PRRT. Whether the absorbed kidney dose could be reduced when a (therapeutic) radiometal with a longer half-life will be used, needs to be further investigated. If NOTA-MI-exendin-4, labeled with a therapeutic radiometal, would show a low absorbed dose in the kidneys, this might enable PRRT with exendin-4.

Like exendin, most radiolabeled peptides show rapid clearance from blood and are predominantly excreted via the kidneys[31]. High renal uptake due to tubular reabsorption is not only seen for exendin, but for other low molecular weight tracers (e.g. minigastrin or octreotide) as well[22]. This makes them less suitable as therapeutic agents or even precludes PRRT, because accumulation of highly radioactive compounds in the kidneys can cause serious nephrotoxicity. Kidneys could therefore be the dose-limiting organs in PRRT[32]. In this regard, it would be interesting to apply this cleavable linker to other peptides or nanobodies in order to reduce the kidney uptake and possibly radiation burden to the kidneys.

Future studies should elucidate the effect of the linker in combination with other (therapeutic) radionuclides and clinical trials are needed to explore the translational value of this new compound.

CONCLUSION

To summarize, [^{68}Ga]Ga-NOTA-MI-exendin-4 showed more than 70% lower renal uptake than [^{68}Ga]Ga-NOTA-exendin-4 in BALB/c nude mice, while uptake in the INS-1 tumor is preserved and might therefore increase the sensitivity of PET/CT to detect insulinomas. Additional studies are required to explore whether this could also apply for therapeutic radionuclides, which would then provide new possibilities for safe and effective use of NOTA-MI-exendin-4 as therapeutic agent for insulinoma treatment.

ACKNOWLEDGEMENTS

The authors thank the animal caretakers of the Central Animal Facility of the Raboudumc for their expertise during the *in vivo* studies.

FUNDING

The research leading to these results has received funding from the European Community's Seventh Framework Programme (FP7/2007-2013) under grant agreement n° 602812.

CONFLICT OF INTEREST

The authors declare that they have no conflict of interest.

ETHICAL APPROVAL

All applicable international, national and/or institutional guidelines for the care and use of animals were followed. All procedures performed in studies involving animals were in accordance with the ethical standards of the institution at which the studies were conducted (Project 2015-0071, approved by the Nijmegen Medical Center animal ethics committee (RUDEC) and the Dutch animal ethics comittee (CCD) of the Radboud University and performed according to the Institute of Laboratory Animal Research Guidelines).

REFERENCES

1. de Herder WW, Niederle B, Scoazec JY, Pauwels S, Kloppel G, Falconi M, *et al.* Well-differentiated pancreatic tumor/carcinoma: insulinoma. *Neuroendocrinology.* **2006**; 84 (3): 183-188.
2. Mehrabi A, Fischer L, Hafezi M, Dirlewanger A, Grenacher L, Diener MK, *et al.* A systematic review of localization, surgical treatment options, and outcome of insulinoma. *Pancreas.* **2014**; 43 (5): 675-686.
3. Christ E, Wild D, Forrer F, Brandle M, Sahli R, Clerici T, *et al.* Glucagon-like peptide-1 receptor imaging for localization of insulinomas. *J Clin Endocrinol Metab.* **2009**; 94 (11): 4398-4405.
4. Wild D, Christ E, Caplin ME, Kurzawinski TR, Forrer F, Brandle M, *et al.* Glucagon-like peptide-1 versus somatostatin receptor targeting reveals 2 distinct forms of malignant insulinomas. *J Nucl Med.* **2011**; 52 (7): 1073-1078.
5. Brom M, Woliner-van der Weg W, Joosten L, Frielink C, Bouckenooghe T, Rijken P, *et al.* Non-invasive quantification of the beta cell mass by SPECT with (1)(1)(1)In-labelled exendin. *Diabetologia.* **2014**; 57 (5): 950-959.
6. Christ E, Wild D, Ederer S, Behe M, Nicolas G, Caplin ME, *et al.* Glucagon-like peptide-1 receptor imaging for the localisation of insulinomas: a prospective multicentre imaging study. *Lancet Diabetes Endocrinol.* **2013**; 1 (2): 115-122.
7. Luo Y, Yu M, Pan Q, Wu W, Zhang T, Kiesewetter DO, *et al.* 68Ga-NOTA-exendin-4 PET/CT in detection of occult insulinoma and evaluation of physiological uptake. *Eur J Nucl Med Mol Imaging.* **2015**; 42 (3): 531-532.
8. Heusser T, Mann P, Rank CM, Schafer M, Dimitrakopoulou-Strauss A, Schlemmer HP, *et al.* Investigation of the halo-artifact in 68Ga-PSMA-11-PET/MRI. *PLoS One.* **2017**; 12 (8): e0183329.
9. van Eerd JE, Vegt E, Wetzels JF, Russel FG, Masereeuw R, Corstens FH, *et al.* Gelatin-based plasma expander effectively reduces renal uptake of 111In-octreotide in mice and rats. *J Nucl Med.* **2006**; 47 (3): 528-533.
10. Vegt E, Wetzels JF, Russel FG, Masereeuw R, Boerman OC, van Eerd JE, *et al.* Renal uptake of radiolabeled octreotide in human subjects is efficiently inhibited by succinylated gelatin. *J Nucl Med.* **2006**; 47 (3): 432-436.
11. Hammond PJ, Wade AF, Gwilliam ME, Peters AM, Myers MJ, Gilbey SG, *et al.* Amino acid infusion blocks renal tubular uptake of an indium-labelled somatostatin analogue. *Br J Cancer.* **1993**; 67 (6): 1437-1439.
12. Rolleman EJ, Valkema R, de Jong M, Kooij PP, Krenning EP. Safe and effective inhibition of renal uptake of radiolabelled octreotide by a combination of lysine and arginine. *Eur J Nucl Med Mol Imaging.* **2003**; 30 (1): 9-15.
13. Gotthardt M, van Eerd-Vismale J, Oyen WJ, de Jong M, Zhang H, Rolleman E, *et al.* Indication for different mechanisms of kidney uptake of radiolabeled peptides. *J Nucl Med.* **2007**; 48 (4): 596-601.
14. Buitinga M, Jansen TJP, van der Kroon I, Woliner-van der Weg W, Boss M, Janssen M, *et al.* Succinylated gelatin improves the theranostic potential of radiolabeled exendin-4 in insulinoma patients. *J Nucl Med.* **2018**;

15. Wu C, Jagoda E, Brechbiel M, Webber KO, Pastan I, Gansow O, *et al*. Biodistribution and catabolism of Ga-67-labeled anti-Tac dsFv fragment. *Bioconjug Chem*. **1997**; 8 (3): 365-369.

16. Uehara T, Rokugawa T, Kinoshita M, Nemoto S, Fransisco Lazaro GG, Hanaoka H, *et al*. (67/68)Ga-labeling agent that liberates (67/68)Ga-NOTA-methionine by lysosomal proteolysis of parental low molecular weight polypeptides to reduce renal radioactivity levels. *Bioconjug Chem*. **2014**; 25 (11): 2038-2045.

17. Brom M, Franssen GM, Joosten L, Gotthardt M, Boerman OC. The effect of purification of Ga-68-labeled exendin on in vivo distribution. *EJNMMI Res*. **2016**; 6 (1): 65.

18. Asfari M, Janjic D, Meda P, Li G, Halban PA, Wollheim CB. Establishment of 2-mercaptoethanol-dependent differentiated insulin-secreting cell lines. *Endocrinology*. **1992**; 130 (1): 167-178.

19. Maina T, Konijnenberg MW, KolencPeitl P, Garnuszek P, Nock BA, Kaloudi A, *et al*. Preclinical pharmacokinetics, biodistribution, radiation dosimetry and toxicity studies required for regulatory approval of a phase I clinical trial with (111)In-CP04 in medullary thyroid carcinoma patients. *Eur J Pharm Sci*. **2016**; 91 236-242.

20. Stabin MG. *Fundamentals of Nuclear Medicine Dosimetry*. New York2008.

21. Schlatter P, Beglinger C, Drewe J, Gutmann H. Glucagon-like peptide 1 receptor expression in primary porcine proximal tubular cells. *Regul Pept*. **2007**; 141 (1-3): 120-128.

22. Vegt E, de Jong M, Wetzels JF, Masereeuw R, Melis M, Oyen WJ, *et al*. Renal toxicity of radiolabeled peptides and antibody fragments: mechanisms, impact on radionuclide therapy, and strategies for prevention. *J Nucl Med*. **2010**; 51 (7): 1049-1058.

23. Vegt E, Melis M, Eek A, de Visser M, Brom M, Oyen WJ, *et al*. Renal uptake of different radiolabelled peptides is mediated by megalin: SPECT and biodistribution studies in megalin-deficient mice. *Eur J Nucl Med Mol Imaging*. **2011**; 38 (4): 623-632.

24. Zhang M, Jacobson O, Kiesewetter DO, Ma Y, Wang Z, Lang L, *et al*. Improving the Theranostic Potential of Exendin 4 by Reducing the Renal Radioactivity through Brush Border Membrane Enzyme-Mediated Degradation. *Bioconjug Chem*. **2019**; 30 (6): 1745-1753.

25. Uehara T, Yokoyama M, Suzuki H, Hanaoka H, Arano Y. A Gallium-67/68-Labeled Antibody Fragment for Immuno-SPECT/PET Shows Low Renal Radioactivity Without Loss of Tumor Uptake. *Clin Cancer Res*. **2018**; 24 (14): 3309-3316.

26. Jodal A, Lankat-Buttgereit B, Brom M, Schibli R, Behe M. A comparison of three (67/68)Ga-labelled exendin-4 derivatives for beta-cell imaging on the GLP-1 receptor: the influence of the conjugation site of NODAGA as chelator. *EJNMMI Res*. **2014**; 4 31.

27. Akizawa H, Arano Y, Mifune M, Iwado A, Saito Y, Uehara T, *et al*. Significance of (111)In-DTPA chelate in renal radioactivity levels of (111)In-DTPA-conjugated peptides. *Nucl Med Biol*. **2001**; 28 (4): 459-468.

28. Yim CB, Mikkola K, Fagerholm V, Elomaa VV, Ishizu T, Rajander J, *et al*. Synthesis and preclinical characterization of [64Cu]NODAGA-MAL-exendin-4 with a Nepsilon-maleoyl-L-lysyl-glycine linkage. *Nucl Med Biol*. **2013**; 40 (8): 1006-1012.

29. Akizawa H, Uehara T, Arano Y. Renal uptake and metabolism of radiopharmaceuticals derived from peptides and proteins. *Adv Drug Deliv Rev*. **2008**; 60 (12): 1319-1328.

30. Mikkola K, Yim CB, Lehtiniemi P, Kauhanen S, Tarkia M, Tolvanen T, *et al*. Low kidney uptake of GLP-1R-targeting, beta cell-specific PET tracer, 18F-labeled [Nle14,Lys40]exendin-4 analog, shows promise for clinical imaging. *EJNMMI Res*. **2016**; 6 (1): 91.

31. Gotthardt M, Lalyko G, van Eerd-Vismale J, Keil B, Schurrat T, Hower M, *et al*. A new technique for in vivo imaging of specific GLP-1 binding sites: first results in small rodents. *Regul Pept*. **2006**; 137 (3): 162-167.

32. Cremonesi M, Ferrari M, Bodei L, Tosi G, Paganelli G. Dosimetry in Peptide radionuclide receptor therapy: a review. *J Nucl Med*. **2006**; 47 (9): 1467-1475.

Part II

Validation of radiolabeled exendin for beta cell mass determination

CHAPTER 7

Strain differences determine the suitability of animal models for non-invasive *in vivo* beta cell mass determination with radiolabeled exendin

Stefanie M. A. Willekens[1], Lieke Joosten[1], Otto C. Boerman[1], Alexander Balhuizen[1], Decio L. Eizirik[2], Martin Gotthardt[1] & Maarten Brom[1]

1 Department of Radiology and Nuclear Medicine, Radboud University Medical Center, Nijmegen, The Netherlands

2 ULB Center for Diabetes Research, Université Libre de Bruxelles, Brussels, Belgium

Molecular Imaging and Biology. **2016**; 18(5):705-714

ABSTRACT

Non-invasive beta cell mass (BCM) quantification is a crucial tool to understand diabetes development and progression. [^{111}In]In-DTPA-exendin is a promising agent for *in vivo* beta cell imaging, but tracer testing has been hampered by the lack of well-defined rodent models.

Biodistribution and pancreatic uptake of [^{111}In]In-DTPA-exendin were compared in rats and mice. In selected models, the amount of [^{111}In]In-DTPA-exendin accumulation in the pancreas and other organs was determined using a model of alloxan-induced beta cell loss. GLP-1R expression levels were analyzed by RT-PCR and immunohistochemistry.

Namely Brown Norway rats showed beta cell specific tracer accumulation and favorable pancreas-to-background ratios for non-invasive BCM determination. Mice displayed receptor mediated [^{111}In]In-DTPA-exendin uptake in endocrine and exocrine pancreas, in spite of very low GLP-1R expression in exocrine tissue.

Rats display better characteristics for *in vivo* BCM determination than mice, and are suggested as a more adequate model for humans.

INTRODUCTION

Diabetes mellitus is characterized by defective glucose homeostasis and consequent chronic hyperglycemia. Maintenance of glycemic control by daily insulin injections or anti-diabetogenic drugs is difficult and patients affected by both type 1 and type 2 diabetes are at risk for severe complications, such as cardiovascular disease, blindness and kidney failure, increasing the risk for premature death. Changes in beta cell mass (BCM) occur in both forms of diabetes [1-3], but the mechanisms and evolution underlying these BCM changes are poorly understood [4, 5].

Beta cell function is usually monitored by measurements of insulin secretion, such as insulin and C-peptide, analyzed in parallel to glucose levels. However, it was shown that beta cell function and BCM do not diminish equally during disease progression [5, 6], indicating that beta cell function is not an adequate measure for BCM. A reliable and reproducible method to monitor BCM dynamics over time, such as longitudinal quantitative imaging, could unravel the importance of BCM during the course of diabetes.

During the past decade, major efforts have been made to image BCM *in vivo* in animal models using a variety of imaging methodologies [7], such as near infrared optical projection tomography (OPT) [8], bioluminescence [9] or magnetic resonance imaging (MRI) [10-12]. While MRI offers the highest resolution (still not allowing resolution of single islets *in vivo*), nuclear medicine imaging modalities, such as single photon emission computed tomography (SPECT) and positron emission tomography (PET) have the potential to reach sufficient sensitivity to detect small numbers of beta cells when targeted with a radiolabeled beta cell specific tracer. Importantly, the first clinical trial results show that SPECT and PET are the most likely approaches to reach human translation at this point in time [13-15].

A variety of antibodies, such as IC2 [16], small molecules, such as ^{18}F-fluorodeoxyglucose ([^{18}F]FDG) [17], neurotransmitter precursors, such as ^{11}C-5-hydroxytryptophan ([^{11}C]5-HTP) [18], organic compounds, such as dihydrotetrabenazine (DTBZ) targeting the vesicular monoamine transporter 2 (VMAT2) [19] and peptides, such as exendin targeting the glucagon-like peptide 1 (GLP-1) receptor [13] have been evaluated as tracers for BCM determination. Very recent findings indicate that [^{11}C]5-HTP can successfully discriminate between rats with severe or moderate beta cell loss [15, 18], while radiolabeled exendin, a stable GLP-1R agonist specifically targeting the pancreatic beta cells [20], was shown to successfully detect small changes in BCM in a preclinical model for beta cell loss [14]. In order to further validate the use of GLP-1R radionuclide imaging to evaluate the dynamics of BCM changes in diabetes, further studies in animal models are required.

A variety of preclinical models have been used to investigate BCM dynamics, but the results obtained showed differences in biodistribution and in tracer uptake in relation to BCM [14, 21-24]. We hypothesize that the observed differences in these studies can be related to the use of animal models. Therefore, in the present study we aimed to evaluate the differences between various animal models to select the most suitable model for preclinical, non-invasive BCM

determination using [^{111}In]In-DTPA-exendin. Ideally, this optimal model should allow accurate, quantitative BCM determination and its features should reflect the human situation. We compared the biodistribution and pancreatic uptake of [^{111}In]In-DTPA-exendin in various rat and mouse strains and compared their specific GLP-1R expression pattern. Finally, we determined the specificity of [^{111}In]In-DTPA-exendin accumulation in beta cells using an alloxan-induced model for beta cell loss.

MATERIALS AND METHODS

Radiolabeling

[Lys^{40}(DTPA)]exendin-3 (Peptides Specialty Laboratories, Heidelberg, Germany) was radiolabeled as previously described (Brom 2012). Briefly, 150 MBq $^{111}InCl_3$ was added to 1 µg [Lys^{40}(DTPA)]exendin-3 dissolved in 0.1 M 2-(*N*-morpholino)ethanesulfonic acid (MES), pH 5.5 (Sigma Aldrich, St. Louis, MO, USA) and incubated for 20 minutes at room temperature. After incubation, EDTA (Sigma Aldrich) and Tween-80 (Sigma Aldrich) were added to a final concentration of 5 mM and 0.1%, respectively. The radiochemical purity of [^{111}In]In-DTPA-exendin-3 was determined by instant thin-layer chromatography (ITLC) (ITLC-SG, Agilent Technologies, Lake Forest, CA, USA), using 0.1 M EDTA in 0.1 M NH_4Ac (Sigma Aldrich), pH 5.5 as a mobile agent.

Animals

All animal experiments were approved by the Animal Welfare Committee of the Radboud University, Nijmegen and carried out in accordance with the local and national guidelines. Six to eight weeks old, male animals were used for all experiments. For the experiments in mice, BALB/c, DBA, CBA and C57Bl/6J mice were purchased from Janvier Labs (Le Genest Saint Isle, France) and the NMRI mice from Harlan (Horst, The Netherlands). For the experiments in rats, Brown Norway, F344, WAG/Rij and Sprague Dawley rats were purchased from Harlan.

Alloxan treatment

To determine the specificity of [^{111}In]In-DTPA-exendin accumulation in the beta cells, animals were injected with various doses (25 – 75 mg/kg) of alloxan monohydrate (Sigma chemicals, St Louis, MO, USA) to deplete the beta cells. Alloxan was dissolved in ice cold 10 mM HCl with a concentration of 0,1 mg/µl and diluted with ice cold PBS. During storage and dilution, alloxan was protected from light and kept on ice. Animals were injected intravenously with 200 µl alloxan solution within five minutes after dilution. Control animals were injected with vehicle (10 mM HCl diluted with PBS). Blood glucose concentrations were monitored for one week after alloxan injection using a blood glucose meter (Accu-Chek Sensor, Roche Diagnostics, Almere, The Netherlands).

Biodistribution studies

Biodistribution studies were performed to compare the [^{111}In]In-DTPA-exendin uptake in different mouse and rat strains. Based on the pancreatic uptake, endocrine-to-exocrine ratio, pancreas-to-stomach ratio and pancreas-to-duodenum ratio, one strain was chosen to determine the specificity of [^{111}In]In-DTPA-exendin accumulation in the beta cells, as described above. To determine the effect of alloxan over time, biodistribution studies were performed on day one, three, five and seven after alloxan injection. All animals used for biodistribution studies were injected intravenously with 15 MBq [^{111}In]In-DTPA-exendin-3 (peptide dose: 20 pmol/rat, mouse). Non-GLP-1R mediated exendin uptake was determined in a separate group of animals that were co-injected with an excess of unlabeled exendin (25 µg/animal). Four hours after injection of the radiolabeled exendin, animals were euthanized and the pancreas and other relevant tissues (blood, muscle, heart, lung, spleen, kidney, liver, stomach and duodenum) were dissected, weighed and counted in a well type gamma counter (Wallac 1480 Wizard, Perkin Elmer, Boston, MA, USA). The percentage injected dose per gram tissue (%ID/g) was determined for each tissue.

Digital autoradiography

Ex vivo autoradiography was performed to visualize the uptake in the islets and the exocrine pancreas. After dissection, pancreata were fixed in 4% formalin (w/v), dehydrated and embedded in paraffin. Sections of the pancreas (4 µm) were prepared and exposed to a phosphorimaging plate (Fuji Film BAS-SR 2025, Raytest, Straubenhardt, Germany) for seven days. Images were acquired with a radioluminography laser images (Fuji Film BAS 1800 II system (Raytest) and analyzed using Aida Image Analyzer software (Raytest).

Endocrine-to-exocrine ratio determination

To quantitatively compare tracer uptake in the islets and the exocrine pancreas, endocrine-exocrine uptake ratios were determined in the autoradiographs of pancreatic sections. The digital images were analyzed using imageJ, a public domain software *(http://imagej.nih.gov/ij/)*. Three pancreatic sections were analyzed per mouse and rat strain. Per pancreatic section, three regions of interest (ROI) were drawn in both the exocrine and endocrine pancreas and the mean density values (photostimulated luminescence) were determined. These values were used to calculate the endocrine-exocrine uptake ratio.

Immunohistochemistry

Pancreatic sections (4 µm) of C57Bl/6 mice, Brown Norway rats and humans were stained for the presence of GLP-1R. Antigen retrieval was performed in 10 mM sodium citrate, pH 6.0 for 10 minutes at 96 °C. Subsequently, sections were incubated for 10 minutes with 3% H_2O_2 in PBS at RT in the dark, to block endogenous peroxidase activity. Non-specific binding was blocked by incubation for 30 minutes with 5% normal swine serum. The primary anti-GLP-1R

antibody (ab39072, Abcam, Cambridge, UK) was diluted in PBS containing 1% BSA (1:500). Primary antibody incubation for 90 minutes was followed by incubation with swine-anti-rabbit peroxidase (1:50) (p0271, DAKO, Copenhagen, Denmark) for 30 min at RT in the dark. Finally, 3,3'diaminobenzidine (DAB) was used to develop the pancreatic sections.

Pancreatic islet isolation, mRNA extraction and real time PCR

mRNA extraction and real time PCR was performed as described previously [25]. Briefly, poly(A)+ mRNA was isolated from pancreatic islets (rat islets were isolated by collagenase digestion and handpicking and mouse islets using the Histopaque method [26]) or exocrine tissue (the tissue remaining after islet isolation) from C57Bl/6 mice and Wistar rats using the Dynabeads mRNA DIRECT™ kit (Invitrogen, Merelbeke, Belgium) and reversely transcribed. Exocrine mRNA samples used in the study were evaluated with Biodrop (Cambridge, United Kingdom) and showed a 260/280 ratio >1.9, suggesting that the mRNA was well preserved. Real time PCR amplification of *Glp-1r* was performed using IQ SyBR Green Supermix on iCycler MyiQ Single Color (BIO-RAD, Hercules, CA, USA) and compared to a standard curve. *amy2* was calculated with the deltaCT method [27]. In all assays the geometrical means of the house keeping genes *β-actin* and *gapdh* was used as a reference. The pancreatic islet and exocrine tissue preparations were selected based on the expression levels of respectively the endocrine marker *pdx1* and the exocrine marker *amy2*. The primers used are listed in Table 1. Standard curves of the reference genes (*β-actin* and *gapdh*) and *Glp1r* mRNA expression assays of both rat and mouse are provided in Figure 1.

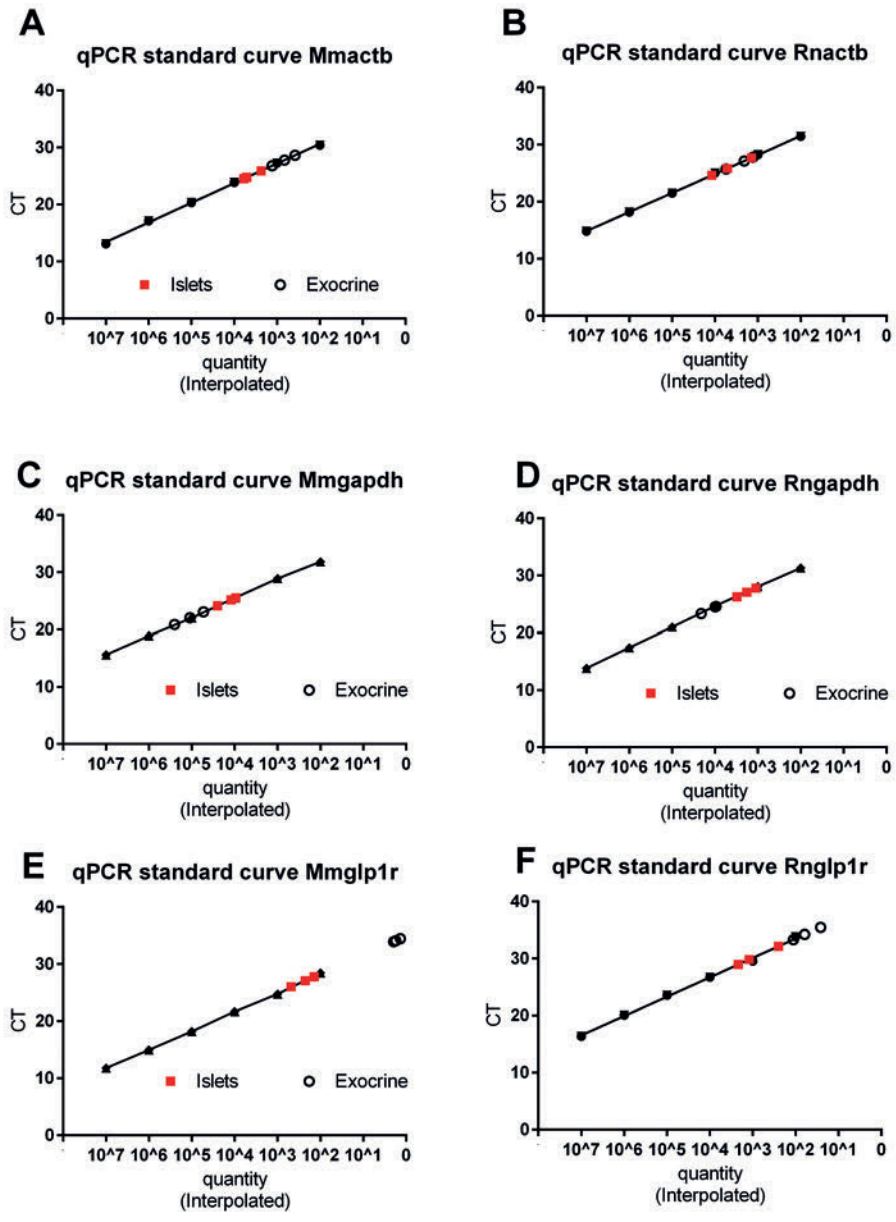

Figure 1. mRNA estimation of glucagon-like peptide 1 receptor (*Glp-1r*) expression was performed by quantitative PCR where beta actin (actb) and glyceraldehyde-3-phosphate dehydrogenase (gapdh) were used as reference genes. Standard curves of *actb*, *gapdh* and *Glp-1r* genes for both mouse (Mm, Mouse musculus, A, C, E) and rat (Rn, Rattus norvegicus, B, D, F) (mRNA expression assays, with plotted CT values of pancreatic islets samples (red squares) and exocrine tissue (black circles).

Table 1. Primers used for quantitative PCR on rat and mouse cDNA with the length of amplification in base pairs.

Primer	Sequence	Base pairs
Rat GLP-1R RT Forward (5'-3') Reverse (5'-3')	 GGCTCCTCTCGTATCAGGAC GATAACGAACAGCAGCGGAAC	200
Rat GLP-1R std Forward (5'-3') Reverse (5'-3')	 ATCCACCTGAACCTGTTTGC CTTGGCTATCACGATGCAGA	468
Mouse GLP-1R RT Forward (5'-3') Reverse (5'-3')	 GCGTGGCAGCCAACTACTA ATAACGAACAGCAGCGGAAC	139
Mouse GLP-1R std Forward (5'-3') Reverse (5'-3')	 ATCCACCTGAACCTGTTTGC AGCTTGATGAAGCGTAGGGT	617
Rat insulin RT Forward (5'-3') Reverse (5'-3')	 TGTGGTTCTCACTTGGTGGA CTCCAGTTGTGCCACTTGTG	111
Rat insulin std Forward (5'-3') Reverse (5'-3')	 TGACCAGCTACAGTCGGAA GTTGCAGTAGTTCTCCAGTTGG	390
Mouse insulin RT Forward (5'-3') Reverse (5'-3')	 GGAAGCCCCGGGGACCTTCAGA GGCGGGTCGAGGTGGGCCTTA	138
Mouse insulin std Forward (5'-3') Reverse (5'-3')	 CACCCAAGTCCCGCCGTGAAG TCAGTGGCATTTACACGGTTGCCTA	449
β-Actin RT Forward (5'-3') Reverse (5'-3')	 CTGTACGCCAACACAGTGCT GCTCAGGAGGAGCAATGATC	127
β-Actin std Forward (5'-3') Reverse (5'-3')	 AAATCTGGCACCACACCTTC CCGATCCACACGGAGTACTT	805
Rat pdx-1 RT Forward (5'-3') Reverse (5'-3')	 GGTATACCAGCGAGATGCT TCAGTTGGGAGCCTGATTCT	152
Rat pdx-1 std Forward (5'-3') Reverse (5'-3')	 GAGGACCCGTACAGCCTACA GGGACCGCTCAAGTTTGTAA	748
Mouse pdx-1 RT Forward (5'-3') Reverse (5'-3')	 GAGGTGCTTACACAGCGGAA GGGCCGGGAGATGTATTTGT	116
Mouse pdx-1 std Forward (5'-3') Reverse (5'-3')	 CCTTTCCCGAATGGAACCGA GCTCTCGTGCCCTCAAGAAT	679

Rat amy2 RT Forward (5'-3') Reverse (5'-3')	 ATTGATCTTGGTGGTGAAGCA GGCTCTGTCAGTAGGCACAA	 174
Rat amy2 std Forward (5'-3') Reverse (5'-3')	 CGAACCAAGGTGGCTGACTAT TCGATGTTCACAGACCCAGT	 636
Mouse amy2 RT Forward (5'-3') Reverse (5'-3')	 CATGGTGACAAGGTGCAACA CAGGTACTGCTTGTTCCTGC	 102
Mouse amy2 std Forward (5'-3') Reverse (5'-3')	 TCTGCACAAGGTCTGGAAATGA ACCCAGATCAATGACCTCTTGG	 500
Gadph RT Forward (5'-3') Reverse (5'-3')	 GCCTGGAGAAACCTGCCAAGTATGA AACCTGGTCCTCAGTGTAGCCC	 101
Gadph std Forward (5'-3') Reverse (5'-3')	 ATGACTCTACCCACGGCAAG TGTGAGGGAGATGCTCAGTG	 975

RESULTS

[^{111}In]In-DTPA-exendin uptake in various mouse strains

Figure 2 shows the biodistribution (2 mice per strain) of [^{111}In]In-DTPA-exendin in five mouse strains. As reported previously [28], tracer uptake was observed not only in the pancreas but also in various other organs, such as the lung, stomach, duodenum and the kidneys. Based on these results, BALB/c mice showed favorable features for *in vivo* beta cell targeting, namely: high pancreatic uptake (36.8 %ID/g) and relatively low uptake in lung (26.4 %ID/g), stomach (7.37 %ID/g) and duodenum (9.42 %ID/g). Therefore, BALB/c mice were selected to determine the specificity of tracer accumulation in the beta cells. C57Bl/6 mice, a strain often used in diabetes research, was also evaluated.

Table 2. Endocrine-exocrine ratio of [^{111}In]In-DTPA-exendin uptake in BALB/c and C57Bl/6 mice calculated from autoradiography of pancreatic sections.

Mouse strain	Endocrine-exocrine ratio
BALB/c	4.11 ± 0.93
C57Bl/6	4.56 ± 0.91

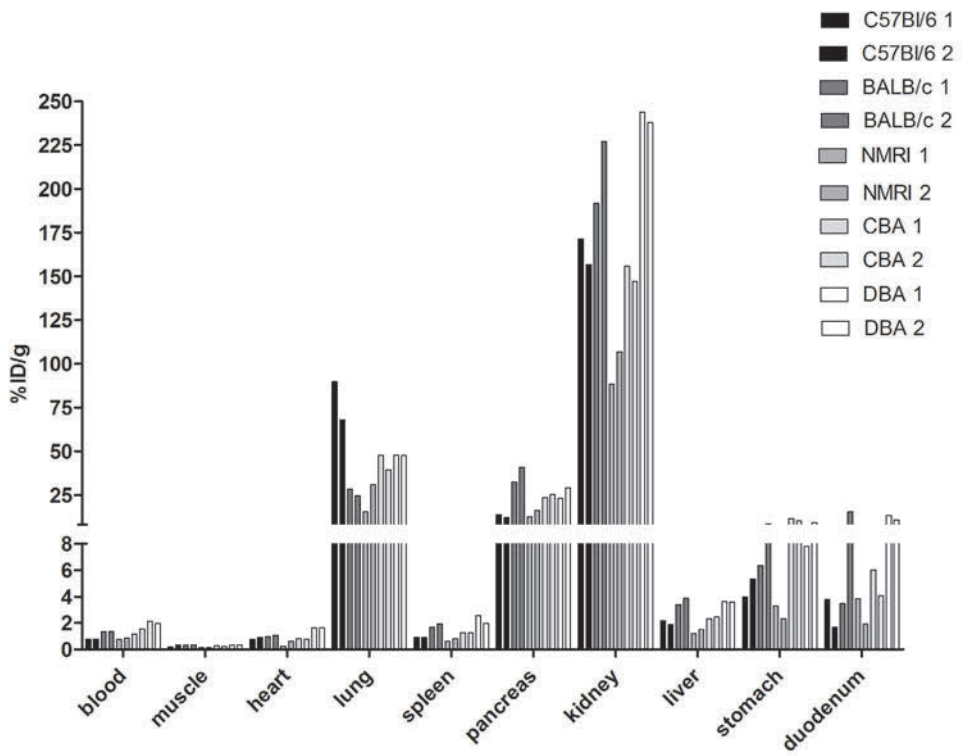

Figure 2. Biodistribution of [^{111}In]In-DTPA-exendin in C57Bl/6, BALB/c, NMRI, CBA and DBA mice. Values are expressed as percentage injected dose per gram tissue (n=2). Mice were dissected four hours after injection.

Beta cell specificity of [^{111}In]In-DTPA-exendin uptake in BALB/c and C57Bl/6 mice

In BALB/c mice, the pancreatic uptake did not decline after injection of 25, 32.5, 50 and 62.5 mg/kg alloxan (Figure 3A). Mice treated with even higher doses of alloxan (75, 100, 150 and 200 mg/kg) showed increased total pancreatic tracer uptake. In animals treated with high alloxan doses, elevated tracer levels in the blood were observed and thus, higher uptake in all other tissues, including the exocrine pancreas (Figure 3A and B). This is most probably the result of dehydration secondary to severe hyperglycemia, leading to slower blood clearance. In addition, direct toxic effects of alloxan cannot be excluded at high doses. Co-injection of an excess unlabeled exendin decreased the pancreatic uptake from 7.9 ± 0.6 %ID/g to 0.23 ± 0.04 %ID/g (Figure 3A) which was also reflected by the autoradiographic images (Figure 3C). Due to the high uptake in exocrine tissue, the endocrine-exocrine ratio in these mice was only 4.11 ± 0.93 (Table 2) which is very low when compared to rats. These results - especially the reduced uptake after co-injection of unlabeled exendin - indicate specific, receptor mediated tracer binding in the exocrine pancreas of BALB/c mice.

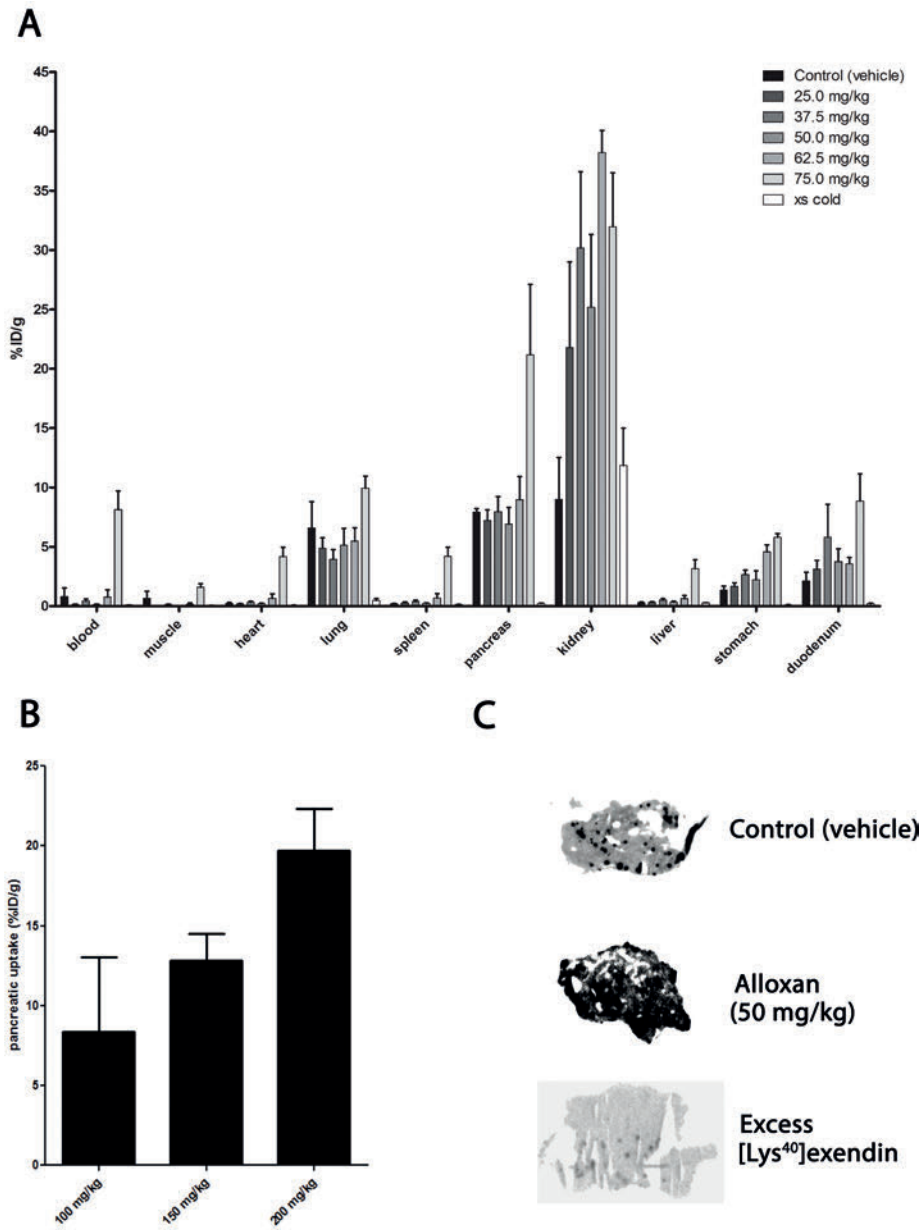

Figure 3. a) Biodistribution of [^{111}In]In-DTPA-exendin in control and alloxan treated BALB/c mice. Values are expressed as percentage injected dose per gram tissue (n=5 mice). Blocking was performed by co-injection of 25 µg unlabeled exendin (n=5). b) Pancreatic uptake of [^{111}In]In-DTPA-exendin in BALB/c mice treated with 100 mg/kg (n=5), 150 mg/kg (n=4) and 200 mg/kg (n=3) of alloxan. Values are expressed as percentage injected dose per gram tissue. c) Ex vivo autoradiography of pancreatic sections of BALB/c mice treated with PBS (control) and 50 mg/kg alloxan. Blocking was performed by co-injection of 25 µg unlabeled exendin.

Because of this high exocrine uptake, [^{111}In]In-DTPA-exendin uptake after alloxan treatment was further investigated in C57Bl/6 mice for validation of the results described above. Figure 4A summarizes pancreatic uptake of [^{111}In]In-DTPA-exendin in C57Bl/6 mice on various days after alloxan treatment. After three days, a clear decrease in pancreatic uptake was observed, while the maximum decrease was observed seven days after alloxan treatment. However, the decrease did not exceed 40% compared to control mice injected with vehicle. Furthermore, similar to the findings observed in BALB/c mice, tracer uptake in the exocrine pancreas of C57Bl/6 mice could be blocked with an excess of unlabeled exendin (Figure 4B and C). Additionally, the calculated endocrine-to-exocrine uptake ratio in these mice (4.56 ± 0.91) (Table 2) was in the same range as the ratio observed in BALB/c mice.

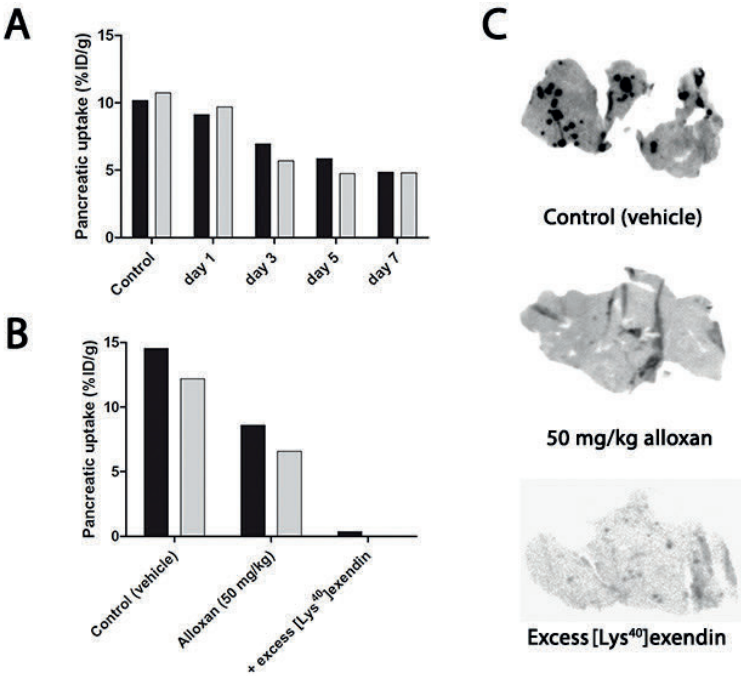

Figure 4. a) Pancreatic uptake of [^{111}In]In-DTPA-exendin in C57Bl/6 mice (n=2) on different days after alloxan treatment (50 mg/kg). b) Pancreatic uptake of [^{111}In]In-DTPA-exendin in C57Bl/6 mice treated with vehicle (control) (n=2) and 50 mg/kg alloxan (n=2). Blocking was performed by co-injection of 25 µg unlabeled exendin (n=1). c) Autoradiography of pancreatic sections of C57Bl/6 mice treated with vehicle (control) and 50 mg/kg alloxan. Blocking was performed by co-injection of 25 µg unlabeled exendin.

[^{111}In]In-DTPA-exendin uptake in different rat strains

Figure 5A summarizes the biodistribution (2 rats per strain) of [^{111}In]In-DTPA-exendin in four rat strains. In all rat strains there was very high lung uptake (> 10%ID/g), which was even higher than the uptake observed in the kidneys. The biodistribution profiles indicated that WAG/

Rij rats have the highest pancreatic [^{111}In]In-DTPA-exendin uptake (0.45%ID/g). In addition, the endocrine-to-exocrine uptake ratio, calculated from the autoradiographs shown in Figure 5B, was highest for WAG/Rij rats as well (Table 3). The uptake in the stomach (1.7 %ID/g) of WAG/Rij rats is relatively high (Figure 5B), resulting in a pancreas-to-stomach uptake ratio of 0.27 ± 0.02 (Table 4). Since high stomach uptake might hamper BCM visualization *in vivo*, we selected Brown Norway rats to investigate the beta cell specificity of pancreatic [^{111}In]In-DTPA-exendin accumulation due to their higher pancreas-to-stomach (1.39 ± 0.11) and acceptable pancreas-to-duodenum (0.70 ± 0.1) ratios (Table 4) despite their lower pancreatic uptake (0.27 %ID/g) (Figure 4A) and endocrine-to-exocrine ratio (57.1 ± 12.5) (Table 3).

Table 3. Overview of the endocrine-exocrine ratios of [^{111}In]In-DTPA-exendin uptake in various rat strains calculated from autoradiography of pancreatic sections.

Rat strain	Endocrine-exocrine ratio
WAG/Rij	105.66 ± 29.84
Brown Norway	57.06 ± 12.53
Sprague Dawley	44.00 ± 13.33
F344	44.83 ± 2.85

Table 4. Overview of the pancreas-to-stomach and pancreas-to-duodenum ratios of [^{111}In]In-DTPA-exendin uptake in the different rat strains.

Rat strain	Pancreas-to-stomach ratio	Pancreas-to-duodenum ratio
Sprague Dawley	0.08 ± 0.02	0.33 ± 0.02
F344	0.11 ± 0.00	0.31 ± 0.07
Wag/Rij	0.27 ± 0.02	1.15 ± 0.78
Brown Norway	1.39 ± 0.11	0.70 ± 0.10

Beta cell specificity of [^{111}In]In-DTPA-exendin uptake in Brown Norway rats

In Brown Norway rats, treated with 60 mg/kg alloxan (2 rats), pancreatic uptake was reduced by more than 80% compared to control rats, that were injected with vehicle (PBS) (2 rats) (Figure 6). Co-administration of an excess unlabeled exendin (1 rat) reduced the pancreatic uptake to similar uptake levels observed in alloxan-treated rats, suggesting no or very low non-specific [^{111}In]In-DTPA-exendin uptake in the exocrine pancreas. Furthermore, autoradiographical analysis showed similar results: high, specific tracer uptake in the islets of Langerhans and low, non-specific uptake in the exocrine pancreas (Figure 5B) resulting in an endocrine-to-exocrine uptake ratio of 57.1 ± 12.5 (Table 4). These results indicate high beta cell specificity of [^{111}In]In-DTPA-exendin in these rats.

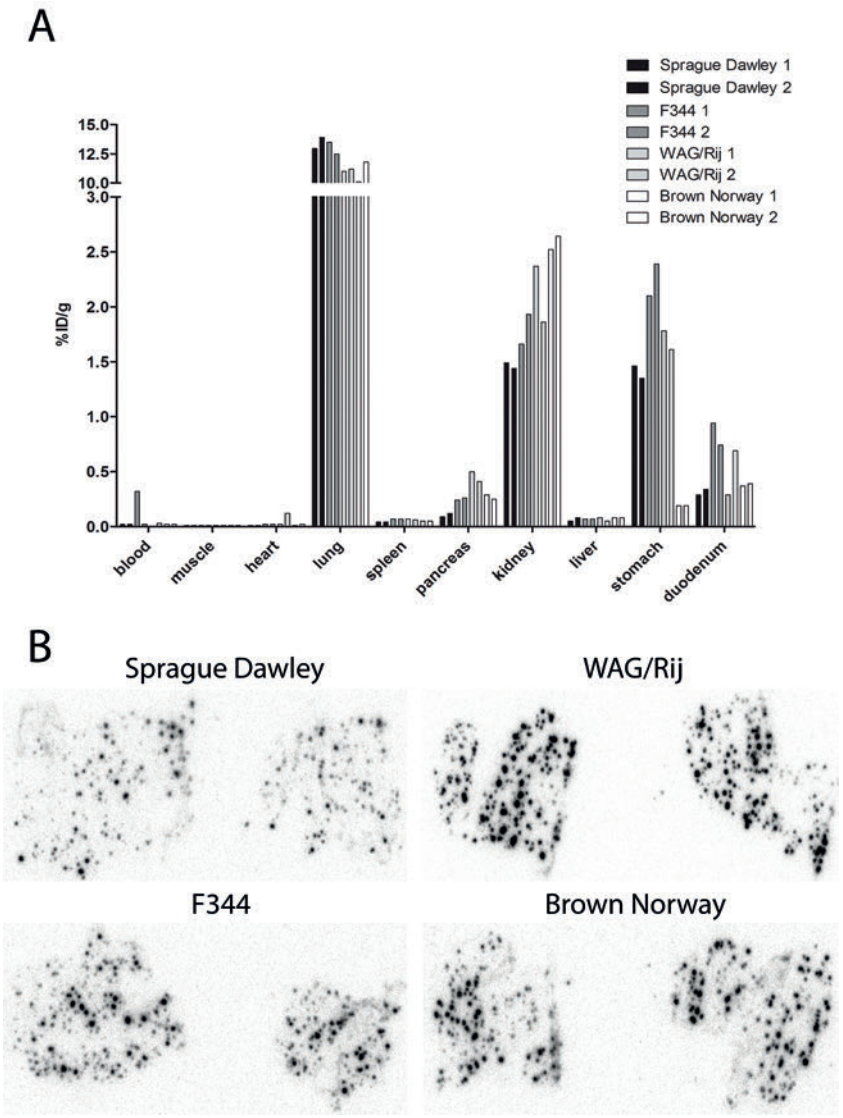

Figure 5. a) Biodistribution of [^{111}In]In-DTPA-exendin in Sprague Dawley, F344, Wag/Rij and Brown Norway rats. Values are expressed as percentage injected dose per gram tissue (n=2 rats). Rats were dissected four hours after injection. b) Autoradiography of pancreatic section of Sprague Dawley, F344, Wag/Rij and Brown Norway rats showing focal hotspots of tracer accumulation representing the islets.

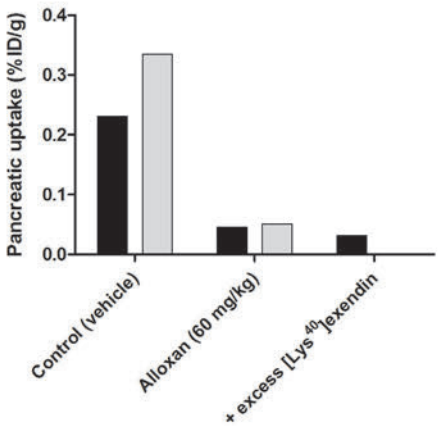

Figure 6. Pancreatic uptake of [^{111}In]In-DTPA-exendin in Brown Norway rats treated with vehicle (control) (n=2) and alloxan (60 mg/kg) (n=2). Values are expressed as percentage injected dose per gram tissue. Blocking was performed by co-injection of 25 µg unlabeled exendin (n=1).

Quantitative PCR

Since receptor mediated [^{111}In]In-DTPA-exendin uptake was observed in exocrine pancreas of mice, *Glp-1r* mRNA expression was compared in endocrine and exocrine pancreatic tissue of rats and mice. Quantitative RT-PCR revealed similar *Glp-1r* mRNA expression levels in endocrine and exocrine tissue of rat and mouse (Figure 7A and B) with endocrine-to-exocrine ratios of 45.8 and 55.6, respectively. Individual expression levels of all cell markers (*Glp-1r, Pdx1, Ins and Amy2b*) in endocrine and exocrine tissue are provided in Figure 8.

Immunohistochemistry

To investigate GLP-1R expression in endocrine and exocrine pancreatic tissue, GLP-1R staining was performed on rat, mouse and human pancreatic tissue. Figures 7C, D and E show the results of the immunohistochemical analysis. In all pancreatic tissues analyzed, the islets of Langerhans showed clear GLP-1R staining while no, or very limited, staining was observed in the exocrine portion of the pancreatic tissue.

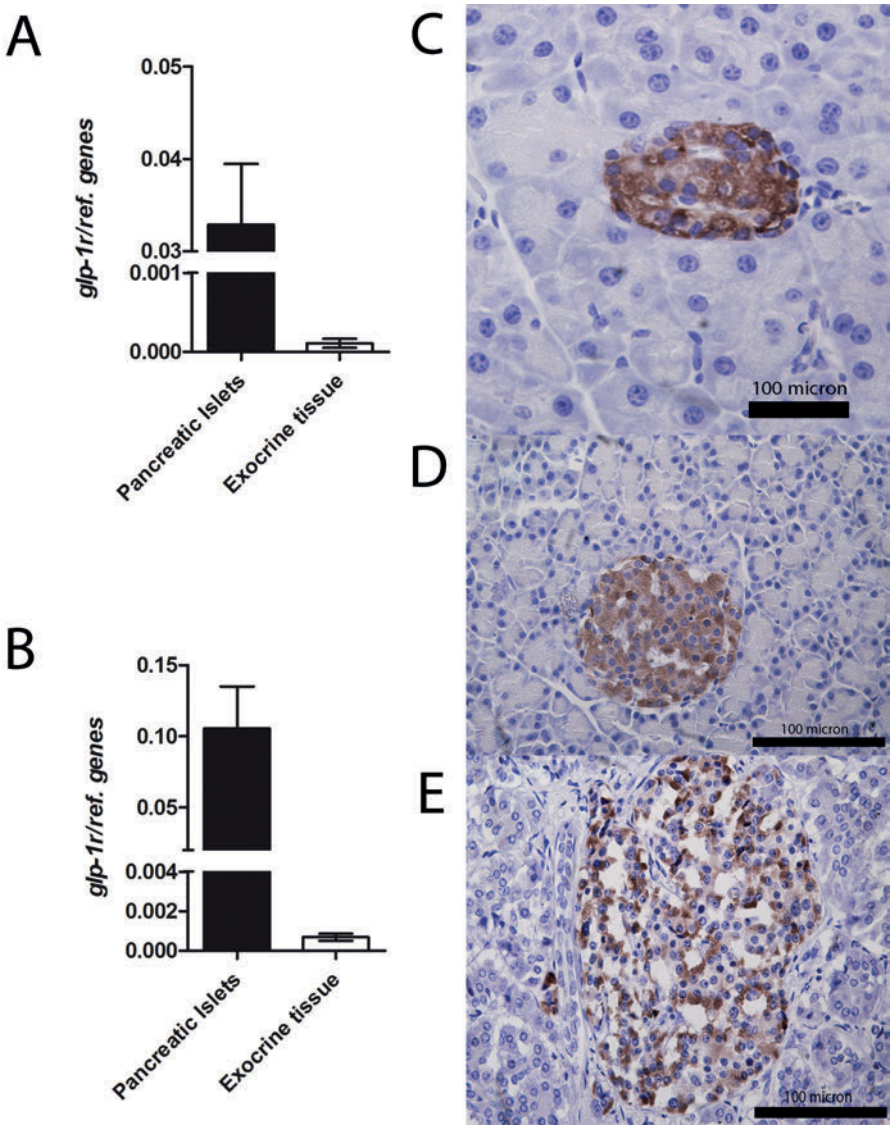

Figure 7. Quantitative PCR for the *Glp-1r* in endocrine and exocrine pancreatic tissue of rat (a) and mouse (b) and immunohistochemical analysis of GLP-1R expression in pancreatic tissue (embedded in paraffin) of rat (c), mouse (c) and human (c). Both analyses show high GLP-1R expression in the islets and no, or very low expression in exocrine tissue. For quantitative PCR, paired t-test was performed and $p < 0.05$ was considered as significant.

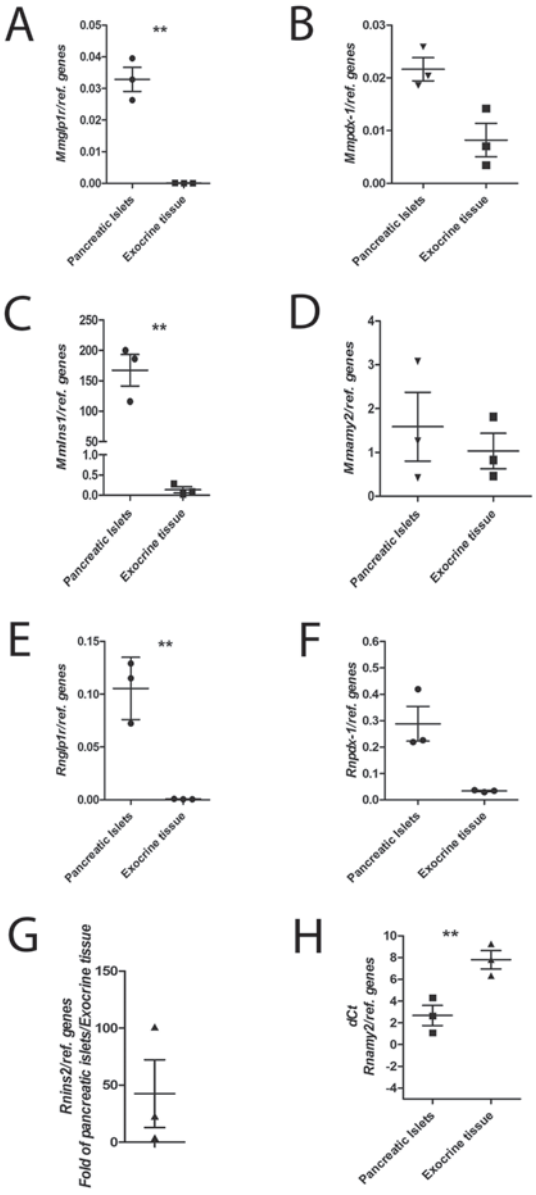

Figure 8. Quantitative PCR of the glucagon-like peptide 1 receptor (*Glp-1r*) mRNA expression in pancreatic islets and exocrine tissue with additional pancreatic endocrine and exocrine cell markers for mouse (Mm, Mouse musculus); A) *Glp-1r*, B) *Pdx1* (Pancreatic and duodenal homeobox 1), and C) *Ins1* (insulin) and D) *Amy2b* (pancreatic α-Amylase), and for rat (Rn, Rattus novergicus); E) *Glp1r*, F) *Pdx1*, G) *Ins2* (Insulin) and H) *Amy2b*. In both species the pancreatic islets were positive for *Glp-1r* and the endocrine cell markers *Pdx1* and *Ins*, while the exocrine material was positive for the exocrine cell marker *Amy2b* but had a decreased expression of *Glp-1r*, *Pdx1* and *Ins*. N=3 in all experimental conditions. Paired t-test was performed and $p<0.05$ was considered significant (**).

DISCUSSION

In this study, we assessed differences between rodent models for non-invasive *in vivo* BCM assessment via GLP-1R targeting. We investigated the biodistribution of [^{111}In]In-DTPA-exendin in various rat and mouse strains and determined the specificity of tracer accumulation in the beta cells. Our present findings indicate that Brown Norway rats display the most favorable characteristics for non-invasive BCM assessment using radiolabeled exendin as a tracer. Mice seem to display receptor mediated tracer uptake in the exocrine pancreas, an observation explaining the limited reduction of exendin uptake in the pancreas of mouse models after beta cell destruction [22, 24].

In view of the spatial resolution of present imaging modalities and the small size of the islets, preventing visualization of single islets *in vivo*, the optimal model for *in vivo* BCM determination must display high and specific [^{111}In]In-DTPA-exendin accumulation in the endocrine pancreas [29, 30] with no or low uptake in the exocrine pancreas and surrounding tissues, in particular stomach and duodenum that are localized in the vicinity of the pancreas. Since [^{111}In]In-DTPA-exendin is excreted via the kidneys, high tracer uptake is observed in this organ, which renders accurate quantification of pancreatic tracer uptake challenging in rodents. However, spill over signal from the kidneys can be excluded by analyzing a particular region of interest in the pancreas localized cranial and anterior of the kidneys [14]. Another option to overcome spillover effects of the kidneys is co-injection of a second radiotracer, specifically targeting the exocrine tissue such as [^{99m}Tc]Tc-demobesin and [^{123}I]I-L-phenylalanine in combination with [^{111}In]In-DTPA-exendin, which facilitates exact delineation of the pancreas and therefore improves accurate quantification of pancreatic [^{111}In]In-DTPA-exendin uptake [22]. Of all investigated rat strains, WAG/Rij rats showed the highest pancreatic [^{111}In]In-DTPA-exendin uptake. However, due to their less favorable pancreas-to-stomach and pancreas-to duodenum ratios, WAG/Rij rats are expected to be less suited for *in vivo* BCM determination using [^{111}In]In-DTPA-exendin SPECT than Brown Norway rats.

To evaluate the beta cell specificity of the tracer, *ex vivo* autoradiography was performed. In rats, focal hotspots of tracer accumulation, representing the beta cells, were observed while there was a low background signal in the exocrine tissue (Figure 5B). Beta cell depletion by alloxan injection resulted in disappearance of the tracer accumulating hotspots, confirming beta cell specificity of GLP-1R targeting using [^{111}In]In-DTPA-exendin allowing accurate BCM determination of BCM. Based on autoradiographic analysis, we showed endocrine-to-exocrine ratios of 105.7 ± 29.8 in WAG/Rij rats, 57.1 ± 12.5 in Brown Norway rats, 44.0 ± 13.3 in Sprague Dawley rats and 44.8 ± 2.9 in F344 rats, which is in line with previous observations [23]. Furthermore, pancreatic [^{111}In]In-DTPA-exendin uptake in Brown Norway rats is similarly decreased after alloxan-induced beta cell depletion and co-injection with an excess unlabeled exendin, confirming beta cell specific tracer accumulation in this model. We have previously shown clear differences in [^{111}In]In-DTPA-exendin uptake in the pancreas of Brown Norway

rats treated with various concentrations of alloxan, resulting in a linear correlation of SPECT signal and BCM [14]. These observations confirm that this rat strain provides an optimal model for *in vivo* BCM assessment via GLP-1R targeting.

Several groups have reported a decrease in pancreatic tracer uptake in mice after alloxan or streptozotocin-induced beta cell destruction [22, 24]. However, the maximum decrease did not exceed 40%, an observation which can be explained by our data. After co-injection of an excess unlabeled exendin in mice, tracer uptake was much lower than the remaining uptake observed after alloxan-induced beta cell depletion. These results strongly suggest that the limited decrease in tracer uptake after alloxan-induced beta cell destruction is caused by receptor mediated [^{111}In]In-DTPA-exendin uptake in the exocrine pancreas of mice. Nevertheless, there was no detectable GLP-1R expression in exocrine pancreatic tissue of mice by immunohistochemistry and only very low *Glp-1r* mRNA expression was observed by RT-PCR. Furthermore, endocrine-to-exocrine ratios of *Glp-1r* mRNA expression are similar in mice and rats. These observations suggest that [^{111}In]In-DTPA-exendin probably binds to a receptor other than the GLP-1R in the exocrine pancreatic tissue of mice, which could also explain the observations of Nalin et al. [31]. These findings preclude the use of this model for additional characterization of [^{111}In]In-DTPA-exendin uptake. In contrast with observations in mice after beta cell destruction [22, 24] (present data), and similar to the above described rat data, patients with long standing type 1 diabetes can show very low [^{111}In]In-DTPA-exendin uptake similar to background values [14], suggesting no or negligible uptake in the exocrine pancreas. Therefore, the situation in humans appears to be better reflected by rat models than by mouse models. At this point in time, it remains unclear which receptor is responsible for exendin uptake in the exocrine pancreas of mice but it is highly likely that this receptor shows differences with the rat and human receptors in a way that only the variant expressed in mice can bind exendin.

CONCLUSION

The choice of a certain rodent model can greatly influence studies investigating BCM dynamics. The present findings indicate that mice have binding in the exocrine pancreas which is mediated by a receptor that is not the GLP-1R, rendering them an inadequate model for BCM assessment by radiolabeled exendin. On the other hand, rats do not show receptor mediated exendin binding in the exocrine pancreas, and are therefore a better suited model for further studies. Among the investigated rat models, Brown Norway rats are the optimal model for non-invasive GLP-1R targeting given their favorable pancreas-to-background uptake ratios. In view of these results and the very low remaining uptake in patients with T1D, rats appear to display better characteristics for *in vivo* investigation of BCM dynamics when compared to mice, and are thus considered a suitable model better reflecting the human situation than other animal models.

ACKNOWLEDGEMENTS

We thank Bianca Lemmers, Henk Arnts, Iris Lamers and Kitty Lemmens for their technical support with the animal experiments. The research leading to these results has received funding from the People Programme (Marie Curie Actions) of the European Union's Seventh Framework Programme FP7/2007-2013/ project BetaTrain under REA grant agreement n° 289932, the European Community's Seventh Framework Programme FP7/2007-2013/ project BetaImage under grant agreement n° 222980, NIH grant 1R01 AG 030328-01 (all to MG) and JDRF grant 3-SRA-2014-32-S-B (to DLE).

CONFLICT OF INTEREST STATEMENT

The authors declare that they have no conflict of interest

STATEMENT OF ANIMAL RIGHTS

All applicable institutional and/or national guidelines for the care and use of animals were followed.

REFERENCES

1. Lohr M, Kloppel G. Residual insulin positivity and pancreatic atrophy in relation to duration of chronic type 1 (insulin-dependent) diabetes mellitus and microangiopathy. *Diabetologia*. **1987**; 30 (10): 757-762.
2. Butler AE, Janson J, Bonner-Weir S, Ritzel R, Rizza RA, Butler PC. Beta-cell deficit and increased beta-cell apoptosis in humans with type 2 diabetes. *Diabetes*. **2003**; 52 (1): 102-110.
3. Steele C, Hagopian WA, Gitelman S, Masharani U, Cavaghan M, Rother KI, *et al*. Insulin secretion in type 1 diabetes. *Diabetes*. **2004**; 53 (2): 426-433.
4. Cnop M, Welsh N, Jonas JC, Jorns A, Lenzen S, Eizirik DL. Mechanisms of pancreatic beta-cell death in type 1 and type 2 diabetes: many differences, few similarities. *Diabetes*. **2005**; 54 Suppl 2 S97-107.
5. Weir GC, Bonner-Weir S. Five stages of evolving beta-cell dysfunction during progression to diabetes. *Diabetes*. **2004**; 53 Suppl 3 S16-21.
6. Ritzel RA, Butler AE, Rizza RA, Veldhuis JD, Butler PC. Relationship between beta-cell mass and fasting blood glucose concentration in humans. *Diabetes care*. **2006**; 29 (3): 717-718.
7. Yang L, Ji W, Xue Y, Chen L. Imaging beta-cell mass and function in situ and in vivo. *Journal of molecular medicine*. **2013**; 91 (8): 929-938.
8. Eriksson AU, Svensson C, Hornblad A, Cheddad A, Kostromina E, Eriksson M, *et al*. Near infrared optical projection tomography for assessments of beta-cell mass distribution in diabetes research. *Journal of visualized experiments : JoVE*. **2013**; (71): e50238.
9. Virostko J, Radhika A, Poffenberger G, Dula AN, Moore DJ, Powers AC. Bioluminescence imaging reveals dynamics of beta cell loss in the non-obese diabetic (NOD) mouse model. *PloS one*. **2013**; 8 (3): e57784.
10. Stasiuk GJ, Minuzzi F, Sae-Heng M, Rivas C, Juretschke HP, Piemonti L, *et al*. Dual-Modal Magnetic Resonance/Fluorescent Zinc Probes for Pancreatic beta-Cell Mass Imaging. *Chemistry*. **2015**; 21 (13): 5023-5033.
11. Vinet L, Lamprianou S, Babic A, Lange N, Thorel F, Herrera PL, *et al*. Targeting GLP-1 receptors for repeated magnetic resonance imaging differentiates graded losses of pancreatic beta cells in mice. *Diabetologia*. **2015**; 58 (2): 304-312.
12. Antkowiak PF, Stevens BK, Nunemaker CS, McDuffie M, Epstein FH. Manganese-enhanced magnetic resonance imaging detects declining pancreatic beta-cell mass in a cyclophosphamide-accelerated mouse model of type 1 diabetes. *Diabetes*. **2013**; 62 (1): 44-48.
13. Pattou F, Kerr-Conte J, Wild D. GLP-1-receptor scanning for imaging of human beta cells transplanted in muscle. *The New England journal of medicine*. **2010**; 363 (13): 1289-1290.
14. Brom M, Woliner-van der Weg W, Joosten L, Frielink C, Bouckenooghe T, Rijken P, *et al*. Non-invasive quantification of the beta cell mass by SPECT with In-labelled exendin. *Diabetologia*. **2014**;
15. Eriksson O, Espes D, Selvaraju RK, Jansson E, Antoni G, Sorensen J, *et al*. Positron emission tomography ligand [11C]5-hydroxy-tryptophan can be used as a surrogate marker for the human endocrine pancreas. *Diabetes*. **2014**; 63 (10): 3428-3437.

16. Aaen K, Rygaard J, Josefsen K, Petersen H, Brogren CH, Horn T, *et al*. Dependence of antigen expression on functional state of beta-cells. *Diabetes*. **1990**; 39 (6): 697-701.

17. Malaisse WJ, Damhaut P, Malaisse-Lagae F, Ladriere L, Olivares E, Goldman S. Fate of 2-deoxy-2-[18F]fluoro-D-glucose in control and diabetic rats. *International journal of molecular medicine*. **2000**; 5 (5): 525-532.

18. Eriksson O, Selvaraju RK, Johansson L, Eriksson JW, Sundin A, Antoni G, *et al*. Quantitative imaging of serotonergic biosynthesis and degradation in the endocrine pancreas. *Journal of nuclear medicine : official publication, Society of Nuclear Medicine*. **2014**; 55 (3): 460-465.

19. Simpson NR, Souza F, Witkowski P, Maffei A, Raffo A, Herron A, *et al*. Visualizing pancreatic beta-cell mass with [11C]DTBZ. *Nuclear medicine and biology*. **2006**; 33 (7): 855-864.

20. Brom M, Joosten L, Frielink C, Boerman O, Gotthardt M. (111)In-exendin uptake in the pancreas correlates with the beta-cell mass and not with the alpha-cell mass. *Diabetes*. **2015**; 64 (4): 1324-1328.

21. Kung MP, Hou C, Lieberman BP, Oya S, Ponde DE, Blankemeyer E, *et al*. In vivo imaging of beta-cell mass in rats using 18F-FP-(+)-DTBZ: a potential PET ligand for studying diabetes mellitus. *Journal of nuclear medicine : official publication, Society of Nuclear Medicine*. **2008**; 49 (7): 1171-1176.

22. Mathijs I, Xavier C, Peleman C, Caveliers V, Brom M, Gotthardt M, *et al*. A standardized method for in vivo mouse pancreas imaging and semiquantitative beta cell mass measurement by dual isotope SPECT. *Molecular imaging and biology : MIB : the official publication of the Academy of Molecular Imaging*. **2015**; 17 (1): 58-66.

23. Mikkola K, Yim CB, Fagerholm V, Ishizu T, Elomaa VV, Rajander J, *et al*. 64Cu- and 68Ga-labelled [Nle(14),Lys(40)(Ahx-NODAGA)NH2]-exendin-4 for pancreatic beta cell imaging in rats. *Molecular imaging and biology : MIB : the official publication of the Academy of Molecular Imaging*. **2014**; 16 (2): 255-263.

24. Reiner T, Thurber G, Gaglia J, Vinegoni C, Liew CW, Upadhyay R, *et al*. Accurate measurement of pancreatic islet beta-cell mass using a second-generation fluorescent exendin-4 analog. *Proceedings of the National Academy of Sciences of the United States of America*. **2011**; 108 (31): 12815-12820.

25. Villate O, Turatsinze JV, Mascali LG, Grieco FA, Nogueira TC, Cunha DA, *et al*. Nova1 is a master regulator of alternative splicing in pancreatic beta cells. *Nucleic acids research*. **2014**; 42 (18): 11818-11830.

26. Fukaya M, Tamura Y, Chiba Y, Tanioka T, Mao J, Inoue Y, *et al*. Protective effects of a nicotinamide derivative, isonicotinamide, against streptozotocin-induced beta-cell damage and diabetes in mice. *Biochemical and biophysical research communications*. **2013**; 442 (1-2): 92-98.

27. Livak KJ, Schmittgen TD. Analysis of relative gene expression data using real-time quantitative PCR and the 2(-Delta Delta C(T)) Method. *Methods*. **2001**; 25 (4): 402-408.

28. Brom M, Joosten L, Oyen WJ, Gotthardt M, Boerman OC. Radiolabelled GLP-1 analogues for in vivo targeting of insulinomas. *Contrast media & molecular imaging*. **2012**; 7 (2): 160-166.

29. Gotthardt M, Boermann OC, Behr TM, Behe MP, Oyen WJ. Development and clinical application of peptide-based radiopharmaceuticals. *Current pharmaceutical design*. **2004**; 10 (24): 2951-2963.

30. Hofland LJ, Lamberts SW. The pathophysiological consequences of somatostatin receptor internalization and resistance. *Endocrine reviews*. **2003**; 24 (1): 28-47.

31. Nalin L, Selvaraju RK, Velikyan I, Berglund M, Andreasson S, Wikstrand A, *et al*. Positron emission tomography imaging of the glucagon-like peptide-1 receptor in healthy and streptozotocin-induced diabetic pigs. *European journal of nuclear medicine and molecular imaging*. **2014**; 41 (9): 1800-1810.

CHAPTER 8

Measuring the pancreatic beta cell mass *in vivo* with exendin SPECT during hyperglycemia and severe insulitis

Lieke Joosten[1], Maarten Brom[1], Hanneke Peeters[1], Desirée Bos[1], Eddy Himpe[2], Luc Bouwens[2], Otto C. Boerman[1] & Martin Gotthardt[1]

1 Department of Radiology and Nuclear Medicine, Radboud University Medical Center, Nijmegen, The Netherlands

2 Department of Cell Differentiation, Vrije Universiteit Brussel, Brussels, Belgium

Molecular Pharmaceutics. **2019**; 16(9):4024-4030

ABSTRACT

Targeting the glucagon like peptide-1 receptor (GLP-1R) with radiolabeled exendin is a very promising method to non-invasively determine the beta cell mass in the pancreas, which is needed to unravel the pathophysiology of type 1 and type 2 diabetes. The present study aimed to explore the effects of both hyperglycemia and insulitis on the uptake of exendin in a spontaneous type 1 diabetes mouse model: Non-Obese Diabetic (NOD) mice.

NOD mice (n = 75, 7-21 weeks old) were injected intravenously with [^{111}In]In-DTPA-exendin-3 and SPECT images were acquired 1 hour p.i.. The pancreatic accumulation of [^{111}In]In-DTPA-exendin-3 was quantified *in vivo* using SPECT and by *ex vivo* counting and correlated to the beta cell mass (BCM). The influence of insulitis and hyperglycemia on the exendin uptake were assessed.

The pancreas could be visualized longitudinally using SPECT. A linear correlation was found between the BCM (%) and pancreatic uptake (%ID/g) as measured by *ex vivo* counting (Pearson $r = 0.64$, $p < 0.001$), which was not affected by either insulitis (Pearson $r = 0.66$, $p = 0.83$) or hyperglycemia (Pearson $r = 0.57$, $p = 0.51$). Biodistribution and *ex vivo* autoradiography revealed remaining [^{111}In]In-DTPA-exendin-3 uptake in the pancreas despite total ablation of BCM.

Despite hyperglycemia and severe insulitis, we have found a good correlation between BCM and pancreatic exendin uptake, even in a suboptimal model with relatively high background activity.

INTRODUCTION

Type 1 diabetes (T1D) is characterized by islet-specific autoimmunity, followed by progressive depletion of the insulin-producing beta cells leading to hyperglycemia [1]. Complete destruction of beta cells in patients with long-standing type 1 diabetes has been believed to be the single cause of hyperglycemia for a long time, however, this theory has been challenged lately. In the last few years, several studies have found evidence of residual insulin-positive beta cells in patients with longstanding T1D [2, 3]. Furthermore, some patients with recent-onset T1D or patients positive for autoantibodies (ICA, GADA and IA-2-Ab) but not (yet) diabetic showed lack of insulitis [4-6], which has been considered to be the pathophysiological key feature required for development of T1D. Insulitis is defined as the presence of lymphocytes infiltrating the islets of Langerhans [4] leading to destruction of the beta cells.

The evidence of remaining but functionally impaired beta cells in longstanding T1D patients and the presence or absence of insulitis underline the population heterogeneity of T1D and with that the crucial need for a non-invasive method to determine the beta cell mass. Beta cell function can be measured by clinical tests determining insulin production capacity following stimulation, but it appears that beta cell mass and functional beta cell mass are not identical [7], emphasizing the relevance for individual monitoring of the beta cell mass in relation to functional capacity. Such a method allows for monitoring of therapies targeting the autoimmune response to protect the beta cells or therapies to increase BCM.

The beta cells can be visualized non-invasively using radiolabeled exendin and SPECT or PET [8, 9]. Exendin is a stable analog of GLP-1 and targets the GLP-1R receptor with high affinity, which is highly expressed on beta cells.

Previously, we have shown the feasibility of radiolabeled exendin to monitor the beta cell mass in a rat model with chemically induced beta cell destruction [8], and in a rat model for spontaneous type 1 diabetes [10]. In both studies a strong good linear correlation between exendin uptake and the beta cell mass was found.

The expression of the GLP-1R can change during the development of diabetes. During insulitis, several cytokines (like Il-1ß and IFN-γ) are released by immune cells, which in turn alter the expression of many genes, amongst which the GLP-1R [11]. Furthermore, previous studies in mice showed that hyperglycemia reduced the expression of the GLP-1R and thereby the beta cell function [12, 13].

To address the effects of longstanding hyperglycemia and longstanding inflammation of the islets on the GLP-1R expression and thus uptake of exendin in the pancreas, we performed a study using Non-Obese Diabetic (NOD) mice. This mouse model is the only well-characterized spontaneous mouse model for studying T1D [14]. The development of diabetes in this model shows a variety of similarities with that in human patients, like the presence of particular immune cells and cytokines (like Il-1ß and IFN-γ) in the diabetic pancreas, and the presence of insulitis [14-16], although the insulitis is much more severe in mice than in men. Furthermore,

this model is suitable to study the effects of hyperglycemia, since these mice do not necessarily require insulin treatment.
Here, we determined the correlation between the BCM and pancreatic uptake of radiolabeled exendin under conditions of severe insulitis and hyperglycemia.

MATERIALS AND METHODS

Animals

All animal experiments were approved by the Animal Ethical Committee of the Radboud University, Nijmegen, The Netherlands, and all experiments were performed according to the Institute of Laboratory Animal Research Guidelines.
Non Obese Diabetic (NOD) female mice were purchased from Charles River Laboratories (L'Arbresle, France). Unilateral nephrectomy of the left kidney had been performed at the age of 5 weeks under isoflurane anesthesia using Buprenorphine as analgesic and the mice arrived at our facility between 6 and 9 weeks of age. One group of mice (n = 6) did not undergo nephrectomy and was euthanized at an age of 12 weeks to determine the distribution of the tracer, without any further measurements. Mice were housed in a pathogen-free environment in ventilated filter-topped cages (5 mice per cage), required to maintain diabetes incidence, and had *ad libitum* access to sterile water and chow. Mice were allowed to adapt to laboratory conditions for 1 week before the start of the experiments.
At least twice a week the body weight of the mice was measured, blood was drawn by venous puncture and blood glucose was measured using a blood glucose meter (Accu-Chek Sensor, Roche Diagnostics, Almere, The Netherlands). Every week a group of 5 mice was studied using SPECT, starting at 7 weeks old until 21 weeks old. Mice were considered diabetic when glucose levels exceeded 11.1 mmol/l [17].

Radiolabeling of DTPA-exendin-3 with ^{111}In

[Lys^{40}(DTPA)]exendin-3 was purchased from Peptide Specialty Laboratories (PSL, Heidelberg, Germany) and referred to as DTPA-exendin-3. DTPA (diethylene triamine penta acetic acid) was conjugated to the ε-amino group of C-terminal Lysine. $^{111}InCl_3$ was obtained from Mallinckrodt Medical (Petten, The Netherlands). DTPA-exendin-3 was labeled with ^{111}In as described previously [18]. Briefly, DTPA-exendin-3 (1 µg, 200 pmol) was incubated for 20 min with 150 MBq $^{111}InCl_3$ and two volumes of 0.1 M MES buffer, pH 5.5. Subsequently, 50 mM EDTA (ethylenediaminetetraacetic acid) (Sigma Aldrich, St. Louis, MO, USA) and 10% Tween-80 (Sigma Aldrich, St. Louis, MO, USA) to a final concentration of 5 mM and 0.1% respectively were added. The radiolabeled peptide was separated from the unbound ^{111}In using solid-phase extraction using an HLB (hydrophilic-lipophilic balance reversed-phase sorbent) cartridge (Waters Oasis©, Milford, MA, USA) as described previously [19]. Pure ethanol was used for

activation of the cartridge and 0.1 M MES buffer was used for conditioning and washing. Quality control was performed by Instant Thin Layer Chromatography (ITLC) on silica gel ITLC strips (ITLC-SG Biodex, Shirley, NY, USA). As a mobile phase 0.1 M EDTA in 0.1 M NH_4Ac, pH 5.5 was used (R_f [^{111}In]In-DTPA-exendin-3 = 0, R_f ^{111}In-EDTA = 1).

Biodistribution and SPECT

Every week 5 mice were injected intravenously with 19.7±1.3 MBq (20 pmol). One hour p.i. mice were anesthetized and subjected to SPECT/CT. Images were acquired with an acquisition time of 50 minutes using a dedicated small animal SPECT scanner (U-SPECT-II, MILabs, Utrecht, The Netherlands) and a 0.1 mm pinhole mouse collimator.

Mice were euthanized after SPECT/CT using CO_2/O_2 suffocation. Blood, muscle, heart, lung, spleen, pancreas, stomach, intestine, kidney and liver were dissected, weighed and the radioactivity concentration was determined in a gamma counter (Wallac 1480-Wizard, Perkin-Elmer, Boston, MA, USA). Pancreata were fixed overnight in formaldehyde, dehydrated and embedded in paraffin.

The U-SPECT-Rec software (MILabs, Utrecht, The Netherlands) was used to reconstruct the SPECT images (OSEM with 16 subsets, 1 iteration and a voxel size of 0.4 mm). The pancreatic uptake of [^{111}In]In-DTPA-exendin-3 was quantified using Inveon Research Workplace (Preclinical Solutions, Siemens Medical Solutions USA, Inc., Knoxville, TN, USA). A volume of interest over the pancreas was drawn manually and corrected for overlapping kidney uptake. For each mouse a volume of 100 mm^3, including the voxels with the highest value, was measured by thresholding.

Macroautoradiography

Pancreatic sections of 5 µm were cut (one mouse per group). Two sections per mouse were exposed to a phosphor screen Fuji Film BAS-SR 2025, Raytest, Straubenhardt, Germany) for 7 days, images were acquired with a radioluminography laser imager (Fuji Film BAS 1800 II System, Raytest) and analyzed using Aida Image Analyzer software (Raytest).

Beta cell mass measurement and insulitis

Four µm thin sections were cut, mounted on glass and stained. Pancreatic sections were stained with guinea pig anti-insulin polyclonal antibody (1:3,000; Van Schravendijk, Brussels) and species-matched Cy3-conjugated secondary antibody (Jackson ImmunoResearch, Cambridgeshire, UK), and counterstained with Hoechst (Sigma Aldrich). Images were acquired with a Carl Zeiss multi-photon confocal laser scanning microscope LSM710 and analyzed using IPLAB pathway 4.0 software. Beta cell mass was estimated morphometrically by quantifying total insulin immunoreactive area within a pancreatic section area of at least 100 mm^2 for each mouse multiplied by the pancreatic weight as previously described [20]. Insulitis was examined histologically after hematoxylin and eosin staining using a bright field microscope (Zeiss

Axioskop, Oberkochen, Germany) and the degree of insulitis was scored as the percentage of islets that were infiltrated. The observer was blinded for the origin of the sections.

Immunohistochemistry

Four µm thin sections were cut, mounted on glass and stained. Pancreatic sections were treated with 10 mM citrate, pH 6.0 for 10 min at 96°C to reverse epitope masking. Blocking was performed by incubating for 10 min at room temperature in 3% H_2O_2, followed by 30 min at RT in 20% normal goat serum. Subsequently, sections were stained with guinea pig anti-insulin (1:3,000; A0564; DAKO, Agilent, Ca, USA) for 60 min at room temperature, followed by goat-anti-guinea pig-HRP (1:1,000; A18775, Thermo Fisher, Massachusetts, USA) for 30 min at RT. Adjacent sections underwent antigen retrieval by a 10 min incubation step at 37°C in 0.1% pronase, followed by blocking in 3% H_2O_2 for 10 min at room temperature and 10 min at room temperature in 1% bovine serum albumin (BSA). Next, sections were stained with mouse-anti-GLP-1R (1:100; 7F382A, Novo Nordisk, Bagsvaerd, Denmark) overnight at 4°C, followed by a 30 min incubation at room temperature with Opal Polymer HRP Ms + Rb (ARH1001EA: Perkin Elmer). Sections were counterstained with hematoxylin and images were acquired using a Leica DM3000 microscope and Leica DMC2900 camera (Leica, Wetzlar, Germany) and Leica Application Suite software (v 4.11, Leica).

Statistical analysis

GraphPad Prism software version 5.03 for Windows was used for data analysis: One-way ANOVA followed by a Tukey test was used to determine significance. A *p*-value below 0.05 was considered significant. All correlation coefficients were calculated with a Pearson correlation coefficient using SPSS (IBM SPSS Statistics 22). To calculate the influence of insulitis and hyperglycemia on the correlation between the beta cell mass and the uptake of radiolabeled exendin, a partial correlation analysis was performed, with hyperglycemia and insulitis as confounding factors. The statistical difference between these correlations was examined by a two-tailed Fisher r-to-z transformation.

RESULTS

Blood glucose

The blood glucose level of the mice was measured at least twice a week. In Figure 1 all measured blood glucose values from 7 to 21 weeks of age of all mice are summarized. During the first 14 weeks all mice were able to control their glucose levels, which ranged between 3.8 and 11.1 mmol/l (normoglycemic). From week 15 onwards elevated glucose levels were measured, that increased rapidly, indicating hyperglycemia.

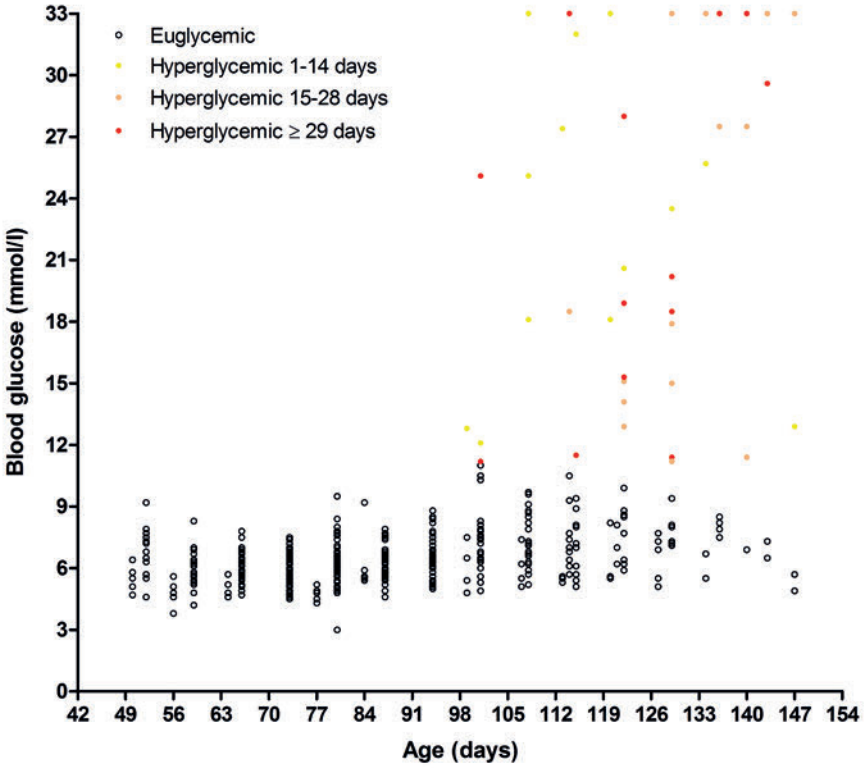

Figure 1. Blood glucose levels (mmol/l) in NOD mice up to 21 weeks of age. Blood glucose was measured twice a week. The duration of hyperglycemia was classified for every mouse: Euglycemic (< 11.1 mmol/l) (open circles) or hyperglycemic (≥ 11.1 mmol/l) for 1 to 14 days (yellow circles) (n=8), 15 – 28 days (brown circles) (n=4) and ≥ 29 days (red circles) (n=3).

Biodistribution and SPECT/CT

The highest pancreatic uptake was found in the group of mice at an age of eight weeks (16.4 ± 3.3 %ID/g), whereas the lowest average uptake was observed in mice of 17 weeks old (6.7 ± 2.0 %ID/g) (p=0.0005). Overall, a clear decrease in exendin uptake was observed over time. The comparative biodistribution between mice that were nephrectomised and mice that were not, is shown in Figure 2.

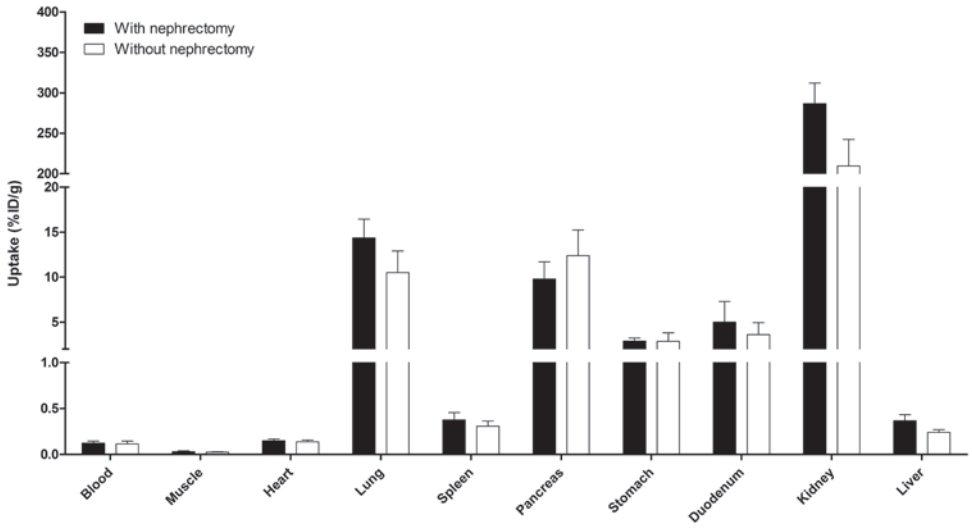

Figure 2. Biodistribution of [^{111}In]In-DTPA-exendin-3 in NOD mice of 12 weeks old. Mice that underwent unilateral nephrectomy are indicated with black bars (n=5), mice without nephrectomy are indicated with white bars (n=6). Values are expressed as a percentage of the injected dose per gram of tissue (error bars is SD).

SPECT with [^{111}In]In-DTPA-exendin-3 clearly visualized the pancreas. Figure 3 shows examples of three mice of different ages and with a different BCM. The decline in [^{111}In]In-DTPA-exendin-3 uptake in the pancreas is clearly visible in these images. Image 3a was obtained from a healthy mouse of 7 weeks old, with an [^{111}In]In-DTPA-exendin-3 uptake in the pancreas of 18.1 %ID/g and a BCM of 0.13 %. Image 3b shows a mouse of 13 weeks old, a pancreatic uptake of 12.2 %ID/g and a BCM of 0.06 %. Both mice had normal blood glucose levels. Finally, image 3c is from a 19-weeks old mouse, with an uptake of 4.5 %ID/g, a BCM of 0.00 % and with high blood glucose levels during several weeks. Notably, there was still uptake of exendin detected in the diabetic mouse. Next to pancreatic uptake, also high uptake of exendin in the kidney was observed.

A linear correlation of 0.68 (Pearson r, $p < 0.001$) between the exendin uptake in the pancreas, measured by *ex vivo* counting and the SPECT signal was found (Figure 4). When the SPECT signal declined, also a decline in the pancreatic uptake measured by *ex vivo* counting was found.

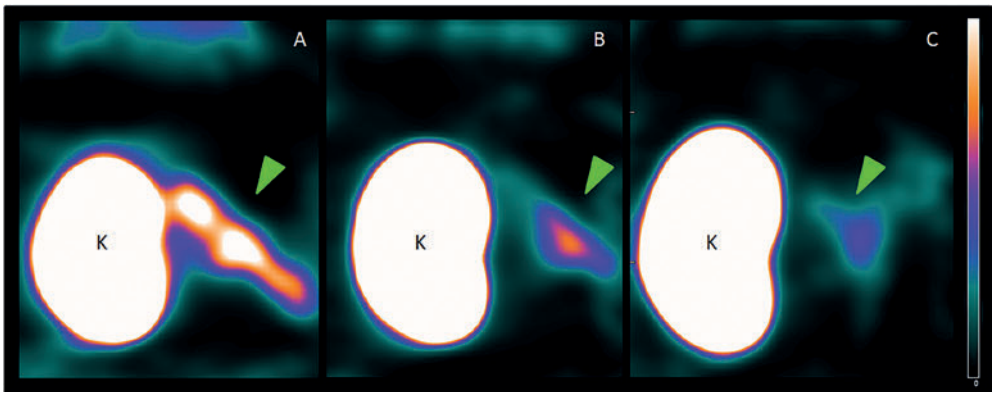

Figure 3. Coronal slices of SPECT images of NOD mice of 7, 13 and 19 weeks old, respectively, with a pancreatic uptake and BCM of (A) 18.1 %ID/g and 0.13 % respectively, (B) 12.2 %ID/g and 0.06 % respectively and (C) 4.5 %ID/g and 0 % respectively. Uptake in kidney is indicated with K and the pancreatic uptake with a green arrow.

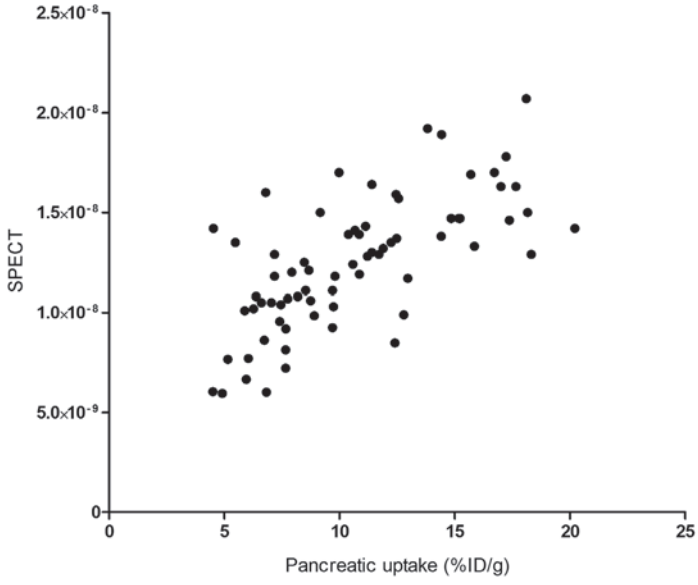

Figure 4. Correlation between the quantified SPECT signal in the pancreas and the uptake of exendin in the pancreas. The uptake is expressed as the percentage injected dose per gram of tissue (%ID/g) and determined by *ex vivo* counting of the pancreas.

Beta cell mass measurement and insulitis

Figure 5 shows that the beta cell mass is linearly correlated with the exendin uptake in the pancreas (Pearson r = 0.64, p < 0.001). A decline in beta cell mass corresponded with a decline in pancreatic uptake. Furthermore, all mice that were mild (11.1 – 22.2 mmol/l) or severe hyperglycemic (> 22.2 mmol/l) at the end of the experiment had a low beta cell mass. However, in mice that had complete absence of beta cells, still uptake of exendin in the pancreas was measured.

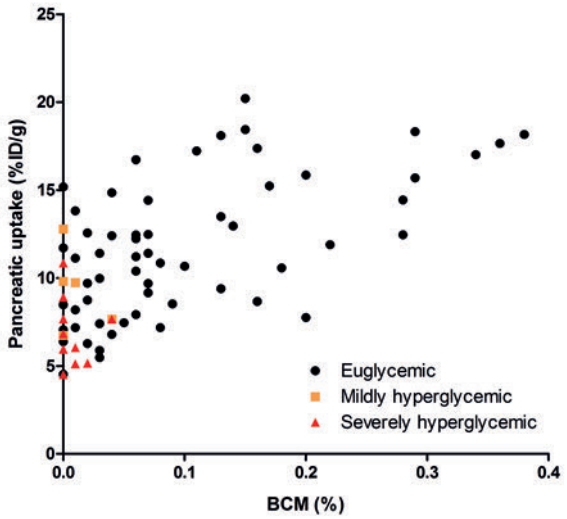

Figure 5. Correlation between the uptake of exendin in the pancreas and the BCM. The uptake is shown as percentage injected dose per gram of tissue (%ID/g) and determined by *ex vivo* counting of the pancreas, the BCM is presented as percentage of the total pancreas and determined by morphometric analysis after immunohistochemical staining with an anti-insulin antibody. The level of glycemia was determined at the endpoint and classified for every mouse: Euglycemic (< 11.1 mmol/l), mildly hyperglycemic (11.1 – 22.2 mmol/l) and severely hyperglycemic (> 22.2 mmol/l).

Already at an early age the first leukocyte infiltrated islets became apparent, and in the few islets that were infiltrated, infiltration was already very severe. With increasing age, more islets were infiltrated by immune cells and from 11 weeks of age onwards more than half of the islets were inflamed (Figure 6).

To investigate if inflammation of the islets influenced the exendin uptake, the correlation between the exendin uptake determined *ex vivo* and the beta cell mass was corrected for insulitis and was found to be 0.66 (Pearson r, covariant analysis) and was not statistically significant (p = 0.83). Insulitis did not significantly affect the uptake of exendin in the beta cells. Furthermore, there was no correlation whatsoever (p = 0.40) between insulitis and exendin uptake (Figure 7).

Correction for the blood glucose value at the time of SPECT imaging resulted in a correlation coefficient of 0.57 (Pearson r, covariant analysis), which was not significantly different than the uncorrected correlation coefficient (p = 0.51). There was, however, a slight negative correlation between blood glucose (at the time of SPECT imaging) and uptake of radiolabeled exendin (Pearson r = -0.44, p < 0.01) (Figure 8).

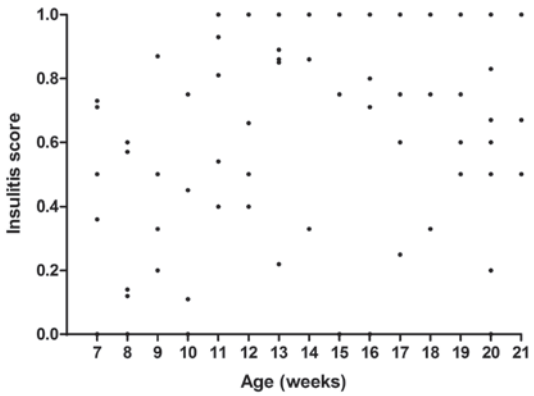

Figure 6. Insulitis score in NOD mice (n=75). The degree of insulitis was scored as the percentage of islets that were infiltrated and was measured at the endpoint (n=5 mice per week).

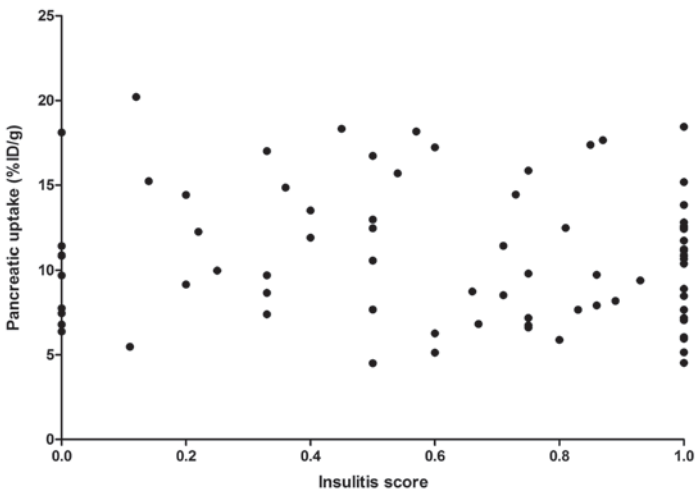

Figure 7. Correlation between insulitis and the uptake of exendin in the pancreas. The degree of insulitis was scored as the percentage of islets that were infiltrated. The uptake is expressed as the percentage injected dose per gram of tissue (%ID/g) and determined by *ex vivo* counting of the pancreas. The correlation coefficient between insulitis and the pancreatic uptake was calculated with a Pearson correlation coefficient (Pearson r = -0.10, p = 0.40).

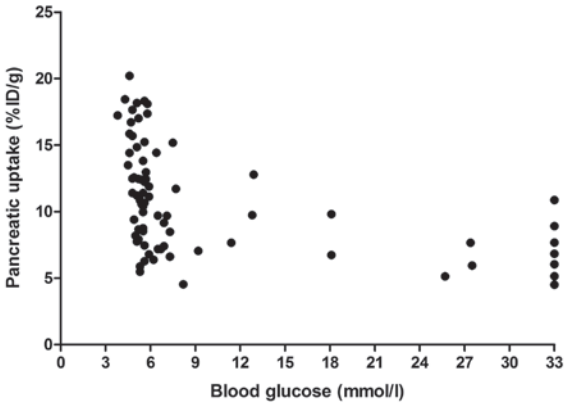

Figure 8. Correlation between the blood glucose and the uptake of exendin in the pancreas. The blood glucose depicted here was measured at the endpoint (mmol/l). The uptake is expressed as the percentage injected dose per gram of tissue (%ID/g) and determined by *ex vivo* counting. The correlation coefficient between the blood glucose levels and pancreatic uptake was calculated with a Pearson correlation coefficient (Pearson r = -0.44 ($p < 0.01$).

Macroautoradiography and immunohistochemistry

Figure 9 illustrates the high uptake of radiolabeled exendin in the islets of Langerhans and moderate uptake in the exocrine pancreas. The images depicted here show a decline of endocrine exendin uptake and thus beta cell mass over time, as diabetes was progressing. When no insulin positive cells were present in the section, there was still radioactive signal detected by macroautoradiography in the exocrine pancreas (Figure 9C).

To confirm the findings in the autoradiography, we have performed immunohistochemical analyses on a mouse with a high exendin uptake (17.7 %ID/g) and with a low exendin uptake (5.1 %ID/g). Figure 10 demonstrates high insulin and GLP-1R expression in the mouse with high exendin uptake (A and B respectively), in contrast to the mouse with low exendin uptake, where the endocrine pancreas was nearly complete negative for both insulin and GLP-1R (D and E respectively). Furthermore, in both mice there was no positive GLP-1R signal in the exocrine pancreas, which verifies that exendin binds to a different receptor than the GLP-1R.

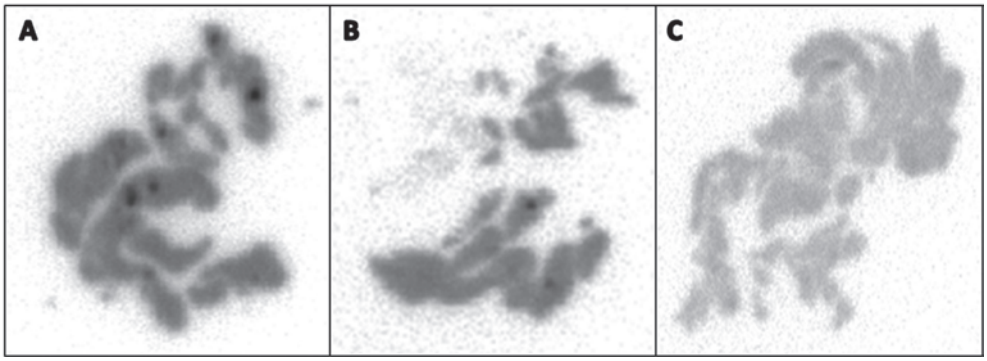

Figure 9. Macroautoradiography of pancreas of NOD mice of 11, 14 and 19 weeks respectively, with a pancreatic uptake and BCM of (A) 15.7 %ID/g and 0.29 % respectively, (B) 8.53 %ID/g and 0.09 % respectively and (C) 5.1 %ID/g and 0.01 % respectively.

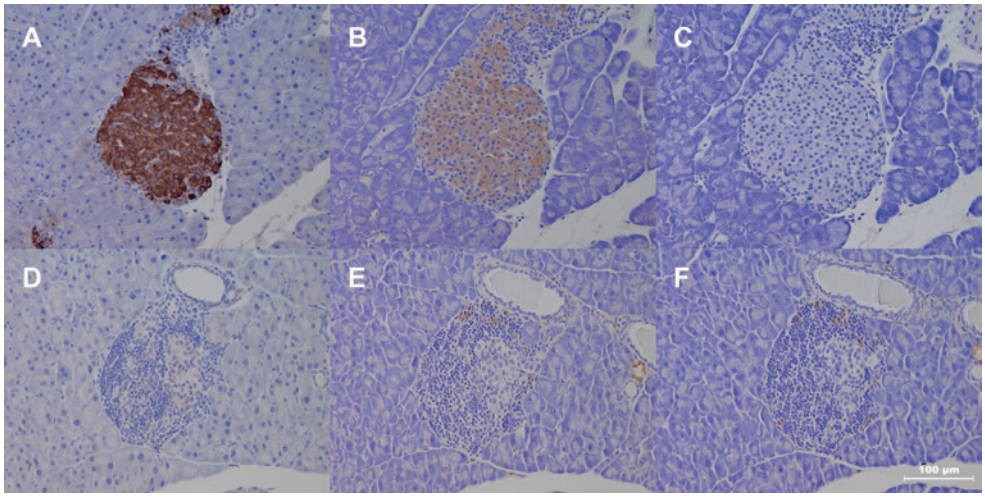

Figure 10. Immunohistochemistry of pancreatic sections of an NOD mouse with high (A-C) and an NOD mouse with low (D-F) exendin uptake. Anti-insulin staining (A+D), anti-GLP-1R staining (B+E) and blanc controls (C+F).

DISCUSSION

In this study, we have validated [^{111}In]In-DTPA-exendin-3 SPECT for determination of the BCM in a type 1 diabetic mouse model. In NOD mice, we were able to visualize the pancreas with SPECT and to quantify the radioactive signal during the progression of the disease. Furthermore, we have found a linear correlation between the BCM and the exendin uptake as determined by *ex vivo* counting, which was not significantly altered by hyperglycemia or insulitis.

A study of Ortis *et al*. demonstrated that the GLP-1R was downregulated upon stimulation of primary rat beta cells with pro-inflammatory cytokines [11]. Although this was an *in vitro* study, it is reasonable that in human T1D or in animal models for T1D, insulitis could also influence the expression of the GLP-1R. We have previously demonstrated in BBDP rats that insulitis has no influence on the strong correlation between BCM and exendin uptake [10]. In the present study we confirm these findings in a mouse model with even stronger insulitis [4]. In nearly all mice insulitis was found, while in diabetic patients the incidence of insulitis is much less. Furthermore, the amount of islets that is infiltrated is hugely different between mice and human [4, 21]. Based on these results, we presume that the weaker insulitis in humans will not have a significant influence on the uptake of exendin. Clinical evaluation is needed to address the influence of insulitis on the uptake of exendin in human, since the cytokines involved in insulitis are not completely identical between mice and human.

The present study demonstrates that despite long term hyperglycemia, there is a good correlation between the beta cell mass and the uptake of exendin. Xu *et al*. and more recently Rajan *et al*. reported the downregulation of the GLP-1R both *in vitro* and *in vivo* after hyperglycemia [12, 13]. We did not observe a significant difference in the correlation between beta cell mass and exendin accumulation when corrected for the blood glucose levels, indicating that the observation of Rajan and co-workers may not be relevant for beta cell quantification by GLP-1R imaging. However, as the duration of hyperglycemia varied in our study, and the blood glucose values at the time of [^{111}In]In-DTPA-exendin-3 and BCM measurement were mainly concentrated at the high and low blood glucose levels, one might consider to perform *in vivo* experiments specifically designed to determine the influence duration and severity of hyperglycemia have on GLP-1R expression and radiolabeled exendin accumulation in the pancreas.

With immunohistochemical staining of insulin we have confirmed a near complete ablation of the beta cells in diabetic mice. However, uptake of the tracer was still found by *ex vivo* counting of the total pancreas in these mice, as well as the presence of a signal on SPECT. Furthermore, autoradiographic images of the pancreas of these mice confirmed the presence of a radioactive signal also in the exocrine pancreas. On the contrary, the validation of this tracer in BBDP rats demonstrated that when the amount of beta cells dropped to zero, also no radioactive signal could be detected with either SPECT or autoradiography [10].

Since there is exendin accumulation in the pancreas of diabetic mice, while immunohistochemistry shows a total depletion of the beta cells, it is plausible that exendin is binding to the exocrine tissue of the pancreas. These data are in line with a previous study, in which we compared GLP-1R targeting using exendin in various mouse and rat strains [22]. We report that in mice the pancreatic uptake of exendin after chemical beta cell destruction is higher than after coinjection of an excess of unlabeled exendin. This stands in contrast to rats, where the accumulation of exendin is similar after beta cell ablation and blocking of uptake by an excess of unlabeled exendin. Because the endocrine-to-exocrine mRNA ratio of GLP-1R was similar in mice and rats, it is likely that in mice exendin has cross-reactivity in the exocrine

tissue with another protein. In accordance, the GLP-1R staining of the murine exocrine tissue was negative in the alloxan study as well as in this study. Similar findings are described by Eriksson *et al.*, who report that the exendin uptake in islets has a larger contribution to the total pancreatic uptake in rats than in mice [23]. Furthermore, we have shown before that the uptake of exendin in patients with T1D drops to background levels, indicating that this cross-reactivity most probably does not play a role in human exocrine pancreas [8].

Diabetes imaging in the NOD mouse model has been described using two different approaches, namely immune imaging [24] or imaging the pancreatic beta cells [25], but thus far none of these approaches were sufficient for proper *in vivo* use. To the best of our knowledge, to date no study reported successful non-invasive *in vivo* imaging of the beta cells using a radioactive tracer in the NOD mouse model. Thus, the NOD mouse model can be used for studying the beta cell mass with radiolabeled exendin, but the uptake of exendin in the exocrine pancreas should be taken into account. In the present study the mice underwent unilateral nephrectomy in order to visualize the pancreas *in vivo*, otherwise the left kidney would mask the pancreas. For clinical SPECT or PET imaging this is not an issue, because there is a larger distance between the pancreas and the kidneys.

Population heterogeneity in T1D and new insights about beta cells underline the necessity to determine the BCM non-invasively [2, 3], as currently all knowledge about beta cells is obtained via autopsies. Detection of remaining beta cells opens possibilities for therapy in which these beta cells could be preserved, regenerated or even activated to proliferate. Immune therapy in diabetic NOD mice revealed recovery of beta cells, while at time of diagnosis no beta cells were detected immunohistochemically [26]. In men, immunotherapy thus far cannot replace standard insulin treatment, due to safety reasons of the therapy or lack of (long term) effects, but shows great potential [27, 28]. Based upon imaging and other (phenotypic) markers patients could be categorised in order to provide patients with optimal therapy. Furthermore, monitoring the efficacy of novel immune-based therapeutic strategies would be of crucial value, especially in an individual-dependent manner [27].

Despite hyperglycemia and severe insulitis, we have found a good correlation between BCM and pancreatic exendin uptake, even in a suboptimal model with relatively low differences in uptake due to high background activity.

ACKNOWLEDGEMENTS

We thank Bianca Lemmers, Kitty Lemmens, Iris Lamers-Elemans and Henk Arnts (Central Animal Facility, Radboud university medical center, Nijmegen, The Netherlands) for their expertise in the *in vivo* studies.

Our work was supported by JDRF International (37-2011-635).

REFERENCES

1. DiMeglio LA, Evans-Molina C, Oram RA. Type 1 diabetes. *Lancet*. **2018**; 391 (10138): 2449-2462.
2. Keenan HA, Sun JK, Levine J, Doria A, Aiello LP, Eisenbarth G, *et al*. Residual insulin production and pancreatic ss-cell turnover after 50 years of diabetes: Joslin Medalist Study. *Diabetes*. **2010**; 59 (11): 2846-2853.
3. Meier JJ, Bhushan A, Butler AE, Rizza RA, Butler PC. Sustained beta cell apoptosis in patients with long-standing type 1 diabetes: indirect evidence for islet regeneration? *Diabetologia*. **2005**; 48 (11): 2221-2228.
4. Campbell-Thompson ML, Atkinson MA, Butler AE, Chapman NM, Frisk G, Gianani R, *et al*. The diagnosis of insulitis in human type 1 diabetes. *Diabetologia*. **2013**; 56 (11): 2541-2543.
5. In't Veld P, Lievens D, De Grijse J, Ling Z, Van der Auwera B, Pipeleers-Marichal M, *et al*. Screening for insulitis in adult autoantibody-positive organ donors. *Diabetes*. **2007**; 56 (9): 2400-2404.
6. Atkinson MA, Eisenbarth GS, Michels AW. Type 1 diabetes. *Lancet*. **2014**; 383 (9911): 69-82.
7. Oram RA, Sims EK, Evans-Molina C. Beta cells in type 1 diabetes: mass and function; sleeping or dead? *Diabetologia*. **2019**; 62 (4): 567-577.
8. Brom M, Woliner-van der Weg W, Joosten L, Frielink C, Bouckenooghe T, Rijken P, *et al*. Non-invasive quantification of the beta cell mass by SPECT with (1)(1)(1)In-labelled exendin. *Diabetologia*. **2014**; 57 (5): 950-959.
9. Selvaraju RK, Velikyan I, Johansson L, Wu Z, Todorov I, Shively J, *et al*. In vivo imaging of the glucagonlike peptide 1 receptor in the pancreas with 68Ga-labeled DO3A-exendin-4. *J Nucl Med*. **2013**; 54 (8): 1458-1463.
10. Brom M, Joosten L, Frielink C, Peeters H, Bos D, van Zanten M, *et al*. Validation of (111)In-Exendin SPECT for the Determination of the beta-Cell Mass in BioBreeding Diabetes-Prone Rats. *Diabetes*. **2018**; 67 (10): 2012-2018.
11. Ortis F, Naamane N, Flamez D, Ladriere L, Moore F, Cunha DA, *et al*. Cytokines interleukin-1beta and tumor necrosis factor-alpha regulate different transcriptional and alternative splicing networks in primary beta-cells. *Diabetes*. **2010**; 59 (2): 358-374.
12. Rajan S, Dickson LM, Mathew E, Orr CM, Ellenbroek JH, Philipson LH, *et al*. Chronic hyperglycemia downregulates GLP-1 receptor signaling in pancreatic beta-cells via protein kinase A. *Mol Metab*. **2015**; 4 (4): 265-276.
13. Xu G, Kaneto H, Laybutt DR, Duvivier-Kali VF, Trivedi N, Suzuma K, *et al*. Downregulation of GLP-1 and GIP receptor expression by hyperglycemia: possible contribution to impaired incretin effects in diabetes. *Diabetes*. **2007**; 56 (6): 1551-1558.
14. Lenzen S. Animal models of human type 1 diabetes for evaluating combination therapies and successful translation to the patient with type 1 diabetes. *Diabetes Metab Res Rev*. **2017**; 33 (7):
15. Avner PR. Sweetness and light: perspectives for rodent models of type 1 diabetes. *Dis Model Mech*. **2010**; 3 (7-8): 426-429.

16. Jorns A, Arndt T, Meyer zu Vilsendorf A, Klempnauer J, Wedekind D, Hedrich HJ, *et al*. Islet infiltration, cytokine expression and beta cell death in the NOD mouse, BB rat, Komeda rat, LEW.1AR1-iddm rat and humans with type 1 diabetes. *Diabetologia*. **2014**; 57 (3): 512-521.

17. Juang JH, Van YH, Kuo CH, Lin MY, Liu YH, Chang HY. Prevention and Reversal of Diabetes by All-Trans Retinoid Acid and Exendin-4 in NOD Mice. *Int J Endocrinol*. **2014**; 2014 435481.

18. Brom M, Joosten L, Oyen WJ, Gotthardt M, Boerman OC. Radiolabelled GLP-1 analogues for in vivo targeting of insulinomas. *Contrast Media Mol Imaging*. **2012**; 7 (2): 160-166.

19. Brom M, Franssen GM, Joosten L, Gotthardt M, Boerman OC. The effect of purification of Ga-68-labeled exendin on in vivo distribution. *EJNMMI research*. **2016**; 6 (1): 65.

20. Mathijs I, Da Cunha DA, Himpe E, Ladriere L, Chellan N, Roux CR, *et al*. Phenylpropenoic acid glucoside augments pancreatic beta cell mass in high-fat diet-fed mice and protects beta cells from ER stress-induced apoptosis. *Mol Nutr Food Res*. **2014**; 58 (10): 1980-1990.

21. In't Veld P. Insulitis in human type 1 diabetes: The quest for an elusive lesion. *Islets*. **2011**; 3 (4): 131-138.

22. Willekens SM, Joosten L, Boerman OC, Balhuizen A, Eizirik DL, Gotthardt M, *et al*. Strain Differences Determine the Suitability of Animal Models for Noninvasive In Vivo Beta Cell Mass Determination with Radiolabeled Exendin. *Molecular imaging and biology : MIB : the official publication of the Academy of Molecular Imaging*. **2016**; 18 (5): 705-714.

23. Eriksson O, Rosenstrom U, Selvaraju RK, Eriksson B, Velikyan I. Species differences in pancreatic binding of DO3A-VS-Cys(40)-Exendin4. *Acta Diabetol*. **2017**; 54 (11): 1039-1045.

24. Kalliokoski T, Simell O, Haaparanta M, Viljanen T, Solin O, Knuuti J, *et al*. An autoradiographic study of [(18)F]FDG uptake to islets of Langerhans in NOD mouse. *Diabetes Res Clin Pract*. **2005**; 70 (3): 217-224.

25. Amartey JK, Shi Y, Al-Jammaz I, Esguerra C, Al-Otaibi B, Al-Mohanna F. Radioiodinated naphthylalanine derivatives targeting pancreatic beta cells in normal and nonobese diabetic mice. *Exp Diabetes Res*. **2008**; 2008 371716.

26. Sherry NA, Kushner JA, Glandt M, Kitamura T, Brillantes AM, Herold KC. Effects of autoimmunity and immune therapy on beta-cell turnover in type 1 diabetes. *Diabetes*. **2006**; 55 (12): 3238-3245.

27. Atkinson MA, Roep BO, Posgai A, Wheeler DCS, Peakman M. The challenge of modulating beta-cell autoimmunity in type 1 diabetes. *Lancet Diabetes Endocrinol*. **2019**; 7 (1): 52-64.

28. Ni Q, Pham NB, Meng WS, Zhu G, Chen X. Advances in immunotherapy of type I diabetes. *Adv Drug Deliv Rev*. **2018**;

CHAPTER 3

Validation of [^{111}In]In-DTPA-exendin SPECT for the determination of the beta cell mass in BioBreeding Diabetes Prone rats

Maarten Brom[1], Lieke Joosten[1], Cathelijne Frielink[1], Hanneke Peeters[1], Desirée Bos[1], Monica van Zanten[2], Otto C. Boerman[1] & Martin Gotthardt[1]

1 Department of Radiology and Nuclear Medicine, Radboud University Medical Center, Nijmegen, The Netherlands
2 Department of Pathology, Radboud University Medical Center, Nijmegen, The Netherlands

Diabetes. **2018**; 67(10): 2012-2018

ABSTRACT

The changes in beta cell mass (BCM) during the development and progression of diabetes could potentially be measured by radionuclide imaging using radiolabeled exendin. In this study we investigated the potential of [^{111}In]In-DTPA-exendin in a rat model that closely mimics the development of type 1 diabetes in humans: BioBreeding Diabetes Prone (BBDP) rats. BBDP rats of 4-18 weeks of age were injected intravenously with [^{111}In]In-DTPA-exendin and SPECT images were acquired. The accumulation of the radiotracer was measured as well as the beta cell mass and grade of insulitis by histology. [^{111}In]In-DTPA-exendin accumulated specifically in the islets, resulting in a linear correlation with the BCM (%) (Pearson $r = 0.89$, $p < 0{,}0001$, $r=0.64$ for SPECT). Insulitis did not have an influence on this correlation. These results indicate that [^{111}In]In-DTPA-exendin is a promising tracer to determine the BCM during the development of type 1 diabetes, irrespective of the degree of insulitis.

INTRODUCTION

Type 1 diabetes (T1D) is the result of autoimmune destruction of the insulin-producing beta cells in the islets of Langerhans in the pancreas. It was long believed that a homogeneous and near-complete destruction of the beta cells occurs, but it has recently been shown that the autoimmune destruction of beta cells is a heterogeneous and chronically ongoing process during the course of T1D [1-3]. As a result, beta cells and insulitic regions were found in pancreatic specimens many years after diagnosis of T1D [2]. In the pancreata of T1D patients, various degrees of beta cell destruction in different areas of the pancreas could be found, including simultaneous detection of apparently healthy islets, early abnormalities, insulitic regions, and islets completely depleted from beta cells and absence of immune cells [3]. More importantly, these studies showed that the degree and pattern of beta cell destruction and immune cell infiltration are unique in every individual. The simultaneous appearance of different states of disease within one pancreas and the highly individual course of T1D would require a method to non-invasively measure the beta cell mass to provide additional information about the number and intrapancreatic distribution of beta cells during T1D and for the selection of patients eligible for novel (immune regulatory based) treatments .

We previously showed that radiolabeled exendin accumulates specifically in the beta cells and could potentially be used to measure the beta cell mass by SPECT in rodents and humans [4].

Despite these promising data, questions remain about the effectiveness of radiolabeled exendin for the determination of the BCM in the complex pathogenesis of diabetes. A concern is the potential variation in the expression of the glucagon-like peptide-1 receptor (GLP-1R), the receptor targeted by radiolabeled exendin, during the course of diabetes including the inflammation-induced physiological changes in the pancreas. For example, it was shown that cytokine treatment of cell sorter-purified rat beta cells reduced the GLP-1R mRNA expression [5]. Furthermore, hyperglycemia results in lower GLP-1R expression in isolated rat islets *in vitro* and in a rat model of partial duct ligation [6]. These results suggest that possibly the GLP-1R expression might change during the progression of T1D, which might result in changes of radiolabeled exendin accumulation impairing the correlation between tracer uptake and BCM. Besides the effects of inflammation and metabolic disease on the GLP-1R expression, changes in blood flow and enhanced vascular permeability due to inflammation could also affect accumulation of the tracer in the pancreas. However, the effect of potential changes in receptor expression on the accumulation of radiolabeled exendin in the beta cells is difficult to predict. We have previously demonstrated a linear correlation between radiolabeled exendin uptake and BCM in an alloxan-induced diabetes model of beta cell reduction[4, 7], but this model does not show the typical patterns of inflammation/insulitis found in T1D. Therefore, for determination of the feasibility of accurately measuring the BCM during T1D, the use of the tracer to determine the BCM noninvasively should be tested in a rodent model mimicking all aspects of the human disease progression.

In the current study, we examine the correlation between the pancreatic uptake of [^{111}In]In-DTPA-exendin and the BCM and the influence of insulitis on the tracer uptake in a rat model for spontaneous T1D: the BioBreeding Diabetes Prone (BBDP) rat. These rats are characterized by severe insulitis, followed by rapid onset of T1D, making this an ideal model to study the effects of insulitis and inflammation and short-term fluctuations in blood glucose levels on the uptake of [^{111}In]In-DTPA-exendin in the pancreas.

MATERIALS AND METHODS

Animals, nephrectomy and housing

Forty-five female Biobreeding Diabetes Prone rats of 3-5 weeks old were obtained from Biomedical Research Models (Worcester, MA, USA). The rats were housed in individually ventilated cages and were fed with sterilized chow and drinking water to maintain their microbiological status to ensure diabetes development. After one week acclimatization in our facility, unilateral nephrectomy (left kidney) was performed to allow accurate estimation of tracer uptake in the pancreas, under inhalation anesthesia with isoflurane (Abbott Laboratories, Toronto, Canada) in O_2:Air (1:4). Carprofen (Rimadyl®, Pfizer Animal Health B.V., Capelle aan de IJssel, The Netherlands) was used as analgesia for two days after surgery, twice daily (5 mg/kg). As from one week after surgery the rats were used for SPECT studies. Every week three rats were subjected for SPECT studies.

Blood glucose levels and body weight were monitored at least twice weekly and the frequency of monitoring was intensified when blood glucose levels rise or body weight drops. For blood glucose level measurements a drop of blood was drawn by puncturing the tail vein with a 25G needle (BD Biosciences, Breda, The Netherlands). Blood glucose was measured with a glucose meter (Accu-Chek Sensor, Roche Diagnostics, Almere, The Netherlands). When rats were hyperglycaemic sustained release insulin implants (Linshin Canada Inc., Toronto, Canada) were injected subcutaneously with a 12G trocar needle to control blood glucose levels.

SPECT

[^{111}In]In-DTPA-exendin-3 was prepared as previously described[8]. Rats were injected intravenously with 15 MBq [^{111}In]In-DTPA-exendin and SPECT scans were acquired 1 hour after injection on a dedicated small animal SPECT/CT scanner U-SPECT-II, MILabs, Utrecht, The Netherlands). SPECT images were acquired with a general purpose 1.0 mm pinhole rat and mouse collimator with an acquisition time of 50 min. The images were reconstructed with OSEM (3 iterations, 8 subsets, voxel size 0.75) using the U-SPECT-Rec software (MILabs, Utrecht, The Netherlands). Mean uptake of [^{111}In]In-DTPA-exendin in the pancreas was quantified using Inveon Research Workplace (Preclinical Solutions, Siemens Medical Solutions USA, Inc., Knoxville, TN, USA). A

volume of interest was drawn over the pancreas and mean uptake (per voxel) was corrected for the injected dose.
After SPECT/CT acquisition the pancreas was dissected, fixed in formalin and embedded in paraffin for autoradiography and histological evaluation.

Histology, autoradiography, immunohistochemistry and beta cell mass determination

Sections (4 µm) were prepared of the paraffin embedded pancreata at 3 levels with an interlevel distance of 100 µm. The sections were mounted and dried and one section per level was exposed to a phosphor imager screen (Fuji Film BAS-SR 2025, Raytest, Straubenhardt, Germany) for 1 week. Images were acquired with a radioluminography laser imager (Fuji Film BAS 1800 II system, Raytest, Straubenhardt, Germany) and analyzed with Aida Image Analyzer software (Raytest, Straubenhardt, Germany).
A consecutive section of the one used for autoradiography was stained for insulin as follows: Deparaffination and antigen retrieval was performed as previously described[4]. Blocking was performed by incubation with PBS containing 1% BSA for 30 min at room temperature. After removal of PBS-BSA, 50-150 µl rabbit-anti-insulin antibody (4 µg/ml diluted in PBS containing 1% BSA, sc9168, Santa Cruz Biotechnology, Inc., Santa Cruz, CA, USA) was added and incubated for 1 hour at room temperature in the dark. The sections were washed three times with PBS and the sections were incubated with Alexa Fluor 594 Donkey Anti-Rabbit IgG (10 µg/ml, Invitrogen, Bleiswijk, the Netherlands) for 30-60 minutes at room temperature in the dark. The sections were counterstained with DAPI. After washing three times with PBS the sections were mounted with Fluoromount (Sigma-Aldrich, St. Louis, MO, USA).
Insulin-stained sections were scanned with an automated microscope (Zeiss Axioskop 2 plus) using a 100 x magnification and a green light filter set. Thresholding was performed on pancreatic tissue in order to determine total pancreatic area semi-automatically using ImageJ (version 1.47, National Institutes of Health, USA). Also a threshold was set for the fluorescently stained beta cells, to discriminate between the endocrine and exocrine tissue. Next, insulin positive beta cells were delineated in iVision (iVision-Mac™ (4.0.16), BioVision Technologies, USA) in order to select only islets and delete autofluorescent regions. Finally, ImageJ was used to calculate the percentage of insulin positive beta cells within the pancreas automatically.

Insulitis score

One section per level was stained with hematoxylin-eosin (3 sections per rat). All islets in the sections were counted and scored for the presence of insulitis as follows: 0, no inflammation; 1, intra-islet inflammation occupying <50% within the islet; 2, intra-islet inflammation occupying >50% within the islet; 3, complete or near complete obliteration of islets by inflammation. The sections were read blindly by two independent observers. The index of insulitis of each rat was calculated according the following formula: $I = (0 \times n_0) + (1 \times n_1) + (2 \times n_2) + (3 \times n_3) / 3 \times (n_0 + n_1 + n_2 + n_3)$[9].

Statistical analysis

The correlation coefficient between the BCM and pancreatic uptake of [^{111}In]In-DTPA-exendin was calculated with a Pearson correlation coefficient with SPSS (IBM SPSS Statistics 22). The influence of insulitis on this correlation was calculated by using insulitis as a covariant. The statistical difference between this correlations was examined by a two-tailed Fisher r-to-z transformation. The levels of significance was set to 0.05.

RESULTS

Blood glucose measurements and onset of diabetes

The results of the blood glucose measurements of BBDP rats during the complete experiments are summarized in Figure 1. All rats were normoglycemic until 8 weeks of age, and hyperglycemia occurred from 9 weeks of age. Hyperglycemic rats were treated with insulin to control the blood glucose levels. Despite insulin treatment, short-term fluctuations in blood glucose levels were observed.

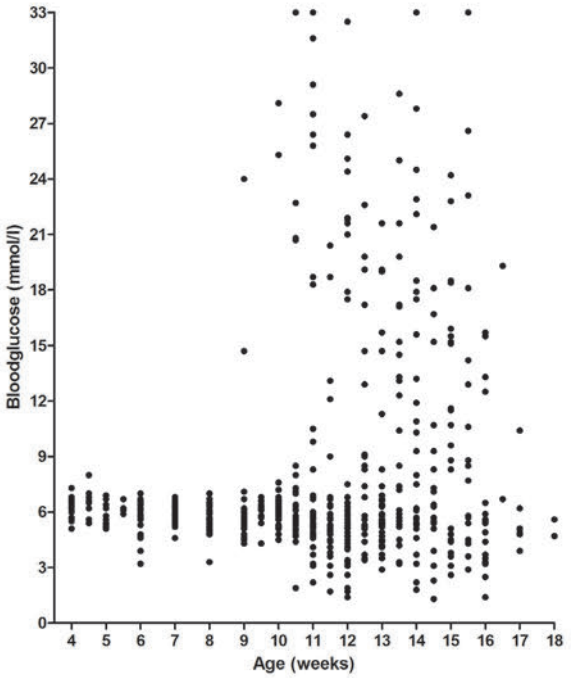

Figure 1. Blood glucose values of BBDP rats. Blood glucose measurements performed twice weekly in BBDP rats (n=45 at 4 weeks of age). Rats were treated with insulin (implantation of an insulin pellet) when hyperglycemia occurred.

[^{111}In]In-DTPA-exendin accumulation and beta cell mass

In animals with a high beta cell fraction, [^{111}In]In-DTPA-exendin accumulated in the pancreas, as measured by *ex vivo* counting. The pancreatic [^{111}In]In-DTPA-exendin uptake decreased in rats with declining beta cell mass leading to a linear correlation between beta cell fraction and [^{111}In]In-DTPA-exendin accumulation in the pancreas (Figure 2, Pearson r = 0.89, p<0.0001). The glycemia levels at the time point of imaging are presented in Figure 2B. The correlation between the beta cell mass and the pancreatic uptake, corrected for the blood glucose levels, was Pearson r = 0.89 and was not significantly different than the uncorrected correlation (p<0.05).

A restricted range correlation coefficient, excluding the animals with a BCM < 0.4%, was calculated, resulting in a Pearson r=0.56.

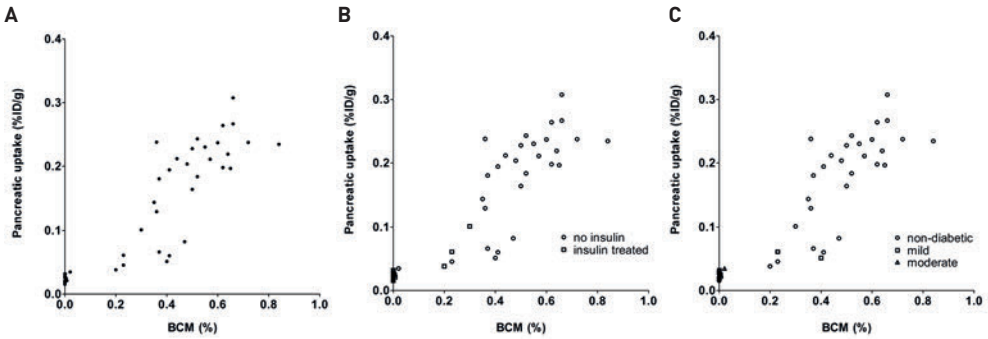

Figure 2. Correlation between pancreatic [^{111}In]In-DTPA-exendin accumulation and beta cell mass.(A). The uptake of [^{111}In]In-DTPA-exendin in the pancreas (n=45), expressed as the percentage of the injected dose per gram of tissue (%ID/g, y-axis, determined y *ex vivo* counting of the entire pancreas) showed a strong correlation with the beta cell mass (expressed as percentage of the total pancreas, x-axis) determined by morphometric analysis (Pearson r = 0.89, p<0.0001). (B). The level of glycemia was plotted for every individual rat. The animals were categorized based on their non-fasting blood glucose levels at the time point of imaging as follows: 1) non-diabetic (<11.1mM) [open circles], mild hyperglycemia (11.1-22.2 mM) [open squares], moderate hyperglycemia (22.2-33.3 mM) [open triangles] and severe hyperglycemia (> 33 mM). (C). The rats treated with insulin are represented as open squares and non-insulin treated rats with open circles.

Insulitis and [^{111}In]In-DTPA-exendin accumulation

Insulitis scored by two independent observers showed a high level of agreement as determined by a Bland-Altman plot (Figure 3). There was no statistical correlation between the difference between the observers and the mean of the observers (One sample t-test, p=0.292). Therefore, there is no level of proportional bias between both observers and the mean insulitis score of both observers were used for further analysis. In young BBDP rats, no infiltration of the islets was observed and first signs of insulitis were observed after 7 weeks of age (Figure 4), preceding the onset of hyperglycemia. The correlation between pancreatic [^{111}In]In-DTPA-exendin accumulation and the beta cell fraction, corrected for the insulitis score, was Pearson

r = 0.81 (partial correlation coefficient) and was not statistically different than the correlation coefficient when not corrected for insulitis (p=0.18).

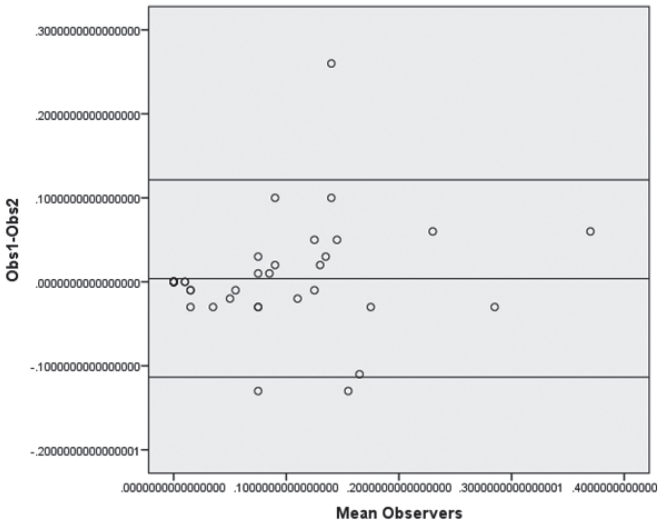

Figure 3. Bland-Altman plot of insulitis score.

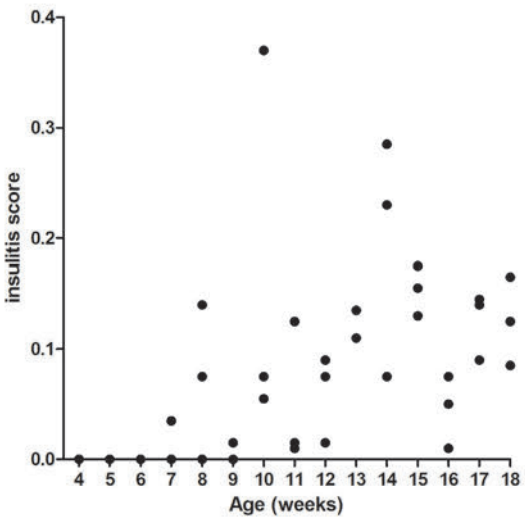

Figure 4. Presence of insulitis in BBDP rats.Insulitis was scored histologically on slides stained with H&E of BBDP rats (n=45) of various ages. Insulitis was observed as soon as 7 weeks of age.

Histology and autoradiography

High accumulation of [^{111}In]In-DTPA-exendin was observed in the islets of Langerhans in the autoradiographic images of rats with high beta cell mass (Figure 5A). Very low accumulation was observed in the exocrine pancreas, and the accumulation of [^{111}In]In-DTPA-exendin colocalized with insulin expression (Figure 5D). The [^{111}In]In-DTPA-exendin uptake decreased with declining amounts of beta cells (Figure 5B) and was not detectable in slides without any beta cells (Figure 5C), which was in line with the decline in insulin positive cells visualized by histology (Figure 5E and F). Furthermore, beta cell identity was verified by Nkx6.1 staining (Figure 6).

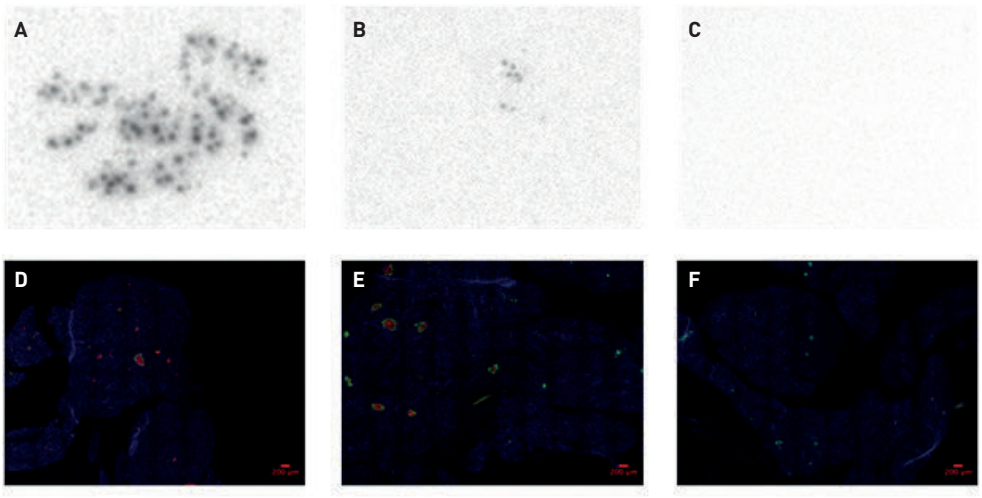

Figure 5. Autoradiography and immunohistochemical staining of pancreatic slides. High accumulation of [^{111}In]In-DTPA-exendin was observed in rats with high BCM (A) where abundant staining for insulin was present (D). In rats with reduced beta cell content (E), lower accumulation of [^{111}In]In-DTPA-exendin was present (B) and [^{111}In]In-DTPA-exendin accumulation was not measurable (C) in rats without beta cells (F).

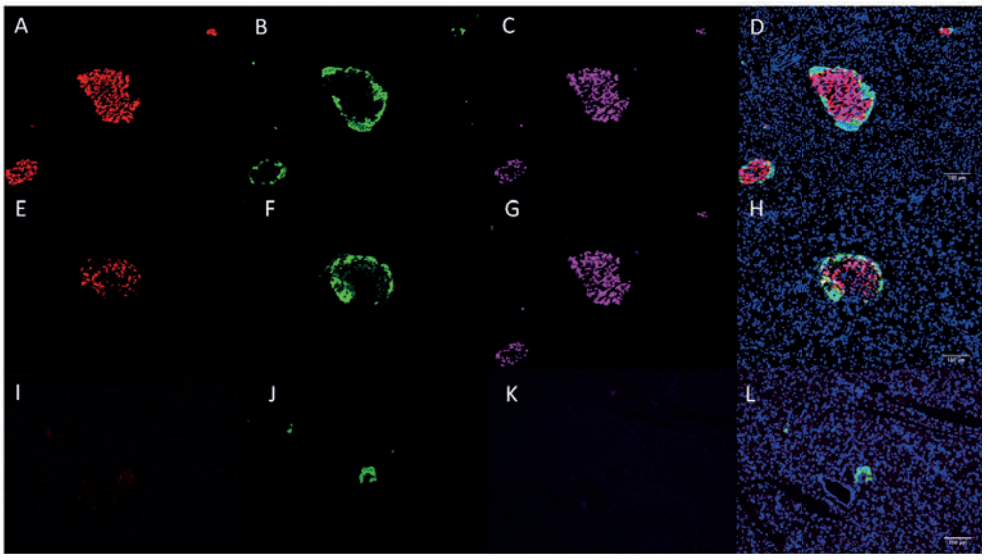

Figure 6. Histological analysis of beta cell identity. Pancreatic sections of a rat with normal (A-D), intermediate (E-H) or no beta cell mass (I-L) were stained for insulin (red), glucagon (green) and an additional marker for beta cells Nkx6.1 (purple). The sections were counterstained with DAPI. The images clearly show co-staining of insulin with Nkx6.1 indicating that a low beta cell mass is not caused by insulin depletion rather than beta cell destruction.

SPECT

SPECT images of rats with a high beta cell mass showed a clear [^{111}In]In-DTPA-exendin accumulation in the pancreas (Figure 7A, beta cell fraction 0.6%). Besides [^{111}In]In-DTPA-exendin accumulation in the pancreas, a high signal was observed in the kidney. The signal in the pancreas decreased in rats with declining beta cell mass (Figure 7B and C). The pancreatic uptake of [^{111}In]In-DTPA-exendin, determined by quantitative analysis of the SPECT images, correlated linearly with the [^{111}In]In-DTPA-exendin accumulation as determined by *ex vivo* counting (Figure 8, Pearson $r = 0.64$, $p<0.0001$). The pancreatic uptake of [^{111}In]In-DTPA-exendin determined by SPECT analysis showed a linear correlation with the beta cell fraction (Pearson $r = 0.50$, $p = 0.0006$).

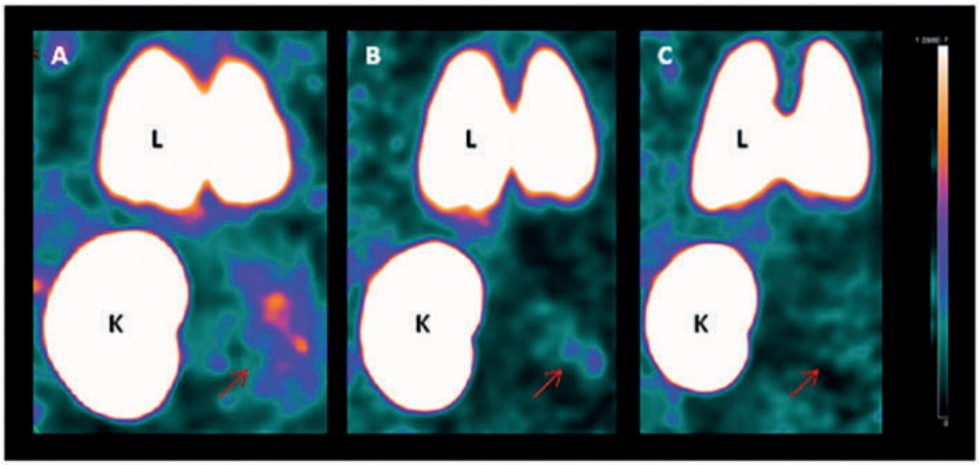

Figure 7. SPECT images of BBDP rats. Coronal images of BBDP rats with normal beta cell mass (A, 0.23%), intermediate (B, 0.13%) and low beta cell mass (C, 0.03%). Pancreatic uptake of [^{111}In]In-DTPA-exendin (indicated with a red arrow) is clearly visible in healthy rats (A) and decreases with declining BCM. Besides pancreatic accumulation, uptake was observed in kidney (K) and lung (L).

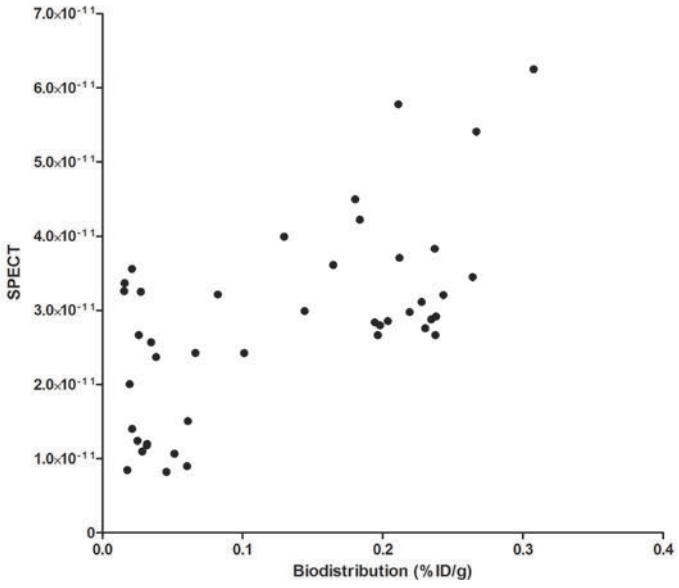

Figure 8. Correlation between pancreatic signal measured by *ex vivo* counting and quantitative analysis of the SPECT images (Pearson r = 0.64, p<0.0001). Due to the low signal in rats with a low beta cell mass the SPECT based quantification is challenging in these animals, as large variation is seen in these animals.

DISCUSSION

In this study we validated [^{111}In]In-DTPA-exendin as a method to determine the beta cell mass noninvasively in BBDP rats, a model for spontaneous type 1 diabetes. We demonstrated a strong correlation between pancreatic [^{111}In]In-DTPA-exendin accumulation, as determined by *ex vivo* counting, and the beta cell mass in this T1D rat model. Moreover, autoradiography revealed that the accumulation is restricted to the islets with very low signal in the exocrine pancreas. Importantly, the signal from the islets completely disappeared when no beta cells were present, while alpha cells could still be observed histologically. These observations indicate high specificity of [^{111}In]In-DTPA-exendin for beta cells and are in line with our previous studies in a rat model for chemically induced beta cell loss, where a strong correlation between pancreatic exendin accumulation and BCM, but not alpha cell mass, was found[4, 7].

The expression of the GLP-1R in the presence of an immune response remains a matter of debate. Previous studies showed a decrease in GLP-1R expression in islets treated with cytokines *in vitro* [5] or after partial duct ligation *in vivo* [6]. Our data clearly demonstrate that in the presence of insulitis also there is a strong linear correlation between the pancreatic uptake of the tracer and the BCM, comparable with the correlation found in chemically induced diabetes without insulitis (Pearson r = 0.89 uncorrected vs. Pearson r = 0.81 corrected for insulitis, p=0.18). This non-significant difference indicates that insulitis has no relevant effect on the correlation between these parameters. The use of the sophisticated rat model for T1D, representing a complete biological system, should reflect the complex pathophysiological processes better than a rather crude *in vitro* model of cytokine treated beta cells. It should be noted that in humans insulitis is described by the infiltration of 3 or more islets with more than 15 leukocytes[10], which is a much milder inflammatory process than the massive infiltration of the islets in rat and mouse models. It is therefore expected that the effect of insulitis on the accumulation of radiolabeled exendin is of even less importance in humans.

Also, changes in GLP-1R expression during hyperglycemia were observed in previous studies. It should be noted that the marked decrease in GLP-1R expression after near complete pancreatectomy was observed after 4 weeks of hyperglycemia [6]. Similar results were observed by glucose infusion experiments, where hyperglycemia was present for 4 days. In our study, the blood glucose levels were controlled by insulin treatment and a strong correlation between radiotracer accumulation and the BCM was observed. Although the rats were treated with insulin, fluctuations in blood glucose were observed (Figure 1), closely mimicking the clinical situation. The strong correlation between ^{111}In-exendin accumulation and BCM suggests a negligible effect of fluctuating glycemic levels in T1D on radiotracer uptake. However, the effects of long term hyperglycemia on the GLP-1R expression and radiolabeled exendin accumulation could not be elucidated in this model.

Besides promising results with radiolabeled and fluorescent exendin analogs for the measurement of the beta cell mass, other radiotracers have been evaluated in animal models

and clinical trials. The first tracer that was evaluated for targeting of the beta cells was DTBZ (which targets VMAT2). Studies in BBDP rats, a spontaneous model for T1D, showed a decrease of 65% in pancreatic standardized uptake value (SUV) of [^{11}C]C-DTBZ in severely diabetic rats[11, 12]. Similar results were obtained with the same radiotracer in streptozotocin induced beta cell loss in Lewis rats: reduced specific binding index (pancreas-to-kidney ratio) in diabetic rats with a variation in degree of reduction between rats[12]. Clinical evaluation of [^{18}F]FP-(+)-DTBZ revealed a reduction of 38% in SUV and 40% in binding potential between healthy subjects and subjects with longstanding type 1 diabetes (>9 years)[13]. Moreover, a linear correlation between arginine stimulated c-peptide and DTBZ binding parameters was observed. A more recent publication showed VMAT2 expression on pp cells and cells of the nervous system in the exocrine part of the pancreas[14], which should be taken into account in evaluating the imaging studies using DTBZ. Recently, Eriksson et al. showed that accumulation of the serotonin receptor tracer [^{11}C]5-HTP is reduced by 66% in the pancreas of C-peptide negative T1D subjects as compared to healthy volunteers implying that this tracer could also be a useful non-invasive marker to determine the total mass of endocrine cells in the pancreas[15]. Since the serotonin receptor is expressed in all endocrine cells, a combination of [^{11}C]5-HTP imaging of serotonin activity and [^{111}In]In-DTPA-exendin imaging could provide useful complementary information about the beta cell and total endocrine mass as well as changes in endocrine cell conformation during the development of diabetes.

Previous studies suggest GLP-1R expression in other endocrine and exocrine cells of the pancreas [16-19]. In the BBDP rat model the accumulation of [^{111}In]In-DTPA-exendin appears to be restricted to beta cells, based on the observation that no signal is observed in autoradiographic images of rats without any beta cells while alpha cells were still present. These observations are in line with our previous findings of a lack of correlation between alpha cell mass and ^{111}In-exendin accumulation in the pancreas[7].

The pancreatic uptake measured by quantitative analysis of the SPECT images showed a linear correlation with the pancreatic uptake as measured by *ex vivo* counting of the activity in the pancreata. The relatively high background activity in the SPECT images represents a challenge for accurate quantification of [^{111}In]In-DTPA-exendin in the pancreas of rats with a low beta cell mass, reducing the correlation coefficient. This phenomenon is of less importance in clinical SPECT or PET imaging, since the background in these images is low and the distance between the pancreas and the kidneys is larger.

The results of this study clearly indicate that radiolabeled exendin imaging represents a reliable technology for the noninvasive determination of the BCM in type 1 diabetes, and the potential of this method should clearly be exploited to study the changes in BCM in clinical studies.

In conclusion, the strong correlation between pancreatic accumulation of [^{111}In]In-DTPA-exendin and the BCM observed in BBDP rats is independent of insulitis and fluctuations in blood glucose levels, suggesting that this non-invasive imaging method holds great promise for clinical determination of BCM in individuals with T1D.

AUTHOR CONTRIBUTIONS

MB, CF, LJ, , DB, HP, MMvZ conducted the experiments. MB, LJ and MG designed the experiments. MB wrote the manuscript. All authors revised and approved the manuscript. MG and MB are guarantors of this work.
MG is consultant of Boehringer Ingelheim and patent holder in the field. All other authors have no conflict of interest.

ACKNOWLEDGEMENTS

We thank Bianca Lemmers, Kitty Lemmens, Iris Lamers and Henk Arnts from the Central Animal Facility for their technical assistance with the animals experiments.
This work was supported by the Juvenile Diabetes Research Foundation under file number 37-2011-635.

REFERENCES

1. Coppieters KT, Roep BO, von Herrath MG. Beta cells under attack: toward a better understanding of type 1 diabetes immunopathology. *Semin Immunopathol*. **2011**; 33 (1): 1-7.
2. Keenan HA, Sun JK, Levine J, Doria A, Aiello LP, Eisenbarth G, *et al*. Residual insulin production and pancreatic ss-cell turnover after 50 years of diabetes: Joslin Medalist Study. *Diabetes*. **2010**; 59 (11): 2846-2853.
3. Coppieters KT, Dotta F, Amirian N, Campbell PD, Kay TW, Atkinson MA, *et al*. Demonstration of islet-autoreactive CD8 T cells in insulitic lesions from recent onset and long-term type 1 diabetes patients. *The Journal of experimental medicine*. **2012**; 209 (1): 51-60.
4. Brom M, Woliner-van der Weg W, Joosten L, Frielink C, Bouckenooghe T, Rijken P, *et al*. Non-invasive quantification of the beta cell mass by SPECT with In-labelled exendin. *Diabetologia*. **2014**;
5. Ortis F, Naamane N, Flamez D, Ladriere L, Moore F, Cunha DA, *et al*. Cytokines interleukin-1beta and tumor necrosis factor-alpha regulate different transcriptional and alternative splicing networks in primary beta-cells. *Diabetes*. **2010**; 59 (2): 358-374.
6. Xu G, Kaneto H, Laybutt DR, Duvivier-Kali VF, Trivedi N, Suzuma K, *et al*. Downregulation of GLP-1 and GIP receptor expression by hyperglycemia - Possible contribution to impaired incretin effects in diabetes. *Diabetes*. **2007**; 56 (6): 1551-1558.
7. Brom M, Joosten L, Frielink C, Boerman O, Gotthardt M. (111)In-exendin uptake in the pancreas correlates with the beta-cell mass and not with the alpha-cell mass. *Diabetes*. **2015**; 64 (4): 1324-1328.
8. Brom M, Oyen WJ, Joosten L, Gotthardt M, Boerman OC. 68Ga-labelled exendin-3, a new agent for the detection of insulinomas with PET. *European journal of nuclear medicine and molecular imaging*. **2010**; 37 (7): 1345-1355.
9. Kamper M, Tsimpoukidi O, Chatzigeorgiou A, Lymberi M, Kamper EF. The antioxidant effect of angiotensin II receptor blocker, losartan, in streptozotocin-induced diabetic rats. *Transl Res*. **2010**; 156 (1): 26-36.
10. Campbell-Thompson ML, Atkinson MA, Butler AE, Chapman NM, Frisk G, Gianani R, *et al*. The diagnosis of insulitis in human type 1 diabetes. *Diabetologia*. **2013**; 56 (11): 2541-2543.
11. Souza F, Simpson N, Raffo A, Saxena C, Maffei A, Hardy M, *et al*. Longitudinal noninvasive PET-based beta cell mass estimates in a spontaneous diabetes rat model. *The Journal of clinical investigation*. **2006**; 116 (6): 1506-1513.
12. Simpson NR, Souza F, Witkowski P, Maffei A, Raffo A, Herron *A, et al*. Visualizing pancreatic beta-cell mass with [11C]DTBZ. *Nuclear medicine and biology*. **2006**; 33 (7): 855-864.
13. Normandin MD, Petersen KF, Ding YS, *et al*. In vivo imaging of endogenous pancreatic beta cell mass in healthy and type 1 diabetic subjects using 18F-fluoropropyl-dihydrotetrabenazine and PET. *Journal of Nuclear Medicine*. **2012**; 53: 908-916.

14. Freeby M, Ichise M, Harris PE. Vesicular monoamine transporter, type 2 (VMAT2) expression as it compares to insulin and pancreatic polypeptide in the head, body and tail of the human pancreas. *Islets*. **2012**; 4: 393-397.

15. Eriksson O, Espes D, Selvaraju RK, Jansson E, Antoni G, Sorensen J, *et al*. The Positron Emission Tomography ligand [11C]5-Hydroxy-Tryptophan can be used as a surrogate marker for the human endocrine pancreas. *Diabetes*. **2014**; 63: 3428-3437.

16. Heller RS, Aponte GW. Intra-islet regulation of hormone secretion by glucagon-like peptide-1-(7--36) amide. *The American journal of physiology*. **1995**; 269 (6 Pt 1): G852-860.

17. Heller RS, Kieffer TJ, Habener JF. Insulinotropic glucagon-like peptide I receptor expression in glucagon-producing alpha-cells of the rat endocrine pancreas. *Diabetes*. **1997**; 46 (5): 785-791.

18. Orskov C, Poulsen SS. Glucagonlike peptide-I-(7-36)-amide receptors only in islets of Langerhans. Autoradiographic survey of extracerebral tissues in rats. *Diabetes*. **1991**; 40 (10): 1292-1296.

19. Kirk RK, Pyke C, von Herrath MG, Hasselby JP, Pedersen L, Mortensen PG, *et al*. Immunohistochemical assessment of glucagon-like peptide 1 receptor (GLP-1R) expression in the pancreas of patients with type 2 diabetes. *Diabetes, obesity & metabolism*. **2017**; 19 (5): 705-712.


9

Epilogue

CHAPTER 10

General discussion and future perspectives

BETA CELLS ARE THE GUARDS OF GLUCOSE BALANCE

Beta cells play a crucial role in the development of diabetes. However, during many years of research the cause of the disease has not yet fully been elucidated. Several possible mechanisms have been proposed that could be involved in its etiology: genetic predisposition (for instance certain variation in HLA genes)[1], inflammation, metabolism, viruses, diet, and environmental factors. Together these factors contribute to the development of diabetes, a very complicated disease. During the course of the disease, beta cells lose their capacity to produce insulin, and finally induced cell death occurs, leading to a reduced beta cell mass. For many years, it was believed that there was total depletion of beta cells in patients suffering from longstanding type 1 diabetes. However, several studies have found evidence of residual insulin-positive beta cells in these patients[2,3]. In fact, new insights into the survival of beta cells in longstanding T1D patients[2] and proliferating beta cells in recent-onset T1D patients[4] have opened a window of opportunities for possible treatments to re-activate beta cells, to stimulate proliferation of beta cells, or to stimulate differentiation of beta cells from other cells.

A non-invasive method to determine the beta cell mass in a living organism could aid in unraveling the pathophysiology of beta cell loss, diabetes development, and monitoring the effect of new therapies. Current data on beta cells is being obtained via either functional tests (c-peptide, oral glucose tolerance test) or post-mortem studies (based on insulin staining), providing information about beta cell function or beta cell mass, respectively. Up to now very little data is available about the dynamics of beta cell mass during the progression of diabetes. A few years ago, our group has shown the potential of [^{111}In]In-DTPA-exendin-3 to non-invasively monitor the beta cell mass in a chemically-induced model for diabetes. Furthermore, our group showed that the uptake of radiolabeled exendin directly correlated with the beta cell mass. In addition, we have shown that the uptake of exendin was lower in patients with T1D than in healthy subjects[5]. Besides, many studies with radiolabeled exendin have been pursued to detect beta cell-derived tumors (insulinomas), with great successes[6].

In this thesis we have explored the feasibility of two additional beta cell markers for imaging beta cells: maxadilan and GIP. In addition, we have modified exendin to enhance its molar activity and to overcome the high kidney uptake. Furthermore, we have defined an optimal rodent model to determine the beta cell mass, and finally, the feasibility of exendin as a non-invasive beta cell marker was investigated in two rodent models for type 1 diabetes.

EXENDIN BEATS MAXADILAN AND GIP

The involvement of beta cell-related incretin receptors in the maintenance of the blood glucose levels makes them interesting targets for imaging beta cells. In this thesis we have shown that targeting the GIP receptor using radiolabeled GIP resulted in specific uptake in GIPR

expressing tumors. Similarly, PAC1 receptor targeting using radiolabeled maxadilan showed specific uptake in PAC1 receptor expressing INS-1 tumors. Therefore, both tracers seem to be suitable ligands for visualizing beta cell-derived tumors.
Radiolabeled exendin showed specific uptake in INS-1 tumors, which was almost four times higher than the uptake of maxadilan. Yet, we cannot make a fair judgement which tracer would perform best in detecting insulinomas. We have used a different tumor model for GIP, a model with artificial expression levels of the receptor, since the GIPR expression in our insulinoma model is very low. In human insulinomas, the incidence of the GLP-1R expression is more than 92%[7]. Interestingly, Wild et al reported that malignant insulinomas often lack the GLP-1R, whereas benign insulinomas do express the GLP-1R[8]. To date, there are no studies describing the expression of the PAC1 receptor in human insulinomas. They only show VPAC1 receptors in more than 95% of the cases, but no VPAC2 receptor expression[7]. Remarkably, a study of Waser and colleagues revealed that 100% of insulinomas were GIPR positive, whereas only 50% of insulinomas where positive for SST receptors[9]. While the latter is currently the most widely used molecular imaging technique for the detection of insulinomas and other NETs.
How about imaging (native) pancreatic beta cells using either radiolabeled maxadilan, GIP or exendin? For radiolabeled maxadilan we have found specific uptake in the pancreas in mice. Although we did observe specific uptake of radiolabeled GIP in isolated human islets, we did not demonstrate specific uptake in mouse pancreas in our biodistribution study. Furthermore, with radiolabeled maxadilan and GIP we were not able to visualize the mouse pancreas with SPECT *in vivo*. Regarding imaging insulinomas, in our tumor models virtually all cells have receptor expression, which leads to a high concentration of the tracer in the tumor. On the contrary, in the pancreas there are less receptor-expressing cells, they are spread throughout the tissue and therefore the concentration of the tracer is lower. In contrast to maxadilan and GIP, it was possible to visualize the pancreatic beta cells using radiolabeled exendin and SPECT in rodents, which is supported by the higher uptake in the pancreas (3 times and 65 times higher for exendin compared with maxadilan and GIP, respectively). The differences in the performance of these ligands may reflect a difference in receptor expression in the islets and/or in the exocrine tissue, receptor affinity, internalisation rate, or stability of the peptide.
Based on these findings, exendin would be the first tracer of choice for imaging beta cell related diseases, as it shows high and specific uptake in both insulinomas and in pancreatic beta cells, which could both be visualized using SPECT.

EXENDIN IS THE CRÈME DE LA CRÈME

In addition to the beta cell targets investigated in this thesis, many other receptors have been studied for imaging insulinomas and islets of Langerhans (Figure 1). A tracer that is currently being studied for this application is the serotonin precursor, 5-hydroxytryptophan (5-HTP).

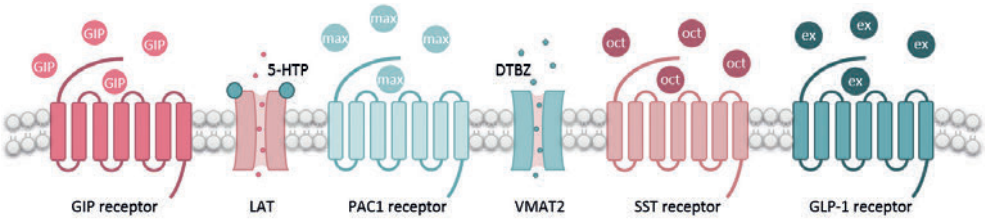

Figure 1. An overview of the most promising targets for beta cell imaging discussed in this chapter. Abbreviations: GIP, glucose-dependent insulinotropic polypeptide; LAT, L-type amino acid transporter; 5-HTP, 5-hydroxytryptophan; PAC1, pituitary adenylate cyclase-activating polypeptide type I; max, maxadilan; VMAT2, vesicular monoamine transporter 2; DTBZ, dihydrotetrabenazine; SST, somatostatin; oct, octreotide; GLP-1, glucagon-like peptide 1; ex, exendin.

5-HTP is taken up by both pancreatic endocrine and exocrine cells, but it is only processed to serotonin and subsequently trapped in vesicles in the endocrine cells. Therefore, it leads to a higher accumulation in endocrine cells than in exocrine cells and it is a potential tracer for islet imaging. However, contradicting results have been reported using radiolabeled 5-HTP as a marker for endocrine cells. Di Gialleonardo *et al.* questioned the feasibility of [^{11}C]5-HTP to image islets, because of the low target-to-background ratio[10]. In contrast, Eriksson *et al.* showed that uptake of [^{11}C]5-HTP in isolated human islets correlated with islet purity. Furthermore, they showed a reduced uptake of [^{11}C]5-HTP in diabetic rats compared to healthy rats, demonstrating the potential of this tracer for noninvasive imaging of the endocrine pancreas[11]. After [^{11}C]5-HTP was used in various clinical studies for diagnosis of neuroendocrine tumors[12], it was more recently also introduced as an imaging biomarker for the islets of Langerhans in the pancreas. In a prospective study, Eriksson *et al.* demonstrated reduced uptake of [^{11}C]5-HTP in the pancreas of T1D patients compared to healthy volunteers. Pancreatic uptake of radiolabeled 5-HTP showed overlap between diabetic patients and healthy volunteers, and showed large variation within these groups. However, the use of the tracer is not only restricted to beta cells, since alpha cells have also been described to take up 5-HTP [13]. It is therefore a tracer for total endocrine mass[14, 15].

Another tracer is based on vesicular monoamine transporter 2 (VMAT2), which is responsible for transporting monoamines (especially neurotransmitters, such as dopamine, histamine and serotonin) from the cytoplasm into synaptic vesicles and is expressed within chromaffin cells, neuron cells and endocrine cells[16, 17]. The use of the VMAT2 antagonist dihydrotetrabenazine (DTBZ) has been extensively studied, with variable results. Several studies, in spontaneous rat models for type 1 diabetes as well as in streptozotocin-induced diabetes, reported a reduced pancreatic uptake of [^{11}C]DTBZ, which was related to progression of diabetes[18-20]. However, the attribution of beta cell related uptake was estimated to be ~25%, as there was significant specific and nonspecific binding of DTBZ to other pancreatic cells[21]. On the contrary, Eriksson

et al. showed no difference in ^{18}F-labeled DTBZ uptake between diabetic and healthy pigs, as uptake in the islets did not exceed the uptake in exocrine tissue[20]. This was confirmed by Fagerholm and colleagues, who reported the same findings in rat and human pancreata[22]. Because of these contradictory results, a study was conducted in different species. VMAT2 expression was identified in islets of pig and human islets, but not in rat and mouse islets, indicating that DTBZ may be suitable for beta cell mass measurements in the clinic[23]. While preclinical studies on the applicability of radiolabeled DTBZ as a tracer for measuring the beta cell mass revealed contradictory results, clinical studies have been performed using this tracer. Goland *et al.* investigated the feasibility of [^{11}C]DTBZ quantification in pancreata of individuals with T1D and healthy controls by dynamic scanning and found a decreased uptake of [^{11}C] DTBZ in T1D patients. However, the functional binding capacity was decreased by a maximum of 40% in patients with longstanding T1D, who almost completely lost the BCM (determined by postmortem analysis), indicating substantial nonspecific VMAT2 uptake in the pancreas[24]. Similarly, ^{18}F-labeled DTBZ showed a reduced uptake in (long-term) T1D patients, compared to healthy individuals[25, 26]. Tracer uptake correlated with stimulated c-peptide levels and a high overlap between insulin and VMAT2 expression was found in human pancreata[27]. Despite encouraging results, the relevance of VMAT2 as an imaging marker for beta cell mass remains a matter of debate, because nonspecific uptake of DTBZ in the exocrine pancreas could limit the ability of the tracer to measure small changes in beta cell mass and expression of VMAT2 is not present in all beta cells [23, 27]. Furthermore, VMAT2 expression has been found in rodent pancreatic mast cells and nerve fibres[23].

Currently, the most widely used tracers for the detection of insulinomas are based on somatostatin (SST) receptor targeting. Reubi et al. have shown that 50-70% of insulinomas express the SST_2 receptor, and 60% express the SST_1 receptor[7]. In addition, Wild and colleagues showed that malignant insulinomas express the SST_2 receptor more often than the GLP-1R and benign insulinomas express the GLP-1R more often than the SST_2 receptor[8]. Furthermore, following SST_1 receptor targeting, a lower uptake in diabetic NOD mice pancreata was found compared with normal mice[28]. However, the expression of the five subtypes of SST receptors has extensively been studied on human pancreatic islets, which showed that there is great overlap of these subtypes in alpha, beta, and delta cells[29].

After careful evaluation of the above mentioned ligands, the performance of exendin seems to best comply the requirements that are needed for an optimal tracer for imaging of beta cells in humans and rats. Exendin seems to exclusively target beta cells, and not other endocrine cells. Furthermore, the uptake of exendin in the exocrine tissue is negligible, since uptake of exendin in severely diabetic rats is corresponding to uptake after receptor blockade[5]. Moreover, exendin is able to visualize insulinomas as well as native beta cells in the pancreas. Yet, using radiolabeled exendin has some drawbacks that we would like to tackle.

DRESSED-UP EXENDIN LIKES TO PERFORM

High molar activity

A number of different factors make native beta cell imaging (compared to tumor imaging) very challenging. First, the beta cell mass represents only 1-2% of the total pancreas and the islets of Langerhans are scattered throughout the pancreas. Second, the targeting agent should be highly specific for the beta cells, since it is surrounded by other endocrine and exocrine cells. Third, the beta cells have lower expression levels of the GLP-1 receptor than tumor cells. As there are less receptors available for binding, these receptors can be more rapidly saturated upon binding of ligands. Thus, to prevent saturation of the beta cell specific receptors, only low doses of exendin can be applied and a high molar activity is required. Therefore, we aimed to increase the molar activity of exendin by adding multiple chelators to incorporate more radioactive molecules per exendin molecule. This has resulted in a massive increase in absolute uptake of radiolabeled exendin in the pancreas of Brown Norway rats and a better visualization of the pancreas using SPECT. Whether this new exendin-based tracer is able to improve the sensitivity of detecting small changes in beta cell mass requires further examination. The methods that have been used so far for increasing the molar activity are mainly based on optimizing labeling conditions[30, 31]. Furthermore, simple purification methods have been described, which separate the unlabeled from the labeled compound before *in vivo* use to prevent receptor saturation by the unlabeled compound[32]. On par with this and our study are the findings of Keller et al.[33] They showed that an increased molar activity enabled them to administer a lower [^{18}F]F-DPA dose *in vivo*. In their study this resulted in a higher tracer binding and retention in the respective organ. In addition, a higher molar dose could allow administration of a reduced peptide dose to patients, thereby preventing pharmacological side-effects.

High kidney uptake

The biggest drawback of radiolabeled exendin and many other small molecules as imaging agents, is the clearance and subsequent reabsorption in the kidneys. Since the kidneys and pancreas are located in close proximity to each other in mice and rats, the high kidney uptake may impair visualization of the pancreas, especially in diabetic animals were the amount of beta cells is very low. When it comes to imaging diabetes in human, the spill-over signal of the kidneys can lead to an overestimation of the signal in the pancreatic tail. For insulinomas, several studies have shown that patients that do have an insulinoma could be diagnosed false negative at early time points after injection, because high uptake in the kidneys could mask the insulinoma in the pancreatic tail in these patients.

Furthermore, if one would like to translate exendin from a diagnostic to a therapeutic agent to treat patients with for example metastasized insulinomas, high renal uptake is a dose limiting factor.

To tackle the problem of high renal uptake, we have modified exendin by incorporating a cleavable linker, namely methionine-isoleucine, between the chelator and the peptide, resulting in NOTA-MI-exendin. Normally, when exendin is cleared from the blood and enters the kidneys, reabsorption in the proximal tubuli causes accumulation of exendin in the kidneys. However, NOTA-MI-exendin showed a massive reduction in renal retention compared to NOTA-exendin, presumably as a consequence of enzymatic cleavage of the linker at the brush border membrane in the kidneys[34]. Very recently, a similar study was carried out, but with a different linker. Introducing a Met-Val-Lys linker to NOTA-exendin resulted in an even faster renal clearance than our compound, NOTA-MI-exendin. Worth noting is that overall, NOTA-Cys^{40}-Leu^{14}-exendin-4 already had a much lower kidney uptake than NOTA-exendin[34]. Another approach is based on introducing an albumin-binding motif (ABM) to exendin. Upon binding to albumin in blood, the circulation time of the radiotracer will be prolonged. Consequently, the ligand has an increased chance of binding the target receptor and the binding to albumin presumably leads to an altered route of clearance. Kaeppeli and colleagues have used this strategy to successfully reduce kidney accumulation[35].

To the best of our knowledge, there is only one clinical study that addressed the high kidney uptake of exendin. In healthy volunteers, succinylated gelatin (Gelofusine) reduced the kidney accumulation of [^{111}In]In-exendin by approximately 18%. Furthermore, in 30% of the patients that received gelofusine, an improved distinction between the pancreatic tail and kidneys was observed, if compared to no Gelofusine administration[36]. To which extend a combination of Gelofusine, a cleavable linker exendin compound, or exendin with an albumin-binding motif would further improve the fast kidney clearance would be an interesting follow-up to these studies.

If we would be able to decrease the accumulation of radiolabeled exendin in the kidneys, this would open a window for exendin to serve as a therapeutic agent. Of course, additional studies are needed to determine the pharmacokinetics of this cleavable exendin labeled with a beta-emitter like Lu-177, and to explore its therapeutic efficacy on insulinomas. Interestingly, one study describes [^{177}Lu]Lu-DOTA-Ahx-Lys^{40}-exendin-4 having specific pancreatic uptake and high kidney uptake in healthy Swiss mice[37] (Guleria 2019), showing that it is feasible to use ^{177}Lu-labeled exendin for targeting GLP-1R expressing organs.

Taken together, a strategy to reduce renal uptake of exendin using a cleavable linker could be of interest for radionuclide therapy using exendin, but for other tracers as well. Actually, this may be the key to develop radiolabeled exendin from a diagnostic to a theranostic agent.

TRANSLATABILITY FROM ANIMAL TO HUMAN (FROM HIGH CUDDLINESS TO HIGH IMPACT)

Are animal studies a reliable predictive surrogate for human studies? Although some animal models are very well-defined, the metabolism, receptor expression and disease progression can greatly vary between species. Critical evaluation of data obtained in animal studies are needed in order to be able to translate them to human application. We have seen that rats seem to be a more suitable model for beta cell imaging than mice, because there is exendin uptake in the exocrine tissue as well. With these exendin results in rodents, the importance of a reliable model has been underlined. Also, for other compounds that have been used for beta cell targeting, large variations between different species have been described. As described previously, VMAT2 expression has been found in human and pig islets, but not in rat and mouse islets[23].

In addition, also the translation of results obtained in subcutaneous tumor models should be evaluated carefully. Often tumor models with artificially high receptor expression are used, which do not always adequately reflect the situation in humans. Furthermore, the tumor location, tumor vasculature, tumor stroma and (lack of) infiltration of immune cells can influence the uptake of the tracer. However, these models can still give a good indication when comparing different tracers.

Stress conditions

In addition to reliably measure the beta cell mass in an appropriate animal model, metabolism plays a crucial role. Changes in the metabolism should not interfere with the expression of the target receptor in order to reliably measure the beta cell mass. Hyperglycemia, which is a consequence of the inability of the beta cells to produce enough insulin, is the hallmark of type 1 and type 2 diabetes. In previous studies, it has been demonstrated that the GLP-1R expression was down-regulated during chronic hyperglycemia[38, 39]. Furthermore, near-normalization of blood glucose levels in patients with type 2 diabetes improved the beta cell sensitivity to GLP-1. These studies indicate that elevated blood glucose levels could influence the expression of the GLP-1R and subsequent quantification of the beta cell mass and imply that close to normal blood glucose levels are needed to reliably measure the beta cell mass[40, 41].

Besides hyperglycemia, also the secretion of certain cytokines has been described to alter GLP-1R expression. Cytokines are released by activated macrophages and T-cells during insulitis, which is known as inflammation of the beta cells. The prevalence and appearance of insulitis in patients with type 1 diabetes and in non-diabetic patients positive for autoantibodies is very heterogeneous[42]. It is important to determine whether (chronic) hyperglycemia and insulitis hamper a reliable beta cell mass quantification using exendin. Our data indicate that severe insulitis and hyperglycemia do not seem to influence the uptake of exendin in preclinical models. Therefore, it is not likely that it influences the determination of the beta cell mass.

Insulitis is less severe in humans than in mice, albeit clinical studies are needed to confirm these findings.

A BRIGHT FUTURE FOR EXENDIN

I believe the use of exendin as a tracer is still in its infancy. The use of exendin in detecting NETs, together with octreotide analogs is becoming a clinical routine in some hospitals. Yet, the role of exendin in diabetes imaging is still not (fully) investigated. In this thesis we have demonstrated the feasibility of exendin to determine the beta cell mass in rodent models for type 1 diabetes, with negligible influence of hyperglycemia and insulitis. A possible next step could be a similar study in an animal model for type 2 diabetes, as the underlying mechanisms for the development of both types differ. Subsequently, it would be of interest to study the beta cell mass in larger patient populations suffering from either type 1 or type 2 diabetes, and relate this to beta cell function. Actually, in a previous study we have shown that there is still exendin uptake in the pancreas of individuals with longstanding type 1 diabetes that have no measurable C-peptide[5]. In this regard, it would be of great interest to find out whether we are detecting non-functional beta cells in these individuals, because this would allow personalized treatment. Stratification of patients, depending on the presence and/or the level of functional beta cells, could aid in choosing the most suitable treatment. For example, patients that still have non-functional beta cells, could possibly benefit from therapies aiming at restoration of beta cell function, rather than regeneration of beta cell mass.

Another approach of radiolabeled exendin is visualization of transplanted islets with SPECT. It has been shown that the accumulation of radiolabeled exendin correlated linearly with transplant size[43]. Therefore, it may qualify to monitor (intrahepatic) islet transplantation in human[44], as exendin shows specific uptake in the beta cells in the islets of Langerhans and has low liver uptake. Transplantation of human donor islets of Langerhans into the liver is one of the explorative treatments that are studied nowadays to restore the insulin production in patients with type 1 diabetes[45]. Visualizing transplanted islets would aid in understanding the spread and survival of these transplants and could give insight into the effectiveness of new therapies aiming at improving intrahepatic islet survival and function.

In this thesis, we have also shown that we are able to reduce the kidney uptake of radiolabeled exendin, which evokes two major questions. First, does the reduced kidney uptake lead to a higher sensitivity in detecting insulinomas, especially the lesions in the vicinity of the kidneys? Second and even more exciting, peptide receptor radionuclide therapy with exendin could now be within reach. Do patients with unresectable or multiple lesions possibly benefit from this new treatment? Both questions need to be further investigated in (pre)clinical studies. So, the road map for exendin (as a theranostic) is yet to be explored.

Finding the most appropriate tracer for beta cell imaging does not necessarily have to be a competition. There is a higher chance on success when working together, and that should be the aim of any research. Using different tracers subsequentially would presumably narrow the area of undetected insulinomas. Furthermore, combining a tracer that detects functional beta cells with a tracer that detects non-functional beta cells, could possibly allow patient stratification, and as such, could offer a personalized treatment.

REFERENCES

1. DiMeglio LA, Evans-Molina C, Oram RA. Type 1 diabetes. *Lancet*. **2018**; 391 (10138): 2449-2462.
2. Keenan HA, Sun JK, Levine J, Doria A, Aiello LP, Eisenbarth G, *et al*. Residual insulin production and pancreatic ss-cell turnover after 50 years of diabetes: Joslin Medalist Study. *Diabetes*. **2010**; 59 (11): 2846-2853.
3. Meier JJ, Bhushan A, Butler AE, Rizza RA, Butler PC. Sustained beta cell apoptosis in patients with long-standing type 1 diabetes: indirect evidence for islet regeneration? *Diabetologia*. **2005**; 48 (11): 2221-2228.
4. Willcox A, Richardson SJ, Bone AJ, Foulis AK, Morgan NG. Evidence of increased islet cell proliferation in patients with recent-onset type 1 diabetes. *Diabetologia*. **2010**; 53 (9): 2020-2028.
5. Brom M, Woliner-van der Weg W, Joosten L, Frielink C, Bouckenooghe T, Rijken P, *et al*. Non-invasive quantification of the beta cell mass by SPECT with (1)(1)(1)In-labelled exendin. *Diabetologia*. **2014**; 57 (5): 950-959.
6. Wild D, Behe M, Wicki A, Storch D, Waser B, Gotthardt M, *et al*. [Lys40(Ahx-DTPA-111In)NH2]exendin-4, a very promising ligand for glucagon-like peptide-1 (GLP-1) receptor targeting. *J Nucl Med*. **2006**; 47 (12): 2025-2033.
7. Reubi JC, Waser B. Concomitant expression of several peptide receptors in neuroendocrine tumours: molecular basis for in vivo multireceptor tumour targeting. *Eur J Nucl Med Mol Imaging*. **2003**; 30 (5): 781-793.
8. Wild D, Christ E, Caplin ME, Kurzawinski TR, Forrer F, Brandle M, *et al*. Glucagon-like peptide-1 versus somatostatin receptor targeting reveals 2 distinct forms of malignant insulinomas. *J Nucl Med*. **2011**; 52 (7): 1073-1078.
9. Waser B, Rehmann R, Sanchez C, Fourmy D, Reubi JC. Glucose-dependent insulinotropic polypeptide receptors in most gastroenteropancreatic and bronchial neuroendocrine tumors. *J Clin Endocrinol Metab*. **2012**; 97 (2): 482-488.
10. Di Gialleonardo V, Signore A, Scheerstra EA, Visser AK, van Waarde A, Dierckx RA, *et al*. 11C-hydroxytryptophan uptake and metabolism in endocrine and exocrine pancreas. *J Nucl Med*. **2012**; 53 (11): 1755-1763.
11. Eriksson O, Selvaraju RK, Johansson L, Eriksson JW, Sundin A, Antoni G, *et al*. Quantitative imaging of serotonergic biosynthesis and degradation in the endocrine pancreas. *J Nucl Med*. **2014**; 55 (3): 460-465.
12. Orlefors H, Sundin A, Ahlstrom H, Bjurling P, Bergstrom M, Lilja A, *et al*. Positron emission tomography with 5-hydroxytryprophan in neuroendocrine tumors. *J Clin Oncol*. **1998**; 16 (7): 2534-2541.
13. Ekholm R, Ericson LE, Lundquist I. Monoamines in the pancreatic islets of the mouse. Subcellular localization of 5-hydroxytryptamine by electron microscopic autoradiography. *Diabetologia*. **1971**; 7 (5): 339-348.

14. Carlbom L, Espes D, Lubberink M, Martinell M, Johansson L, Ahlstrom H, *et al.* [(11)C]5-hydroxy-tryptophan PET for Assessment of Islet Mass During Progression of Type 2 Diabetes. *Diabetes.* **2017**; 66 (5): 1286-1292.

15. Eriksson O, Espes D, Selvaraju RK, Jansson E, Antoni G, Sorensen J, *et al.* Positron emission tomography ligand [11C]5-hydroxy-tryptophan can be used as a surrogate marker for the human endocrine pancreas. *Diabetes.* **2014**; 63 (10): 3428-3437.

16. Anlauf M, Eissele R, Schafer MK, Eiden LE, Arnold R, Pauser U, *et al.* Expression of the two isoforms of the vesicular monoamine transporter (VMAT1 and VMAT2) in the endocrine pancreas and pancreatic endocrine tumors. *J Histochem Cytochem.* **2003**; 51 (8): 1027-1040.

17. Maffei A, Liu Z, Witkowski P, Moschella F, Del Pozzo G, Liu E, *et al.* Identification of tissue-restricted transcripts in human islets. *Endocrinology.* **2004**; 145 (10): 4513-4521.

18. Simpson NR, Souza F, Witkowski P, Maffei A, Raffo A, Herron A, *et al.* Visualizing pancreatic beta-cell mass with [11C]DTBZ. *Nucl Med Biol.* **2006**; 33 (7): 855-864.

19. Souza F, Simpson N, Raffo A, Saxena C, Maffei A, Hardy M, *et al.* Longitudinal noninvasive PET-based beta cell mass estimates in a spontaneous diabetes rat model. *The Journal of clinical investigation.* **2006**; 116 (6): 1506-1513.

20. Freeby M, Goland R, Ichise M, Maffei A, Leibel R, Harris P. VMAT2 quantitation by PET as a biomarker for beta-cell mass in health and disease. *Diabetes Obes Metab.* **2008**; 10 Suppl 4 98-108.

21. Singhal T, Ding YS, Weinzimmer D, Normandin MD, Labaree D, Ropchan J, *et al.* Pancreatic beta cell mass PET imaging and quantification with [11C]DTBZ and [18F]FP-(+)-DTBZ in rodent models of diabetes. *Mol Imaging Biol.* **2011**; 13 (5): 973-984.

22. Fagerholm V, Mikkola KK, Ishizu T, Arponen E, Kauhanen S, Nagren K, *et al.* Assessment of islet specificity of dihydrotetrabenazine radiotracer binding in rat pancreas and human pancreas. *J Nucl Med.* **2010**; 51 (9): 1439-1446.

23. Schafer MK, Hartwig NR, Kalmbach N, Klietz M, Anlauf M, Eiden LE, *et al.* Species-specific vesicular monoamine transporter 2 (VMAT2) expression in mammalian pancreatic beta cells: implications for optimising radioligand-based human beta cell mass (BCM) imaging in animal models. *Diabetologia.* **2013**; 56 (5): 1047-1056.

24. Goland R, Freeby M, Parsey R, Saisho Y, Kumar D, Simpson N, *et al.* 11C-dihydrotetrabenazine PET of the pancreas in subjects with long-standing type 1 diabetes and in healthy controls. *J Nucl Med.* **2009**; 50 (3): 382-389.

25. Freeby MJ, Kringas P, Goland RS, Leibel RL, Maffei A, Divgi C, *et al.* Cross-sectional and Test-Retest Characterization of PET with [(18)F]FP-(+)-DTBZ for beta Cell Mass Estimates in Diabetes. *Mol Imaging Biol.* **2016**; 18 (2): 292-301.

26. Normandin MD, Petersen KF, Ding YS, Lin SF, Naik S, Fowles K, *et al.* In vivo imaging of endogenous pancreatic beta-cell mass in healthy and type 1 diabetic subjects using 18F-fluoropropyl-dihydrotetrabenazine and PET. *J Nucl Med.* **2012**; 53 (6): 908-916.

27. Saisho Y, Harris PE, Butler AE, Galasso R, Gurlo T, Rizza RA, *et al*. Relationship between pancreatic vesicular monoamine transporter 2 (VMAT2) and insulin expression in human pancreas. *J Mol Histol*. **2008**; 39 (5): 543-551.

28. Amartey JK, Shi Y, Al-Jammaz I, Esguerra C, Al-Otaibi B, Al-Mohanna F. Radioiodinated naphthylalanine derivatives targeting pancreatic beta cells in normal and nonobese diabetic mice. *Exp Diabetes Res*. **2008**; 2008 371716.

29. Kumar U, Sasi R, Suresh S, Patel A, Thangaraju M, Metrakos P, *et al*. Subtype-selective expression of the five somatostatin receptors (hSSTR1-5) in human pancreatic islet cells: a quantitative double-label immunohistochemical analysis. *Diabetes*. **1999**; 48 (1): 77-85.

30. Breeman WA, De Jong M, Visser TJ, Erion JL, Krenning EP. Optimising conditions for radiolabelling of DOTA-peptides with 90Y, 111In and 177Lu at high specific activities. *Eur J Nucl Med Mol Imaging*. **2003**; 30 (6): 917-920.

31. Brom M, Joosten L, Oyen WJ, Gotthardt M, Boerman OC. Improved labelling of DTPA- and DOTA-conjugated peptides and antibodies with 111In in HEPES and MES buffer. *EJNMMI Res*. **2012**; 2 4.

32. von Hacht JL, Erdmann S, Niederstadt L, Prasad S, Wagener A, Exner S, *et al*. Increasing molar activity by HPLC purification improves 68Ga-DOTA-NAPamide tumor accumulation in a B16/F1 melanoma xenograft model. *PLoS One*. **2019**; 14 (6): e0217883.

33. Keller T, Lopez-Picon FR, Krzyczmonik A, Forsback S, Takkinen JS, Rajander J, *et al*. Comparison of high and low molar activity TSPO tracer [(18)F]F-DPA in a mouse model of Alzheimer's disease. *J Cereb Blood Flow Metab*. **2019**; 271678X19853117.

34. Zhang M, Jacobson O, Kiesewetter DO, Ma Y, Wang Z, Lang L, *et al*. Improving the Theranostic Potential of Exendin 4 by Reducing the Renal Radioactivity through Brush Border Membrane Enzyme-Mediated Degradation. *Bioconjug Chem*. **2019**; 30 (6): 1745-1753.

35. Kaeppeli SAM, Jodal A, Gotthardt M, Schibli R, Behe M. Exendin-4 Derivatives with an Albumin-Binding Moiety Show Decreased Renal Retention and Improved GLP-1 Receptor Targeting. *Mol Pharm*. **2019**; 16 (9): 3760-3769.

36. Buitinga M, Jansen T, van der Kroon I, Woliner-van der Weg W, Boss M, Janssen M, *et al*. Succinylated Gelatin Improves the Theranostic Potential of Radiolabeled Exendin-4 in Insulinoma Patients. *J Nucl Med*. **2019**; 60 (6): 812-816.

37. Guleria M, Das T, Amirdhanayagam J, Sarma HD, Dash A. Preparation of [(177)Lu]Lu-DOTA-Ahx-Lys40-Exendin-4 for radiotherapy of insulinoma: a detailed insight into the radiochemical intricacies. *Nucl Med Biol*. **2019**; 78-79 31-40.

38. Rajan S, Dickson LM, Mathew E, Orr CM, Ellenbroek JH, Philipson LH, *et al*. Chronic hyperglycemia downregulates GLP-1 receptor signaling in pancreatic beta-cells via protein kinase A. *Mol Metab*. **2015**; 4 (4): 265-276.

39. Xu G, Kaneto H, Laybutt DR, Duvivier-Kali VF, Trivedi N, Suzuma K, *et al*. Downregulation of GLP-1 and GIP receptor expression by hyperglycemia: possible contribution to impaired incretin effects in diabetes. *Diabetes*. **2007**; 56 (6): 1551-1558.

40. Hojberg PV, Vilsboll T, Rabol R, Knop FK, Bache M, Krarup T, *et al*. Four weeks of near-normalisation of blood glucose improves the insulin response to glucagon-like peptide-1 and glucose-dependent insulinotropic polypeptide in patients with type 2 diabetes. *Diabetologia*. **2009**; 52 (2): 199-207.

41. Hojberg PV, Zander M, Vilsboll T, Knop FK, Krarup T, Volund A, *et al*. Near normalisation of blood glucose improves the potentiating effect of GLP-1 on glucose-induced insulin secretion in patients with type 2 diabetes. *Diabetologia*. **2008**; 51 (4): 632-640.

42. Campbell-Thompson ML, Atkinson MA, Butler AE, Chapman NM, Frisk G, Gianani R, *et al*. The diagnosis of insulitis in human type 1 diabetes. *Diabetologia*. **2013**; 56 (11): 2541-2543.

43. Eter WA, Van der Kroon I, Andralojc K, Buitinga M, Willekens SMA, Frielink C, *et al*. Non-invasive in vivo determination of viable islet graft volume by (111)In-exendin-3. *Sci Rep*. **2017**; 7 (1): 7232.

44. Pattou F, Kerr-Conte J, Wild D. GLP-1-receptor scanning for imaging of human beta cells transplanted in muscle. *N Engl J Med*. **2010**; 363 (13): 1289-1290.

45. de Kort H, de Koning EJ, Rabelink TJ, Bruijn JA, Bajema IM. Islet transplantation in type 1 diabetes. *BMJ*. **2011**; 342 d217.

SUMMARY

Diabetes is one of the leading causes of death worldwide, according to the WHO. Type 1 diabetes develops as a result of an autoimmune attack directed towards the insulin-producing beta cells. Type 2 diabetes is characterized by an ineffective use of insulin by the peripheral organs. Little is known about beta cell dynamics during the onset and progression of diabetes. A non-invasive imaging method would allow monitoring of the beta cell mass longitudinally and could identify changes in the beta cell mass during development of diabetes. Subsequently, it could provide information to individualize diabetes treatment. The ideal tracer should meet certain prerequisites to qualify as a suitable tracer for beta cell imaging, for example, specific uptake in the beta cells and not in non-target cells, high target affinity, and fast blood clearance. In the recent years, several tracers for beta cell imaging have been proposed and some have been tested in clinical trials. Yet, none of these tracers has been implemented for routinely visualizing beta cells in diabetic patients.

Preferably, the tracer should also be able to visualize insulinomas, tumors in the pancreas derived from insulin-producing beta cells. Currently, the most widely used imaging method to diagnose insulinomas is based on somatostatin receptor targeting using radiolabeled octreotide visualized by PET or SPECT. However, it has been shown that only part of insulinomas express the somatostatin receptor, and it is not a suitable tracer to image beta cell mass. Therefore, the search for new agents that are able to image beta-cell related diseases is ongoing. Currently, the glucagon-like peptide 1 receptor (GLP-1R) targeting peptide exendin is the most promising tracer for imaging beta cells. Peptides, targeting specific receptors on beta cells, best comply the requirements for a suitable tracer. Hence, the search for new beta cell imaging agents, as described in the next studies, have been focused on peptides.

THE SEARCH FOR NEW TRACERS FOR BETA CELL IMAGING

Insulinomas have high expression of the pituitary adenylate cyclase-activating polypeptide type I (PAC1) receptor and the glucose-dependent insulinotropic polypeptide receptor (GIPR). In **chapter 3** we have investigated the feasibility of radiolabeled maxadilan, a PAC1 receptor targeting agent, to detect insulinomas by SPECT imaging in a mouse model with subcutaneous insulinomas (INS-1 tumors). Maxadilan-DTPA-[^{111}In]In accumulated specifically in INS-1 tumors and in the pancreas. Furthermore, we were able to clearly visualize INS-1 tumors using SPECT/CT. Next, another promising tracer has been investigated as a beta cell imaging agent. **Chapter 4** describes the characterization of ^{111}In-labeled GIP for visualizing neuroendocrine tumors. [^{111}In]In-DTPA-GIP$_{1-42}$ showed receptor-mediated binding to BHK-GIPR positive cells, NES2Y cells (human beta cell-like insulin secreting cell line) and isolated

islets *in vitro*. Furthermore, the *in vivo* studies showed that GIP receptor transfected tumors and NES2Y tumors could be visualized with SPECT/CT using [^{111}In[In]-DTPA-GIP$_{1-42}$ as a tracer. Exendin has been shown to specifically target the GLP-1R on beta cells in the pancreas and is able to visualize GLP-1R expressing insulinomas. Native beta cells, in contrast to tumor cells, display physiological levels of the receptor and are spread throughout the pancreas. As there are less receptors available for binding, a low peptide dose should be administered to avoid receptor saturation. Hence, to be able to be detected, a high molar activity is needed in order to get a sufficient amount of radioactive signal in the beta cells. This issue has been addressed in **chapter 5**, which focusses on the improvement of the molar activity of ^{111}In-labeled exendin. In this study, exendin has been modified by addition of six lysine residues and by conjugation of one, two or six DTPA moieties to these lysine residues, resulting in five new compounds. Addition of multiple DTPA molecules increased the molar activity, and was most pronounced for hexendin(40-45), which has six DTPA moieties. As a result of the enhanced molar activity, the absolute pancreatic uptake of hexendin(40-45) in Brown Norway rats increased considerably, enabling an improved visualization of the pancreas with SPECT/CT.

Chapter 6 is devoted to one of the main challenges when using radiolabeled exendin *in vivo*. Radiolabeled exendin accumulates at high concentrations in the kidneys, which could hamper the detection of small insulinomas in the vicinity of the kidneys. Reduction of the accumulation in the kidney would greatly improve the visualization of insulinomas. In this study, exendin-4 was extended with a Met-Ile-linker and subsequently conjugated with NOTA. Biodistribution studies in BALB/c nude mice bearing a subcutaneous INS-1 tumor showed stable tumor uptake over time for [^{68}Ga]Ga-NOTA-MI-exendin-4 and the INS-1 tumor was clearly visualized using SPECT/CT. Most importantly, kidney uptake was significantly lower for this extended exendin analog compared to [^{68}Ga]Ga-NOTA-exendin-4.

BETA CELL IMAGING APPLIED IN RODENT MODELS

To validate the clinical potential of radiolabeled exendin as a native beta cell imaging agent, we first determined the most suitable animal model for non-invasive determination of the beta cell mass using [^{111}In]In-DTPA-exendin-3 (**chapter 7**). The most important finding of this study was that rats seem to represent a more adequate model for beta cell mass assessment than mice. In rats, the uptake of exendin after alloxan treatment was similar to the uptake after a blocking dose, whereas in mice there was a considerable amount of exendin uptake after alloxan treatment. These results indicate that there was exendin uptake in the exocrine tissue as well. Considering the fact that exocrine GLP-1R expression measured on mRNA and protein level was very low, it is likely that [^{111}In]In-DTPA-exendin-3 binds to a binding site, other than the GLP-1R, in exocrine mouse pancreas. Therefore, determination of the beta cell mass using radiolabeled exendin may be more specific for the beta cells in rats than in mice.

Next, we have examined the use of [^{111}In]In-DTPA-exendin-3 for determining the beta cell mass in two rodent models for spontaneous type 1 diabetes. In **chapter 8** nonobese diabetic (NOD) mice were monitored until 21 weeks of age by measuring blood glucose and performing SPECT/CT after injection of [^{111}In]In-DTPA-exendin-3. A linear correlation was found between the beta cell mass in these mice and the uptake of exendin in the pancreas, which was not affected by either insulitis or hyperglycemia. However, there was remaining [^{111}In]In-DTPA-exendin-3 uptake in the pancreas, despite total ablation of the beta cells, rendering this a suboptimal animal model for exendin imaging as mentioned above. A more favorable correlation between exendin uptake and the beta cell mass was found in BioBreeding Diabetes Prone rats (**Chapter 9**). Also, in this model we have shown that the correlation between radiolabeled exendin uptake and beta cell mass was independent of insulitis and fluctuations in blood glucose levels. The results of this study clearly indicate that imaging with radiolabeled exendin represents a reliable and robust technology for non-invasive determination of the beta cell mass in type 1 diabetes.

In **chapter 10** the results of the studies described and the future perspectives of beta cell and insulinoma imaging are discussed.

SAMENVATTING

Diabetes is een chronische, metabole ziekte, waarbij het lichaam niet in staat is om de bloedglucose in goede balans te houden. De beta cellen, gelokaliseerd in de eilandjes van Langerhans in de pancreas zorgen voor deze balans door het produceren van insuline. Onder invloed van insuline wordt glucose in het bloed opgeslagen in onder andere spieren en de lever, waardoor de concentratie glucose daalt naar normale waarden. Type 1 diabetes ontstaat als gevolg van een auto-immuunreactie gericht tegen de beta cellen, waarbij deze cellen sterven. Type 2 diabetes kenmerkt zich door insuline-resistentie van weefsels die normaliter wel gevoelig zijn voor insuline. Beide oorzaken leiden tot verhoogde bloedglucosewaarden (hyperglycemie). Er is weinig bekend over de hoeveelheid beta cellen (beta cel massa) tijdens het ontstaan en de ontwikkeling van diabetes. Momenteel wordt alleen de beta cel functie gemeten door het bepalen van bijvoorbeeld bloedglucosewaardes of glucose tolerantie. Vaak wordt de beta cel functie gezien als een maat van de beta cel massa, maar de beta cel massa en functie komen niet per definitie overeen. Wanneer de beta cel massa op een niet-invasieve manier gevisualiseerd kan worden, geeft dit de mogelijkheid om de beta cel massa langdurig te volgen en zo mogelijke veranderingen in de beta cel massa waar te nemen tijdens de ontwikkeling van diabetes. Om beta cellen te kunnen visualiseren is een merkstof (tracer) nodig die specifiek bindt aan de beta cellen. De beta cellen zijn geclusterd in de eilandjes van Langerhans, welke verspreid liggen over de pancreas. Dit maakt het moeilijk om de beta cellen af te beelden. De ideale beta cel tracer moet aan bepaalde eisen voldoen. De tracer moet bijvoorbeeld I) specifiek accumuleren in de beta cellen en niet in andere organen, II) hoge affiniteit hebben voor de receptor op de cellen waar de tracer specifiek aan kan binden en III) snel uit het bloed worden geklaard. Er is een verscheidenheid aan beta cel tracers onderzocht, waarvan sommigen in klinische trials zijn getest. Toch is er tot op heden nog geen beta cel tracer die routinematig wordt gebruikt om de beta cel massa in mensen met diabetes te bepalen.

Naast het in beeld brengen van diabetes, zou het van toegevoegde waarde zijn als de tracer ook insulinomen kan detecteren. Insulinomen zijn tumoren in de pancreas, die zijn ontstaan door ongeremde groei van de insuline-producerende beta cellen. De meest gebruikte nucleaire methode voor het visualiseren van insulinomen is gebaseerd op somatostatine receptor targeting met behulp van radioactief octreotide en PET of SPECT. Het is echter aangetoond dat niet alle insulinomen de somatostatine receptor tot expressie brengen, en octreotide is ook geen geschikte tracer voor het visualiseren van de beta cel massa, omdat octreotide ook bindt aan andere endocriene cellen. De vraag naar nieuwe tracers voor het zichtbaar maken van beta cel gerelateerde aandoeningen blijft dus bestaan. In dit proefschrift wordt de toepasbaarheid van nieuwe en geoptimaliseerde tracers voor het visualiseren van beta cellen en insulinomas en voor het bepalen van de beta cel massa onderzocht.

DE ZOEKTOCHT NAAR NIEUWE TRACERS VOOR BETA CEL IMAGING

In **deel 1** (H3 – H6) van dit proefschrift onderzoeken we nieuwe en geoptimaliseerde radioactieve tracers voor beta cel imaging. Insulinomen brengen de pituitary adenylate cyclase-activating polypeptide type I (PAC1) receptor en de glucose-dependent insulinotropic polypeptide receptor (GIPR) verhoogd tot expressie. In **hoofdstuk 3** hebben we onderzocht of het PAC1 receptor bindende peptide maxadilan toepasbaar is voor het detecteren van insulinomen. In muizen met een subcutane insulinoom (INS-1 tumor) werd receptor gemedieerde tumor opname gezien na injectie van maxadilan-DTPA-[^{111}In]In. Ook in de pancreas werd PAC1-gemedieerde opname van deze tracer waargenomen. Verder hebben we laten zien dat de INS-1 tumoren konden worden afgebeeld met SPECT/CT na injectie van maxadilan-DTPA-[^{111}In]In. **Hoofdstuk 4** beschrijft de karakterisatie van ^{111}In-gelabeld GIP voor het visualiseren van neuroendocriene tumoren. [^{111}In]In-DTPA-GIP$_{1-42}$ liet receptor gemedieerde opname zien in BHK-GIPR positieve cellen, in NES2Y cellen (humane insuline-secreterende (beta)-cellijn) en in geïsoleerde eilandjes van Langerhans *in vitro*. Daarnaast toonden *in vivo* studies aan dat GIP getransfecteerde tumoren en NES2Y tumoren konden worden afgebeeld met SPECT/CT na injectie van [^{111}In]In-DTPA-GIP1-$_{42}$. Deze resultaten tonen aan dat zowel maxadilan als GIP veelbelovende tracers zijn voor het afbeelden van neuroendocriene tumoren.

Momenteel is het peptide exendin de meest veelbelovende tracer voor het in beeld brengen van beta cellen. Eerdere studies hebben aangetoond dat exendin specifiek bindt aan de glucagon-like peptide-1 receptor (GLP-1R), welke tot expressie komt op beta cellen in de pancreas en dat exendin gebruikt kan worden om GLP-1R expresserende tumoren in beeld te brengen. In tegenstelling tot tumorcellen, waar bepaalde receptoren/eiwitten tot overexpressie worden gebracht, hebben de beta cellen in de pancreas fysiologische expressie van de GLP-1R. Omdat deze niet-neoplastische beta cellen minder receptoren beschikbaar hebben waar gelabeld exendin aan kan binden (ten opzichte van tumoren), is er een lage peptide dosis nodig om verzadiging van de receptoren te voorkomen. Om deze cellen toch zichtbaar te kunnen maken, is het dus belangrijk om voldoende radioactiviteit toe te dienen. Dit kan door middel van het behalen van een hoge molaire activiteit (de hoeveelheid radioactiviteit per massaeenheid van de tracer). In **hoofdstuk 5** richten we ons op een betere visualisatie van de pancreas door het verbeteren van de molaire activiteit van ^{111}In-gelabeld exendin. In deze studie worden vijf nieuwe exendin verbindingen beschreven waarbij exendin werd gemodificeerd door het toevoegen van zes lysines (hexendin) en de conjugatie van één, twee of zes DTPA moleculen. In Brown Norway ratten hebben we de visualisatie van de pancreas met deze tracers met elkaar vergeleken. Het toevoegen van meerdere DTPA moleculen resulteerde in een verhoogde molaire activiteit, vooral voor hexendin(40-45), welke in totaal zes DTPA moleculen heeft. Als gevolg van de verhoogde molaire activiteit konden we een grotere hoeveelheid radioactiviteit in de beta cellen in de pancreas krijgen. Hierdoor zagen we een verbeterde visualisatie van de pancreas in Brown Norway ratten met SPECT/CT na injectie van ^{111}In-gelabeld hexendin(40-45).

Kleine hydrofiele moleculen, zoals exendin, worden via de nieren uit het bloed geklaard. Een deel hiervan zal via de urine worden uitgescheiden, maar een significant deel zal door middel van reabsorptie via bepaalde receptoren in de nieren blijven. Het exendin zelf wordt daar afgebroken, maar het radionuclide zal in de nieren blijven, wat leidt tot hoge concentraties radioactiviteit in de nieren. Dit kan de aanwezigheid van kleine insulinomen in de nabijheid van de nieren maskeren. Maar ook de beta cel massa bepaling met behulp van radioactief exendin kan bemoeilijkt worden, doordat de staart van de pancreas dichtbij de nieren ligt. Een reductie van de exendin opname in de nieren zou daarom de visualisatie van bepaalde insulinomen sterk kunnen verbeteren. In **hoofdstuk 6** hebben we exendin-4 verlengd met een methionine-isoleucine (Met-Ile) linker, waaraan NOTA is geconjugeerd. Bepaalde enzymen in de nieren zullen deze linker in het radioactieve exendin knippen, waardoor er twee delen ontstaan. Het exendin deel zal in de nieren worden opgenomen en daar worden afgebroken, terwijl het radioactieve deel niet zal worden gereabsorbeerd, maar via de urine worden uitgescheiden. Biodistributie studies in muizen met een subcutane INS-1 tumor lieten stabiele tumor opname van [^{68}Ga]Ga-NOTA-MI-exendin-4 zien gedurende vier uur na injectie. Ook met behulp van SPECT/CT konden de INS-1 tumoren duidelijk zichtbaar worden afgebeeld. Het toevoegen van de Met-Ile linker tussen exendin en NOTA leidde tot 70 procent minder nier opname vergeleken met [^{68}Ga]Ga-NOTA-exendin-4.

BETA CEL IMAGING IN DIERMODELLEN

Deel 2 van dit proefschrift richt zich op de validatie van radioactief exendin voor het niet-invasief bepalen van de beta cel massa in verschillende diermodellen. Om de klinische toepasbaarheid van radioactief exendin te onderzoeken, hebben we eerst gezocht naar de meest optimale diersoort voor het bepalen van de beta cel massa met behulp van [^{111}In]In-DTPA-exendin-3 (**hoofdstuk 7**). We hebben de opname en distributie van [^{111}In]In-DTPA-exendin-3 in muizen en ratten pancreas bepaald door middel van biodistributie en autoradiografie. Deze resultaten hebben we vervolgens vergeleken met de GLP-1R expressie op basis van immunohistochemie en qPCR. Met autoradiografie zagen we hotspots in de pancreas (de eilandjes van Langerhans), die verdwenen na alloxaan geïnduceerde depletie van de beta cellen. In ratten ging de depletie van beta cellen gepaard met een 80% afname van radioactief exendin in de pancreas, in tegenstelling tot in muizen, waar we na het toedienen van alloxaan nog steeds een flinke pancreas opname van exendin zagen. Deze resultaten impliceren dat er in muizen, naast opname in de beta cellen, er ook opname is in de exocriene pancreas. Aangezien er met immunohistochemie en qPCR geen expressie van de GLP-1R is aangetoond in de exocriene pancreas, is het aannemelijk dat [^{111}In]In-DTPA-exendin-3 in muizen exocrien pancreasweefsel aan een andere receptor bindt dan de GLP-1R. Deze resultaten leiden tot de bevinding dat voor

het bepalen van de beta cel massa met behulp van exendin ratten een geschikter model zijn dan muizen.

Vervolgens hebben we het gebruik van [^{111}In]In-DTPA-exendin-3 voor het bepalen van de beta cel massa onderzocht in twee type 1 diabetes diermodellen. **Hoofdstuk 8** beschrijft het monitoren van nonobese diabetic (NOD) muizen. Type 1 diabetes ontwikkelt zich bij de NOD muizen als gevolg van een spontane auto-immuunreactie tegen de beta cellen, wat gekarakteriseerd wordt door hyperglycemie (verhoogde bloedglucose) en insulitis (ontsteking van de eilandjes van Langerhans). Bij deze muizen is gedurende een leeftijd van 21 weken wekelijks de bloedglucose bepaald en wekelijks een SPECT/CT uitgevoerd 1 uur na injectie van [^{111}In]In-DTPA-exendin-3. In deze muizen is een lineaire correlatie gevonden tussen de beta cel massa en de opname van exendin in de pancreas. Insulitis en hyperglycemie leken geen invloed te hebben op deze correlatie. Terwijl we na immunohistochemische analyse geen beta cellen meer zagen in de pancreas, maten we wel nog opname van [^{111}In]In-DTPA-exendin-3 in de pancreas. Deze bevindingen bevestigen dat muizen een suboptimaal model zijn voor het bepalen van de beta cel massa met exendin imaging.

Er is ook een ratten model waarbij type 1 diabetes spontaan ontwikkelt na een auto-immuunreactie tegen de beta cellen. Diabetes wordt in deze BioBreeding Diabetes Prone (BBDP) ratten gekarakteriseerd door ernstige insulitis, waarna diabetes zich snel ontwikkelt. In **hoofdstuk 9** staat beschreven hoe deze ratten zijn gemonitord tot een leeftijd van 18 weken, waarbij wekelijks de bloedglucose werd gemeten, en wekelijks een SPECT/CT werd uitgevoerd 1 uur na injectie van [^{111}In]In-DTPA-exendin-3. Door middel van autoradiografie zagen we specifieke accumulatie van radioactief exendin in de eilandjes van Langerhans. Wanneer we met autoradiografie geen signaal in de eilandjes zagen, kwam dit overeen met de immunohistochemische analyse, waar ook geen beta cellen werden aangetoond. We hebben een goede correlatie tussen de pancreas opname van radioactief exendin en de beta cel massa aangetoond. Ook in dit model hebben we laten zien dat deze correlatie niet werd beïnvloedt door insulitis en bloedglucose waarden. De resultaten van deze studie tonen aan dat imaging met radioactief exendin een veelbelovende methode is om niet-invasief de beta cel massa in type 1 diabetes te bepalen.

In **hoofdstuk 10** worden de resultaten van de beschreven studies en het toekomstperspectief van beta cel en insulinoom imaging besproken.

LIST OF PUBLICATIONS

1. Buitinga M, Cohrs CM, Eter WA, **Claessens-Joosten** L, Frielink C, Bos D, Sandker G, Brom M, Speier S, Gotthardt M. Non-Invasive Monitoring of Glycemia-Induced Regulation Of GLP-1R Expression in Murine and Human Islets of Langerhans. *Diabetes*. 2020;
2. Lobeek D, Rijpkema M, Terry SYA, Molkenboer-Kuenen JDM, **Joosten** L, van Genugten EAJ, van Engen-van Grunsven ACH, Kaanders J, Pegge SAH, Boerman OC, Weijs WLJ, Merkx MAW, van Herpen CML, Takes RP, Aarntzen E, Oyen WJG. Imaging angiogenesis in patients with head and neck squamous cell carcinomas by [(68)Ga]Ga-DOTA-E-[c(RGDfK)]2 PET/CT. *European journal of nuclear medicine and molecular imaging*. 2020;
3. Michelotti FC, Bowden G, Kuppers A, **Joosten** L, Maczewsky J, Nischwitz V, Drews G, Maurer A, Gotthardt M, Schmid AM, Pichler BJ. PET/MRI enables simultaneous in vivo quantification of beta-cell mass and function. *Theranostics*. 2020;10:398-410.
4. Jansen TJP, van Lith SAM, Boss M, Brom M, **Joosten** L, Behe M, Buitinga M, Gotthardt M. Exendin-4 analogs in insulinoma theranostics. *J Labelled Comp Radiopharm*. 2019;
5. **Joosten** L, Brom M, Peeters H, Bos D, Himpe E, Bouwens L, Boerman O, Gotthardt M. Measuring the pancreatic beta cell mass in vivo with exendin SPECT during hyperglycemia and severe insulitis. *Molecular pharmaceutics*. 2019;
6. Op 't Veld RC, **Joosten** L, van den Boomen OI, Boerman OC, Kouwer P, Middelkoop E, Rowan AE, Jansen JA, Walboomers XF, Wagener F. Monitoring (111)In-labelled polyisocyanopeptide (PIC) hydrogel wound dressings in full-thickness wounds. *Biomater Sci*. 2019;
7. Brom M, **Joosten** L, Frielink C, Peeters H, Bos D, van Zanten M, Boerman O, Gotthardt M. Validation of (111)In-Exendin SPECT for the Determination of the Beta Cell Mass in BioBreeding Diabetes Prone Rats. *Diabetes*. 2018;
8. Demine S, Balhuizen A, Debaille V, **Joosten** L, Fereau M, Chilla SNM, Millard I, Scharfmann R, Egrise D, Goldman S, Marchetti P, Gotthardt M, Laurent S, Burtea C, Eizirik DL. Imaging of Human Insulin Secreting Cells with Gd-DOTA-P88, a Paramagnetic Contrast Agent Targeting the Beta Cell Biomarker FXYD2gammaa. *Molecules*. 2018;23:
9. **Joosten** L, Brom M, Peeters H, Heskamp S, Behe M, Boerman O, Gotthardt M. Enhanced Specific Activity by Multichelation of Exendin-3 Leads To Improved Image Quality and In Vivo Beta Cell Imaging. *Molecular pharmaceutics*. 2018;15:486-494.
10. Willekens SMA, **Joosten** L, Boerman OC, Brom M, Gotthardt M. Characterization of (111)In-labeled Glucose-Dependent Insulinotropic Polypeptide as a Radiotracer for Neuroendocrine Tumors. *Scientific reports*. 2018;8:2948.
11. Eter WA, Van der Kroon I, Andralojc K, Buitinga M, Willekens SMA, Frielink C, Bos D, **Joosten** L, Boerman OC, Brom M, Gotthardt M. Non-invasive in vivo determination of viable islet graft volume by 111In-exendin-3. *Scientific reports*. 2017;7:7232.

12. **Joosten** L, Brom M, Schafer MKH, Boerman OC, Weihe E, Gotthardt M. Preclinical evaluation of PAC1 targeting with radiolabeled Maxadilan. *Scientific reports.* 2017;7:1751.

13. van der Kroon I, Woliner-van der Weg W, Brom M, **Joosten** L, Frielink C, Konijnenberg MW, Visser EP, Gotthardt M. Whole organ and islet of Langerhans dosimetry for calculation of absorbed doses resulting from imaging with radiolabeled exendin. *Scientific reports.* 2017;7:39800.

14. Brom M, Franssen GM, **Joosten** L, Gotthardt M, Boerman OC. The effect of purification of Ga-68-labeled exendin on in vivo distribution. *EJNMMI research.* 2016;6:65.

15. Eter WA, Parween S, **Joosten** L, Frielink C, Eriksson M, Brom M, Ahlgren U, Gotthardt M. SPECT-OPT multimodal imaging enables accurate evaluation of radiotracers for beta-cell mass assessments. *Scientific reports.* 2016;6:24576.

16. van der Kroon I, Andralojc K, Willekens SM, Bos D, **Joosten** L, Boerman OC, Brom M, Gotthardt M. Noninvasive Imaging of Islet Transplants with 111In-Exendin-3 SPECT/CT. *Journal of nuclear medicine : official publication, Society of Nuclear Medicine.* 2016;57:799-804.

17. van der Kroon I, **Joosten** L, Nock BA, Maina T, Boerman OC, Brom M, Gotthardt M. Improved Quantification of the Beta Cell Mass after Pancreas Visualization with 99mTc-demobesin-4 and Beta Cell Imaging with 111In-exendin-3 in Rodents. *Molecular pharmaceutics.* 2016;13:3478-3483.

18. Willekens SM, **Joosten** L, Boerman OC, Balhuizen A, Eizirik DL, Gotthardt M, Brom M. Strain Differences Determine the Suitability of Animal Models for Noninvasive In Vivo Beta Cell Mass Determination with Radiolabeled Exendin. *Molecular imaging and biology : MIB : the official publication of the Academy of Molecular Imaging.* 2016;18:705-714.

19. Willekens SM, van der Kroon I, Bos D, **Joosten** L, Frielink C, Boerman OC, Brom M, Gotthardt M. Quantitative and longitudinal imaging of intramuscular transplanted islets of Langerhans with SPECT using [123 I]IBZM. *Diabetes, obesity & metabolism.* 2016;

20. Willekens SM, van der Kroon I, **Joosten** L, Frielink C, Boerman OC, van den Broek SA, Brom M, Gotthardt M. SPECT of Transplanted Islets of Langerhans by Dopamine 2 Receptor Targeting in a Rat Model. *Molecular pharmaceutics.* 2016;13:85-91.

21. Berclaz C, Pache C, Bouwens A, Szlag D, Lopez A, **Joosten** L, Ekim S, Brom M, Gotthardt M, Grapin-Botton A, Lasser T. Combined Optical Coherence and Fluorescence Microscopy to assess dynamics and specificity of pancreatic beta-cell tracers. *Scientific reports.* 2015;5:10385.

22. Brom M, **Joosten** L, Frielink C, Boerman O, Gotthardt M. (111)In-exendin uptake in the pancreas correlates with the beta-cell mass and not with the alpha-cell mass. *Diabetes.* 2015;64:1324-1328.

23. Brom M, Woliner-van der Weg W, **Joosten** L, Frielink C, Bouckenooghe T, Rijken P, Andralojc K, Goke BJ, de Jong M, Eizirik DL, Behe M, Lahoutte T, Oyen WJ, Tack CJ,

Janssen M, Boerman OC, Gotthardt M. Non-invasive quantification of the beta cell mass by SPECT with (1)(1)(1)In-labelled exendin. *Diabetologia.* 2014;57:950-959.

24. Roosenburg S, Laverman P, **Joosten** L, Cooper MS, Kolenc-Peitl PK, Foster JM, Hudson C, Leyton J, Burnet J, Oyen WJ, Blower PJ, Mather SJ, Boerman OC, Sosabowski JK. PET and SPECT imaging of a radiolabeled minigastrin analogue conjugated with DOTA, NOTA, and NODAGA and labeled with (64)Cu, (68)Ga, and (111)In. *Molecular pharmaceutics.* 2014;11:3930-3937.

25. Andralojc K, Srinivas M, Brom M, **Joosten** L, de Vries IJ, Eizirik DL, Boerman OC, Meda P, Gotthardt M. Obstacles on the way to the clinical visualisation of beta cells: looking for the Aeneas of molecular imaging to navigate between Scylla and Charybdis. *Diabetologia.* 2012;55:1247-1257.

26. Brom M, **Joosten** L, Oyen WJ, Gotthardt M, Boerman OC. Improved labelling of DTPA- and DOTA-conjugated peptides and antibodies with 111In in HEPES and MES buffer. *EJNMMI research.* 2012;2:4.

27. Brom M, **Joosten** L, Oyen WJ, Gotthardt M, Boerman OC. Radiolabelled GLP-1 analogues for in vivo targeting of insulinomas. *Contrast media & molecular imaging.* 2012;7:160-166.

28. Roosenburg S, Laverman P, **Joosten** L, Eek A, Rutjes FP, van Delft FL, Boerman OC. In vitro and in vivo characterization of three 68Ga- and 111In-labeled peptides for cholecystokinin receptor imaging. *Molecular imaging.* 2012;11:401-407.

29. Aloj L, Aurilio M, Rinaldi V, D'Ambrosio L, Tesauro D, Peitl PK, Maina T, Mansi R, von Guggenberg E, **Joosten** L, Sosabowski JK, Breeman WA, De Blois E, Koelewijn S, Melis M, Waser B, Beetschen K, Reubi JC, de Jong M. Comparison of the binding and internalization properties of 12 DOTA-coupled and (1)(1)(1)In-labelled CCK2/gastrin receptor binding peptides: a collaborative project under COST Action BM0607. *European journal of nuclear medicine and molecular imaging.* 2011;38:1417-1425.

30. Brom M, **Joosten** L, Laverman P, Oyen WJ, Behe M, Gotthardt M, Boerman OC. Preclinical evaluation of 68Ga-DOTA-minigastrin for the detection of cholecystokinin-2/gastrin receptor-positive tumors. *Molecular imaging.* 2011;10:144-152.

31. Laverman P, **Joosten** L, Eek A, Roosenburg S, Peitl PK, Maina T, Macke H, Aloj L, von Guggenberg E, Sosabowski JK, de Jong M, Reubi JC, Oyen WJ, Boerman OC. Comparative biodistribution of 12 (1)(1)(1)In-labelled gastrin/CCK2 receptor-targeting peptides. *European journal of nuclear medicine and molecular imaging.* 2011;38:1410-1416.

32. Yim CB, van der Wildt B, Dijkgraaf I, **Joosten** L, Eek A, Versluis C, Rijkers DT, Boerman OC, Liskamp RM. Spacer effects on in vivo properties of DOTA-conjugated dimeric [Tyr3] octreotate peptides synthesized by a "Cu(I)-click" and "sulfo-click" ligation method. *Chembiochem : a European journal of chemical biology.* 2011;12:750-760.

33. Brom M, Oyen WJ, **Joosten** L, Gotthardt M, Boerman OC. 68Ga-labelled exendin-3, a new agent for the detection of insulinomas with PET. *European journal of nuclear medicine and molecular imaging*. 2010;37:1345-1355.

34. Laverman P, McBride WJ, Sharkey RM, Eek A, **Joosten** L, Oyen WJ, Goldenberg DM, Boerman OC. A novel facile method of labeling octreotide with (18)F-fluorine. *Journal of nuclear medicine : official publication, Society of Nuclear Medicine*. 2010;51:454-461.

35. Roosenburg S, Laverman P, **Joosten** L, Eek A, Oyen WJ, de Jong M, Rutjes FP, van Delft FL, Boerman OC. Stabilized (111)in-labeled sCCK8 analogues for targeting CCK2-receptor positive tumors: synthesis and evaluation. *Bioconjugate chemistry*. 2010;21:663-670.

36. Weijers EM, van Wijhe MH, **Joosten** L, Horrevoets AJ, de Maat MP, van Hinsbergh VW, Koolwijk P. Molecular weight fibrinogen variants alter gene expression and functional characteristics of human endothelial cells. *Journal of thrombosis and haemostasis : JTH*. 2010;8:2800-2809.

DANKWOORD

Hoi! Leuk dat je het dankwoord leest. Neem een kopje thee en ga er even voor zitten. Het is vrij lang namelijk, want ik heb het werk wat hier beschreven staat natuurlijk niet alleen gedaan. Zonder het enthousiasme, harde werk en goede input én output van vele anderen is het een compleet boekwerk geworden. Met zoveel samenwerkingen en zoveel collega's waar ik mee heb mogen samenwerken, weet ik zeker dat ik personen ga vergeten te bedanken. Dus bij deze: voel je je ook maar enigszins aangesproken, dan wil ik je graag bedanken voor hetgeen jij voor mij hebt gedaan. Ik heb mezelf vast ingedekt. Mocht je je overigens niet aangesproken voelen, dan evengoed bedankt. We hebben vast een keer samen gelachen. Voor jullie allemaal een bloemetje!

Ten eerste wil ik mijn beide promotoren, Martin en Otto, bedanken voor de mogelijkheid om op deze wijze promotieonderzoek te doen. Naast mijn analistenfunctie en ook nog eens parttime hebben jullie het nodige geduld moeten hebben.

Lieve Otto, mijn woord van dank aan jou gaat heel ver terug. Door jouw enthousiaste rondleiding op het lab wilde ik niets liever dan mijn afstudeerstage bij jullie uitvoeren. Toen ik ook nog de mogelijkheid kreeg om na mijn studie als analist te mogen blijven hoefde ik daar niet over na te denken. Voor mijn gevoel heb jij de basis gelegd voor de open en goede sfeer die er op de afdeling heerst. Samenwerken met jou was heel fijn, mede door je razendsnelle correcties, enthousiasme en positieve kijk op dingen. Ook al waren de resultaten niet altijd zoals verwacht, dan wist jij er toch iets positiefs uit te halen. Ik ben blij dat je, ondanks je vertrek naar een andere afdeling, toch mijn promotor wilt zijn. Dankjewel!

Lieve Martin, het is fijn om met je samen te werken. Jouw grapjes en anekdotes over de meest uiteenlopende (soms vieze) onderwerpen zijn een welkome afwisseling met werk. Jouw ideeën voor nieuw onderzoek tijdens werkbesprekingen werken aanstekelijk. Meestal dan, ik heb

inmiddels geleerd om de ideeën die je hebt te filteren en heb me er ook bij neergelegd dat ik niet alles meteen hoef te begrijpen wanneer je hardop aan het brainstormen bent over waar exendin mogelijk nog meer voor ingezet kan worden. Jouw pad van logica kan ik dan niet altijd volgen, en laat me des te meer inzien dat dus ook niet iedereen mijn, voor mij zeer logische, denkwijze kan volgen. Ook jouw rake vragen: 'Lieke, gaat het echt goed met je?' waren af en toe nodig. Waar jij vaak met wilde ideeën kwam, wist Otto dit in kleinere stapjes te hakken om te weten waar te beginnen. Voor mij waren jullie een goede aanvulling op elkaar. Dankjewel!

Lieve Maarten, jij hebt me wegwijs gemaakt op zowel het nucleaire lab, het celkweeklab en het dierenlab en hebt me de fijne kneepjes van het vak geleerd. Wat ook wel nodig was, gezien ik vond dat de mannetjes muizen toch wel rare billen hadden... We hebben veel gelachen op het lab, met name onze kleurrijke josti-codering maakte de mega experimenten enigszins overzichtelijk en haalbaar. Je functioneerde tevens als mijn externe harde schijf, want ik moest dikwijls aan jou vragen welke experimenten ik alweer had gedaan en wat daar de uitkomst van was. Mede dankzij jou heb ik nu een mooie vervolgfunctie die bij me past. Ik vind het jammer dat we geen collega's meer zijn, maar ik hoop dat we toch nog eens kunnen samenwerken. Dankjewel!

Lieve Sandra, we zijn beiden begonnen als student in het Aquarium op de Nucleaire en hebben een heel ander pad bewandeld. Je gaat als een trein, en je neemt onderweg heel veel personen mee in deze trein, om ze op een verder traject in hun carrière netjes af te zetten, met een koffer vol bruikbare bagage. Ik vraag me vaak af hoe je het toch allemaal doet. Ik vind het fijn dat je deel uitmaakt van mijn promotieteam en dat we nu samen een nieuw project aan gaan. Een project waar ik met veel plezier aan werk. Ik ga nog ontzettend veel van je leren de komende jaren. Je bent een voorbeeld voor velen. Dankjewel!

Lieve Peter, je verdient het om een apart stukje te krijgen in het dankwoord. In het verleden hebben we bij veel studies mogen samenwerken, wat geleid heeft tot mooie resultaten. Ik vind het dan ook leuk om in mijn nieuwe onderzoek weer nauw met je te kunnen samenwerken. Met jouw kritische en vooruitkijkende blik gaan we dit project ook tot een succes maken. Bovenal wil ik je bedanken voor je luisterend oor, als 'papa' van de afdeling kunnen we wel bijna zeggen. Het is niet altijd even makkelijk geweest, en je nam tijd om ook over niet-werk gerelateerde dingen te praten. Dankjewel!

Lieve analisten, Gerben, Cathelijne, Desirée, Janneke, Danny, Annemarie, Milou en Hanneke, jullie houden de afdeling draaiende. Ik heb het altijd fijn gevonden om één van jullie te zijn, en zo voelt het nog steeds een beetje. Iets met niet kunnen loslaten. Ik moet eraan wennen om nu 'aan de andere kant' te staan en jullie om hulp moet vragen voor het uitvoeren van experimenten. Niet dat ik geen vertrouwen in jullie heb, want dat heb ik zeker wel, maar... ik

weet eigenlijk niet waarom. Jullie staan altijd voor iedereen klaar en zonder jullie is er geen nucmed. Gerben, ik kan je geen hele bladzijde in mijn boekje geven, dus ik hoop dat ik je niet teleurstel. Ik hoop nog lang van jouw kennis gebruik te mogen maken, en dat we samen het 'lood-project' tot een mooi resultaat kunnen brengen. Hanneke, je kwam als geroepen ons 'beta' team versterken. Er liepen veel grote projecten door elkaar heen, waardoor we nauwelijks tijd over hadden om tussendoor goed bij te praten. Ik realiseer me dat we af en toe veel van je verwachtten, je werkte immers nog maar net bij ons op de afdeling. Mede door jouw zeer nauwkeurig bijgehouden labjournaal en je mega tabellen die overigens heel overzichtelijk waren, kon ik uiteindelijk alle resultaten bundelen. Ik hoop dat je geen *muis*arm (haha) of nachtmerries hebt overgehouden aan het eindeloos tekenen van ontplofte eilandjes. Desirée en Cath, uren en uren hebben we gepland, gelabeld, gescand, geofferd, geperfuseerd, geïsoleerd, gekleurd, getekend, geanalyseerd. Maar altijd met gezellig geklets. Cath, meestal heb jij een experiment al uitgevoerd voordat ik mijn vraag af heb. Je werkt super efficiënt en doet alles met evenveel enthousiasme. Samenwerken met jou is een plezier, dus ik hoop dat we dat ook nog veel kunnen blijven doen. Desirée, dat je mijn schets van een celmembraan met receptoren, getekend met mijn uitzonderlijke (verreweg van goede) tekentalent, hebt weten om te zetten in mooie digitale plaatjes (zie H2 en H10), laat toch wel enig talent aan jouw zijde zien. Ik zou er niet raar van opkijken als de aanvragen nu binnenstromen (sorry?). Naast de fijne samenwerking hebben we ook veel goede gesprekken gehad. Ik ben blij dat je mijn paranimf bent, want je verdient het. Dankjewel!

Lieve Erik, ik wil je toch even apart bedanken voor je geduld en afleiding tijdens het vliegen. Zelfs toen ik op weg naar San Sebastian al een afscheidsberichtje naar mijn familie wilde gaan versturen omdat de steward iets te hard van de achterkant van het vliegtuig naar voren rende en ik dacht dat we via de glijbaan de zee in zouden moeten duiken. Uiteindelijk had jij gelijk en had de piloot waarschijnlijk gewoon graag een kauwgumpje. Dankjewel!

Lieve Beta-groep, Martin, Maarten, Tom, Sanne, Cath, Estel, Daphne D, Marti, ook al zijn onze meetings niet altijd efficiënt (meestal wel uiteraard), ze zijn wel altijd gezellig. Het is erg fijn om met jullie samen te werken, ik denk dat we een goede aanvulling zijn op elkaar. Tom en Daphne L, zonder jullie hulp had ik de ingewikkelde dosimetrie berekeningen nooit voor elkaar gekregen. Dankjewel!

Lieve Stefanie, het was ontzettend fijn om met jou samen te werken en dat heeft ook twee mooie hoofdstukken opgeleverd. Maar nog meer waardeer ik de tijd buiten werk. We hebben samen veel gelachen, gedronken, geluisterd en gepraat. Jammer dat we geen collega's meer zijn, maar erg dankbaar dat we nog steeds contact hebben. Ik kijk uit naar ons volgende weekendje naar Leuven! Want dat gaat er zeker komen! Dankjewel!

Lieve kamergenoten, Sanne, René en Marti, opeens zit ik bij jullie op de kamer, bij de seniors, wat een serieuze bedoeling. Nooit eens tijd voor een praatje of een grapje. Altijd volledige concentratie op het werk, alle deadlines worden gehaald, nooit wordt er geklaagd. Niets is minder waar. Toch fijn dat thuiswerken, anders krijg ik niks gedaan ;-). Ik vind het leuk met jullie en goed dat we toch nog enige tijd onze 'ellende' samen kunnen delen. Dankjewel!

Lieve (oud) collega's van de nucleaire, studenten, laboranten, hotlab, staf, artsen, PhD's, seniors, mede dankzij jullie heerst er een ontzettend fijne sfeer op de afdeling. De vele borrels (soms iets teveel voor mij als moeder en forens), dagjes uit, research lunch, weekendjes weg, workshop vlaai bakken, workshop paaldansen, dagje Volendam (nee, ik ben niet zo goed in onverwachte dingen) en vooral ook de memorabele congressen (hét IBA-feest in Milaan is nooit meer geëvenaard), één en al gezelligheid. Ik ben blij dat ik hier deel van uitmaak en hoop dat nog lange tijd te mogen doen. Dankjewel!

Dear Martin Schäfer, Eberhard Weihe, Decio Eizirik, Alexander Balhuizen, Fritz Andreae, Martin Béhé, it was a real pleasure working with you. Thank you for your scientific input for several of my chapters. I hope we will get the chance to work together again. Thank you!

Lieve Monica van Zanten, Luc Bouwens en Eddy Himpe, ik heb onze samenwerking als zeer prettig ervaren. Ook al lag het werk een hele tijd stil, ik vind het fijn dat we het zo vlug weer konden oppakken en waardeer jullie input enorm! Dankjewel!

Lieve collega's van pathologie, urologie en radiotherapie, ik heb vele uurtjes doorgebracht op jullie afdelingen, waar ik me altijd welkom heb gevoeld. Jullie gastvrijheid en behulpzaamheid stel ik zeer op prijs. Dankjewel!

Lieve collega's van PRIME, Bianca, Kitty, Iris, Henk, Wilma, jullie zijn onmisbaar voor ons onderzoek. Door jullie flexibiliteit, meedenkendheid (is dat een woord? Bij deze), vaardigheid, oplettendheid en uiteraard gezelligheid is het fijn om met jullie samen te werken. Ik ben blij dat we dit in de toekomst kunnen voortzetten. Dankjewel!

Lieve carpoolers, Cindy, Claudia, Hanneke, Najat, José. We hebben het er vaak over gehad. Is je dankwoord nou al af? We komen er wel in he? Tadaa, hier staan jullie dan! Welverdiend! We kletsen wat af tijdens onze ritjes, al doe ik ook graag even mijn ogen dicht in de auto. Alle ins en outs worden besproken en het is fijn om mijn ei kwijt te kunnen bij jullie. De meest hilarische momenten waren toch vaak wanneer we in een file terecht kwamen en spijt hadden dat we geen snoepjes in de auto hadden liggen of probeerden met een foto op het nieuws te komen. Helaas is dat één keer wel gelukt, maar toch hebben we toen ook veel gelachen.

Waarschijnlijk van de schrik. Ook Nico, Alice, Bart, Suzanne, Marian, Ria, Karen, Monique en Kim wil ik bedanken voor de gezellige ritjes. Dankjewel!

Dear Bridget Collins (Flora Forager), your work inspires me. I am really grateful that I could use your botanical artworks to illustrate my book. They are a perfect match with the work that I have done. Thank you!

Lieve Bregje, jij voelde precies goed aan welke kant ik op wilde met de lay out van mijn boekje, vooral omdat het toch iets afwijkt van de meeste boekjes. Ik ben blij dat je mijn 'More is more' hebt weten in te dammen. Het moest herkenbaar zijn als een echt 'Lieke-boekje', en ik geloof dat dat is gelukt. Dankjewel!

Het leven draait niet alleen om werken, en ik mag me gelukkig prijzen dat ik zoveel mensen om me heen heb voor de nodige ontspanning en afleiding.

Lieve Lay's, spreekt voor zich. Dankjewel!

Lieve familie, ik kijk altijd weer uit naar onze familiedagen, weekendjes weg en op zondagochtend chocola eten bij Omi. Dankjewel!

Lieve vrienden, René, Cindy, Sjors, Sonja, Tom, Anda, Erik, Sandra, Johan, Christel, Roos, Niels, Leonie, Rob, Aniek (Buisbubs 2.0), Richard en Veerle, een feestje, verhuizen, klussen of gewoon een gezellig avondje, we kunnen altijd op elkaar rekenen. Op handen en voeten door tunnels kruipen, met kleren aan in de sloot vallen of een ouderwets potje beugelen. Ik vind het fijn om samen te zijn. Hopelijk kan dat snel weer, dan gaan we proosten en dan zeggen we net zo vaak: "Nog eine dan", tot we er bij neervallen. Christel, je staat altijd voor ons klaar, "doe bis de leefste". Dankjewel!

Lieve Golden Girls (volgens Remco de Grey Girls) Marloes, Christine en Leonie, we hebben al vele mooie herinneringen gemaakt sinds we elkaar hebben leren kennen op de Bouwens. Ons plan om elk jaar een Escape Room te gaan doen is niet helemaal gelukt, en het is al een puzzel op zich om een avondje te prikken om te daten. Ik denk graag terug aan onze jaarlijkse (wat ging er mis?) kermis date (waar ik me niet alles van kan herinneren), de PM-sessies in Panningen, etentjes (met en met zonder kinderen en aanhang), en het eten van ijsjes met alcohol. Ik hoop nog meer mooie herinneringen met jullie te maken. Dankjewel!
Lieve Thom en Chris, ik geniet van de spontane etentjes en gezellige avonden samen (en zwempartijtjes die onze dochters regelen). Dankjewel!
Lieve Leonie en Niels, we kenden elkaar al toen we nog niet konden lopen. We raken nooit uitgepraat, terwijl we eigenlijk aan één woord genoeg hebben. Als we samen zijn is het altijd

gezellig, moet er altijd een etentje bij en wordt het altijd te laat. En dat is fijn. Laten we hiermee doorgaan tot we niet meer kunnen lopen. Dankjewel!

Lieve schoonfamilie, Leo, Jeanne, Lotte, Lucas, Pien en Richard, alweer 19 jaar geleden stapte ik bij jullie naar binnen. Een beetje onwennig in het begin, maar ik ben blij met zo'n lieve schoonfamilie. Dankjewel!

Lieve papa en mama, de grootste dank gaat uit naar jullie! Jullie hebben de basis gelegd, en dat is denk ik het halve werk. Dankzij jullie heb ik het zover kunnen schoppen. Jullie liefde en steun is onvoorwaardelijk. Niet alleen voor mij, maar ook voor de kinderen. De wetenschap dat jullie altijd voor ons klaar staan geeft rust. Op de kindjes passen, verbouwen, huis op orde houden, op de kindjes passen, tuin op orde houden, op de kindjes passen. Het is nooit teveel voor jullie en daarom kon ik met een gerust hart aan mijn promotie werken. Dankjewel!

Lieve Rob, Aniek en Evy, ik vind het ontzettend fijn dat we elkaar nu vaker zien, ondanks dat we niet bij elkaar in de buurt wonen. Ik ben trots op jullie, als kersvers gezin. Evy, wat gaan we samen nog vele leuke dingen meemaken. Ik kan niet wachten om je weer te knuffelen. Aniek, het lijkt alsof ik je al jaren kent en dat voelt goed. Rob, ik ben ontzettend trots dat jij hier vandaag bij me staat. Dankjewel!

Lieve Zsofi en Timo, als er iets is wat ik jullie wil leren, is dat je nooit moet opgeven en vertrouwen moet hebben in jezelf. Die woorden krijg ik ook meteen van jullie terug als ik me weer druk maak om de verdediging. Door onze momenten samen kan ik echt alles even loslaten en genieten. Genieten, dat doe ik van jullie, met volle teugen. Dankjewel voor jullie knuffels, ondeugendheid, gekkigheid, eerlijkheid, vertrouwen en liefde. Jullie zijn mijn alles! De tijd staat jullie goed! Dankjewel!

Lieve Remco! Mijn liefje, mijn maatje, mijn best vriend, mijn rem... Dankjewel voor je onvoorwaardelijke steun. Je kent me door en door. Je kent me beter dan dat ik mezelf ken. Wanneer ik weer eens meerdere achtbanen in mijn hoofd heb, weet jij ze in goede banen te leiden, zodat er geen kan ontsporen. Je begrijpt het als geen ander wanneer ik toch even moet werken om mijn hoofd leeg te krijgen, of wanneer ik echt even tijd voor mezelf nodig heb. We hebben ontzettend veel meegemaakt samen, en dat heeft ons alleen maar sterker gemaakt. Je hebt me tevens het allermooiste gegeven wat er bestaat, ons gezin. Ik kijk er heel erg naar uit om samen met jullie mooie nieuwe herinneringen te maken. Dankjewel lief!

CURRICULUM VITAE

Lieke Joosten was born in Tegelen, The Netherlands, on November 2nd 1983. In 2002, she graduated from the Bouwens van der Boijecollege (VWO) in Panningen. In the same year, she started her study Applied Science, Biomedical Science at the Fontys Hogeschool in Eindhoven. Her first internship was at the Netherlands Forensic Institute in The Hague, where she investigated a method to obtain reliable 'fingerprints' from bacteria in soil samples. Her final internship started in 2005 at the Erasmus Medical Center in Rotterdam, where she performed the study entitled: "MCL-1 as therapeutic target for infants with Acute Lymphoblastic Leukemia". She obtained her Bachelor of Science degree after 3.5 years and to fill the gap between two studies, she worked as a technician at the Netherlands Institute for Neuroscience in Amsterdam, where she performed research on gene inhibition by RNA interference. In 2006, she started the master Oncology at the Vrije Universiteit in Amsterdam. Her first internship was performed at the Department of Physiology at the VU University Medical Center in Amsterdam, studying the development of a fibrin coating using different variants of fibrinogen and their influence on endothelial cell characteristics. In 2007, she started her final internship at the Radboud University Medical Center at the Department of Radiology and Nuclear Medicine, where she worked on the project "PET imaging of CCK2/gastrin receptor expressing tumors". She obtained the degree of Master of Science in 2008 and she stayed at the Department of Radiology and Nuclear Medicine to work as a research technician. While working as a senior research technician, she started her PhD project at the same department. Her project is focused on the development and characterization of novel beta cell tracers. From September 2019 she continues her work at the Department of Radiology and Nuclear Medicine as a Scientific Researcher on the project 'Development of a new alpha-based-PSMA therapy for prostate cancer'.

PORTFOLIO

Name PhD candidate: Lieke Joosten	PhD period: 01-04-2015 – 31-12-2019
Department: Radiology and Nuclear Medicine	Promotor(s): Prof. M. Gotthardt
Graduate School: Radboud Institute for Molecular Life Sciences	Prof. O. C. Boerman
	Co-promotor(s): Dr. M. Brom
	Dr. S. Heskamp

Training activities		**Year(s)**	**ECTS**
a)	Courses & Workshops		
	- Statistics	2016	0.8
	- Within sight of my PhD	2017	0.5
	- FIJI microscopic imaging	2017	0.5
	- RIMLS PhD Retreat	2018	0.5
	- How to write a medical scientific paper	2018	0.5
	- Scientific integrity	2018	0.5
	- RIMLS PhD Retreat*	2019	0.75
	- InDesign course	2019	0.1
	- The art of presenting science	2019	0.75
	- Teaching sessions	2019	0.5
b)	Seminars & lectures		
	- Journal clubs	2017	0.1
	- Radboud Research Rounds*	2017, 2018	0.35
	- Paper Awards*	2017 - 2019	0.5
c)	Symposia & congresses		
	- BELNUC Maastricht*	2015	1.0
	- NKRV*#	2015 - 2019	1.75
	- EASD*	2015	1.5
	- Symposium beta cell imaging	2015	0.5
	- EANM*#	2015 - 2017	5.25
	- NVDO*	2016	1.0
	- EMIM*	2018	1.5
	- New frontiers symposium	2018	0.5
	- ENABLE symposium	2019	1.25
d)	Other		
	- Organization symposium beta cell imaging	2015	1
	- Organization ENABLE symposium	2019	2
	- Review scientific publication	2019	0.1
	- Review scientific abstracts WMIC	2019	0.5
Teaching activities			
e)	Teaching PhD students		
	- Selen Ekim	2015	5
	- Inge vd Kroon	2015 - 2017	10
	- Stefanie Willekens	2015 - 2016	5
	- Gregory Bowden	2015	1.5
	- Marko Kröselj	2015 - 2016	2.5
	- Roel Op 't Veld	2016 - 2019	3.5
f)	Other		
Total			51.7

RESEARCH DATA MANAGEMENT

Findable

All raw and processed data obtained during my PhD and described in this thesis have been stored on the hard drive of the department of Radiology, Nuclear Medicine and Anatomy at the Radboud university medical center. This hard drive is password protected and automatic back-ups are made several times a day. Most of the data is captured in notebooks and a digital copy of these notebooks is stored on the hard drive as well. A small part of the data in chapters 6 and 8 is captured and stored on Labguru, a digital lab book client, which is centrally stored and daily backed-up on the local Radboudumc server. Raw data from equipment (*e.g.* SPECT/CT, gamma counter) are backed-up on university servers belonging to the department. Big data, for example SPECT/CT images and immunohistochemical images are stored on external hard-drives and are located at the department of Radiology, Nuclear Medicine and Anatomy.
All mouse studies were performed according to the Institute of Laboratory Animal Research Guidelines. Animal experiments were approved by the Animal Ethical Committee of the Radboud University, Nijmegen, The Netherlands.

Accessible

All protocols and data are accessible by contacting the corresponding author or one of the researchers involved in these studies.

Interoperable

All protocols and data are documented in English.

Reusable

All data will be saved for at least 15 years after publication of the respective study. All used methods and data analyzed during these studies are available upon request from the corresponding author.